INVESTIGATING THE MECHANISM OF GABA NEURON DEGENERATION IN A MODEL OF COENZYME Q DEFICIENCY

By

Mallory Louise Hacker

Dissertation

Submitted to the Faculty of the

Graduate School of Vanderbilt University

in partial fulfillment of the requirements for

the degree of

DOCTOR OF PHILOSOPHY

in

Cell and Developmental Biology

August, 2013

Nashville, Tennessee

Approved:

Aaron B. Bowman, Ph.D.

Joshua T. Gamse, Ph.D.

Kathleen L. Gould, Ph.D.

Laura A. Lee, Ph.D.

David M. Miller III, Ph.D.

To the memory of my father, Tim Hacker

ACKNOWLEDGEMENTS

I must first thank my mentor, David Miller. David's research expertise is in developmental neurobiology, but I am very thankful that he allowed me to work on the lab's only neurodegeneration project. I knew during my rotation that the environment of the Miller lab was the perfect fit for me and David's willingness to accommodate my desire to work on this project solidified his lab as the ideal place to do my graduate research. David's teaching style struck the perfect balance of providing mentorship and yet also allowing me to work very independently. This allowed me to learn from him while also growing tremendously as a scientist. My communication skills (verbal and written) have also improved vastly thanks to David. Finally, David understands the importance of having a work-life balance, and I will forever be grateful for his compassion that allowed me to be with my family when I needed to the most.

I thank the members of my thesis committee, Aaron Bowman, Josh Gamse, Kathy Gould, and Laurie Lee, for their feedback and encouragement. I am especially grateful for the numerous letters of recommendation they have written on my behalf. I give special thanks to my committee chair, Kathy Gould. Since my first day at Vanderbilt (where she was assigned my IMPACT mentor), Kathy has been someone I can go to for advice and I am thankful for her support over the years.

I thank the Department of Cell & Developmental Biology, the Program in Developmental Biology, and the Neurodegeneration Research Group for opportunities to present my work, give journal club presentations, and discuss science collaboratively.

I would also like to thank my funding sources, which have included the Cellular, Molecular, Biochemical Science (CBMS) training program (T32GM08554) and predoctoral fellowships from the American Heart Association (AHA) (10PRE4230025) and (12PRE11650022).

My chemistry research mentor at UT-Chattanooga, Dr. Manuel Santiago, saw my potential and encouraged me to apply for Vanderbilt's IGP program. I am very thankful to have had that support as an undergraduate, because I would not be where I am today without it.

I had the great fortune of working in a wonderful laboratory environment. My coworkers happily embraced the many silly traditions that I started in the lab (such as Jack Friday, "cake" timer, beer birthdays, and the lab trophy). Cody was my scientific sibling (he and I joined the Miller lab at the same time). Both inside and outside of the lab, Cody has been a great friend and I am thankful to have gone through graduate school with him. Rachel has not only been a great bay mate but also a close friend. I'm fortunate to have spent most of my graduate years working beside her. Tyne joined the lab a couple of years ago, and she perfectly fit in with the lab dynamic. I am thankful to have had her here these past few years. Clay, Sarah and Jud were the older graduate students whose advice and assistance made the first years in lab much easier. Tim, Becky and Kathie were essential to keep the lab running smoothly.

I am very thankful for the many friendships I have made with fellow graduate students at Vanderbilt. It has been invaluable to have peers that understand the trials, tribulations and triumphs that accompany this journey.

Finally, I lovingly acknowledge my family for their support. Henry has been my rock throughout graduate school, and I am very thankful for his unconditional understanding and encouragement. I am also thankful for my second family, the Hornes. They have provided so much encouragement and support over the years, and their genuine interest in (and respect for) my work is something that I have always cherished. My mom has always supported me and also showed me how to be a strong, independent woman. Lastly, I must thank my late father. From an early age, he convinced me that I could do anything that I put my mind to. He was truly my biggest fan, and I never once doubted that he was proud of me.

TABLE OF CONTENTS

LIST OF TABLES

LIST OF FIGURES

LIST OF ABBREVIATIONS

Abbreviation	Description	Abbreviation	Description
Ach	Cholinergic	GFP	Green Flurorescent Protein
AD	Alzheimer's Disease	HBx	Hepatitis B Virus X
AECOM	Albert Einstein College of Medicine	HD	Huntington's Disease
ALS	Amyotrophic Lateral Sclerosis	HPF	High-Pressure Freezing
ANT	Adenine Nucleotide Translocator	KAP-1	Kinesin-Associated Protein 1
Apaf-1	Apoptosis Protease Activating Factor 1	LAS-AF	Leica Application Suite Advanced Fluorescence
APTX	Aprataxin	LB	Luria-Bertani
ATP	Adenosine TriPhosphate	LMP	Lysosomal Membrane Permeabilization
AU	Arbitrary Units	MPT	Mitochondrial Permeability Transition
CARD	Caspase Activation Recruitment Domain	mRFP	monomeric Red Fluorescent Protein
CGC	Caenorhabditis Genetics Center	mtHtt	Mutant Huntingtin
CNS	Central Nervous System	NBRP	National BioResource Project
CoQ	Coenzyme Q	NO	Nitric Oxide
CoQOX	CoQ - Oxidized	OD	Optical Density
CoQRED	CoQ - Reduced	PD	Parkinson's Disease
CRT-1	Calreticulin	PDSS1/2	Polyprenyl Diphosphate Synthesase Subunit 1/2
d	day	PTP	Permeability Transition Pore
DA	Dorsal A-type	Q	Coenzyme Q
DB	Dorsal B-type	rec-CED-3	Reconstituted CED-3
DD	Dorsal D-type	RNAi	RNA Interference
DIC	Differential Interference Contrast	ROS	Reactive Oxygen Species
DMQ	Demthoxy-Coenzyme Q	RPM	Revolutions Per Minute
DRP-1	Dynamin-Related Protein 1	*sbo*	*small boy*
dsRNA	double-stranded RiboNucleic Acid	SOD-1	SuperOxide Dismutase 1
Egl	Egg-Laying Defective	TEM	Transmission Electron Microscopy
EGTA	Ethylene Glycol Tetraacetic Acid	Unc	Uncoordinated
ETC	Electron Transport Chain	VD	Ventral D-type
ETFDH	Electron-Transferring-Flavoprotein Dehydrogenase	VNC	Ventral Nerve Cord
EV	Empty Vector	WAN-1	Worm Adenine Nucleotide translocator 1
GABA	Gamma Amino isoButyric Acid	WT	Wild-Type

CHAPTER I

INTRODUCTION

Neurons are specialized cells that transmit information through electrochemical signals. The nervous system is composed of various types of neurons, or nerve cells, that form elaborate signaling networks to control many processes, including movement, behavior and learning. Neurodegenerative diseases are characterized by dysfunction or death of discrete neuronal populations. The pathogenic outcome of this neuronal loss includes impaired movement (i.e., ataxias) and/or reduced mental capacity (i.e., dementia). Despite the wide range of symptoms presented by these diseases, they share features such as an age-dependent onset and progressive death of specific neuronal subtypes. Studies based on genetic mutations linked to these diseases are beginning to reveal the underling molecular mechanisms of neuronal degeneration. This work has identified a wide variety of putative disease-causing events (i.e., oxidative stress, energy depletion, calcium overload) and show that these cellular stresses are associated with mitochondrial dysfunction, a universal denominator of neurodegenerative diseases. Mitochondria are key energy-providing organelles and their impairment causes adverse cellular effects, including increased reactive oxygen species (ROS) and deficient ATP production (Brookes et al. 2004). The deleterious effects of these insults and the central role that mitochondria play in cell death regulation underlie the need to understand how dysfunction of this organelle contributes to disease pathogenesis.

Despite recent progress, much is still unknown about how age-dependent cellular changes lead to the selective death of specific types of neurons. Part of the challenge of understanding basic biological responses to injury in the nervous system is due to the complexity of the mammalian brain, which is composed of billions of neurons that make trillions of neuronal connections (Wang 2010). To circumvent this challenge, I have used the nematode *C. elegans* as a model system to

study how mitochondrial dysfunction leads to neuronal degeneration. In contrast to the mammalian brain, the *C. elegans* nervous system is composed of only 302 neurons (White et al. 1986). The strong conservation of key biological pathways between *C. elegans* and mammals suggests that my findings could enhance the understanding of how mitochondrial impairment contributes to neurodegenerative disease. In this **Introduction**, common features of neurodegenerative diseases are reviewed, with a focus on cellular stresses that are shared among these disorders. These injuries trigger cell death responses that are also prominent in neurodegenerative diseases. Finally, many aspects of Coenzyme Q (an essential mitochondrial molecule that antagonizes many of these cellular stresses) are discussed. These features of Coenzyme Q include its diverse functions, its association with neurodegenerative disease and the advantages of using *C. elegans* to study Coenzyme Q deficiency.

Neurodegenerative diseases share common features

Age-dependent disease onset

Advanced age is the primary risk factor for neurodegenerative diseases (T. Farooqui & A. A. Farooqui 2009) and enhanced life expectancy is projected to correlate with a dramatic increase in the frequency of these disorders. An unfortunate consequence of aerobic metabolism is the generation of reactive oxygen species (ROS). Overproduction of ROS damages biomolecules such as proteins, lipids and DNA. To counteract these insults, cells use several adaptive mechanisms (i.e., antioxidant molecules and enzymes) that reduce ROS levels below toxic thresholds. However, these defenses decrease with age, leading to overall increased oxidative stress (Mattson & Magnus 2006). Resultant damage to proteins, membranes and nucleotides accumulates over time, impairing other cellular processes (i.e., energy production, calcium buffering, DNA stability). Thus, the inherent cellular changes that accompany aging may sensitize neurons to genetic or environmental factors

that contribute to a neurodegenerative condition. Additionally, familial forms of neurodegenerative disorders have earlier disease onset than sporadic cases (Fig. 1.1A) due to inherited genetic mutations whose impaired function adversely affects neuron viability (Bertram 2005). Similarities in clinical and pathological presentations between both early- and late-onset forms of these diseases are suggestive of shared cellular events that may be accelerated by specific genetic mutations (Mattson & Magnus 2006).

Selective neuronal vulnerability

Another hallmark of neurodegenerative diseases is the selective degeneration of distinct neuronal populations (Fig. 1.1B). These disorders manifest with unique clinical outcomes that originate with dysfunction or degeneration of specific brain regions. For example, neuronal loss in the hippocampus and cerebral cortex in Alzheimer's Disease is correlated with symptoms of impaired learning and memory (Bird et al. 1983). Motor dysfunction is a hallmark of Parkinson's disease due to degeneration of dopaminergic neurons of the substantia nigra (Obeso et al. 2008). Amyotrophic Lateral Sclerosis (ALS) is characterized by loss of motor neurons of the cerebrospinal axis that control voluntary muscles (Kawamura et al. 1981). Huntington's Disease is associated with discoordinated movement (i.e., chorea) and degraded cognitive function that are linked to degeneration of glutamatergic neurons in the striatum (Martin & Gusella 1986). Although the types of neurons injured in these diseases are known, the molecular foundation for their selective hypersensitivity in each of these diseases is not well-understood.

Efforts to delineate the basis for neuron vulnerability have revealed that common cellular processes are often disrupted in these sensitive neuronal populations. These studies compared affected versus resistant populations of neurons from similar brain regions and reported potentially harmful differences in oxidative stress load, energy production, calcium regulation and

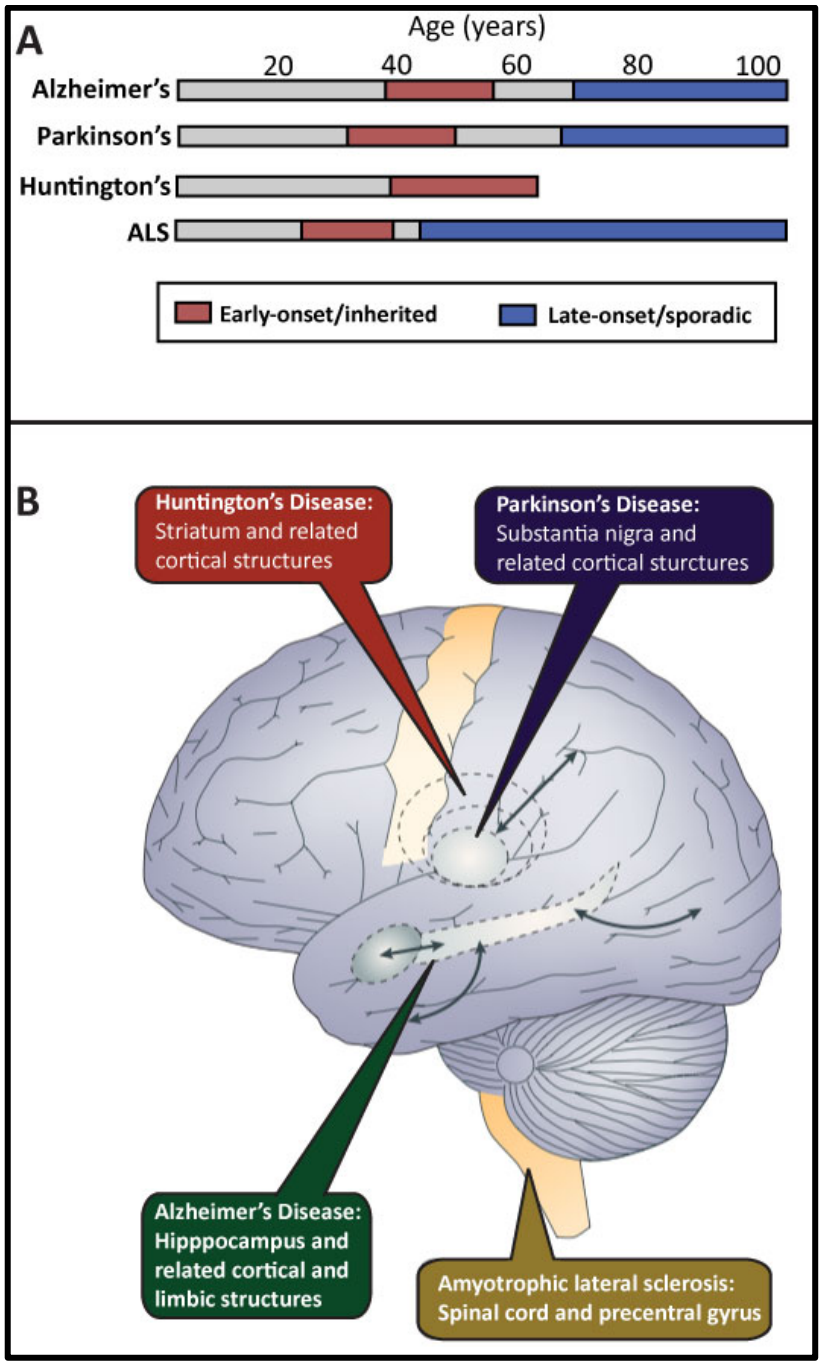

Figure 1.1: Age-related disease onset and selective neuronal vulnerability are common features of neurodegenerative diseases. A. Both familial and sporadic types have age-related disease onset, with familial forms of neurodegenerative disorders having earlier onset than sporadic cases. **B.** Affected brain regions of major neurodegenerative diseases correlate with clinical symptoms. Figure modified from (Mattson & Magnus 2006).

mitochondrial function (Wang 2010). These variances do not solely cause vulnerable neurons to die but are predicted to confer sensitivity to subsequent insults that can lead to their demise. Additionally, expression profiling of neurons with distinct vulnerabilities in murine models of Parkinson's Disease (C. Y. Chung et al. 2005) and Amyotrophic Lateral Sclerosis (Hedlund et al. 2010) uncovered many gene classes that are differentially expressed compared to resistant neurons. Notably, mitochondrial and apoptosis-related genes are differentially expressed in vulnerable versus resistant populations. Despite these correlations between altered cellular homeostasis and unique gene expression, a clear causal connection between these changes and disease state remains elusive.

Mitochondrial dysfunction

Mitochondria are essential organelles that provide many important functions for the cell, such as ATP production, antioxidant defense and calcium homeostasis (Petrozzi et al. 2007). Not surprisingly, disruption of these mitochondrial-dependent processes is associated with neurodegenerative diseases (Beal 2005). Additionally, both age-related cellular changes and differential neuronal sensitivities implicate oxidative stress as a key event in neurodegenerative diseases. Oxidative stress arises from damage to molecules (i.e., proteins, lipids, nucleotides) by reactive oxygen species (ROS). The highly reactive superoxide anion is one of the major ROS produced, and it is primarily generated as a by-product of the energy-producing process of oxidative phosphorylation in the mitochondrial electron transport chain (ETC) (Zeevalk et al. 2005).

Genetic analyses of patients with familial forms of neurodegenerative diseases identified mutations in proteins associated with the mitochondria. For example, many of the genes linked to Parkinson's Disease (i.e., PINK1, Parkin, DJ-1) have mitochondrial roles (Valente et al. 2004; Darios 2003; Taira et al. 2004). Several genetic mutations linked to these diseases also disrupt the function

of the electron transport chain (ETC) (**Fig. 1.2**) (Lin & Beal 2006). For example, β-amyloid deposits in the brain are a hallmark pathology of Alzheimer's Disease and a fragment of β-amyloid disrupts the activity of ETC Complex IV (Canevari et al. 1999). Additionally, chemical inhibitors of the ETC produce symptoms reminiscent of neurodegenerative diseases, providing further evidence of a connection between ETC dysfunction and neuronal degeneration (Knott et al. 2008). Specifically, 3-nitropropionic acid (3-NP), an inhibitor of Complex II of the ETC, causes selective degeneration of GABAergic neurons in the striatum which is also a prominent feature of Huntington's Disease (Brouillet et al. 1999). Thus, ETC dysfunction resulting in decreased ATP synthesis, or alternatively, increased ROS production is linked to neurodegenerative disease.

Types of cell death associated with neurodegenerative pathology

Aberrant neuronal cell death underlies the pathogenesis of neurodegenerative diseases. Cell death pathways, initiated by a wide-range of cellular stressors, have been implicated in these disorders. Two of the most well-characterized types of cell death associated with neurodegeneration are apoptosis and necrosis (Bredesen et al. 2006). Neuronal death by apoptosis or necrosis is linked to Alzheimer's (Bonfoco et al. 1995), Huntington's (Portera-Cailliau et al. 1995), Parkinson's Diseases (Jellinger 2000), and Amyotrophic Lateral Sclerosis (Matyja et al. 2005). Evidence for both of these death pathways in neurodegenerative diseases suggests that a common set of insults and proteins may regulate the killing mechanisms that remove damaged neurons.

Apoptosis

Programmed cell death (i.e., apoptosis) is important for embryonic development and adult tissue homeostasis (Kerr et al. 1972). However, misregulation of this process is associated with disease. For example, insufficient apoptosis is linked to the pathogenesis of cancer

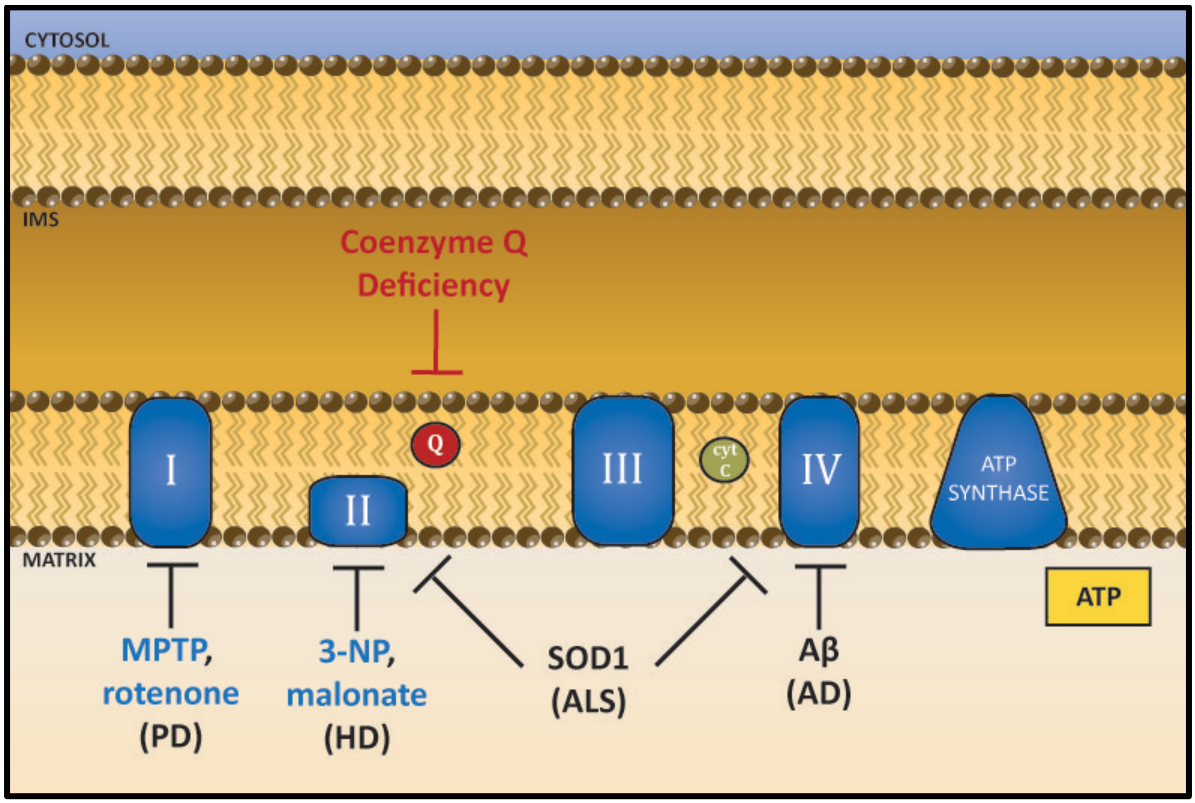

Figure 1.2: The mitochondrial electron transport chain (ETC) is often disrupted in neurodegenerative diseases. Genetic mutations linked to neurodegenerative diseases, SOD1 and amyloid beta (Aβ), reduce the activity of ETC complexes in models of Amyotrophic Lateral Sclerosis (ALS) (Menzies et al. 2002) and Alzheimer's Disease (AD) (Canevari et al. 1999), respectively. Pharmacological inhibitors of Complex I (MPTP and rotenone) induce Parkinsonian (PD) symptoms (Langston et al. 1983; Betarbet et al. 2000) and 3-nitropropionic acid (3-NP) and malonate interfere with Complex II and produce symptoms associated with Huntington's Disease (HD) (Brouillet et al. 1999). Coenzyme Q deficiency reduces the levels of Coenzyme Q (Q) and often presents with neurological symptoms such as cerebellar ataxia. IMS = intermembrane space, cyt c = cytochrome C.

(Bergmann & Steller 2010) and excessive apoptosis leads to inappropriate cell loss in neurodegenerative disease (Mattson 2000). Oxidative stress and DNA damage are established apoptotic triggers that are also commonly found in stressed or aging neurons.

Apoptosis (i.e., Type I cell death) is an energy-driven process that largely functions through a family of cysteine proteases known as caspases. Forward genetic screens in *C. elegans* identified conserved apoptotic machinery (Fig. 1.3) and outlined a cascade of events that leads to apoptotic death (Metzstein et al. 1998). Whereas apoptosis in vertebrates is inherently more complex, central events such as the anti-apoptotic activity of CED-9/Bcl2 and CED-3/caspase activation by CED-4/Apaf-1 are maintained. Because of the conservation of core death machinery, the simple anatomy and defined nervous system of *C. elegans* make it a useful organism for studies of how cellular injury activates neuron death pathways.

Apoptosis in *C. elegans*

In *C. elegans*, 131 of 1090 somatic cells reproducibly die by apoptosis during development (Dong et al. 2009) and 80% of these cells are derived from neuronal lineages (Putcha & E. M. Johnson 2004). Apoptotic cells show a raised button-like morphology and are readily distinguished by differential interference contrast (DIC) microscopy (Ellis & Horvitz 1986). In this genetically programmed pathway (Fig. 1.3), an apoptotic signal stimulates transcriptional upregulation of EGL-1, a BH3-only protein (Conradt & Horvitz 1998; Thellmann et al. 2003). EGL-1 binds to CED-9, a Bcl-2 family member that normally sequesters CED-4/Apaf-1 at the outer mitochondrial membrane. The EGL-1-CED-9 interaction releases CED-4 to aggregate as an active "apoptosome" (Yan et al. 2004). The CED-4 oligomer interacts with CED-3/caspase to trigger an intramolecular cleavage at specific sites that activates CED-3 (X. Yang et al. 1998). The resultant CED-3 caspase activity executes the apoptotic program by targeting downstream substrates for proteolytic degradation.

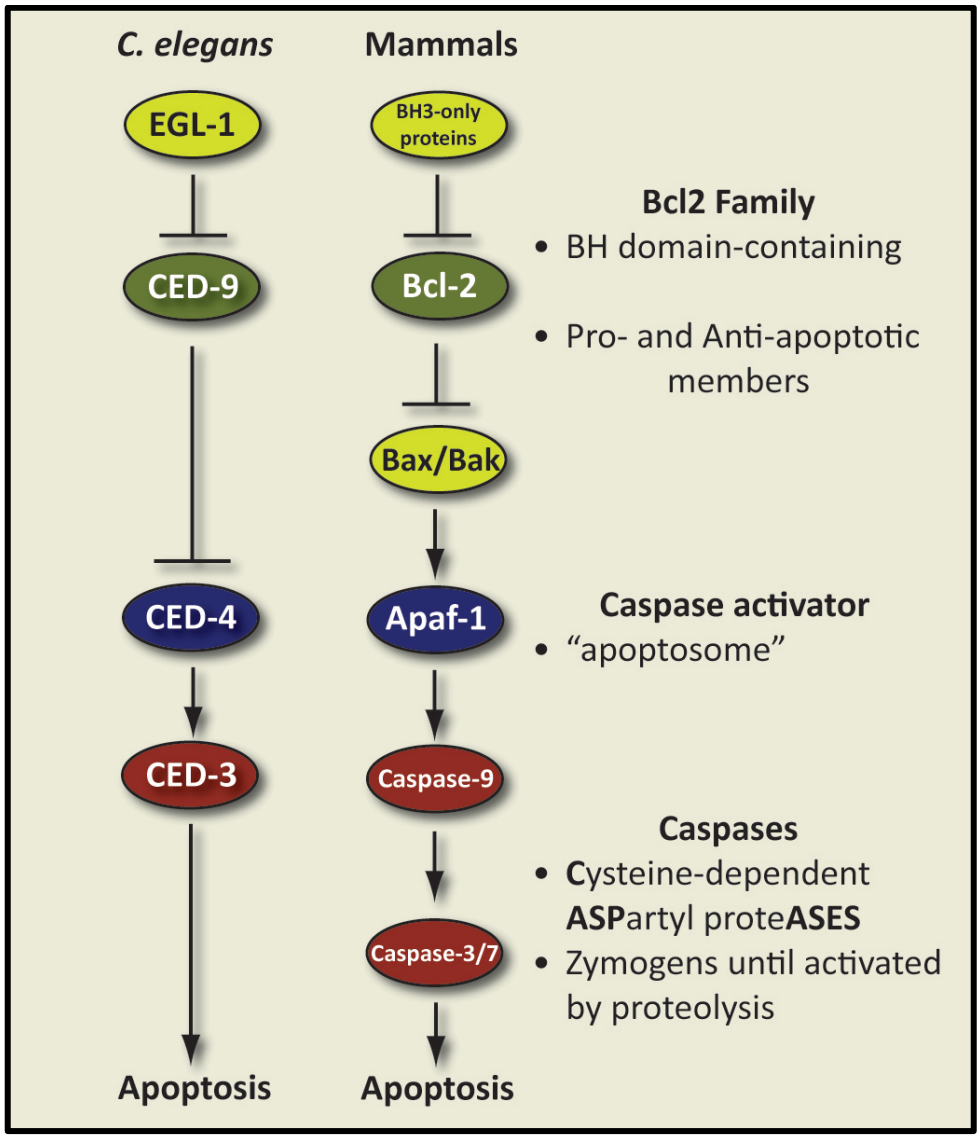

Figure 1.3: Apoptotic regulators are conserved from *C. eleagns* to mammals. Programmed cell death in *C. elegans* is regulated by four core components that have clear mammalian homologues: EGL-1/BH3-only, CED-9/Bcl2, CED-4/Apaf-1, CED-3/caspase. Additionally, the cascade of apoptotic events is also conserved between *C. elegans* and mammals: BH3-only proteins inhibit the anti-apoptotic Bcl2 regulator leading to Apaf-1-dependent activation of caspases. Adapted from (Yi & Yuan 2009).

This genetically programmed pathway is widely studied in developmental contexts but stress-induced apoptosis has also been observed. DNA damage-induced germ cell apoptosis requires the core apoptotic machinery (Fig. 1.3) and is regulated by CEP-1, the p53 tumor suppressor homologue (Gartner et al. 2008). Additionally, in a *C. elegans* model of Huntington's disease, loss-of-function mutations in *ced-3*/caspase prevented neuronal cell death (Faber et al. 1999). The existence of non-programmed apoptotic deaths in the worm suggests that apoptotic machinery responds to both developmental and stress-related cues to facilitate cell death execution.

Necrosis

Necrotic cell death is morphologically distinct from apoptosis and typically occurs under conditions of severe cellular injury (i.e., high levels of oxidative stress, calcium overload, drastic energy depletion). Necrotic cells exhibit prominent cellular swelling, distortion of organelles such as the mitochondria and endoplasmic reticulum, and vacuolization of the cytoplasm (Hall et al. 1997). In contrast to the tightly regulated mechanism of apoptosis, necrosis (i.e., Type III death) was initially regarded as a chaotic, uncontrollable process. However, recent studies reveal that inhibition of key proteolytic events prevents necrosis, thus paralleling the pivotal enzymatic regulation of the apoptotic program.

The "Calpain-Cathepsin Hypothesis" originated with studies of ischemia in mammals (Yamashima 2000) and involves the activation of two proteolytic families (calpains and cathepsins) to execute necrotic cell death. In this model (Fig. 1.4), necrotic stimuli trigger increased intracellular calcium that then activates calcium-dependent calpain proteases. Calpain activation leads to lysosomal membrane permeabilization (LMP) and the consequent release of harmful cathepsin proteases into the cytosol. Robust proteolysis by the combined effects of activated calpains and

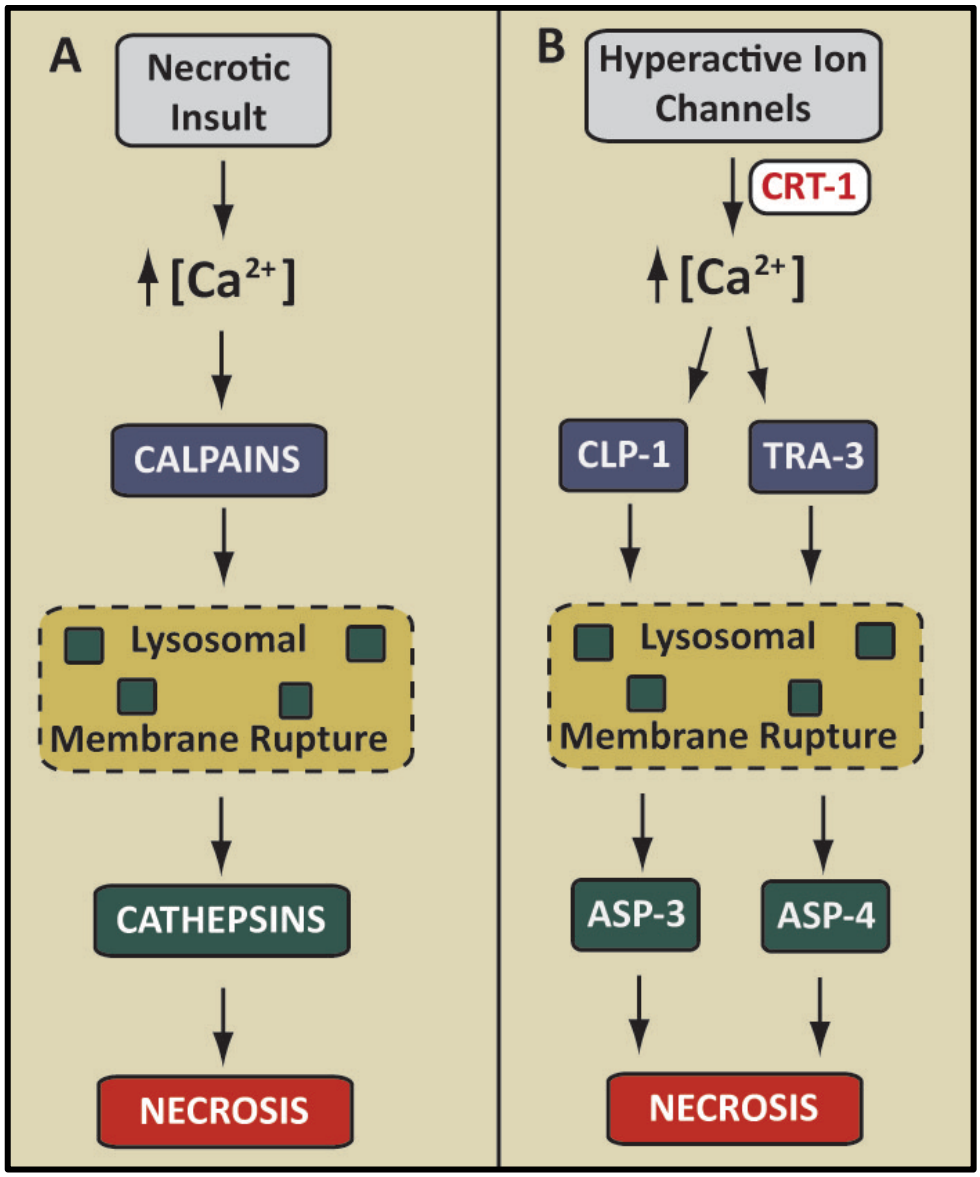

Figure 1.4: Necrotic events are conserved in *C. elegans*. A. According to the "Calpain-Cathepsin Hypothesis," necrosis-initiating insults stimulate a rise in intracellular calcium that activates a family of calcium-dependent proteases (calpains). Activated calpains trigger lysosomal membrane permeabilization and rupture that releases harmful cathepsin proteases into the cytosol. This proteolytic cascade leads to necrotic cell death. **B.** Key events in this pathway are conserved in *C. elegans.* Hyperactive ion channels stimulate a CRT-1/calreticulin-dependent increase in cytosolic calcium levels. Two calpain proteases (CLP-1 and TRA-3) are activated and lead to the subsequent release of two cathepsin proteases (ASP-3 and ASP-4) from the lysosome. Genetic inhibition of these proteins inhibits necrosis in *C. elegans*.

cathepsins results in necrotic cellular demise. As is also the case for apoptosis, key events in necrotic pathway are conserved in *C. elegans*.

Necrosis in *C. elegans*

Mutations that result in constitutive cation channel activity have been shown to trigger necrotic cell death in *C. elegans* (Syntichaki et al. 2002). As was previously reported for necrotic cell death in mammals, necrosis in *C. elegans* requires elevated intracellular calcium that activates a series of proteases ultimately leading to cell destruction (Xu et al. 2001). Specific members of the calpain (CLP-1, TRA-3) and cathepsin (ASP-3, ASP-4) protease families are required for necrotic cell death (**Fig. 1.4)** (Syntichaki et al. 2002) in this pathway. These proteases promote necrotic death initiated by several mechanisms, including hyperactive ion channels (i.e., degenerin channels *deg-1* and *mec-4,* acetylcholine receptor channel subunit *deg-3*, and the G_s protein α-subunit *gsa-1* (Syntichaki et al. 2002)) and by ectopic expression of Hepatitis B virus X protein (Geng et al. 2012). Alternatively, SRP-6 (an intracellular serpin that inhibits cysteine peptidases) protects against intestinal necrotic death in a pathway requires TRA-3 and ASP-3 but not CLP-1 or ASP-4 (Luke et al. 2007). Furthermore, additional calpain and cathepsins that do not control hyperactive ion channel-mediated necrosis (i.e., W05G11.4 and ASP-1) were also identified in the SRP-6 pathway. This result suggests that members of these protease families respond differently to necrotic signals, depending on the cellular context (i.e., cell type, necrotic stimulus).

Intermediate cell death pathways

Despite the wealth of literature describing apoptosis and necrosis as two distinct, mutually exclusive forms of cell death, recent studies have revealed extensive cross talk between these two pathways. “Aponecrosis” is one such alternative form of cell death that shares morphological

features of apoptosis (i.e., nuclear chromatin fragmentation) and necrosis (i.e., mitochondrial swelling, translucent cytoplasm, and plasma membrane rupture) (Formigli et al. 2000). Additionally, common molecular mechanisms have been connected to both apoptosis and necrosis (Brennan & Cookson 2000; Wang et al. 2003). For example, the apoptotic components caspase-8 and Bid (a Bcl-2 family member) regulate necrotic cell death resulting from oxidative stress (Brennan & Cookson 2000; Wang et al. 2003). Another shared regulator of these two forms of cell death is the mitochondrion, as release of mitochondrial factors into the cytosol is implicated in both apoptosis and necrosis (Galluzzi et al. 2007). This finding suggests that the cellular response to mitochondrial dysfunction may activate either of these pathways or specific elements of both.

Mitochondria in cell death

A role for mitochondria in mammalian cell death is well-established. Mitochondrial membrane permeabilization (MMP) is linked to both apoptosis and necrosis, with two mechanisms that can cause MMP (Kroemer et al. 2007). For apoptosis, mitochondrial outer membrane permeabilization (MOMP) mediated by pro-apoptotic Bcl-2 family members form a protein-permeable pore that releases factors such as cytochrome c (X. Liu et al. 1996) and DIABLO/Smac (Du et al. 2000), which stimulate caspase activation. Additionally, MMP can occur with the opening of the mitochondrial permeability transition pore (PTP) (Galluzzi et al. 2010). PTP is a multisubunit structure spanning from the mitochondrial matrix to the outer mitochondrial membrane. The precise composition is unclear but three components have been identified: the voltage-gated anion channel (VDAC), the adenine nucleotide translocase (ANT) and cyclophilin D (CypD). Following pore opening, mitochondrial membrane potential drops and osmotic swelling occurs as solutes enter the mitochondria. Ultimately, outer mitochondrial membrane breakdown leads to release of mitochondrial contents into the cytosol. Since energy collapse (due to loss mitochondrial membrane

potential) and release of apoptogenic factors both occur with PTP opening, the cell can undergo necrosis or apoptosis. Inhibition of permeability transition pore opening can block both types of cell death (Roy et al. 2006). The key role of the mitochondrion in cell death mechanisms might explain why dysfunction of this organelle is so tightly correlated with neurodegenerative diseases.

Unlike mammalian systems in which mitochondria have been closely linked to cell death mechanisms, evidence of mitochondrial death regulation in *C. elegans* is controversial. Homologs of mammalian Endonuclease G (EndoG/*csp-6*) and Apoptosis Inducing Factor (AIF/*wah-1*) contribute to apoptotic death by mediating DNA degradation and phosphatidyl serine exposure, respectively (Parrish et al. 2001; Wang et al. 2007). A recent study identified a specific interaction between CED-4/Apaf-1 and a member of the adenine nucleotide translocase (ANT) family, *wan-1*, that serves as a key regulator of programmed cell death in *C. elegans* (Q. Shen et al. 2009). ANT is a core component of the mitochondrial permeability transition pore (MPTP) whose opening releases death-promoting factors in mammals (Kroemer et al. 2007). This finding supports the hypothesis that mitochondria also serve as important regulators of cell death in the nematode.

Further evidence for the role of mitochondrial dysfunction in cell death is provided by the observation that excessive mitochondrial fission (i.e., fragmentation) is an early event in apoptosis that precedes caspase activation. Mitochondria normally divide and fuse to meet the cell's changing energy demands (Knott et al. 2008; Knott & Bossy-Wetzel 2008). An imbalance in the fission/fusion cycle has been implicated in various neurodegenerative diseases (Knott & Bossy-Wetzel 2008). Drp1 is a conserved large GTPase that is essential in the regulation of mitochondrial fission (Bossy-Wetzel et al. 2003). In mammals, overexpression of Drp1 initiates apoptosis and expression of a dominant-negative Drp1 can prevent apoptotic cell death (Shani et al. 2001). A Drp1-mediated necrotic cell death pathway has also been identified (Bras et al. 2007). These findings suggest that changes in mitochondrial morphology may be linked with the execution of cell death.

An integrated model of necrosis and apoptosis

The shared features of pathways leading to both apoptosis and necrosis are suggestive of the idea of a continuum of cell death signals can lead to either outcome (Fig. 1.5) (Yakovlev & Faden 2004). In this model, cellular damage such as oxidative stress or impaired calcium homeostasis is in a balance with ATP levels to dictate whether an injured cell undergoes apoptosis or necrosis. For example, mild cellular damage provides a cell-killing signal that is transduced by an energy-dependent apoptotic program. Conversely, severe intracellular damage coupled with a sharp decrease in cellular ATP levels triggers a necrotic death pathway. This continuum explains how similar cellular insults, depending on severity, can activate necrotic or apoptotic pathways and may also explain how common upstream regulators (i.e., Bcl2 family, caspase, calpains) can promote either an apoptotic or necrotic response.

Interestingly, CED-9/Bcl2 was recently identified as a key regulator of Hepatitis B virus X (HBx)-induced cell death in *C. elegans* (Geng et al. 2012). Ectopic expression of HBx triggers apoptotic and necrotic death, both of which rely on CED-9 function. CED-9-dependent apoptosis occurs through the canonical pathway (i.e., CED-4 release and CED-3 activation, Fig. 1.3), whereas CED-9-dependent necrosis requires mitochondrial permeability transition (MPT) to increase Ca^{2+} levels and activate necrotic proteases (i.e., TRA-3, CLP-1, ASP-3, ASP-4, Fig. 1.4). The dual function of CED-9 in *C. elegans* is suggestive of an evolutionarily ancient link between key cell killing functions and alternative cell death pathways.

It is clear that mitochondrial dysfunction plays a key role in cell death mechanisms; however, less is known about how dysfunction of this organelle results in the degeneration of specific types of neurons. Hallmarks of aging and vulnerable neurons, such as increased oxidative stress, impaired calcium homeostasis, and disrupted energy metabolism, are also associated with mitochondrial dysfunction and ultimately trigger apoptotic or necrotic cell death. Cells have

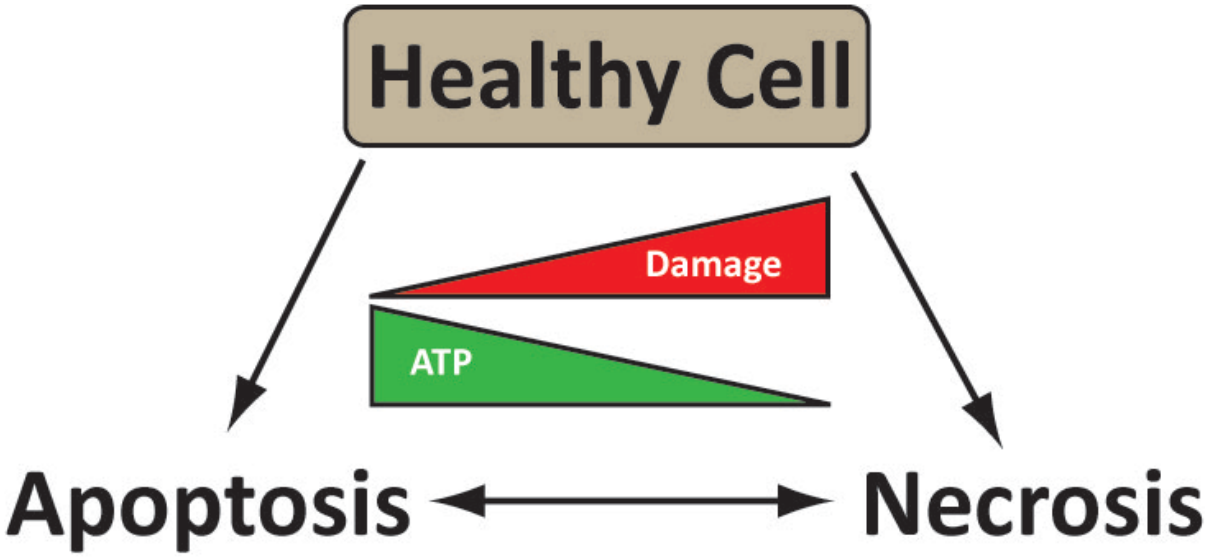

Figure 1.5: Common insults account for a cell death continuum between apoptosis and necrosis. Mild cellular damage coupled with abundant ATP levels allows cells to expend the energy required for apoptotic cell death. Severe damage in the absence of ATP triggers a necrotic death pathway that occurs through an energy-independent mechanism. Intermediate levels of damage and ATP can lead to cell death that shares features of both apoptosis and necrosis.

numerous adaptive mechanisms that defend against stress-induced cell death. The next section highlights one of these protective molecules, Coenzyme Q.

Coenzyme Q is important for cellular homeostasis and viability

Coenzyme Q (CoQ) is a highly conserved lipophilic molecule present in all tissues, cells and membranes (Turunen et al. 2004). CoQ primarily functions as an electron carrier in the ATP-producing mitochondrial oxidative respiratory chain (Fig 1.2) (Crane et al. 1957), but other roles for this fat-soluble molecule have been described, including electron transfer for plasma and lysosomal membranes (I. L. Sun et al. 1992; Nohl & Gille 2001), regulation of apoptosis through the mitochondrial permeability transition pore (PTP) (Fontaine et al. 1998; Papucci et al. 2003; Devun et al. 2010; Sahach et al. 2007), and as a membrane antioxidant (Navas et al. 2002). The variety of these CoQ-dependent cellular processes highlights the importance of biosynthesis, maintenance and distribution of this vitamin-like quinone.

Coenzyme Q functions

Coenzyme Q has a prominent role in the mitochondria where it shuttles electrons from Complexes I and II to Complex III in the electron transport chain (ETC) (Crane et al. 1957) (Fig. 1.2). Coenzyme Q is therefore essential for ATP production. In addition, the close association of CoQ with the free radical-generating ETC likely accounts for its key antioxidant role to prevent oxidative mitochondrial overload. CoQ also has energy coupling roles in lysosomal acidification (Gille & Nohl 2000) and plasma membrane Na^+/H^+ exchange (Crane 2001). Furthermore, as the only endogenously synthesized lipid-soluble antioxidant (Ernster & Dallner 1995), Coenzyme Q is essential for protecting against free radical damage in cellular membranes. Interestingly, studies have shown that Coenzyme Q prevents apoptotic death by preventing mitochondrial permeability

transition pore (PTP) opening (Fontaine et al. 1998; Papucci et al. 2003; Devun et al. 2010; Sahach et al. 2007). These diverse roles of Coenzyme Q are indicative of a key regulator that protects against cell death, either by direct (i.e., PTP inhibition) or indirect (i.e.,. ATP production, ROS reduction) mechanisms.

Coenzyme Q biosynthesis

Coenzyme Q biosynthesis requires at least nine genes (Coq1-Coq9) that are conserved from yeast to humans (Fig. 1.6) (Tran & Clarke 2007). These nuclear genes encode proteins with both catalytic (Coq1, Coq2, Coq3, Coq5, Coq6, Coq7/Clk1) and regulatory functions (Coq4, Coq8, Coq9), and most of these proteins are predicted to form a multisubunit complex in the mitochondria (Tran & Clarke 2007). CoQ structure is conserved among species, with the exception of length of the isoprene tail (Table 1.1), which ranges from CoQ_6 (*S. cerevisiae*) to CoQ_{10} (humans). The polyprenyl diphosphate synthase (COQ-1 enzyme) determines the length of this tail and thus dictates the CoQ isoform synthesized in each organism (Okada et al. 1996; K et al. 1997). Many biological functions of Coenzyme Q are correlated with its molecular structure: the lipid-soluble isoprene tail anchors CoQ in cellular membranes and the benzoquinone ring accounts for its redox properties (Fig. 1.6A).

Table 1.1: Isoprene tail length of Coenzyme Q varies among species. The COQ1 gene encodes polyprenyl diphosphate synthase that determines species-specific isoprene tail length (Tran & Clarke 2007).

Species	Coenzyme Q Isoform
S. cerevisiae	CoQ_6
E. coli	CoQ_8
C. elegans	CoQ_9
S. pombe	CoQ_{10}
M. musculus	CoQ_9
H. sapiens	CoQ_{10}

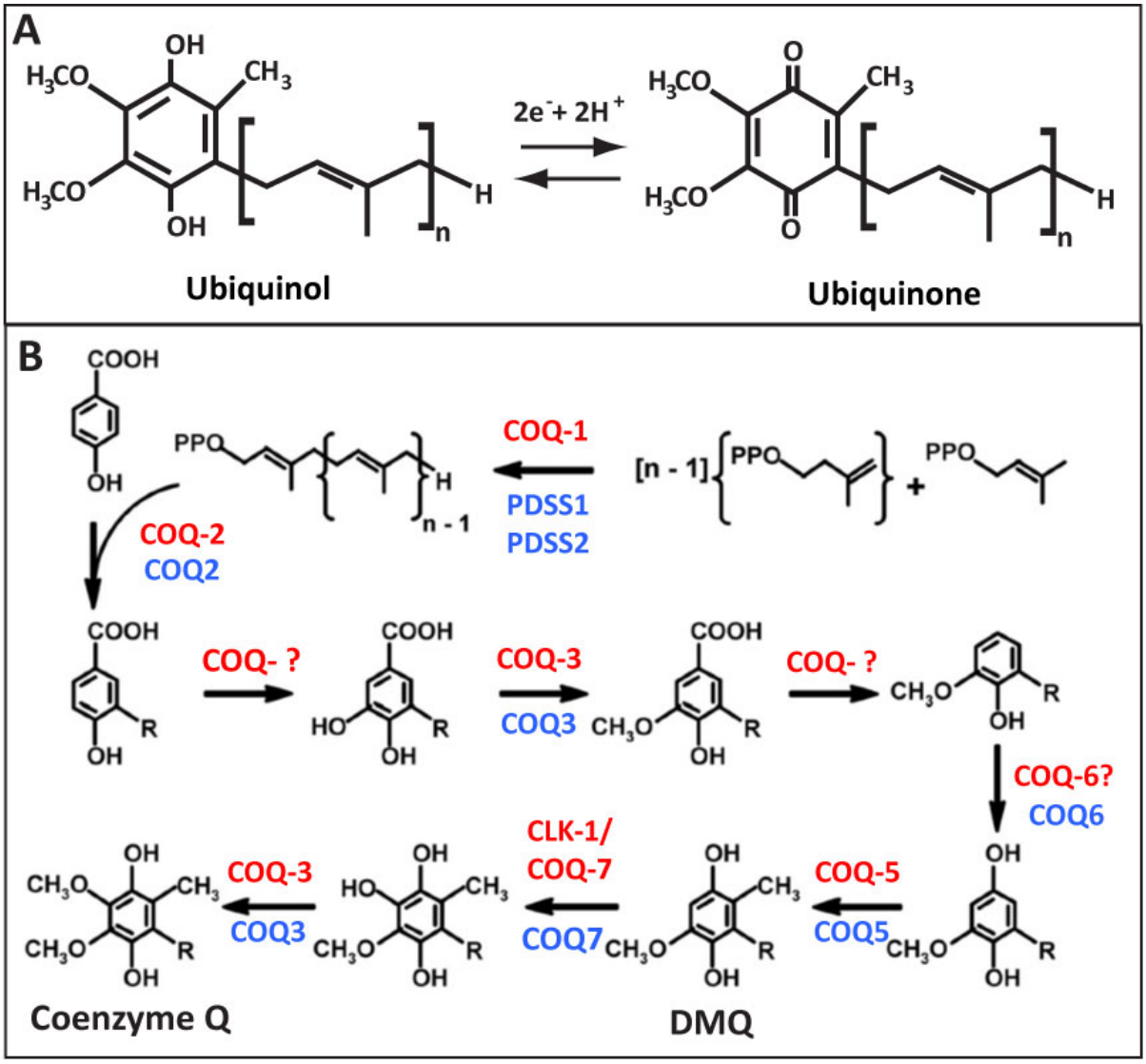

Figure 1.6: Coenzyme Q and its biosynthetic proteins are highly conserved. A. Coenzyme Q is a redox molecule that switches between reduced (ubiquinol/CoQ_{RED}) and oxidized (ubiquinone/ CoQ_{OX}) states. The number of isoprene units (n) varies among species (Table 1.1). **B.** The CoQ biosynthetic pathway with enzymes at each step indicated (*C. elegans* in red, *H. sapiens* in blue). DMQ = demethoxy ubiquinone. Panel B is adapted from Tran and Clarke *Mitochondrion* 2007 (Tran & Clarke 2007; Beal 2005; Metzstein et al. 1998).

Coenzyme Q deficiencies

Coenzyme Q deficiency is a rare, autosomal recessive mitochondrial syndrome that is both clinically and genetically heterogeneous (Emmanuele et al. 2012). The most common clinical presentations are myopathy (Horvath et al. 2006) and the neurological motor disorder, cerebellar ataxia (Emmanuele et al. 2012). This neuromuscular pathology is likely due to mitochondrial dysfunction, as ETC activity is significantly reduced in patients with CoQ deficiency (Nohl & Gille 2001; Catarina M Quinzii 2007; Canevari et al. 1999; Ellis & Horvitz 1986).

There are two types of Coenzyme Q deficiency, primary and secondary. Primary CoQ deficiency results from mutations in Coenzyme Q biosynthetic genes (Fig. 1.6). Patients with mutations in PDSS1 (Mollet et al. 2007), PDSS2 (López et al. 2006), COQ2 (Mollet et al. 2007; Jakobs et al. 2013; Quinzii et al. 2006; Diomedi-Camassei et al. 2007), COQ6 (Heeringa et al. 2011), ADCK3/CABC1 (Mollet et al. 2008), COQ9 (Andrew J Duncan 2009) have been identified. A reduction of CoQ levels that is not attributed directly to mutations in the Coenzyme Q biosynthetic pathway is known as secondary Coenzyme Q deficiency. The mechanism of how these defects impact CoQ levels is not well-understood. For example, a mutation in the electron-transferring-flavoprotein dehydrogenase (ETFDH) gene is linked to secondary CoQ deficiency (Gempel et al. 2007). Because ETFDH directly transfers electrons to CoQ, it is postulated that impaired ETFDH function either causes down-regulation or degradation of Coenzyme Q. Other mutations associated with secondary CoQ deficiency, such as the DNA repair gene aprataxin (APTX), do not have a clear relationship to CoQ homeostasis (Quinzii et al. 2005). The heterogeneity of clinical presentations of CoQ deficiency is likely due to both the diverse cellular functions of Coenzyme Q as well the variety of mutations linked to the disease.

Coenzyme Q supplementation

Coenzyme Q deficiency is the only treatable mitochondrial disorder; early CoQ_{10} supplementation shows significant improvement of clinical symptoms (Rötig et al. 2000; Montini et al. 2008). The rationale for CoQ supplementation in CoQ deficiency is clear and its potent antioxidant properties make it a reasonable therapeutic candidate for administration during neurodegenerative diseases, which are tightly linked to both oxidative stress and mitochondrial dysfunction. Additionally, increased levels of oxidized CoQ_{10} was detected in Amyotrophic Lateral Sclerosis (ALS) patients and is strongly correlated with disease progression (Sohmiya et al. 2005). Decreased Coenzyme Q levels are reported in Parkinson's Disease patients (Hargreaves et al. 2008) and normal declines in CoQ levels also occur with aging (Kalén et al. 1989). Animal neurodegeneration models show neuroprotective effects of Coenzyme Q administration in affected brain regions (Matthews et al. 1998; Ferrante et al. 2002). Despite success in murine models, clinical supplementation of CoQ_{10} in neurodegenerative diseases has produced mixed outcomes (Galpern & Cudkowicz 2007). The lack of significant neuronal improvement might be due to poor bioavailability of Coenzyme Q and its difficulty crossing the blood-brain barrier (Mancuso et al. 2009). Nevertheless, the positive impact of CoQ_{10} supplementation on CoQ deficiency patients implicates the existence of active mechanisms of distributing this lipophilic molecule to deficient tissues and subcellular compartments.

Currently, the process of exogenous CoQ incorporation into cells is not well understood. Limited information about this mechanism indicates that the endomembrane system is required for CoQ uptake and intracellular distribution (Padilla-López et al. 2009; Fernández-Ayala et al. 2005). My work in **Chapter 3** discusses observations in *C. elegans* that support a model of intercellular CoQ transport between tissues. This experimental paradigm could provide a useful genetic tool for an

unbiased approach to identify regulators of CoQ transport. An enhanced understanding of this process may help develop more effective CoQ treatment strategies.

Models of Coenzyme Q deficiency

Genes in the Coenzyme Q biosynthetic pathway were initially discovered as *S. cerevisiae* mutants with impaired respiration (Tran & Clarke 2007). Strong sequence homology indicates that these genes are highly conserved in aerobic organisms. Characterization of corresponding proteins in single-cell systems significantly advanced our understanding of biochemical function during Coenzyme Q synthesis (Tran & Clarke 2007). However, analysis of CoQ deficiency in multicellular organisms is needed to understand the tissue-specific effects of CoQ depletion.

Two *Drosophila* CoQ biosynthetic pathway mutants have been characterized. A mutation in the COQ2 homologue, *small boy (sbo),* results in larval arrest but the authors did not investigate neuronal or muscular defects (J. Liu et al. 2011). A missense mutation in *qless,* the human PDSS1 orthologue (Fig. 1.6), results in embryonic lethality accompanied with neuroblast growth defects (Grant et al. 2010). The central nervous system (CNS) of *qless* larvae showed signs of mitochondrial stress and caspase activation, and expression of the pan-caspase inhibitor p35 was sufficient to rescue neuroblast clonal growth in *qless* mutants. This result demonstrates death-promoting caspases likely contribute to neuron inviability in CoQ-deficient animals.

Vertebrate models of CoQ deficiency primarily exist in mice and include reports of loss-of-function Pdss2 (Peng et al. 2008; Saiki, Lunceford, Shi, et al. 2008b), COQ7 (Nakai et al. 2001; Levavasseur et al. 2001) and COQ9 (Garcia-Corzo et al. 2012) genes (Fig. 1.6). A spontaneous missense mutation in Pdss2 results in renal dysfunction (Peng et al. 2008). Interestingly, liver-specific conditional knockout of Pdss2 did not develop an overt phenotype while knockouts targeted

to podocytes caused renal disease. This finding is suggestive of tissue-specific metabolic requirements for Coenzyme Q that are revealed under deficiency conditions.

A role of Coenzyme Q in *C. elegans* was initially suggested by studies of mutations in *coq-7/clk-1* mutants. COQ-7/CLK-1 is a hydroxylase that modifies the quinone ring at a step late in the CoQ synthesis pathway (Fig. 1.6). Impaired COQ-7/CLK-1 function causes accumulation of a CoQ intermediate, demethoxy-CoQ (DMQ). Additionally, *clk-1/coq-7* mutants live longer than wild-type animals (Larsen & Clarke 2002). While the mechanism responsible for lifespan extension is controversial, *coq-7/clk-1* mutants have decreased mitochondrial membrane potential (Lemire et al. 2009), reduced ROS damage, and decreased mitochondrial respiration (Y.-Y. Yang et al. 2009) compared to wild-type. Notably, *coq-7/clk-1* mutants still produce small amounts of CoQ_9 (Hihi et al. 2003) and the intermediate 5-demethoxylated ubiquinone (DMQ) is sufficient to permit fertility if animals also receive CoQ_8 from their *E. coli* diet (Jonassen et al. 2001). The DMQ intermediate that accumulates partially supports respiration but does not substitute for CoQ in non-mitochondrial sites (Arroyo et al. 2006; Hihi et al. 2002), where exogenous CoQ is necessary for viability. These findings suggest that dietary CoQ can be functionally incorporated in *C. elegans* CoQ-deficiency mutants.

Studies describing other Coenzyme Q biosynthetic mutants are limited, likely due to the lethality that accompanies these genetic knockouts (Gavilan et al. 2005). Developmental and sterility defects are reported phenotypes of *coq-3* (Gomez et al. 2012) and *coq-8* mutants (Asencio et al. 2009). The viability of *coq-7/clk-1* animals compared to other CoQ knockouts suggests that these mutants represent varying degrees of Coenzyme Q deficiency. Indeed, lifespan extension occurs with moderate levels of CoQ depletion (< 50%) (as in *coq-7/clk-1* mutants (Larsen & Clarke 2002)) but is not supported by severe CoQ depletion (as reported for *coq-3* (Hihi et al. 2002) and *coq-8*

mutants (Asencio et al. 2009)). These results are supportive of a model in which distinct Coenzyme Q levels regulate diverse processes including development, fertility and lifespan.

Interestingly, unlike Coenzyme Q pathway mutants in other organisms that invariably result in early lethality (J. Liu et al. 2011; Grant et al. 2010; Peng et al. 2004; Peng et al. 2008; Nakai et al. 2001; Levavasseur et al. 2001; Garcia-Corzo et al. 2012), some loss-of-function *C. elegans* CoQ pathway mutants animals reach adulthood (Gavilan et al. 2005; Gomez et al. 2012; Asencio et al. 2009). This developmental progression is attributed both to maternally supplied mRNA and/or Coenzyme Q as well as CoQ_8 obtained from the *E. coli* diet. In any case, the availability of an adult Coenzyme Q-deficient population is useful for experimental studies of the potential role of mitochondrial function in neurological disease.

Coenzyme Q deficiency in *C. elegans* as a model for neurodegenerative disease

The common features of neurodegenerative diseases such as age-dependent onset, selective neuronal vulnerability and mitochondrial dysfunction-associated pathogenesis suggest that shared pathways regulate these clinically distinct disorders. To understand mechanisms that underlie mitochondrial dysfunction-associated neuronal degeneration, we developed a Coenzyme Q deficiency model of neurodegeneration in *C. elegans*. This model parallels hallmarks of human neurodegeneration, with an age-related and selective degeneration of GABA motor neurons arising from deficiency of CoQ (an essential mitochondrial component). GABA neurons produce Gamma-Aminobutryic Acid (GABA), the main inhibitory neurotransmitter in the nervous system. Based on the observation that GABA neurons (Fig. 1.7) are the most sensitive neuronal population to reduced CoQ levels, I focused my studies on characterizing the cell death pathway activated in GABA neurons that leads to their selective degeneration (**Chapters 2, 4, 5**). A candidate gene approach identified distinct components of apoptotic (**Chapter 2** and **Chapter 4**) and necrotic (**Chapter 2** and **Chapter 5**)

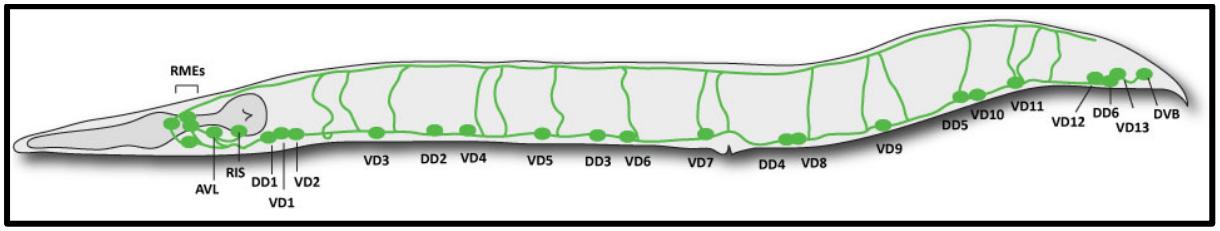

Figure 1.7 *C. elegans* GABA nervous system. Schematic depicts adult hermaphrodite, anterior left, ventral down. 26 GABA neurons control movement (D-type motor neurons: 6 DD, 13 VD), head foraging (4 RME motor neurons) or defecation (AVL and DVB motor neurons). Adapted from (Schuske et al. 2004)

pathways that adopt both killing and neuroprotective roles in CoQ-deficient GABA neurons. The relevance of these studies is underscored by the functional conservation of a human CoQ biosynthetic protein through its rescue of *C. elegans* defects (**Chapter 3**).

With its simple body plan and powerful genetic tools, *C. elegans* is especially well-suited to an experimental approach that uses genetic manipulation to identify key neurodegenerative disease genes. The strong conservation of known components of *C. elegans* necrotic and apoptotic pathways suggests that the signals that deploy these processes may also provide similar functions in mammals. Thus, an understanding of the mechanisms whereby mitochondrial dysfunction initiates cell death in *C. elegans* could lead to possible therapies that prevent neurodegeneration in humans.

CHAPTER II

COENZYME Q PROTECTS CAENORHABDITIS ELEGANS GABA NEURONS FROM CALCIUM-DEPENDENT DEGENERATION

Laurie R. Earls [a,1,2], Mallory L. Hacker [a,1], Joseph D. Watson [a,b,3], David M. Miller III [a,b]

[1] L.R.E and M.L.H contributed equally to this paper

[a] Department of Cell and Developmental Biology, Vanderbilt University, Nashville, TN 37232-8240

[b] Program in Neuroscience, Vanderbilt University, Nashville, TN 37232-8240

Present addresses:

[2] Department of Developmental Neurobiology, St. Jude Children's Research Hospital, Memphis, TN 38105

[3] Department of Biochemistry and Biophysics, University of North Carolina, Chapel Hill, NC 27599

This paper has been published in PNAS, 107:32, 14460-14465.

Author contributions

Laurie Earls discovered the GABA neuron selectivity with *coq-1* RNAi and identified *ced-4, crt-1* and EGTA treatment as suppressors of neurodegeneration. The suppression of degeneration by *drp-1* was first identified by combinatorial RNAi (Laurie Earls) and was later confirmed with a genetic mutant (Mallory Hacker). Joseph Watson characterized the necrotic death of *coq-1(ok749)* animals. Mallory Hacker performed all other experiments and validated the *ced-4, crt-1* and EGTA results.

INTRODUCTION

Mitochondrial dysfunction, selective neuronal vulnerability, and progressive onset are unifying features of major human neurodegenerative diseases including amyotrophic lateral sclerosis (ALS), Alzheimer's disease (AD), Parkinson's disease (PD), and Huntington's disease (HD) (Petrozzi et al. 2007). Genetic mutations linked to these diseases have been shown to disrupt the electron transport chain (ETC) (Fig. 1.2) (Lin & Beal 2006), a mitochondrial pathway that accounts for the majority of cellular energy production. Chemical inhibitors of the ETC can also produce symptoms reminiscent of neurodegenerative diseases (Brouillet et al. 1999). Despite the broad disruption of mitochondrial function in these cases, specific neuron classes are preferentially targeted. The molecular basis for this selectivity is largely unknown (Bossy-Wetzel et al. 2008).

The key role of mitochondrial fragmentation in both necrosis and apoptosis (Young et al. 2010) parallels emerging evidence that excessive mitochondrial fission may contribute to neurodegenerative disease (Knott et al. 2008). Inhibition of the fission-promoting dynamin GTPase, Drp-1, for example, blocks mitochondrial fragmentation and death induced by overexpression of the mutant Huntingtin protein (mtHtt) in cultured cells (Wang et al. 2008). The progressive onset of these diseases is correlated with an age-dependent decline in mitochondrial function, but the mechanistic link between diminished mitochondrial activity and neurodegeneration is poorly understood.

Although the cell death pathways of necrosis and apoptosis feature distinct biochemical and morphological components, recent studies have revealed “aponecrotic” cell killing pathways that include elements of both mechanisms (Formigli et al. 2000). Additionally, apoptosis and necrosis share common molecular triggers, such as oxidative stress and energy depletion, two hallmarks of mitochondrial dysfunction (Wochna et al. 2007; Zhang et al. 2009). These findings suggest that

apoptotic and necrotic pathways may represent related cell death responses and can be activated by mitochondrial impairment.

Coenzyme Q (CoQ) transfers electrons from complexes I and II to complex III in the mitochondrial ETC (Fig. 1.2) and fulfills a critical role in mitochondrial ATP production (Crane et al. 1957). CoQ also limits the production of reactive oxygen species that can damage cellular processes. Human patients with CoQ deficiency exhibit diverse symptoms ranging in severity from infantile multiorgan disease (Quinzii et al. 2006; Mollet et al. 2007) to discrete late onset cerebellar ataxia (Lagier-Tourenne et al. 2008; Mollet et al. 2008). Although the essential roles of CoQ in mitochondrial energy production and cell survival are likely to account for these deficits, the molecular basis for this heterogeneity is unclear, as are the specific cellular pathologies arising from CoQ deficiency (DiMauro et al. 2007).

We developed a model of CoQ deficiency for the purpose of delineating the molecular events that contribute to cell death arising from mitochondrial dysfunction. Because of its short life span, anatomic simplicity, and genetic tractability, the nematode *Caenorhabditis elegans* is particularly amenable to this approach. We used RNA interference (RNAi) and genetic ablation to knock down genes in the CoQ synthesis pathway (Fig. 1.6) (*coq-1*, *coq-2, coq-3*) to mimic CoQ deficiency. These treatments result in age-dependent loss of motor coordination that is correlated with progressive degeneration of GABA neurons (Fig. 1.7). Our results show that CoQ deficiency in *C. elegans* results in a selective cell death pathway that includes features of both apoptotic and necrotic processes and, therefore, suggest that this experimental model may be useful for delineating the mechanism of neuron cell death in human CoQ deficiency and in related neurodegenerative diseases that are also linked to defective mitochondrial function.

MATERIALS AND METHODS

Strains and Maintenance

C. elegans mutants and strains used in this chapter are listed in Table 2.1 and Table 2.2, respectively. Strains were maintained at 20°C unless otherwise indicated (Brenner 1974). GFP reporters and the *ced-3(n717), ced-4(n1162), crt-1(bz30),* and *drp-1(tm1108)* mutant alleles were crossed into the RNAi-hypersensitive strain *eri-1(mg366).* The *unc-25::mCherry* was generated by bombardment (Praitis et al. 2001) with the plasmid pMLH41 [*punc-25::mCherry, unc-119(+)*] (see Molecular Biology).

RNAi

RNAi assays were performed by feeding (Kamath et al. 2003). Briefly, 3 mL of LB/ampicillin (50 mg/mL) was inoculated with 30 µL of overnight culture and grown in a 37 °C shaker. At OD_{600} ≈ 0.800, the culture was diluted to 6 mL with LB/amp + IPTG (40 mM final concentration) and incubated at 37 °C for another 4 h. Bacteria were pelleted, dispersed in 250 mL of M9/IPTG, and spread onto 60-mm NGM plates. L4 larvae were added to plates and incubated at 20 °C for 5 d before scoring progeny. RNAi clones were sequenced to confirm inserts. EGTA (0.5 mM) was added to media before pouring plates.

Combinatorial RNAi

Cultures for combinatorial RNAi experiments (i.e., *coq-1 + drp-1, coq-1 + kap-1, coq-1 + fzo-1*) were grown separately and then mixed before plating. *kap-1* is an unrelated gene that has no visible phenotype by RNAi and was used as a control for potential competitive effects of combining two RNAi constructs (Fig. 2.9).

Table 2.1. Mutant alleles (or transgenic arrays), their source, and genotyping primers that were used in this chapter.

Mutant	Source	Genotyping Primers	Reference
ced-3 (n717) IV	CGC	AGACTTTGCCAAACACGAATCA	(Yuan et al. 1993)
		TCAGCAGCTCAACAACATCC	
ced-4 (n1162) III	CGC	TCATCCACGACTTTGAACCA	(Yuan & Horvitz 1992)
		GCAAGCGTCACGAAATATCA	
ced-9 (n1950gf) III	CGC	CGGACAACTCGCTGACGAAT	(Hengartner & Horvitz 1994)
		TTCCTTCCAGTTGTTGCGGA	
coq-1 (ok749) I	CGC	AAAAATGTTACGGCCGACTG	(Gavilan et al. 2005)
		CGTGTCCCTCAAAATGACCT	
		AGTCAGTGCTCGTCGGAGAT	
coq-2 (ok1066) III	CGC	ATGCACATGGAGCATAGCAATG	(Gavilan et al. 2005)
		GCGTGGTTTCACACAGATACAA	
coq-3(ok506) IV	CGC	GCTGTAAGGGAGATTTTCCCAT	(Gomez et al. 2012)
		ACGGCGAGCAAAATAGGGAAAT	
crt-1(bz30) V	CGC	ACGTTATCCTTAACTACAAGGG	(Xu et al. 2001)
		CCAGCTTTCATAAGAGTAGAGT	
drp-1(tm1108) IV	Ding Xue	CCGGAAAGTCTTCAGTGCTC	(Breckenridge et al. 2008)
		CTGGTACGAAAAGAGCTGGC	
eri-1 (mg366) IV	CGC	CATGCAATTTCAATGCCTTTTA	(Kennedy et al. 2004)
		TGCATCATCCAATCCACTATGT	
egl-1 (n1084 n3082) V	CGC	CCGATTAGTCGTATTCTAACTTC	(Conradt & Horvitz 1998)
		TCATGGTACAAATTGGAGAAAAGT	
egl-1(ok1418) V	CGC	GTCTGTGACGTCACATGAGGTT	N/A
		GCTTGCCTTGTGCCTTCGCCTG	
eri-1(mg366) IV	CGC	CATGCAATTTCAATGCCTTTTA	(Kennedy et al. 2004)
		TGCATCATCCAATCCACTATGT	
Transgene	**Source**	**Array**	**Reference**
juIs76 II	CGC	*punc-25::GFP, lin-15(+)*	(Jin et al. 1999)
hT2 (I;III)	CGC	*bli-4(e937) let(q782) qIs48*	(McKim et al. 1993)
juIs14	CGC	*pacr-2::GFP, lin-15(+)*	(Hallam et al. 2000)
adI1240	CGC	*peat-4::sGFP, lin-15(+)*	(Lee et al. 1999)
stEx30	CGC	*pmyo-3::MYO-3::GFP, rol-6(d)*	(Campagnola et al. 2002)
mgIs42	CGC	*ptph-1::GFP, rol-6(d)*	(Sze et al. 2000)
pRN2003	Randy Blakely	*pdat-1::GFP*	(Nass et al. 2002)

Table 2.2: Strains generated for analysis in this study.

Strain	Genotype
NC1400	*pRN2003[pdat-1::GFP rol-6(su1006)]; juIs96 [punc-25::GFP lin-15(+)]; eri-1(mg366); lin-15B(n744*)
NC1404	*juIs14[pacr-2::GFP lin-15(+)]; eri-1(mg366); lin-15B(n744)*
NC1405	*juIs76[punc-25::GFP lin-15(+)]; eri-1(mg366);lin-15B(n744)*
NC1407	*juIs76[punc-25::GFP lin-15(+)]; ced-4(n1162); eri-1(mg366); lin-15B(n744)*
NC1420	*myo-3(st386); eri-1(mg366); lin-15B(n744); stEx30[myo-3::GFP rol-6(su1006)]*
NC1436	*adIs1240[eat-4::GFP lin-15(+)]; eri-1(mg366); lin-15B(n744)*
NC1437	*juIs76[punc-25::GFP lin-15(+)]; eri-1(mg366); crt-1(bz30); lin-15B(n744)*
NC1439	*mgIs42[tph-1::GFP rol-6(su1006)]; eri-1(mg366); lin-15B(n744)*
NC1778	*juIs76[punc-25::GFP lin-15(+)]; eri-1(mg366) drp-1(tm1108)*
NC1635	*coq-1(ok749)/dpy-5(e61); juIs14[acr-2::GFP lin-15(+)]*
NC1660	*coq-1(ok749)/dpy-5(e61); juIs76[punc-25::GFP lin-15(+)]*
NC1647	*juIs76[punc-25::GFP lin-15(+)]; eri-1(mg366) ced-3(n717)*
NC1941	*juIs76[punc-25::GFP lin-15(+)]; eri-1(mg366); egl-1(n1084n3082)*
NC1959	*juIs76[punc-25::GFP lin-15(+)]; coq-2(ok1066)/hT2*
NC1974	*juIs76[punc-25::GFP lin-15(+)]; coq-3(ok506)/nT1*
NC1993	*coq-2(ok1066)/hT2; juIs14[pacr-2::GFP lin-15(+)]*
NC1999	*juIs76[punc-25::GFP lin-15(+)]; ced-4(n1162); coq-3(ok506)/nT1*
NC2020	*coq-2(ok1066)/hT2; juIs14[pacr-2::GFP lin-15(+)]; wdEx658[punc-25::mcherry unc-119(+)]*
NC2026	*juIs76[punc-25::GFP lin-15(+)]; eri-1(mg366); egl-1(ok1418)*

Thrashing assay

Swimming assays were performed as described (Miller et al. 1996). In brief, individual worms treated with either control (empty vector, EV) or *coq-1* RNAi were placed in 60µL M9 and thrashes were counted for 2 minutes (following a 2 minute stabilization period), with an average number of thrashes per minute reported.

Neuron degeneration assays

Animals were anesthetized in 0.1% tricaine/tetramisole on 2% agar pads (McCarter et al. 1997). Percent (%) degeneration was determined by counting the number of degenerating (i.e., neurite beading) or missing (i.e., break in GFP signal) GABAergic processes (using *juIs76 [punc-25::GFP*]) between cell soma and dividing by the total number of segments. There are ten total segments that are divided as follows: DD1/VD1/VD2 -(1)- VD3 -(2)- DD2/VD4 -(3)- VD5 -(4)- DD3/VD6 -(5)- VD7 -(6)- DD4/VD8 -(7)- VD9 -(8)- DD5/VD10 -(9)- VD11 -(10)- VD12/DD6/VD13 (see Fig. 1.7). For example, if 3 VNC intervals are scored as degenerating of a total of 10 total intervals in a given animal, the percent VNC degeneration would be 3/10 or 30%. Commissures were scored similarly, with the number of degenerating commissures divided by the total number of discrete GABA neuron commissures per animal (16 total). A 63x objective on a Zeiss Axioplan microscope was used for scoring. The observer was blinded to experimental versus control samples to avoid bias. *punc-25::GFP(juIs76)* was used to mark GABA neurons for experiments with *coq-1* RNAi, *coq-1(ok749), coq-2(ok1066),* and *coq-3(ok506). punc-25::mCherry(wdEx658)* was also used to mark GABA neurons in *coq-2(ok1066)* for results shown in Fig. 2.2. *coq-3(ok506)* and *coq-3(ok506); ced-4(n1162)* animals were scored as 7 day-old adults (Fig. 2.6B). The following mutants and treatments did not perturb GABA neuron morphology: *ced-4(n1162), ced-3(n717); crt-1(bz30); drp-1(tm1108),* CoQ_{10}, 0.5 mM EGTA. GABA neuron degeneration was observed in *coq-1(ok749)* maintained at 15°C.

Cholinergic neurons marked with *pacr-2::GFP* (Hallam et al. 2000) were quantified in the same manner, and no significant degeneration was detected. Additional neuron classes were examined (Fig. 2.7), but no differences between control (empty vector) and *coq-1* RNAi knockdown animals were observed in these neurons. For GFP knockdown in reporter strains (Fig. 2.7), quantification of fluorescence in Z series of confocal optically sectioned images was done by using histogram analysis in ImageJ.

Molecular biology

unc-25 Promoter (GABA neurons)

pG2M60 (a gift from Yishi Jin) was used as template to amplify 1.8 kb of the *unc-25* promoter (GoTaq, Promega). The amplicon was inserted into a pENTR D-TOPO vector (pMLH001) using a TOPO TA reaction.

punc-25::mCherry + unc-119 minigene (pMLH41)

The *unc-25* promoter was added to pCJS53 by using 5'SphI and 3'AscI. pCJS53 already contained the *unc-119* minigene from pG2M41 (Maduro & Pilgrim 1995) that inserted into the vector backbone between 5'ApaI and 3'PacI.

ATP measurement

Crude mitochondria were isolated from lysates (Bossy-Wetzel et al. 2008; Grad et al. 2007) obtained from a mixed population of *eri-1; unc-25::GFP(juIs76)* animals treated with either empty vector (EV) or *coq-1* RNAi. A Roche Cell-Titer Glow Luminescent Cell Viability Assay kit was used to measure ATP levels with a FluorStar Optima luminometer. ATP levels were normalized to protein concentrations and represented in arbitrary units. A Bio-Rad protein assay kit was used to measure

protein concentrations in a BioRad3 spectrophotometer. Each measurement was replicated in three independent experiments.

Microscopy

Animals were imaged in a Zeiss Axioplan compound microscope with a CCD camera (ORCA I; Hamamatsu). Confocal images were obtained on a Zeiss LSM 510 confocal microscope and on a Leica TCS SP5 confocal microscope.

RESULTS

Knockdown of *coq-1* results in age-dependent loss of coordinated movement

COQ-1 catalyzes the first step in Coenzyme Q synthesis (Fig. 1.6), the assembly of the lipophillic polyisoprenoid tail (Tran & Clarke 2007). RNAi knockdown of *coq-1* is reported to induce uncoordinated (Unc) and Egg-laying defective (Egl) phenotypes, but the mechanism of these effects has not been studied (Rodríguez-Aguilera et al. 2005). We replicated this experiment, using the RNAi "feeding" method to expose an RNAi-hypersensitive strain, *eri-1(mg366)* (Kennedy et al. 2004), to bacteria expressing *coq-1* double-stranded RNA (dsRNA). Loss of motor coordination first appeared at the L4 larval stage as a kink in the normal sinusoidal wave that drives locomotion. Movement then gradually declined in adults, often culminating in paralysis (Fig. 2.1A). Quantification of movement loss with a swimming assay (Miller et al. 1996) verified the developmental progression of the Unc phenotype (Fig. 2.1B).

RNAi or genetic depletion of CoQ induces age-dependent degeneration of GABA neurons

Observation of GABA motor neurons in the ventral nerve cord (Fig. 1.7), labeled with the *unc-25::GFP* reporter (Fig. 2.2A), suggested a possible explanation for the loss in motor coordination. These GABA neurons degenerate in *coq-1* knockdown animals, and cell bodies, viewed under differential interference contrast (DIC), demonstrated the swollen appearance characteristic of necrotic cell death (Fig. 2.2C). GABAergic processes in the ventral nerve cord, circumferential commissures and GABAergic processes in the dorsal cord appear discontinuous with apparent breaks (Fig. 2.2B). These morphological defects first appeared in late larval development and progressed as animals aged (Fig. 2.2D), thereby mirroring the age-dependent pattern of the Unc phenotype.

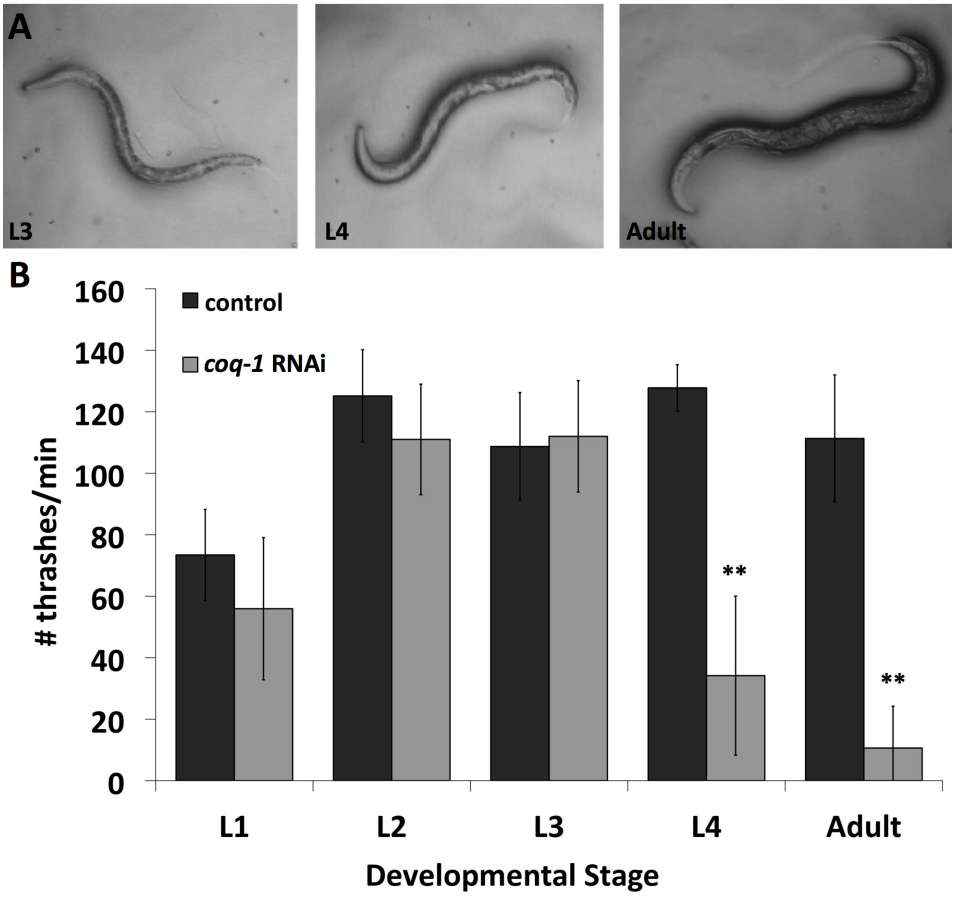

Figure 2.1: RNAi knockdown of *coq-1* results in progressive loss of motor coordination.
A. Examples of the abnormal postures adopted by L4 larvae and adults after exposure to *coq-1* RNAi.
B. Swimming assay quantifying movement defects (bars represent avg ± SD, ** $p < 0.005$, $n = 10$).

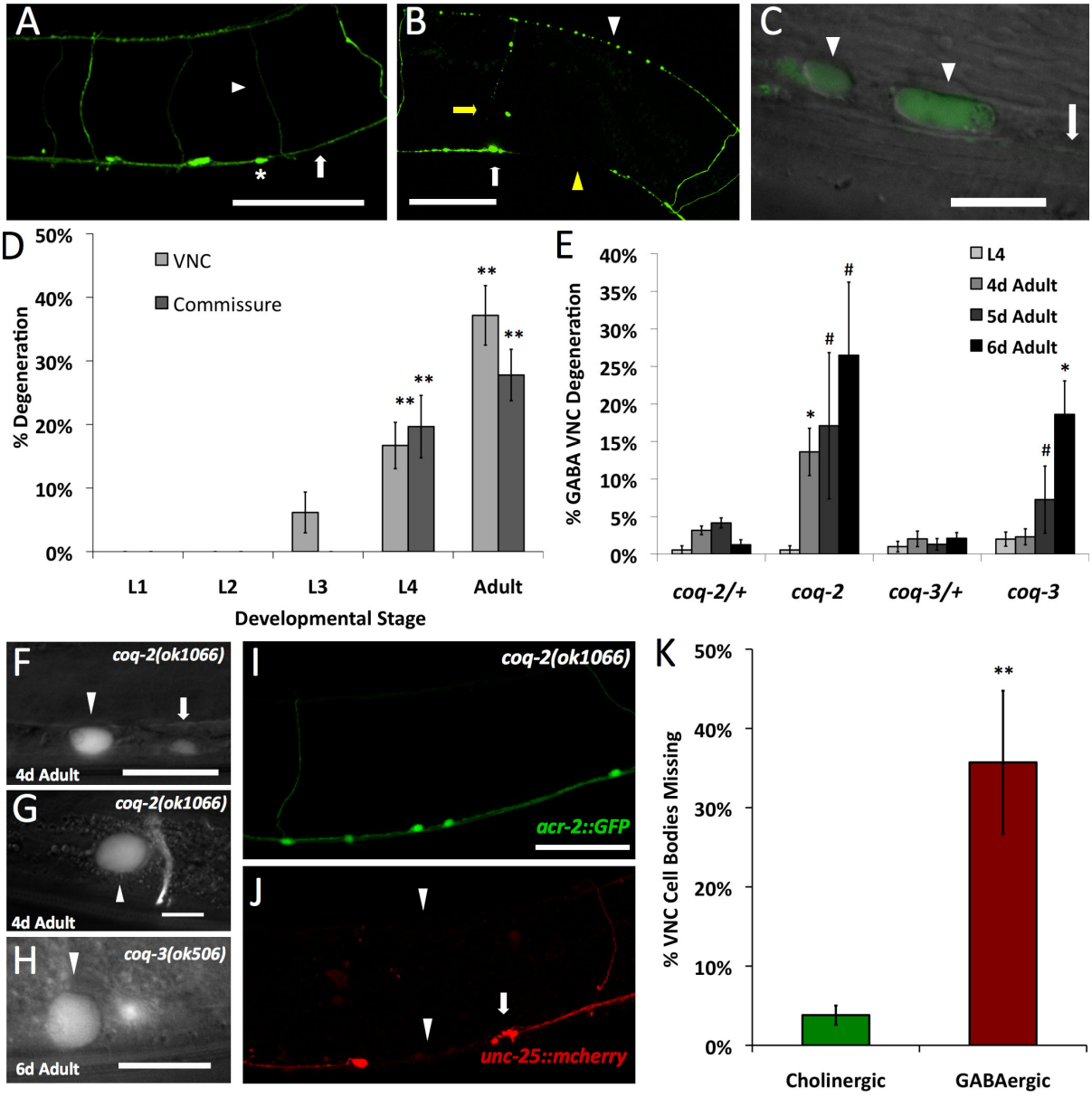
A
B
C
D
VNC
Commissure
% Degeneration
50%
40%
30%
20%
10%
0%
L1
L2
L3
L4
Adult
Developmental Stage
E
% GABA VNC Degeneration
40%
35%
30%
25%
20%
15%
10%
5%
0%
L4
4d Adult
5d Adult
6d Adult
coq-2/+
coq-2
coq-3/+
coq-3
F
coq-2(ok1066)
4d Adult
G
coq-2(ok1066)
4d Adult
H
coq-3(ok506)
6d Adult
I
coq-2(ok1066)
acr-2::GFP
J
unc-25::mcherry
K
% VNC Cell Bodies Missing
50%
40%
30%
20%
10%
0%
Cholinergic
GABAergic

Figure 2.2: CoQ depletion results in GABA neuron degeneration. A. Wild-type adult GABA neuron cell bodies (asterisks), processes in the ventral nerve cord (VNC) (arrow), and dorsally projecting commissures (arrowhead) labeled with *unc-25::GFP*. **B.** Adult *coq-1* RNAi-treated worm showing signs of degeneration (white arrowhead, dorsal process beading; white arrow, degenerating GABA cell body; yellow arrow, degenerating commissure; yellow arrowhead, VNC process break). (Scale bars: 50 µm.) **C.** *unc-25::GFP*-labeled GABA neurons appear swollen in *coq-1* RNAi-treated adults. Shown is the ventral view of GABAergic cell bodies (arrowheads) and VNC (arrow). (Scale bar: 10 µm.) **D.** Quantification of progressive degeneration of GABA neuron VNC processes and commissures ($n \geq 3$, error bars = SEM; $^{**}p < 0.001$ vs. empty vector-treated animals). No degeneration was observed in empty vector-treated animals. **E.** Progressive GABA neuron degeneration in *coq-2(ok1066)* and *coq-3(ok506)* mutants. GABA neuron degeneration was not observed in L1–L3 larval stages but was detectable in L4 larvae and pronounced in adults (day, d). $^{\#}p < 0.04$ and $^{*}p < 0.001$ vs. heterozygous controls, $n \geq 20$ for each developmental stage. **F.** Enlarged cell size of degenerating GABA neuron (arrowhead) compared with an unaffected GABA neuron cell body (arrow). (**F–H**) Swollen D-class (**F** and **H**) and RME GABA neurons (**G**) in *coq-2(ok1066)* (**F** and **G**) and *coq-3(ok506)* (**H**) mutants visualized with unc-25::GFP. (Scale bars: 10 µm.) Cholinergic neurons (*acr-2::GFP*) (**I**) are unaffected, whereas GABA neurons (*unc-25::mcherry*) (**J**) show degenerating processes (arrowheads) and cell bodies (arrows) in a single *coq-2(ok1066)* animal. (Scale bar: 30 µm.) **K.** VNC *acr-2::GFP*-cholinergic neurons were counted from VA2–VA11 (30 total) and VNC *unc-25::mcherry*-GABA neurons from VD3–VD11 (13 total). Fraction of missing cholinergic vs. GABA neurons in *coq-2(ok1066).* $^{**}P < 0.001$, $n = 16$. Anterior left, ventral down in **A–C** and **F–J**.

We also validated the *coq-1* RNAi results by examining *coq-1(ok749)* mutant animals (Fig. 2.3). The *ok749* deletion removes a C-terminal region comprising ≈70% of the coding sequence and is therefore a likely null allele (Fig. 3.1). Prior studies of *coq-1(ok749)* reported paralysis and early larval lethality (Gavilan et al. 2005). We observed that homozygous *coq-1* animals develop to at least the third larval stage with a few adult escapers. This finding is likely to mean that the *coq-1(ok749)* mutation results in a maternal effect lethal phenotype in which the first generation of viable offspring progress through larval development with maternally provided CoQ (Hihi et al. 2002). Homozygous *coq-1* mutants appear Unc as L3 larvae. Degeneration of GABA neurons is initially observed in young adults (Fig. 2.3B-C); a swollen ventral cord cholinergic motor neuron was observed in a single animal at this stage (n = 20). Older *coq-1(ok749)* animals show extensive swelling and degeneration of other tissues as reported (Gavilan et al. 2005).

We tested deletion mutants for *coq-2* and *coq-3* to ask whether genetic ablation of other CoQ biosynthetic genes phenocopies *coq-1* knockdown (Asencio et al. 2003). GABA neurons of *coq-2(ok1066)* and *coq-3(ok506)* animals also show the swollen morphology (Fig. 2.2F-H) and progressive degeneration of *coq-1*-deficient animals (Fig. 2.2E). The similar phenotypes displayed by *coq-2* and *coq-3* mutants substantiate the idea that the movement and degenerative defects result from reduced CoQ synthesis, rather than off-target effects or additional roles of the COQ-1 enzyme.

The similar degenerative pattern and age-dependence shown by the *coq-1, coq-2*, and *coq-3* knockout animals validates the specificity of the *coq-1* RNAi treatment. Hence, for most subsequent experiments in this chapter, we used RNAi knockdown of *coq-1* to bypass the developmental delay of the CoQ pathway mutants and to produce large numbers of viable adult animals with CoQ-deficient phenotype.

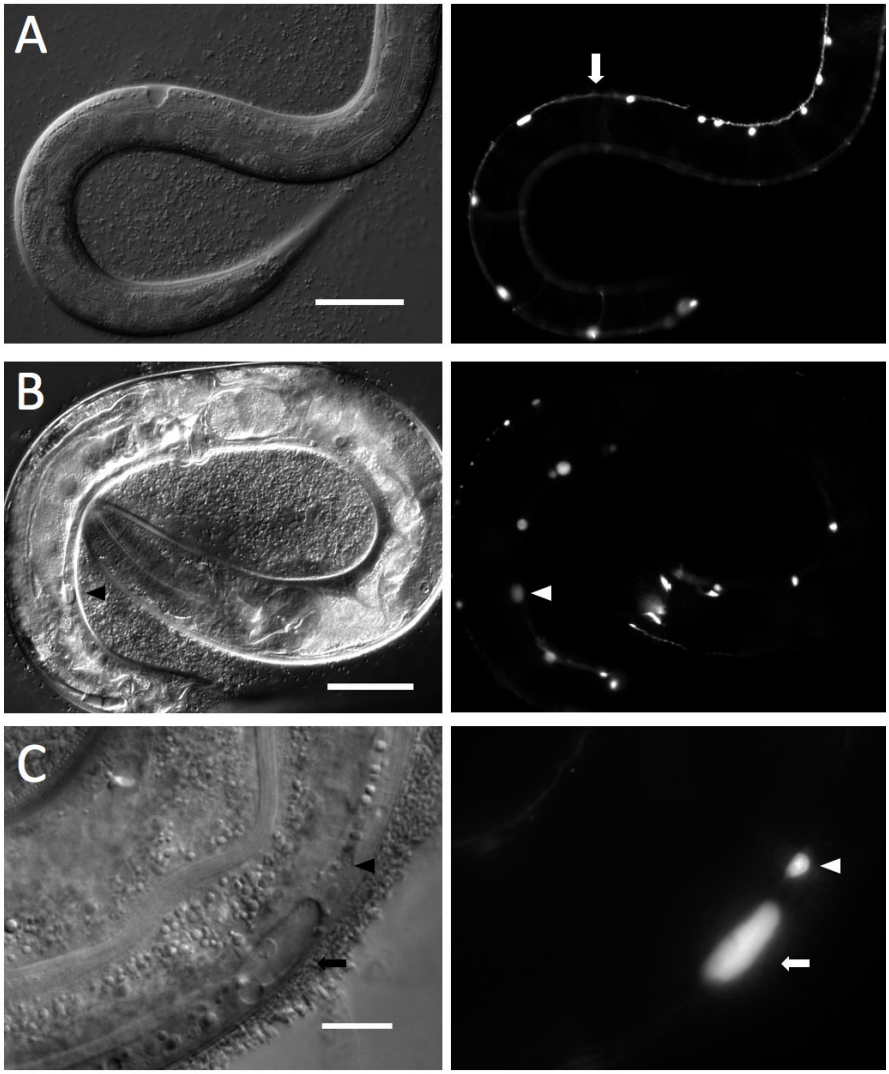

Figure 2.3: GABA neuron degeneration in *coq-1(ok749)* animals. A-B. DIC (Left) and GFP (Right) views of *unc-25::GFP*-labeled GABA neurons in *coq-1(ok749)* at the L3 (**A**) and adult (**B**) stages. Arrow denotes intact ventral nerve cord (VNC) in L3 larva (**A)** and arrowhead marks swollen GABAergic motor neuron cell body in adult (**B**). **C.** Enlarged (arrow) and normal (arrowhead) GABAergic cell bodies in the VNC. Scale bars: **A** and **B**, 20 µm; **C**, 10 µm.

GABA neurons are preferentially sensitive to CoQ Depletion-induced degeneration

Having observed that CoQ deficiency results in GABA neuron degeneration, we asked whether nearby cholinergic motor neurons in the ventral nerve cord were similarly affected. The results of this analysis revealed that GABA neurons are significantly more sensitive to CoQ depletion (Fig. 2.2I-J and Fig. 2.4). For example, in *coq-2(ok1066)* adults in which >35% of GABA neurons have degenerated, <5% of ventral cord cholinergic motor neurons are affected (Fig. 2.2K).

We next used cell-specific GFP reporters to evaluate the sensitivity of additional neuron subtypes to CoQ depletion by *coq-1* RNAi. Populations tested were cholinergic (*acr-2::GFP*), serotonergic (*tph-1::GFP*), glutamatergic (*eat-4::GFP*), and dopaminergic (*dat-1::GFP*) neurons. Although all animals displayed age-dependent Unc phenotype with *coq-1* RNAi, none of these neuron classes showed signs of degeneration comparable with that observed for GABA neurons at a similar developmental stage (Fig. 2.5A-E). We considered the possibility that this differential effect could be due to the relative insensitivity of these neuron classes to RNAi. This explanation is made less likely, however, by the finding that all of these neuronal types were equally vulnerable to RNAi against GFP (Fig. 2.5G).

Like neurons, muscle is also a highly metabolic tissue, and muscle degeneration is seen in some cases of CoQ deficiency (Lalani et al. 2005). Therefore, we used a GFP-labeled myosin heavy chain protein (MYO-3::GFP) (Campagnola et al. 2002) to examine muscle structure in the *coq-1* RNAi knockdown animals. We detected no morphological abnormalities in body wall muscle (Fig. 2.5F), verifying that the Unc phenotype associated with this RNAi construct is not the result of muscle degeneration. We also examined vulval muscle, reasoning that defects in these muscles might explain the Egl phenotype. However, we observed no structural differences between vulval muscles in control versus *coq-1* RNAi-treated animals.

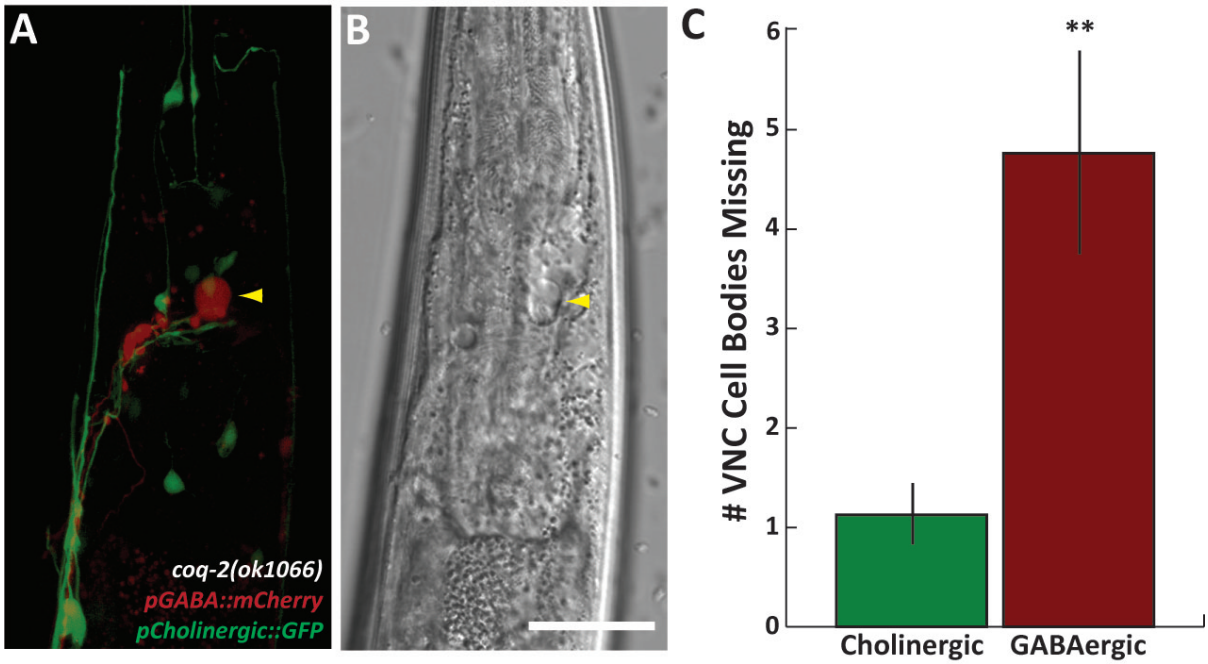

Figure 2.4: GABA neurons are more sensitive than neighboring cholinergic neurons to *coq-2* depletion. A. A swollen GABAergic neuron (yellow arrowhead, *punc-25*::mcherry) next to unaffected cholinergic neurons (*pacr-2*::GFP) in the head of a *coq-2(ok1066)* animal. Scale bar = 25µM. **B.** DIC image shows a large, swollen necrotic GABA neuron (yellow arrowhead). **C.** The number of absent cholinergic (*acr-2::GFP*) and GABAergic (*unc-25::mcherry*) neurons (between VA2-VA11 and VD3-VD11, respectively) in adult *coq-2* animals.**$p < 0.002$; n = 16.

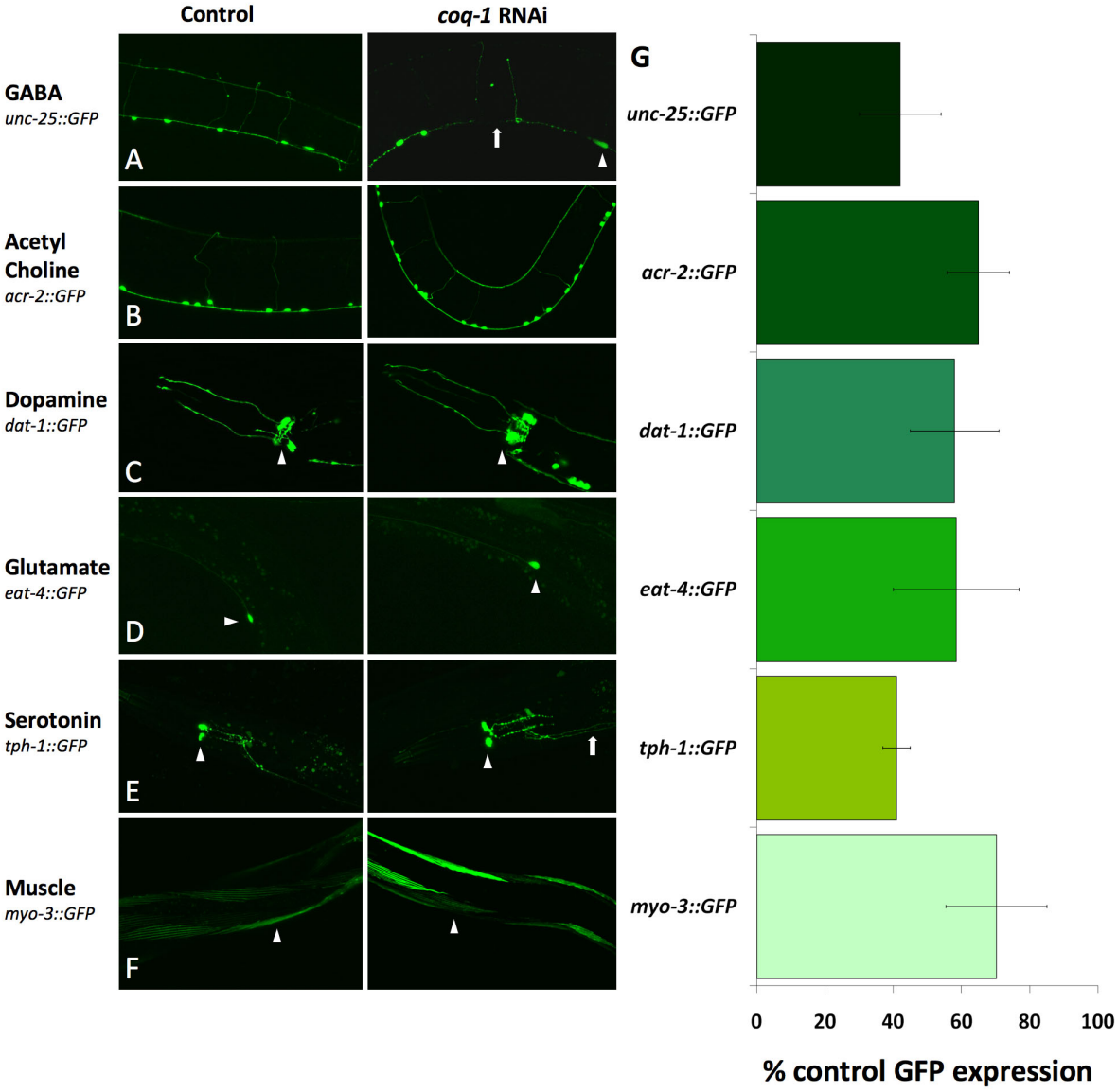
Control
coq-1 RNAi
GABA
unc-25::GFP
A
Acetyl
Choline
acr-2::GFP
B
Dopamine
dat-1::GFP
C
Glutamate
eat-4::GFP
D
Serotonin
tph-1::GFP
E
Muscle
myo-3::GFP
F
G
unc-25::GFP
acr-2::GFP
dat-1::GFP
eat-4::GFP
tph-1::GFP
myo-3::GFP
0
20
40
60
80
100
% control GFP expression

Figure 2.5: *coq-1* RNAi triggers preferential degeneration of GABA neurons. Confocal images (40×) of empty vector treated control or *coq-1* RNAi-treated animals expressing GFP reporters specific for different neurotransmitter classes of neurons. **A.** GABAergic neurons detected by *unc-25::GFP. coq-1* RNAi-treated animals show both VNC degeneration (arrow) and swollen neurons (arrowhead). Other classes of neurons and muscle cells do not show degeneration in age-matched animals subject to coq-1 RNAi-treatment for the same period. **B.** Cholinergic neurons, *acr-2::GFP*. **C.** Dopaminergic neurons, *dat-1::GFP*. Arrowhead, CEP neuron. **D.** Glutamatergic neurons, *eat-4::GFP*. Arrowheads point to AVM (Left) and ALM (Right). **E.** Serotonergic neurons, *tph-1::GFP*. NSM cell body (arrowheads) and HSN axonal projection (arrow) are shown. **F.** Muscle, *myo-3::GFP*. Arrowheads point to body wall muscle cells. **G.** Sensitivity to RNAi knockdown in each GFP-labeled cell type was determined by measuring GFP fluorescence after RNAi against GFP. GFP fluorescence intensity values were obtained from a through focus Z-series collected in a confocal microscope and quantified by histogram analysis in ImageJ (n = 6, avg ± SD). Fluorescence intensities for each GFP strain were normalized to measurements obtained from a control (RNAi with empty vector) to calculate % control GFP expression.

Although our results do not preclude the possibility that non-GABAergic neurons or muscle are functionally affected by *coq-1* RNAi, the earliest degenerative phenotype was exclusively observed in GABA neurons. In fact, functional deficits in other neurons or muscle are likely because the movement defects of mutants in which GABA neurons are selectively disabled are less severe than the paralyzed adult phenotype that results from RNAi ablation of *coq-1* (McIntire, Jorgensen, Kaplan, et al. 1993b). Ultimately, *coq-1* RNAi-treated adults and become completely paralyzed and show widespread cell swelling and tissue necrosis after 5 days of RNAi treatment; non-GABA neuron cell types were similarly affected in older *coq-2* and *coq-3* adults.

coq-1 RNAi-mediated degeneration is calcium-dependent

Calcium is a key effector of neurodegenerative diseases involving mitochondrial dysfunction (Mattson 2007). Calreticulin (*crt-1*) functions in the ER lumen to maintain Ca^{2+} levels for ready release on appropriate stimuli (Michalak et al. 1999). In *C. elegans*, *crt-1* mutants block necrotic degeneration of motor neurons (Xu et al. 2001). We tested a *crt-1* null mutant (*bz30*) in our paradigm and found that it prevented the progressive degeneration of GABA neurons in *coq-1* RNAi-treated animals (Fig. 2.6A). The calcium-chelating agent EGTA (0.5 mM) was similarly protective (Fig. 2.6A). Taken together, these results demonstrate that Ca^{2+} signaling is important for *coq-1* RNAi-mediated degeneration of GABA neurons.

Specific apoptotic genes are required for GABA neuron cell death in CoQ-depleted animals

Ca^{2+} release from the endoplasmic reticulum can result in necrotic (Driscoll & Gerstbrein 2003) or apoptotic (Demaurex & Distelhorst 2003) cell death. The cell swelling observed in *coq-1* knockdown mutants is consistent with a necrotic mechanism. To investigate whether apoptotic genes are required for GABA cell death, we tested mutants of the canonical apoptotic pathway, *egl-*

1, *ced-9, ced-4,* and *ced*-3 (Fig. 2.6 and Fig. 2.7). In apoptotic cells, the BH3-only protein, EGL-1, interacts with CED-9 (Bcl-2) to release CED-4 (Apaf-1) for activation of CED-3 (caspase) that, in turn dismembers sensitive target proteins that normally maintain cellular integrity (Fig. 1.3) (Lettre & Hengartner 2006). Loss-of-function mutations in *egl-1* did not prevent GABA neuron degeneration after *coq-1* knockdown. A gain-of-function allele of the anti-apoptotic protein CED-9 was similarly ineffective (Fig. 2.7). Surprisingly, mutations in *ced-4* and *ced-3* attenuated both the *coq-1* RNAi-dependent GABA neuron degeneration and Unc phenotype (Fig. 2.6A, C). These genetic results indicate that CED-4 is activated in *coq-1*–depleted GABA neurons by a pathway that is not regulated by either *egl-1* or *ced-9*. In addition to strongly suppressing degeneration of GABA ventral nerve cord (VNC) processes, the *ced-4* mutation also attenuates the elimination of GABA neuron cell bodies in *coq-1* RNAi-treated animals (Fig. 2.8), which suggests that GABA neuron cell death is blocked. This result is supported by our finding of comparably strong *ced-4* suppression of GABA neuron degeneration in *coq-3(ok506)* animals (Fig. 2.6B). Curiously, we note that a strong loss-of-function allele of *ced-3* (*n717)* only partially rescued the uncoordinated and GABA neuron degeneration phenotypes, whereas the *ced-4* mutation affords almost complete suppression of both defects in *coq-1* RNAi-treated animals (Fig. 2.6). In **Chapter 4**, we describe a more comprehensive analysis of *ced-3* loss-of-function in an RNAi-independent CoQ deficiency model that surprisingly suggests the opposite role for CED-3 as a negative regulator of GABA neuron death. Nonetheless, the cytoplasmic swelling of CoQ-depleted GABA neurons in conjunction with the essential roles of CED-4/Apaf-1 and CRT-1/calreticulin suggest that loss of CoQ synthetic activity triggers selected components of both programmed cell death and necrotic pathways.

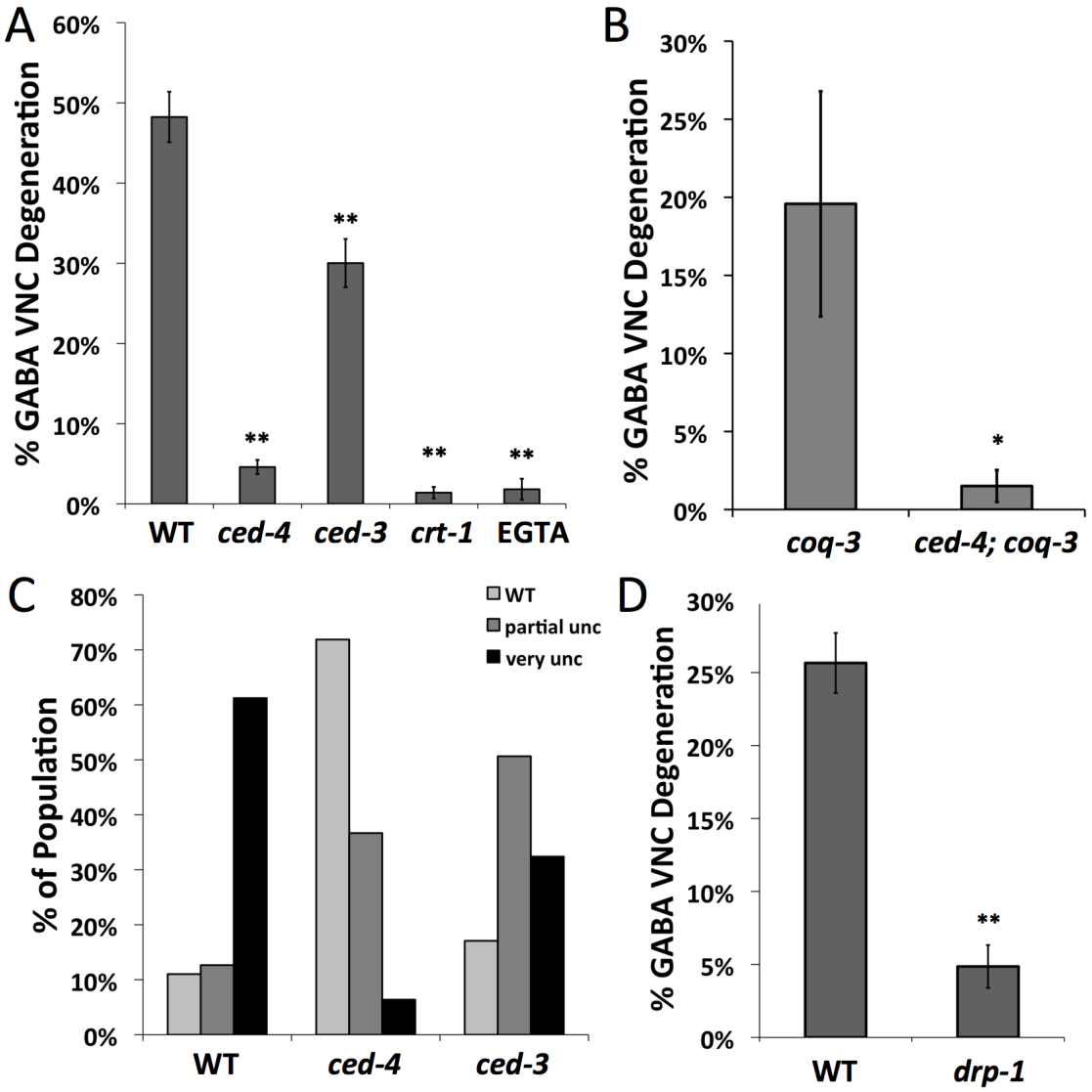

Figure 2.6: Apoptotic genes and calcium and are required for *coq-1* RNAi-induced GABA neuron degeneration. A. *ced-4(n1162), ced-3(n717), crt-1(bz30)*, and EGTA (0.5 mM)-treated animals were tested for *coq-1* knockdown-induced GABA neuron degeneration. All results were obtained from *coq-1* RNAi-treated animals containing *eri-1(mg366); unc-25::GFP*. GABA neurons were scored in adults as in Fig. 2.2. n ≥ 3 experiments for each genotype. Error bars = SEM, **p < 0.0001 vs. WT (wild-type). **B.** *ced-4(n1162)* suppresses GABA neuron degeneration in *coq-3(ok506)* adults, *p < 0.02 vs. *coq-3(ok506*), n > 14. **C.** Movement assay of *ced-4* and *ced-3* mutants treated with *coq-1* RNAi. Adults were tapped on the head and the tail and scored for movement: "partial unc" worms are uncoordinated and "very unc" worms are unable to move, n > 100 worms. **D.** *drp-1 (tm1108)* suppresses *coq-1* knockdown-induced GABA degeneration, **p < 0.001 vs. WT, n > 60.

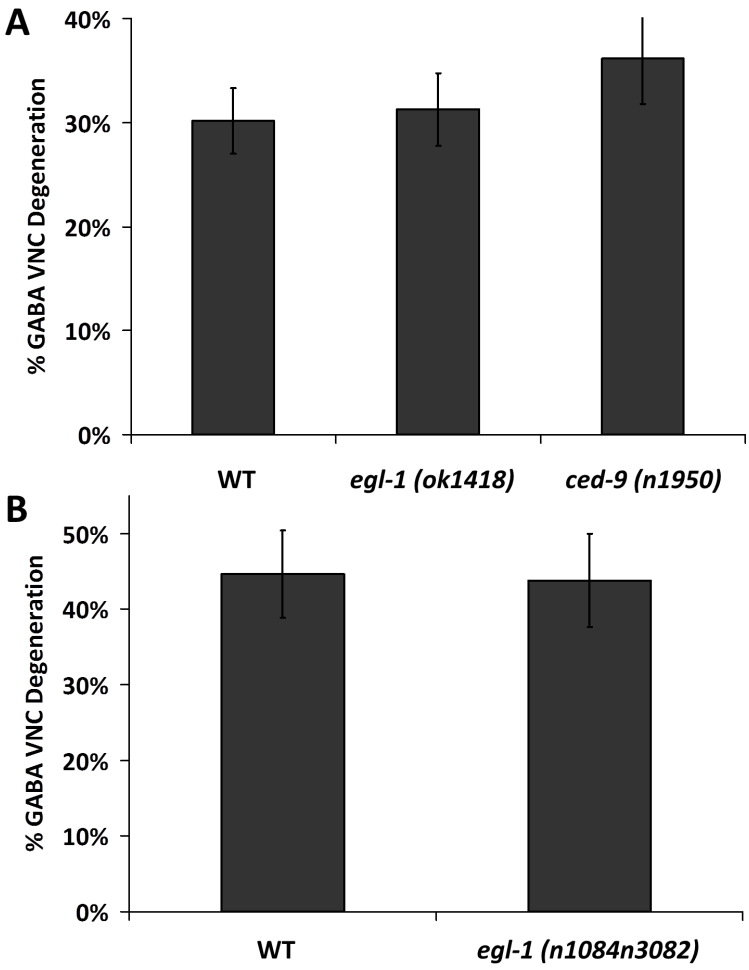

Figure 2.7: Apoptotic genes *egl-1* and *ced-9* are not required for *coq-1* RNAi-induced GABA neuron degeneration. A. *egl-1(ok1418) and ced-9(n1950)* were assayed for GABA neuron degeneration after *coq-1* knockdown as in Fig. 2.2 (n > 40). Results with *egl-1* and *ced-9* do no differ significantly from the wild-type control in these experiments. **B.** In a separate experiment, another *egl-1* loss-of-function allele, *n1084n3082*, was treated with *coq-1* RNAi and assayed for GABA neuron degeneration (n > 20), with no significant difference from the wild-type control.

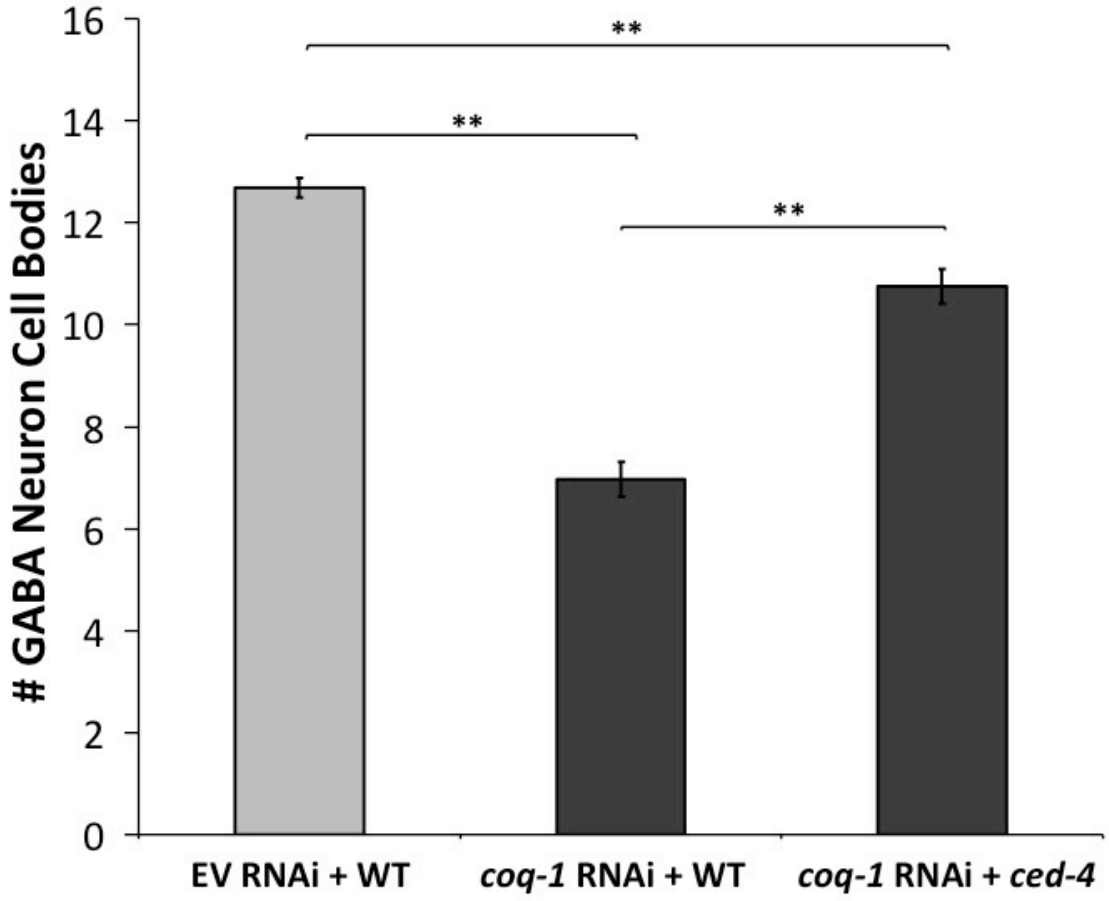

Figure 2.8: *ced-4* suppresses degeneration of GABA neuron cell bodies in *coq-1* RNAi-treated animals. *punc-25::GFP*-positive GABA neurons in the VNC interval from VD3-DD11 (13 total cells) were counted in *coq-1* RNAi-treated wild-type (WT) and *ced-4(n1162)* and for the negative control of wild-type treated with empty vector (EV RNAi + WT), **p < 0.0001, n > 50. All strains include the *eri-1(mg366)* mutant allele.

coq-1* knockdown-induced cell death depends on the mitochondrial fission gene *drp-1

Calcium has been shown to stimulate mitochondrial fission (Breckenridge et al. 2003), which, in turn, has been linked to both apoptosis and necrosis in mammals (Young et al. 2010; Youle & Karbowski 2005) and in *C. elegans* (Dacey et al. 2005). We reasoned that CoQ deficiency might sensitize mitochondria to Ca^{2+}-dependent fission-related cell death. To test this idea, we used RNAi knockdown of *coq-1* in *drp-1* mutant animals (Fig. 2.6D) DRP-1 (dynamin-related protein) has been shown to function in both mitochondrial fission (Dacey et al. 2005) and in a *ced-3*–dependent and *ced-9*–independent cell death pathway (Breckenridge et al. 2008). The *drp-1* mutant blocked GABA neuron degeneration (Fig. 2.6D), thereby implicating the fission machinery in the pathology associated with *coq-1* knockdown in *C. elegans*. Similar results were obtained in *coq-1*+*drp-1* double RNAi experiments (Fig. 2.9A). We also used double RNAi to test *fzo-1,* a gene required for mitochondrial fusion (Takayuki Kanazawa 2008). In this case, *fzo-1* knockdown actually enhances the GABA neuron degeneration phenotype of *coq-1*–deficient animals as expected for a treatment that impairs mitochondrial fusion (Fig. 2.9B-C). The conclusion that mitochondrial function is defective in CoQ-depleted animals is also supported by our finding that mitochondrial ATP levels are significantly reduced by *coq-1* RNAi treatment (Fig. 2.10). Together, these results indicate that CoQ depletion disrupts mitochondrial function and activates a cell death pathway that depends on the mitochondrial morphogenesis gene, *drp-1.*

DISCUSSION

We have shown that depletion of Coenzyme Q (CoQ) through RNAi and genetic ablation of CoQ biosynthetic genes, *coq-1*, *coq-2*, and *coq-3*, leads to the progressive loss of motor coordination and preferential degeneration of GABA neurons. The mechanism of cell death relies strongly on the

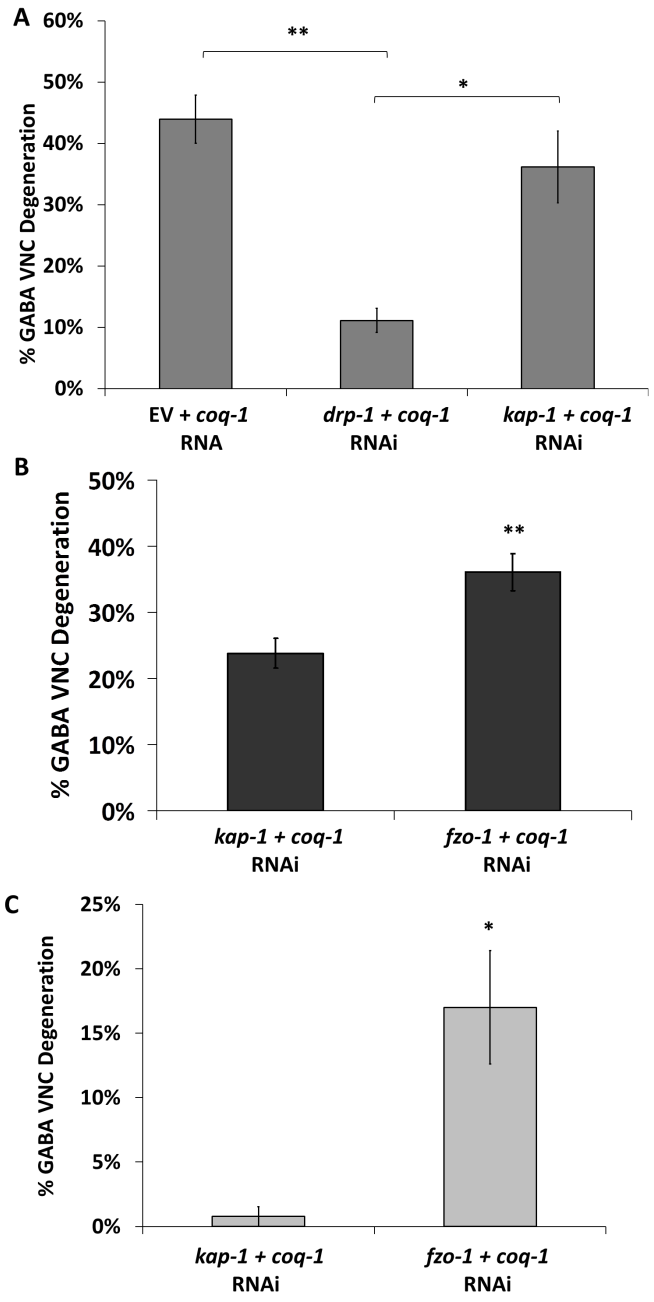

Figure 2.9: RNAi of mitochondrial fission and fusion genes influences GABA neuron degeneration induced by *coq-1* RNAi. A. Double RNAi with empty vector (EV) and *coq-1* results in GABA neuron degeneration (≈44%). Double RNAi of *coq-1* with the mitochondrial fission gene *drp-1* results in significantly less GABA neuron degeneration than EV + *coq-1* RNAi control. Double RNAi with a randomly selected control gene *kap-1* (kinesin-associated protein) did not inhibit *coq-1* RNAi-induced GABA neuron degeneration. n = 60, **P < 0.0001; *p < 0.0003. **B.** Combinatorial RNAi with *fzo-1* (mitochondrial outer membrane fusion gene) and *coq-1* enhance the GABA neurodegeneration observed with coq-1 and an unrelated gene, *kap-1*, n > 100, **p < 0.0001. **C.** *fzo-1* RNAi enhances *coq-1* knockdown-induced GABA neuron degeneration in animals lacking the RNAi sensitive mutation *eri-1(mg366).* n > 15, *p < 0.002 (Student's t test).

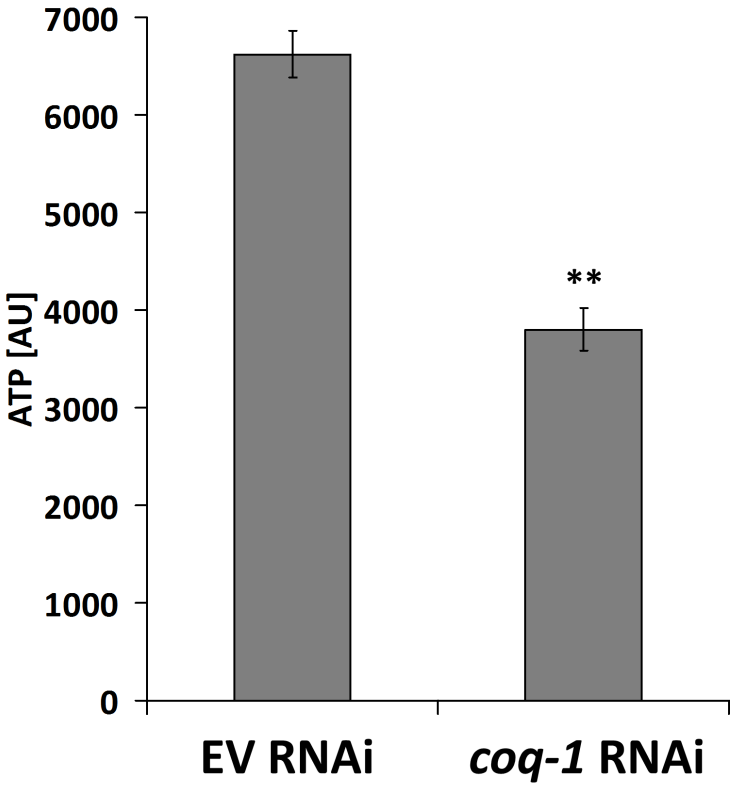

Figure 2.10: Mitochondrial ATP levels are reduced in CoQ-depleted animals. ATP levels in mitochondria isolated from whole animal lysates are reduced in *coq-1* RNAi-treated animals versus empty vector-treated control (EV RNAi). **p < 0.0008, n = 3. Each sample contained 0.2 µg of total protein. Relative ATP levels are denoted (AU, arbitrary units). ATP levels were measured by using a luminescence assay and normalized to protein concentration

function of *ced-4* (Apaf-1). The GABA neuron pathology that accompanies CoQ depletion also involves calcium signaling, possibly from ER stores, and the mitochondrial fission protein DRP-1. These results emphasize an important role for CoQ in neuron survival and link mitochondrial dysfunction to a calcium-dependent mechanism of selective neuron degeneration in *C. elegans.*

CoQ depletion triggers a cell death pathway featuring elements of both apoptosis and necrosis

Our findings suggest that CoQ depletion in *C. elegans* GABA neurons triggers a cell death mechanism that includes features of both apoptotic and necrotic pathways. The affected GABA neurons morphologically resemble necrotic cells (i.e., swollen soma) yet requires a downstream component of apoptosis, *ced-4*. In *C. elegans*, necrosis and apoptosis have been reported to function as separate pathways (S. Chung et al. 2000); however, our results indicate that a subset of apoptotic genes is required for a pathology (cell swelling) normally restricted to a necrotic mechanism. In the canonical apoptotic pathway (Fig. 1.3), CED-9 tethers CED-4 to the outer mitochondrial membrane. EGL-1 binding to CED-9 releases CED-4 for incorporation into the apoptosome and subsequent activation of CED-3/caspase (Lettre & Hengartner 2006). Our finding that neither EGL-1 nor CED-9 affects *coq-1* RNAi-induced GABA neuron death indicates that CED-4 must be activated by an alternative mechanism in this case. Our results also suggest that CED-4 is likely to activate novel downstream effectors. CED-4–dependent, CED-3–independent cell killing programs have been reported for yeast in which CED-4 is overexpressed (Tao et al. 1999) and in *C. elegans* with RNAi knockdown of the presumptive anti-apoptotic protein, ICD-1 (Bloss et al. 2003). Mechanisms whereby CED-4 might activate these pathways are unknown. In the future, it will be interesting to determine whether the downstream CED-3-independent program that is triggered in CoQ-depleted GABA neurons includes other members of the *C. elegans* caspase family (Shaham 1998) or novel components (Barsoum et al. 2006).

Mitochondrial morphogenesis protein, DRP-1, is required for the death of CoQ-depleted GABA neurons

Mitochondrial fragmentation, which can trigger apoptosis, depends on the dynamin-related protein, DRP-1 (Knott et al. 2008). Previous studies have shown that *coq-1* RNAi induces mitochondrial fragmentation in *C. elegans* (Ichishita et al. 2008). Thus, our finding that DRP-1 is required for the execution of GABA neurons in CoQ-deficient animals (Fig. 2.6, Fig. 2.9) is consistent with a model in which the mitochondrial fragmentation or "excessive fission" accounts for the neurodegenerative effect of CoQ depletion. Enhancement of this effect by RNAi knockdown of the mitochondrial fusion gene, *fzo-1*, also supports this idea (Fig. 2.9). In addition to mediating mitochondrial fusion, the mammalian homolog of FZO-1, Mfn2, promotes expression of ETC proteins (Pich et al. 2005). This finding suggests that the loss of mitochondrial energy production in *fzo-1*–deficient animals could also contribute to cell death in CoQ-depleted GABA neurons. Although mitochondrial fission has been linked to apoptosis in mammals, conflicting results have been obtained in *C. elegans* (Dacey et al. 2005; Breckenridge et al. 2008). However, our finding that DRP-1 is required for GABA neuron degeneration in *C. elegans* parallels results with mammalian cells showing that mitochondrial fission is a necessary step in experimental models of neurodegenerative disease resulting from mitochondrial injury. For example, exposure of cortical neurons to high concentrations of the neurotransmitter NO (nitric oxide) triggers a caspase-independent death pathway that requires mitochondrial fission (Barsoum et al. 2006). NO-induced degeneration is accompanied by ATP depletion and production of free radicals. Both of these traits are also induced by either environmental or genetic defects that block mitochondrial ETC (Bossy-Wetzel et al. 2008; Wallace & Starkov 2000; Atamna & Frey 2007). We therefore speculate that CoQ depletion in *C. elegans* disrupts mitochondrial ETC function (discussed in **Chapter 5**), which in turn, triggers a

degenerative pathway that shares common features such as downstream signals and effector molecules that also mediate neurodegeneration in mammalian neurons.

CoQ deficiency in *C. elegans* as a model for human disease

The selective, age-dependent death of GABA neurons and loss of coordinated movement seen in CoQ-depleted worms are shared features of CoQ deficiency in humans. The most common outcome of this deficiency is cerebellar ataxia (Montero et al. 2007), although mutations that disrupt CoQ biosynthesis can also result in a more severe early-onset pathology involving multiple tissues (Mollet et al. 2007; Catarina M Quinzii 2007).

Despite the rarity of CoQ deficiency in humans, it shares important pathologies with prevalent glutamine repeat diseases. These include the autosomal dominant Huntington's Disease (HD) and spinocerebellar ataxias. The age-related death of medium spiny GABAergic neurons of the striatum occurs in HD (Martin & Gusella 1986) and GABAergic Purkinje cells are significant targets for degeneration in the cerebellar ataxias (Zoghbi 1995). Recent studies have linked neuronal degeneration in HD to disrupted mitochondrial function (Orr et al. 2008). For example, exogenous CoQ is neuroprotective in mouse models of HD (Ferrante et al. 2002). In addition, the pathology induced by overexpression of mutant Huntingtin (mtHtt) in mammalian cells or in C. *elegans* depends on the mitochondrial fission machinery (Wang et al. 2008). Lastly, *coq-1* RNAi in *C. elegans* enhances the toxicity of a mutant form of human tau that has been implicated in the pathology of AD (Kraemer et al. 2006). It is striking that salient features of these human genetic diseases including selective neuron sensitivity, mitochondrial dysfunction, Ca^{2+} dependence, and aberrant cell death (Dueñas et al. 2006; Kwong et al. 2006) are observed in *C. elegans* with the depletion of CoQ. These parallels suggest that neurodegenerative mechanisms arising from

mitochondrial dysfunction are conserved and, thus, can be effectively delineated by studies in *C. elegans*.

Acknowledgements

We thank D. Xue (University of Colorado, Boulder, CO) for *drp-1(tm1108*), Y. Jin (University of California, San Diego, CA) for plasmid pSC392, and C. Thorne (Vanderbilt University, Nashville, TN) for help with the ATP assays. Other strains were obtained from the *C. elegans* Genetics Center, which is supported by National Institutes of Health National Center for Research Resources. We thank A. Bowman (Vanderbilt University, Nashville, TN), B. McLaughlin (Vanderbilt University, Nashville, TN), and M. Driscoll (Rutgers University, Piscataway, NJ) for comments on the manuscript. This work was supported by National Institutes of Health Grants R01 NS26115 and R21 MH77302, a Vanderbilt Kennedy Center Hobbs Discovery Grant (to D.M.M.), National Institutes of Health Grant F31 NS49743 (to J.D.W.), and National Institutes of Health Grant T32 GM08554.

CHAPTER III

CHARACTERIZATION OF A CONSERVED COENZYME Q BIOSYNTHESIS PATHWAY IMPLICATES INTERCELLULAR UBIQUINONE TRANSPORT MECHANISMS

INTRODUCTION

Coenzyme Q is synthesized in the mitochondria and is incorporated into all cellular membranes (Kalén et al. 2002). Because of robust *de novo* production, exogenous CoQ is not required under normal conditions. However, symptoms arising from Coenzyme Q deficiency are improved with oral Coenzyme Q_{10} supplementation (Rötig et al. 2000; Montini et al. 2008). The therapeutic benefit of CoQ treatment implicates active mechanisms of cellular uptake and distribution under conditions in which biosynthesis or maintenance of CoQ is impaired. Unfortunately, the bioavailability of Coenzyme Q limits its efficiency as a dietary supplement. Coenzyme Q is a large, insoluble molecule that requires high doses and long-term administration for successful clinical improvement (Catarina M Quinzii 2007). Therefore, treatments that enhance utilization of exogenous CoQ are of significant therapeutic value. In addition to mechanisms that control its uptake, externally provided CoQ must also be distributed to a variety of membranes in the cell. Normally, intracellular distribution mechanisms are active, because Coenzyme Q is synthesized in the mitochondria but is also present in other membranes (Tran & Clarke 2007). Our current understanding of CoQ uptake and distribution is based on limited reports that implicate the endomembrane system (Fernández-Ayala et al. 2005; Padilla-López et al. 2009). However, these studies used single-cell models and therefore do not recapitulate the complex, cell-cell interactions that must occur during CoQ transport in multicellular organisms. Additionally, specific Coenzyme Q-binding proteins that regulate CoQ uptake or intracellular trafficking have not been identified. Active transport of Coenzyme Q to specific cellular locations is suggested by the function of Coq10p, a

protein that captures CoQ from its site of biosynthesis (matrix side of the inner mitochondrial membrane) and transports it to the mitochondrial electron transport chain (ETC) (Barros et al. 2005; Busso et al. 2010). It therefore seems likely that other CoQ-binding proteins could facilitate the movement of CoQ among tissues and CoQ localization within specific cellular membranes.

This chapter focuses on fundamental aspects of Coenzyme Q deficiency that are conserved in *C. elegans*. Coenzyme Q deficiency is a clinically heterogeneous disorder, with mutations in different genes of this pathway producing a wide range of symptoms. Mutations in *C. elegans* CoQ biosynthetic pathway genes share this heterogeneity as evident by diverse developmental and neurodegenerative defects. Additionally, experiments in this chapter reveal that GABA neurons do not require endogenous CoQ biosynthesis to maintain viability. This finding suggests that CoQ-deficient GABA neurons are rescued by importation of CoQ from other tissues. An intercellular Coenzyme Q transport model is also supported by the discovery that restoration of CoQ synthesis exclusively in body muscle rescues developmental and fertility defects of *coq-1* mutants. These findings indicate that mechanisms of uptake and distribution of exogenous CoQ could be conserved between nematodes and mammals. Additionally, this work reports the first functional complementation of a CoQ mutant with a human Coenzyme Q biosynthetic gene. The pathogenic effects of a patient-isolated COQ2 mutation are also recapitulated in our *C. elegans* model. Taken together, this chapter describes several aspects of human CoQ deficiency that are conserved in *C. elegans* and therefore, underscores its strengths as a genetic model of mechanisms that control the efficacy of CoQ uptake and function.

MATERIALS AND METHODS

Nematode Strains and Genetics

Nematodes were cultured using standard methods (Brenner 1974). Mutants, genotyping primers, and strain sources are listed in Table 3.1. A list of strains generated for this study is located in Table 3.2.

Molecular Biology and Transgenic Strains

Molecular cloning primers and plasmids used for this work are listed in Tables 3.3 and 3.4, respectively. Table 3.5 contains the DNA concentrations used to generate transgenic arrays for this study. Refer to **Materials and Methods** section of **Chapter 2** for *unc-25* promoter construction.

cDNA Preparation

cDNA was synthesized from by RT-PCR from total RNA derived from the N2 (wild-type) strain. (poly-dT primers (Affy 100) and Superscript II Reverse Transcriptase (Invitrogen)).

coq-1 cDNA RNAi

A complete *coq-1* cDNA clone pG2M57 (yk1514f03) was obtained from Yuji Kohara (National Institute of Genetics, Japan) and used as template to amplify *coq-1*, which was TOPO TA cloned into pCR8/GW/TOPO (Invitrogen) to make pMLH003. The *coq-1* cDNA was then inserted into pL4440-Gateway (pG2M13) via an LR Clonase Gateway reaction (Invitrogen) to yield pMLH018. pMLH018 was transformed in HT115 (DE3), an RNAse III-deficient *E. coli* strain with T7 polymerase activity that is IPTG-inducible for enhanced dsRNA production/RNAi efficiency (Timmons et al. 2001).

Table 3.1: Alleles, genotyping primers and sources of mutants used in this study.

Mutant	Source	Genotyping Primers	Reference
coq-1 (ok749) I	Caenorhabditis Genetics Center	AAAAATGTTACGGCCGACTG	(Gavilan et al. 2005)
		CGTGTCCCTCAAAATGACCT	
		AGTCAGTGCTCGTCGGAGAT	
coq-2 (ok1066) III	Caenorhabditis Genetics Center	ATGCACATGGAGCATAGCAATG	(Gavilan et al. 2005)
		GCGTGGTTTCACACAGATACAA	
coq-3 (ok506) IV	Caenorhabditis Genetics Center	GCTGTAAGGGAGATTTTCCCAT	(Gomez et al. 2009)
		ACGGCGAGCAAAATAGGGAAAT	
coq-4 (ok1490) I	Caenorhabditis Genetics Center	ATTGGAGGAGGTGACACTGC	N/A
		AGAGTTGAAGAGAATGCGGC	
		TGCTCGGCGAGGTAACAGTC	
coq-5/tag-277 (gk379) III	Caenorhabditis Genetics Center	N/A	N/A
		N/A	
coq-8 (ok840) III	Caenorhabditis Genetics Center	ATGGCAGCAAAGCGGC	(Asencio et al. 2009)
		CGGGATACTGTACTTTTACAGC	
		CAAGTCTTCCGATACGA	
eri-1 (mg366) IV	Caenorhabditis Genetics Center	CATGCAATTTCAATGCCTTTTA	(Kennedy et al. 2004)
		TGCATCATCCAATCCACTATGT	
Transgene	**Source**	**Array or Translocation**	**Reference**
hT2 (I;III)	Caenorhabditis Genetics Center	*bli-4(e937) let(q782) qIs48*	(McKim et al. 1993)
juIs76 II	Caenorhabditis Genetics Center	*punc-25::GFP, lin-15(+)*	(Jin et al. 1999)
trIs10 I	Caenorhabditis Genetics Center	*pmyo-3::MB::YFP, pmyo-2::YFP, pceh-23::HcRed, punc-25::DsRed, unc-129nsp::CFP*	(Dixon 2006)
wpIs36 I	Marc Hammarlund	*punc-47::mCherry*	Unpublished
wpIs39 X	Marc Hammarlund	*punc-47::mCherry*	Unpublished
wpSi1 II	Marc Hammarlund	*punc-47::rde-1:SL2:sid-1, C. briggsae unc-119(+)*	Unpublished

Table 3.2: List of strains that were used in this study.

Strain	Genotype
NC1405	*juIs76 [punc-25::GFP, lin-15(+)] II; eri-1 (mg366) IV*
NC1958	*juIs76 [punc-25::GFP, lin-15(+)] II; coq-5+tag-277(gk379) III / hT2 (I; III)*
NC1959	*juIs76 [punc-25::GFP, lin-15(+)] II; coq-2(ok1066) III / hT2 (I; III)*
NC1974	*juIs76 [punc-25::GFP, lin-15(+)] II; coq-3(ok506) IV/ nT1 (IV; V)*
NC2066	*juIs76 [punc-25::GFP, lin-15(+)] II; coq-8(ok840) III / hT2 (I; III)*
NC2513	*juIs76 [punc-25::GFP, lin-15(+)] II; eri-1(mg366)IV; wdEx831 [pttr-39::coq-1 RNAi FWD, pttr-39::coq-1 RNAi REV, punc-25::mCherry, pceh-22::GFP]*
NC2556	*juIs76 [punc-25::GFP, lin-15(+)] II; coq-1(ok749) I; wdEx807 [psur-5::C.briggsae coq-1 cDNA, psur-5::NLS::GFP]*
NC2617	*trIs10 [pmyo-3::MB::YFP, pmyo-2::YFP, pceh-23::HcRed, punc-25::DsRed, unc-129nsp::CFP] I; eri-1 (mg366) IV*
NC2627	*trIs10 [pmyo-3::MB::YFP, pmyo-2::YFP, pceh-23::HcRed, punc-25::DsRed, unc-129nsp::CFP] I; ced-3 (ok2734) eri-1 (mg366) IV*
NC2743	*juIs76 [punc-25::GFP, lin-15(+)] II; coq-1(ok749) I / hT2 (I; III)*
NC2750	*coq-1(ok749) I; juIs223 [pttr-39::mcherry, pttx-3::GFP]; wdEx926 [psur-5::coq-1::GFP, podr-1::mCherry]*
NC2792	*coq-1(ok749)/hT2 (I; III); juIs223 [pttr-39::mcherry, pttx-3::GFP]; wdEx933 [punc-25::COQ-1::GFP, coel::GFP]*
NC2793	*coq-1(ok749)/hT2 (I; III); juIs223 [pttr-39::mcherry, pttx-3::GFP]; wdEx934 [pmyo-3::COQ-1::GFP, coel::GFP]*
NC2795	*wdEx935 [pmyo-3::coq-1::GFP, pmyo-3::TOM20mRFP, rol-6(d)]*
NC2810	*wdEx938 [pmyo-3::hPDSS2::GFP, pmyo-3::TOM20::mRFP, rol-6(d)]*
NC2821	*coq-1(ok749)/hT2 (I; III); wdEx939 [pceh-22::COQ-1::GFP, rol-6(d)]*
NC2822	*coq-1(ok749)/hT2 (I; III); wdEx940 [pF25B3.3::COQ-1::GFP, rol-6(d)]*
NC2823	*coq-1(ok749)/hT2 (I; III); wdEx941 [pelt-2::COQ-1::GFP, rol-6(d)]*
NC2824	*wdEx942 [psur-5::human COQ2-wt, psur-5::NLS::GFP]; coq-2(ok1066) III; wpIs39 [punc-47::mCherry] X*
NC2826	*wdEx943 [psur-5::human COQ2-mutant, psur-5::NLS::GFP]; coq-2(ok1066) III; wpIs39 [punc-47::mCherry] X*
XE1375	*lin-15(n744) X ; eri-1(mg366) IV ; rde-1(ne219) V ; wpSi1[Punc-47::rde-1:SL2:sid-1, Cbunc-119(+)] II ; wpIs36[Punc-47::mCherry] I*

Table 3.3: Primers used for molecular biology in this study.

DNA amplified	Primer Name	Primer Sequence
coq-1 cDNA	coq-1_5p_AscI	GGGGCGCGCCATGGGTGTTCTACCGAAAAT
	coq-1_3p_SacII	CCCCGCGGTTAGAATTTTCGATCCG
coq-1::GFP	coq-1_5p_AscI	GGGGCGCGCCATGGGTGTTCTACCGAAAAT
	coq-1_3p_SacII_nostop	AACCGCGGGAATTTTCGATCCGACTGTGAC
Miller *coq-1* RNAi	coq1RNAi_5p_AscI+PmeI	AAGGCGCGCCGTTTAAACGAAGAGTACCTG
	coq1RNAi_3p_PmeI+SpeI+ApaI	GGGCCCACTAGTGTTTAAACGCGGCCACAGGTTTTCCCAT
C. briggsae coq-1	br-coq-1_5p_AscI	ATGGCGCGCCATGGGTGTACTTCCAAAAATT
	br-coq-1_3p_SacII	ATCCGCGGTTAGAATTTCCTATCCGTTTGA
Human *PDSS1*	PDSS1_5p_AscI	AAGGCGCGCCATGGCCTCGCGCTGGTGG
	PDSS1_r3p_SacII	CCCCGCGGTCATTTATCTCTTGTGAGTACAATTTC
PDSS1::mCherry	PDSS1_5p_AscI	AAGGCGCGCCATGGCCTCGCGCTGGTGG
	PDSS1_tag3p_SacII	CCCCGCGGTTTATCTCTTGTGAGTACAATTTCTGAA
Human *PDSS2*	PDSS2_5p_AscI	GGGGCGCGCCATGAACTTTCGGCAGCTGCT
	PDSS2_3p_SacII	CCCCGCGGTCATGAAAATCTGGTCACAGCA
Human *PDSS2::GFP*	PDSS2_5p_AscI	GGGGCGCGCCATGAACTTTCGGCAGCTGCT
	PDSS2_tag3p_SacII	CCCCGCGGTGAAAATCTGGTCACAGCAAAC
Human *COQ2*	hQ2_5p_KpnI	GGGGTACCTAAGCTCGCCCTTATGACCC
	pYESQ2_3p_EcoRIstop	TTGAATTCTCGAAGCTCGCCCTTAATTTTCTATT
C-terminal GFP	GFP-C-tag_5p_SacII	GGGCCGCGGAGAGAAAAAATGAGTAAAGGA
	unc-54_3p_ApaI	GGGGGCCCGTACGGCCGACTAGTAGGAAAC
C-terminal mCherry	C-Mcherry-5p_SacII	GGGCCGCGGGTAGAAAAAATGCTCGAGATG
	unc-54_3p_ApaI	GGGGGCCCGTACGGCCGACTAGTAGGAAAC
TOM20::mRFP	TOM20_5p_AscI	AAGGCGCGCCAATGTCGGACACAATTCTTG
	mRFP_3p_SacII	TTCCGCGGTTAGGCGCCGGTGGAGTG
ttr-39 promoter	pC04G2.1_5p_SphI	GGGCATGCATTATTATTTCTATCGGCTAC
	pC04G2.1_3p_AscI	GGGGCGCGCCATGATTTTTTGTTTTAACAA
unc-25 promoter	punc-25_5p_HindIIISphI	GGAAGCTTGCATGCAAAAAACACCCAC
	punc-25_3p_AscI	GGGGCGCGCCATTTTTGGCGGTGAACTGAGC
sur-5 promoter	psur-5_5p_SphI	GGGCATGCCTGCATTGCTAAATTGCAACCC
	psur-5_3p_AscI	GGGGCGCGCCAAAATGTAAAGTTCAAAGGT

Table 3.4: Plasmids that were used and/or produced for this chapter.

Vector	DNA	Notes
pMBM009	*unc-25* RNAi in pL4440 in HT115 *E. coli*	
pMLH001	*punc-25* (5'SphI/3'AscI) FWD in pENTR D-TOPO	
pMLH004	*pttr-39* (5'SphI/3'AscI) FWD in pENTR D-TOPO	
pMLH009	*punc-25::gateway::mCherry::unc-10 3'UTR*	
pMLH035	*punc-25::TOM20::mRFP*	
pMLH018	*coq-1 cDNA* RNAi clone	
pMLH080	*psur-5* (5'SphI/3'AscI) REV in pCR8/GW/TOPO	
pMLH081	*pF25B3.3* minus 5'106bp in pCR8/GW/TOPO	
pMLH103	*pttr-39::mCherry::unc-54 3'UTR*	
pMLH107	*pttr-39::coq-1 RNAi FWD + punc-25::mCherry*	
pMLH112	*pttr-39::coq-1 RNAi REV*	
pMLH129	"Miller *coq-1*" RNAi clone	
pMLH132	*punc-25::mcherry::unc-54 3'UTR*	
pMLH158	*ced-9* RNAi in pL4440 in HT115 *E. coli*	
pMLH167	*punc-25::C. briggsae coq-1 cDNA*	
pMLH171	*psur-5::C.briggsae coq-1 cDNA*	
pMLH181	*psur-5::SOD-2::GFP::unc-54 3'UTR*	
pMLH235	*pmyo-3::GFP::unc-10 3'UTR*	
pMLH258	*psur-5::COQ-1::GFP::unc-54 3'UTR*	
pMLH260	*punc-25::COQ-1::GFP::unc-54 3'UTR*	
pMLH262	*punc-25(HindIII-SphI—XbaI-AscI)::TOM20::GFP*	
pMLH263	*pceh-22::TOM20::GFP::unc-10 3'UTR*	
pMLH264	*pmyo-3::TOM20::GFP::unc-10 3'UTR*	
pMLH269	*pceh-22::COQ-1::GFP::unc-54 3'UTR*	
pMLH270	*pmyo-3::COQ-1-GFP::unc-54 3'UTR*	
pMLH272	*pmyo-3::COQ-1::mCherry::unc-54 3'UTR*	
pMLH271	*pmyo-3::TOM20mRFP::unc-10 3'UTR*	
pMLH284	*pmyo-3::PDSS2::GFP::unc-54 3'UTR*	
pMLH289	*pF25B3.3::COQ-1::GFP::unc-54 3'UTR*	
pMLH290	*pdpy-7::COQ-1::GFP::unc-54 3'UTR*	
pMLH291	*pelt-2::COQ-1::GFP::unc-54 3'UTR*	
pMLH297	*pmyo-3::PDSS1::mCherry::unc-54 3'UTR*	
pMLH298	*punc-25(SphI-XbaI—KpnI-AscI)::COQ-1::GFP*	
pMLH300	*psur-5::human PDSS1::mCherry::unc-54 3'UTR*	
pMLH301	*psur-5::human COQ2::unc-54 3'UTR*	
pMLH302	*psur-5::human COQ2 (N401fsX415)*	
pMLH303	*psur-5::PDSS2-GFP::unc-54 3'UTR*	
pG2M02	*pmyo-3::TOM20::mRFP*	a gift from Toshihiko Oka
pG2M07	*podr-1::mCherry*	a gift from Geraldine Maro
pG2M10	*psur-5::NLS::GFP (pTG96)*	a gift from David Fay
pG2M19	*pceh-22::GFP (pCW2.1)*	a gift from Oliver Hobert
pG2M20	*punc-122::GFP*	a gift from Daniel Colon-Ramoz

pG2M26	GD1 (delta ubiG *E. coli*)	a gift from Cathy Clarke
pG2M27	KO229::pSN18 (Q9)	a gift from Cathy Clarke
pG2M30	*pBlueScript II*	
pG2M31	*rol-6(d) (pRF4)*	
pG2M36	*pmyo-3::dsRed (pJER1)*	
pG2M43	Human PDSS1 wild-type	a gift from Agnes Rotig
pG2M44	Human PDSS1 D308E	a gift from Agnes Rotig
pG2M45	Human PDSS2 wild-type	a gift from Agnes Rotig
pG2M46	Human PDSS2 S382L	a gift from Agnes Rotig
pG2M47	Human COQ2 wild-type	a gift from Agnes Rotig
pG2M48	Human COQ2 *N401fsX415*	a gift from Agnes Rotig
pG2M49	*elt-2 promoter*	a gift from Jim McGhee
pG2M50	*pdpy-7::swip-10::unc-54 3'UTR*	a gift from A. Hardaway
pG2M52	*psur-5::luc+GFP (pSLGCV)*	a gift from Cristina Lagido
pG2M57	yk1514f03 in pME18S-FL3	a gift from Yuji Kohara
pG2M58	yk1479d10 in pME18S-FL3	a gift from Yuji Kohara
pG2M60	*punc-25::CFP (pSC392)*	a gift from Yishi Jin
pG2M61	KO229:pKA3 (Q8)	a gift from Cathy Clarke
pG2M62	KO229:pLD23 (Q10)	a gift from Cathy Clarke
pRLS26	*goa-1* RNAi in pL4440	made by Rachel Skelton

Table 3.5: Transgenic arrays that were generated for this work.

Transgenic Array	Genotype Injected	Plasmid Name	Concentration
wdEx807 [psur-5::C.briggsae coq-1 cDNA, psur-5::NLS::GFP]	N2	pMLH171	25 ng/µL
		pG2M30	25 ng/µL
		pG2M10	25 ng/µL
wdEx831 [pttr-39::coq-1 RNAi FWD, pttr-39::coq-1 RNAi REV, punc-25::mCherry, pceh-22::GFP]	*eri-1(mg366) juIs223* IV	pMLH107	10 ng/µL
		pMLH112	10 ng/µL
		pMLH132	15 ng/µL
		pG2M19	15 ng/µL
		pG2M30	30 ng/µL
wdEx926 [psur-5::coq-1::GFP, podr-1::mCherry]	*coq-1(ok749)/hT2 (I; III); juIs223 IV*	pMLH258	25 ng/µL
		pG2M07	25 ng/µL
		pG2M30	50 ng/µL
wdEx933 [punc-25::COQ-1::GFP, coel::GFP]	*coq-1(ok749)/hT2 (I; III); juIs223 IV*	pMLH260	25 ng/µL
		pG2M20	25 ng/µL
		pG2M30	50 ng/µL
wdEx934 [pmyo-3::COQ-1::GFP, coel::GFP]	*coq-1(ok749)/hT2 (I; III); juIs223 IV*	pMLH270	20 ng/µL
		pG2M20	25 ng/µL
		pG2M30	55 ng/µL
wdEx935 [pmyo-3::coq-1::GFP, pmyo-3::TOM20mRFP, rol-6(d)]	N2	pMLH270	20 ng/µL
		pMLH271	20 ng/µL
		pG2M31	25 ng/µL
		pG2M30	35 ng/µL
wdEx938 [pmyo-3::hPDSS2::GFP, pmyo-3::TOM20::mRFP, rol-6(d)]	N2	pMLH271	20 ng/µL
		pMLH284	20 ng/µL
		pG2M31	25 ng/µL
		pG2M30	35 ng/µL
wdEx939 [pceh-22::COQ-1::GFP, rol-6(d)]	*coq-1(ok749)/hT2 (I; III)*	pMLH269	10 ng/µL
		pG2M31	25 ng/µL
		pG2M30	65 ng/µL
wdEx940 [pF25B3.3::COQ-1::GFP, rol-6(d)]	*coq-1(ok749)/hT2 (I; III)*	pMLH289	20 ng/µL
		pG2M31	25 ng/µL
		pG2M30	55 ng/µL
wdEx941 [pelt-2::COQ-1::GFP, rol-6(d)]	*coq-1(ok749)/hT2 (I; III)*	pMLH291	10 ng/µL
		pG2M31	25 ng/µL
		pG2M30	650ng/µL
wdEx942 [psur-5::human COQ2-wt, psur-5::NLS::GFP]	*coq-2(ok1066)/hT2 (III;I); wpIs39 X*	pMLH301	25 ng/µL
		pG2M10	25 ng/µL
		pG2M30	50 ng/µL
wdEx943 [psur-5::human COQ2-mutant, psur-5::NLS::GFP]	*coq-2(ok1066)/hT2 (III;I); wpIs39 X*	pMLH302	25 ng/µL
		pG2M10	25 ng/µL
		pG2M30	50 ng/µL

Miller coq-1 RNAi

The Miller *coq-1* RNAi clone (573bp of *coq-1* cDNA, Fig. 3.4A) was amplified (GoTaq, Promega) from pMLH018 and inserted into pCR8/GW/TOPO using a TOPO TA reaction to make pMLH104. PmeI (added to both primers) was used to subclone the Miller *coq-1* RNAi into pRLS26 to create pMLH129 that was subsequently transformed into HT115 (DE3) *E. coli* for RNAi studies (Timmons et al. 2001).

Miller *unc-25* RNAi

The Miller *unc-25* RNAi clone was generated by amplifying (GoTaq, Promega) 1.1kb of the *unc-25* cDNA from N2 cDNA using primers that flanked the amplicon with PmeI restriction sites. *unc-25* RNAi was inserted into pMLH158 between PmeI sites to create pMBM009 which is in HT115 (DE3) *E. coli* (Timmons et al. 2001).

C-terminal GFP and mCherry tags

pCJS93 used as a template to PCR amplify *GFP::unc-54 3'UTR* (Phusion High-Fidelity DNA Polymerase, New England Biolabs) for insertion into pMLH171 with 5'SacII/3'ApaI (added to the primers). *mCherry::unc-54 3'UTR* was amplified from pMLH103 (Phusion High-Fidelity DNA Polymerase, New England Biolabs) and inserted into pMLH270 with 5'SacII/3'ApaI (added to the primers) to make pMLH272.

Both mCherry and GFP are kept in frame by removing the stop codon (last three nucleotides) of the CDS (coding DNA sequence); this C-terminal fluorescent tag is linked to the protein by a 5 amino acid linker (PREEK). COQ-1, PDSS1 and PDSS2 were fluorescently tagged using this method.

coq-1::GFP

Due to a frame-shifting nucleotide insertion in exon 8 of *coq-1* in pG2M57 (yk1514f03), a second *coq-1* cDNA clone pG2M58 (yk1479d10) was obtained from Yuji Kohara (National Institute of Genetics, Japan). yk1479d10 was PCR amplified (GoTaq, Promega) and TOPO TA cloned into pCR8/GW/TOPO to create pMLH023. A *coq-1::GFP* fusion construct was generated by amplifying *coq-1* from pMLH023 (Phusion High-Fidelity DNA Polymerase, New England Biolabs) and inserting it into pMLH188 using 5'AscI/3'SacII (added to the primers) to create pMLH260.

C. briggsae coq-1 cDNA

Whole-animal *C. briggsae* cDNA was obtained by RT-PCR from total RNA from AF16 (obtained from the CGC). The *C. briggsae coq-1* cDNA (1.2kb) was amplified (Phusion High-Fidelity DNA Polymerase, New England Biolabs) and inserted into pMLH35 with 5'AscI/3'SacII (added to the primers) to make pMLH167. The *sur-5* promoter was subcloned from pMLH90 (5'SphI/3'AscI') to make pMLH171.

ttr-39 Promoter (D-Type GABA Neurons)

The 891 bp *ttr-39* promoter was amplified (GoTaq, Promega) from N2 genomic DNA with primers that added 5'SphI/3'AscI sites and TA TOPO cloned into a pENTR D-TOPO (Invitrogen) vector to make pMLH004. The *ttr-39* promoter inserted via 5'SphI/3'AscI to make pMLH107 and pMLH112.

sur-5 Promoter (All Cells)

The 3.7kb *sur-5* promoter (Gu et al. 1998) was amplified (GoTaq, Promega) from pG2M52 (Lagido et al. 2008) with primers that added 5'SphI/3'AscI and cloned into pCR8-TOPO (Invitrogen)

using a TOPO TA reaction (pMLH080). pMLH258 was created by subcloning *sur-5* from pMLH080 (5'SphI/3'AscI) into pMLH256.

myo-3 Promoter (Body Wall Muscle)

The *unc-25* promoter from pMLH132 was amplified (adding 5'HindIII/SphI and 3'XbaI/AscI/XbaI restriction sites to the primers) to create the intermediate vector (pMLH262) used to subclone the *myo-3* promoter. A 5'HindIII/3'XbaI digest added *pmyo-3* (2.4 kb) (Okkema et al. 1995) from pG2M36 to make pMLH264 and 5'AscI/3'ApaI was used to add COQ-1::GFP from pMLH260 to create pMLH270.

ceh-22 Promoter (Pharynx)

The intermediate vector (pMLH262) described above for the *myo-3* promoter was also used to subclone *pceh-22* (2.8 kb) 5'SphI/3'XbaI from pG2M19 (Okkema et al. 1997) to create pMLH263. pMLH269 was made by digesting COQ-1::GFP 5'AscI/3'ApaI from pMLH260 and adding it to pMLH263.

dpy-7 Promoter (Hypodermis)

pMLH290 was created by subcloning the *dpy-7* promoter (346 bp) (Gilleard et al. 1997) from pG2M50 (a gift from Andrew Hardaway, Blakely lab) with 5'SphI/3'AscI into pMLH260.

elt-2 Promoter (Intestine)

pMLH298 is an intermediate plasmid that was generated by PCR amplifying the *unc-25* promoter from pMLH132 (with primers that add 5'SphI/XbaI and 3'AscI/KpnI) and inserting it into

pMLH290 (5'SphI/3'AscI). The *elt-2* promoter (5 kb) (Fukushige et al. 1998) was subcloned from pG2M49 (a gift from Jim McGhee) into pMLH298 with 5'XbaI/3'KpnI to create pMLH291.

F25B3.3/rgef-1 Promoter (All Neurons)

The *F25B3.3*/pan-neural promoter (3.5kb) (Altun-Gultekin et al. 2001) was PCR amplified (GoTaq, Promega) from pG2M59 and inserted into pCR8-TOPO (Invitrogen) using a TOPO TA reaction to create pMLH081. The pan-neural promoter was then inserted into pMLH102 with 5'SphI/3'AscI (added to the primers) to produce pMLH113. Due to an SphI site 100bp into the F25B3.3 promoter, a second SphI digest was performed to include this 5' fragment from pMLH081, which was lost in pMLH113, to make pMLH121. COQ-1::GFP from pMLH270 was added using a 5'AscI/3'PacI digest to create pMLH289.

TOM20::mRFP (Outer Mitochondrial Membrane Localization)

The outer mitochondrial membrane marker, TOM20::mRFP, was created by fusing the first 54 nucleotides of TOM20 (*F23H12.2*) to mRFP (Ichishita et al. 2008). TOM20::mRFP was PCR amplified (GoTaq, Promega) from pG2M002 (a gift from Toshihiko Oka) and inserted into pMLH009 using 5'AscI/3'SacII added to primers to create pMLH035.

Human PDSS1

PDSS1 was amplified (Phusion High-Fidelity DNA Polymerase, New England Biolabs) from pG2M43 (Mollet et al. 2007) and ligated into pMLH272 (5'AscI/3'SacII) to make pMLH297.

Human PDSS2

PDSS2 was amplified (Phusion High-Fidelity DNA Polymerase, New England Biolabs) from pG2M45 (López et al. 2006) and inserted into pMLH270 (5'AscI/3'SacII) to make pMLH284.

Human COQ2

Wild-type and mutant COQ2 were amplified (KAPA HiFi DNA Polymerase) from pG2M47 and pG2M48 (Mollet et al. 2007), respectively, and inserted into pMLH280 with 5'KpnI/3'EcorI (added to the primers) to make pMLH301 and pMLH302.

Generation of CoQ_9-producing bacterial feeding plates

KO229 *E. coli* (pKA3/Q_8 or pSN18/Q_9) was grown overnight in Luria-Bertani (LB) ampicillin (AMP) + chloramphenicol (CAM) cultures. This overnight starter culture (125uL) was used to inoculate 12.5mL LB + AMP cultures. After approximately 8 hours of growth (OD ~1.0), cultures were centrifuged (3.8K RPM, 6 minutes) and the pellet was resuspended in 0.5mL M9. NGM plates (60mm) were seeded with 0.25mL bacterial slurry. *E. coli* strains (KO229:pKA3 (Q_8), KO229:pSN18) were provide by Cathy Clarke (UCLA) (Gomez et al. 2009; Saiki, Lunceford, Bixler, et al. 2008a).

RNAi

Feeding RNAi was performed as described in **Chapter 2 – Materials and Methods**. DNA concentrations used to create the transgenic *coq-1*-csRNAi array are listed in Table 3.5.

Brood size assays

For COQ-1::GFP rescue experiments, WT*, coq-1(ok749)*, or transgenic *coq-1* mutants (all sharing the *juIs223* transgene to mark D-type GABA neurons) were picked at the L4 stage to individual plates and maintained at 20°C. The number of hatched L1s per animal was quantified and averaged across a population to generate the average brood size per genotype (Hodgkin & Barnes 1991). The Human COQ2 rescue experiment used the same technique except that all strains contained *wpIs39* to label GABA neurons instead of *juIs223*.

GABA neurodegeneration assay

Percent GABA neurodegeneration was performed as described in **Chapter 2 – Materials and Methods**. RME and D-type neurons were counted for the data in Figure 3.5D; wild-type animals have four RME and 19 D-type neurons. The experimenter was blinded to genotype to avoid bias.

Protein sequence alignments and phylogenetic tree generation

The DNAstar Megalign software (use provided by the Blakely lab) was used for Clustal V protein sequence alignments and phylogenetic tree generation. Accession numbers for proteins used are as follows: *M. musculus*: NP_062374.2 (PDSS1); *D. rerio*: NP_001017656.1 (pdss1); *H. sapiens*: NP_055132.2 (PDSS1), NP_065114.3 (PDSS2), NP_056512.5 (COQ2); *D. melanogaster*: NP_733425.1 (qless); *C. elegans*: NP_491588.1 (COQ-1), NP_498513.1 (COQ-2A), NP_498512.1 (COQ-2B), NP_871682.1 (COQ-2C), NP_871683.1 (COQ-2D), NP_871684.1 (COQ-2E); *C. briggsae*: XP_002639605.1 (COQ-1); *S. pombe:* NP_595276.1 (dps1); *S. cerevisiae*: NP_009557.1 (COQ1).

Microscopy

A Zeiss Axioplan compound microscope with a 100x objective was used to capture the images in Figure 3.2 and 3.4. The representative images collected for Figure 3.5 and 3.7 were taken on a Leica TCS-SP5 confocal microscope with a 63x objective using the Leica Application Suite Advanced Fluorescence (LAS-AF) software.

Experimental contributions

Meg Mitchell built pMBM009 (*unc-25* RNAi).

RESULTS

Mutations that disrupt different steps in the CoQ biosynthetic pathway display heterogeneous phenotypes

We have previously shown that RNAi knockdown of the biosynthetic enzyme *coq-1* results in selective degeneration of GABAergic neurons in *C. elegans* (Earls et al. 2010) (**Chapter 2**). However, given my recent discovery that RNAi efficacy can vary with genotype (see **Appendix A**), I have also pursued an RNAi-independent method to induce CoQ deficiency. For this approach, GABA neurodegeneration was assayed in mutants with defects in the Coenzyme Q biosynthetic pathway genes *coq-1, coq-2*, *coq-3, coq-4, coq-5* and *coq-8* (Fig. 3.1, Table 3.6).

Chapter 2 describes experiments with *coq-1, coq-2*, and *coq-3* mutants that resulted in necrotic cell death (i.e., swollen cell soma) of adult GABA motor neurons (Fig. 2.2, Fig. 2.3). The similar neurodegenerative phenotypes of mutants in these three different CoQ biosynthetic pathway genes confirm the hypothesis that CoQ deficiency is responsible for GABA neuron death. However, these mutants also showed phenotypic differences in other traits that are indicative of heterogeneous effects. For example, most *coq-1(ok749*) animals arrest at the L3 larval stage, with few adult escapers. L3 arrest has been observed for other mitochondrial-impaired mutants and has been attributed the need for a large mitochondrial expansion (at the L3-to-L4 transition) to meet increasing energy demands (Tsang et al. 2001). In contrast, *coq-2* and *coq-3* mutants develop to become sterile adults (Table 3.6). Thus, mutations affecting distinct steps in the CoQ biosynthetic pathway (*coq-1* versus *coq-2*, *coq-3*) result in developmental arrest at different developmental ages (L3 versus adult). Our analysis determined that mutations in other CoQ biosynthetic genes also display a range of phenotypic defects. For example, *coq-4* mutants are viable, *coq-5* animals arrest larvae and *coq-8* mutants reach the adult stage but are sterile (Table 3.6). Of these three mutants, only *coq-8* shows a GABA neuron degeneration defect (Fig. 3.2). This phenotype could not be scored

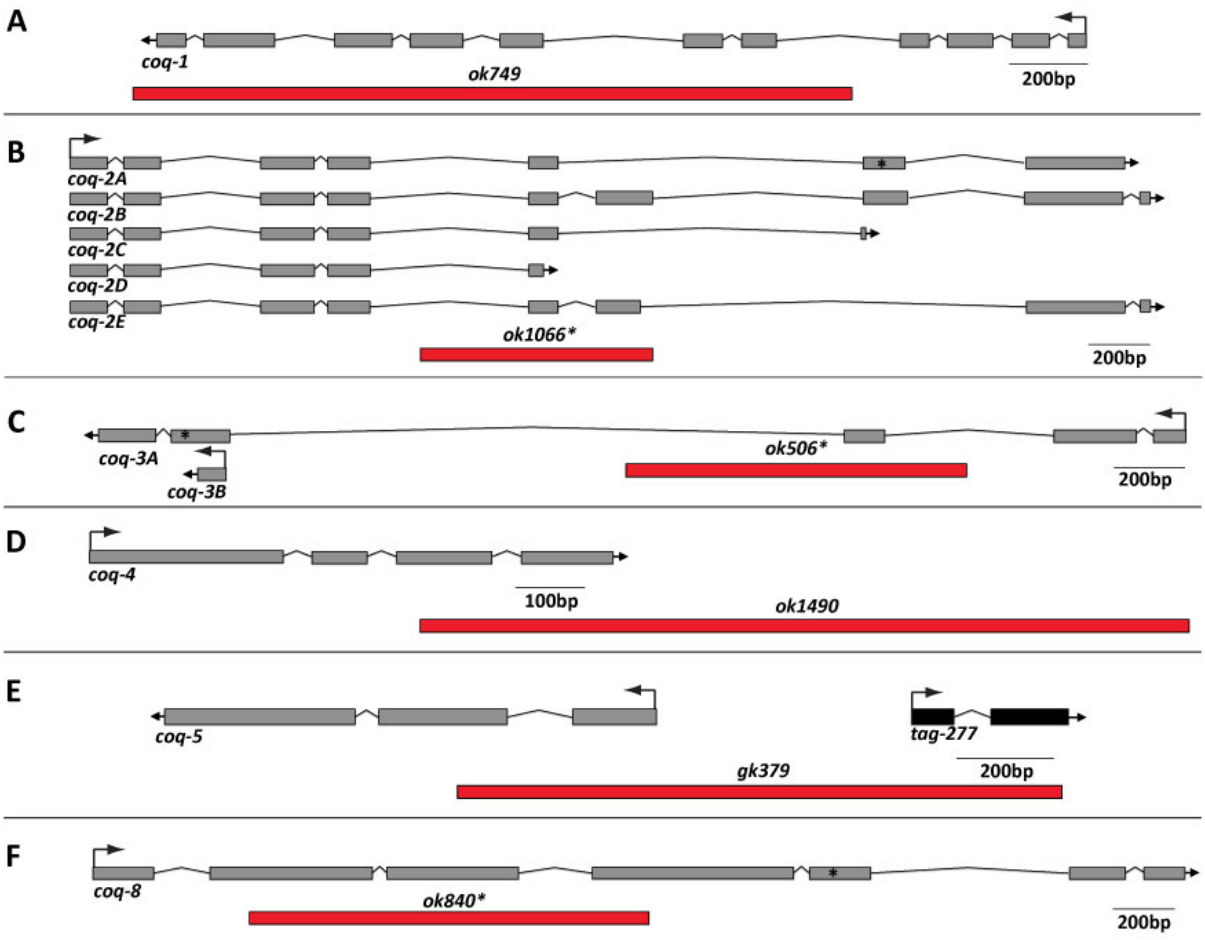

Figure 3.1: Deletion alleles of Coenzyme Q biosynthetic genes. A. *ok749* is an 1860bp deletion that removes the C-terminal 7 exons of (of 11 total) of *coq-1.* **B.** *coq-2* is predicted to encode five isoforms, and *ok1066* corresponds to a 708 bp deletion that disrupts all five *coq-2* splice variants. *ok1066* also introduces a premature stop codon (*). **C.** There are two predicted isoforms of *coq-3*. The *ok506* allele deletes 957bp of the genomic sequence, removing the third exon of *coq-3A* and adds an early stop codon in exon 4 (*). **D.** The N-terminus of *coq-4* is not affected by the *ok1490* deletion (1210bp). **E.** The *gk379* mutation (1228 bp deletion) removes 5' terminal exons of *coq-5* and adjacent gene, *tag-277.* **F.** *coq-8(ok840)* is a 1238bp deletion that removes sequences from exons 2, 3, and 4 and creating a premature stop codon in exon 5 (*). Genomic regions and deletions were compiled from genomic models provided on WormBase.

Table 3.6: Mutants of Coenzyme Q biosynthetic pathway genes display a range of phenotypes. The developmental and GABA neurodegeneration phenotypes of homozygous CoQ biosynthetic pathway mutants are listed. Adults with mutations in *coq-1, coq-2, coq-3,* or *coq-8* display features of necrotic GABA neurodegeneration. There are no signs of GABA neuron degeneration in *coq-4* mutants and *coq-5* animals arrest before cell death can be assayed.

Gene (Allele)	Developmental Phenotype	GABA Neurodegeneration
coq-1(ok749)	larval arrest	Yes (in adult escapers)
coq-2(ok1066)	sterile adults	Yes
coq-3(ok506)	sterile adults	Yes
coq-4(ok1490)	viable	No
coq-5(gk379)	larval lethal	N/A*
coq-8(ok840)	sterile adults	Yes

* no adults to score

in *coq-5* animals due to their early larval arrest. The severe phenotype of *coq-5* animals could result from the *gk379* deletion that is predicted to disable both *coq-5* and the adjacent *tag-277* gene. In contrast, *coq-4* mutant animals are viable and fertile and do not show evidence of GABA neuron degeneration. Although the exact enzymatic function of COQ-4 has not been directly determined, it is predicted to serve as a hydroxylase or carboxylase to modify the benzoquinone ring (Tran & Clarke 2007). The relatively mild *coq-4* phenotype could also be indicative of a hypomorphic effect arising from the C-terminal *ok1490* deletion (Fig. 3.1). Additionally, Coenzyme Q deficiency is a clinically heterogeneous syndrome that presents with symptoms ranging from severe infantile multisystem disease to adult-onset cerebellar ataxia (Emmanuele et al. 2012). These differences could arise from a combination of gene-specific effects and allelic differences. The diverse phenotypic effects of mutations in different genes of the *C. elegans* CoQ pathway parallel observations of CoQ deficiency in humans and thus could be useful for modeling the roles of specific genetic alleles in pathological effects arising from inadequate biosynthesis of CoQ.

The regulatory Coenzyme Q gene coq-8 is also required for GABA neuron viability

Examination of *coq-8(ok840)* animals confirmed previous reports of an adult sterile phenotype (Table 3.6) (Asencio et al. 2006; Asencio et al. 2009). Other CoQ knockouts (*coq-2* and *coq-3*) show signs of GABA neuron cell death early in adulthood, typically within 4-6 days after hatching (Fig. 2.2). Notably, *coq-8* mutants do not display characteristics of GABA neurodegeneration (i.e., defasciculation, neuronal process beading or breaks, cell soma loss) until a later stage, 7-8 days after hatching (Fig. 3.2A). Nonetheless, degenerating GABA neurons in *coq-8* animals share morphological

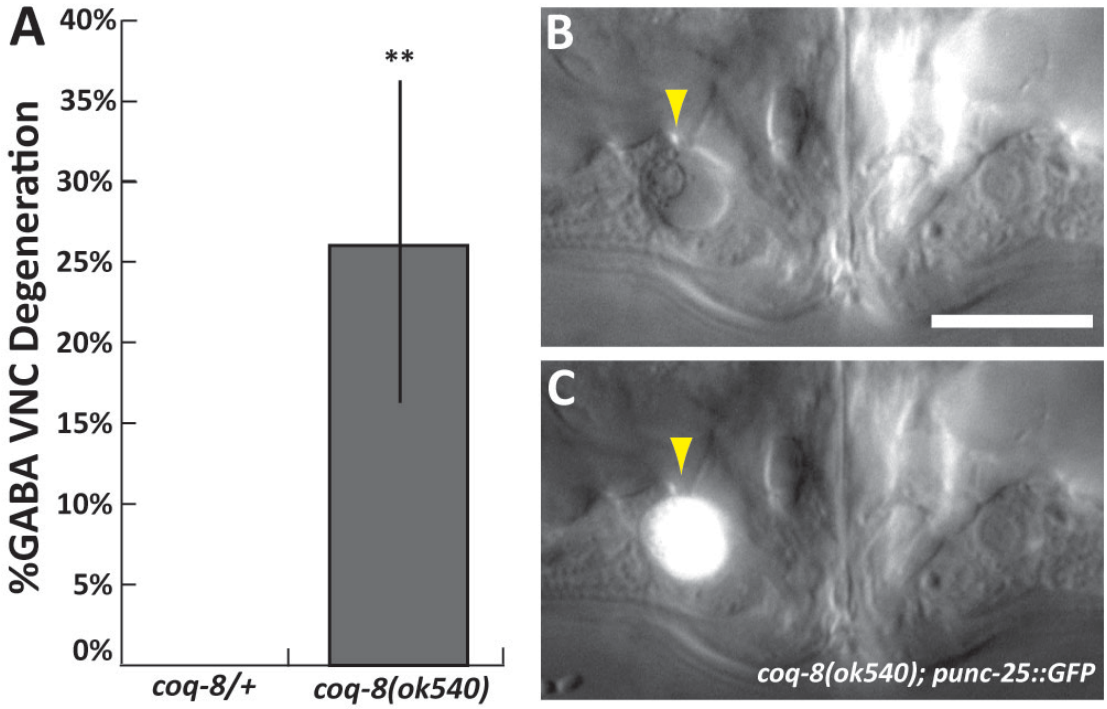

Figure 3.2: Necrotic GABA neuron degeneration occurs in older *coq-8(ok540)* adults. A. GABA neuron degeneration is pronounced in 8 day old homozygous *coq-8(ok540)* mutants but not in *coq-8* heterozygous animals. ** p<0.0001. **B.** The VD7 GABAergic neuron, adjacent to the vulva, shows a swollen, necrotic appearance (yellow arrowhead). Scale bar = 10µM. **C.** *punc-25::GFP* expression confirms GABAergic identity (yellow arrowhead).

features (i.e., swollen, necrotic-like soma) of other CoQ biosynthetic pathway mutants and thus suggest activation of a comparable death program with later onset of degeneration (Fig. 3.2B-C).

The function of COQ-8 in the CoQ biosynthetic pathway is not well understood. As with other CoQ synthetic mutant strains, yeast Coq8 mutants are CoQ-deficient and show respiratory defects (Do et al. 2001). However, unlike other CoQ synthetic proteins, COQ-8 is not believed to directly modify CoQ intermediates during biosynthesis. Instead, COQ-8 is predicted to have a regulatory role, based on its homology to the ABC-1 family of protein kinases (Asencio et al. 2006; Asencio et al. 2009). Kinase-dependent activation of other CoQ enzymes by COQ8 has been proposed, and Coq3p, Coq5p and Coq7p are phosphorylated in a Coq8p-dependent manner (Xie et al. 2011). However, Coq8 kinase activity has not been experimentally confirmed. Interestingly, patients with ADCK3/COQ8 mutations present with milder symptoms compared to those with mutations that disrupt catalytic CoQ enzymes (Lagier-Tourenne et al. 2008). This finding parallels the mild GABA neurodegeneration defect (i.e., late-onset) in *coq-8* animals compared to other CoQ biosynthetic pathway mutants (e.g., *coq-2)* and could reflect similar roles for the COQ-8 protein in nematodes and humans.

Except for *coq-4(ok1490),* which may not result in a null phenotype, GABA neuron degeneration is observed in CoQ pathway mutants that develop to adult stages (Fig. 2.2, Fig. 3.2, Table 3.6). As noted above, GABA neuron degeneration is not observed in mutant animals that die during larval development (e.g., *coq-5*). The correlation between developmental stage and neurodegeneration also suggests that age-dependent mechanism contribute to GABA neuron death arising from CoQ depletion.

Dietary CoQ influences developmental progression and GABA neurodegeneration

Experimental use of *coq-1(ok749)* is limited because the majority of these animals fail reach the adult stage at which GABA neuron degeneration is observed. This severe phenotype is observed even for *coq-1* animals grown on an *E. coli* strain (OP50) which produces CoQ_8. *coq-1(ok749)* viability is substantially enhanced, however, by growth on an *E. coli* strain that produces CoQ_9 (the endogenous *C. elegans* CoQ isoform, Table 1.1) (Rodríguez-Aguilera et al. 2005). This observation suggests that *coq-1* mutants fed CoQ_9-producing bacteria incorporate sufficient levels of CoQ_9 from their diet to develop to adulthood and thereby increase the frequency of the GABA neurodegeneration phenotype. I have confirmed this result by growing *coq-1* animals on a CoQ_9-producing bacterial strain. An *E. coli* strain (KO229) that is mutant for the *coq-1* homolog (ispB) was used for this experiment. The ispB mutation is lethal but can be complemented with plasmids encoding polyprenyl diphosphate transferases from other species (K et al. 1997; Okada et al. 1998). With this approach, it is possible to engineer viable bacterial strains that produce CoQ derivatives with isoprenoid side chains of different lengths. For example, the ispB mutant strain KO229:pSN18 produces CoQ_9. *coq-1* mutants fed CoQ_9-producing KO229 bacteria showed a significant shift from L3 arrest to the adult stage (Fig. 3.3B) thus confirming earlier results suggesting that a CoQ_9-containing diet is sufficient to restore viability to *coq-1* mutant animals. Although the presence of a mature vulva indicated that these *coq-1* animals were adults, they were significantly smaller than heterozygous siblings (Figure 3.3A) and displayed severe morphological abnormalities including large vacuolated regions in various tissues (Fig. 3.3D). This result suggests that uptake and utilization of exogenous CoQ_9 may be less efficient than that of endogenously synthesized CoQ. Nonetheless, *coq-1* adults fed CoQ_9-producing *E. coli* (KO229) showed significantly more degenerating GABA neurons (Fig. 3.3C) than animals grown on the CoQ_8-producing OP50 *E. coli* strain (arrest at the L3

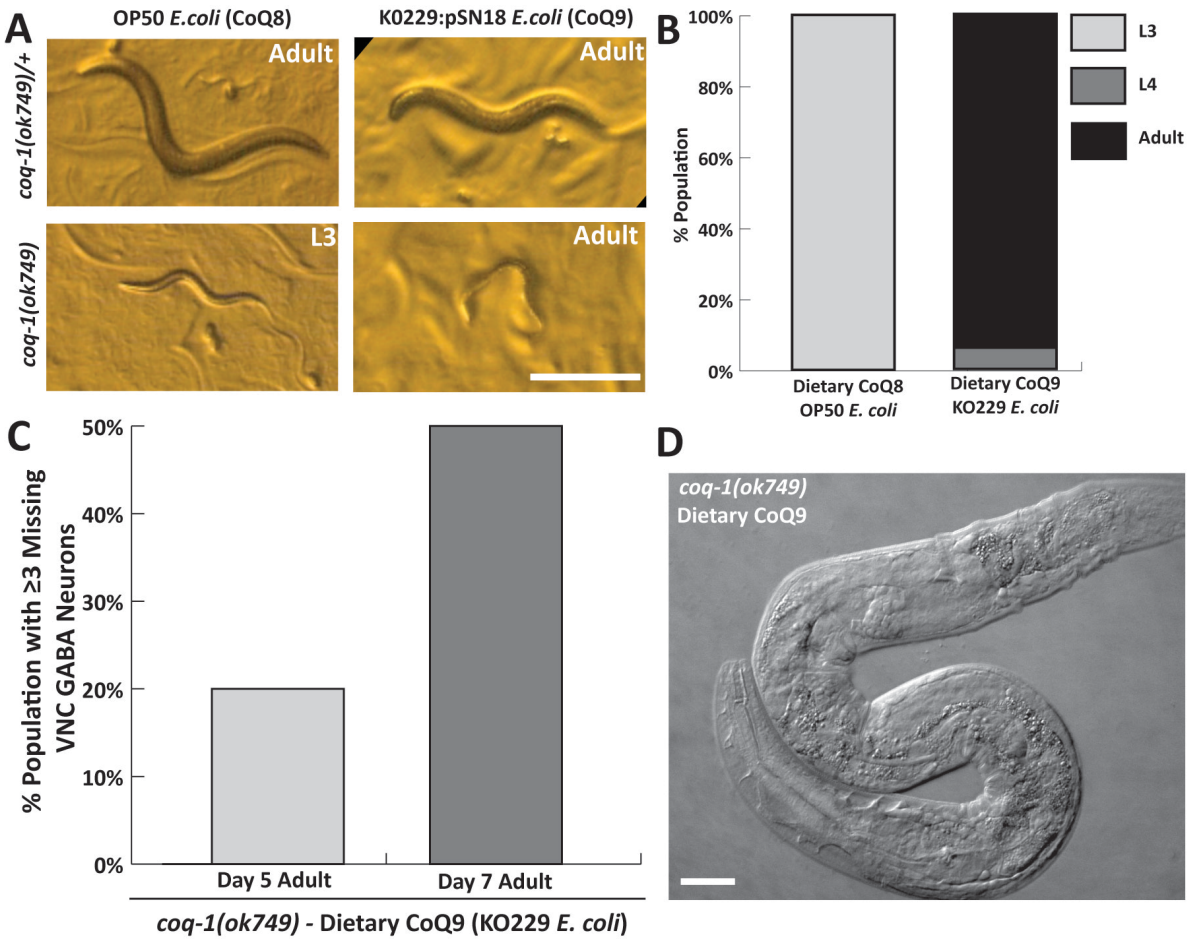

Figure 3.3: Bacterial diet influences developmental progression and GABA neurodegeneration of *coq-1(ok749)* mutants. A. Homozygous *coq-1* animals cultured on OP50 (CoQ_8-producing) bacteria arrest as L3 larvae. Dietary CoQ_9 from KO229 *E. coli* allows *coq-1* mutants to develop to adults that are significantly smaller than heterozygous animals siblings. Scale bar = 500µM. **B.** *coq-1* mutants fed a CoQ_8-producing diet (OP50) arrest at the L3 stage; homozygous *coq-1* animals cultured on KO229 (CoQ_9-producing) progress to adult stages. **C.** GABA neuron cell death increases with age in CoQ_9/KO229 fed *coq-1* animals. Animals grown on OP50 (CoQ_8) arrest at the L3 stage without missing GABA neurons (data not shown) **D.** *coq-1* adults show severe morphological defects. Scale bar = 20 µM.

stage without GABA neuron death, data not shown). These results are consistent with the hypothesis that provision of the dietary CoQ_9 isoform promotes development to the adult stage and consequent appearance of the GABA neuron degeneration phenotype.

Apoptotic GABA neuron death can occur rarely under distinct dietary CoQ conditions

CoQ deficiency arising from *coq-1* RNAi (Fig. 2.2C) or knockouts of *coq-1* (Fig. 2.3B-C)*, coq-2* (Fig. 2.2F-G)*, coq-3* (Fig. 2.2H)*,* or *coq-8* (Fig. 3.2B) reproducibly induces necrotic (i.e., swollen) GABA neurons. These experiments were performed animals with growth on either HT115 *E. coli* (*coq-1* RNAi) or OP50 *E. coli* (*coq-1, coq-2, coq-3, coq-8* mutants). Growth on the CoQ_9-producing *E. coli* strain KO229, however, resulted in rare instances of apoptotic GABA neurons for *coq-1* and *coq-2* mutants (Fig. 4.6, Fig. 3.4A-B). Apoptotic (i.e., raised, button-like) GABA neurons were also identified in *coq-1* mutants fed KO229:pKA3 (Q_8-producing diet) (Fig. 3.4C-D) (Fig. 4.6). It is currently unclear why GABA neurons predominantly die through necrosis under most CoQ deficiency paradigms and occasionally switch to death by apoptosis with other dietary conditions. Nevertheless, this finding indicates that CoQ-deficient GABA neurons are competent to undergo apoptotic as well as necrotic death.

Knockdown of *coq-1* exclusively in GABA neurons does not induce degeneration

Global reduction of *coq-1* in *C. elegans* produces an age-dependent loss in motor coordination and preferential degeneration of GABA motor neurons (see **Chapter 2**) (Earls et al. 2010). This finding highlights the importance of CoQ for GABA neuron viability but does not distinguish between cell autonomous verses non-cell autonomous roles of CoQ in GABA neuron survival. To investigate whether GABA neuron-specific production of *coq-1* is required to prevent neurodegeneration, I used two methods to induce cell-specific RNAi (csRNAi) knockdown of *coq-1* in

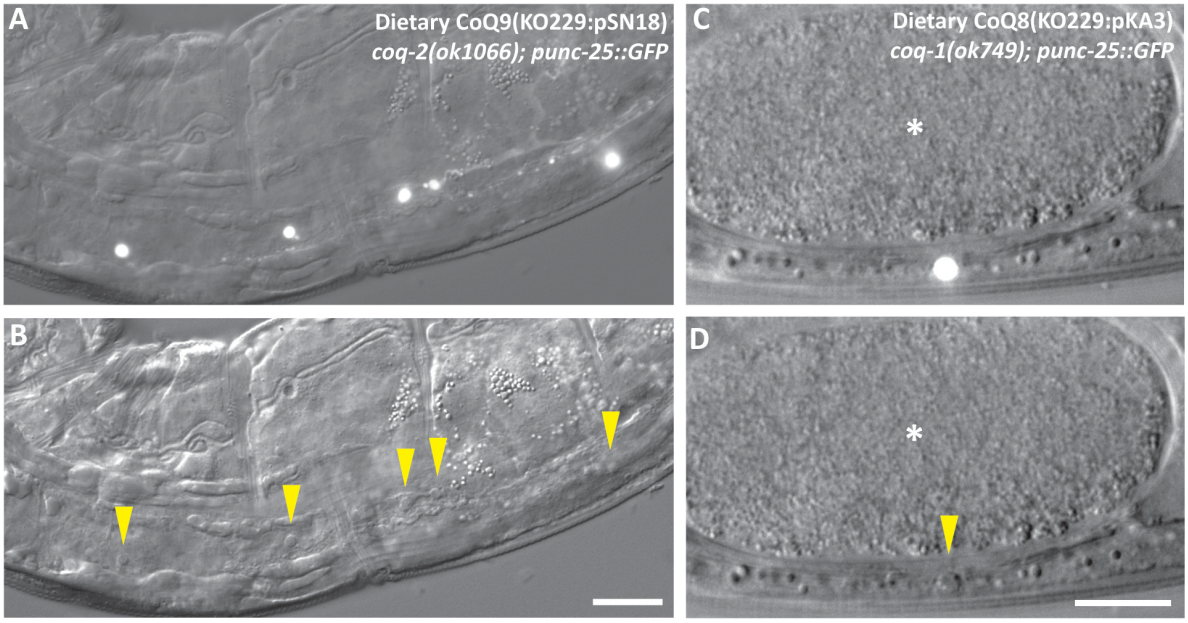

Figure 3.4: GABA neurons adopt apoptotic morphology in *coq-1* and *coq-2* mutants fed an alternative *E. coli* strain KO229. A. Five GABA neurons are marked by *punc-25::GFP* expression in a *coq-2(ok1066)* animal cultured on KO229:pSN18 (Q_9-diet). **B.** All five GABA neurons show a button-like morphology (yellow arrowheads) consistent with apoptotic death. **C.** A single GABA neuron in a *coq-1(ok749)* animal fed KO229:pKA3 (Q_8-diet). **D.** The apoptotic GABA neuron (yellow arrowhead) lies in the ventral nerve cord immediately beneath a single cell embryo (*) in the uterus. Scale bars = 10μM.

GABA neurons (Fig. 3.5). First, a *coq-1* feeding RNAi experiment was performed using transgenic strain XE1375 (provided by Marc Hammarlund, described in **Chapter 5**) in which GABA neurons are specifically sensitized to the RNAi effect. This experiment failed to produce evidence of dying GABA neurons in adult animals (data not shown) despite the fact that XE1375 includes the RNAi-sensitizing mutation, *eri-1(mg366)*, that facilitated global *coq-1* knockdown and GABA neuron degeneration in the earlier RNAi feeding experiments (Fig. 2.2). Control RNAi knockdown of *unc-25*/glutamic acid decarboxylase (GAD) generated a robust "shrinker" phenotype and therefore confirmed that GABA neurons are sensitive to RNAi in the XE1375 genetic background (Fig. 5.1). This result suggests that cell-specific knockdown of CoQ synthesis in GABA neurons is not sufficient to induce degeneration.

In a second independent experimental paradigm, I used an established method of cell-specific gene knockdown in which the forward and reverse strands of a *coq-1* cDNA sequence ("Miller *coq-1* RNAi", Fig. 3.5A) are transgenically expressed under the control of a GABA neuron-specific promoter (Tavernarakis et al. 2000; Petersen et al. 2011). The *coq-1* RNAi sequence in these constructs does not share significant homology with any other regions of the *C. elegans* genome (from BLAST sequence analysis) and therefore should selectively target the *coq-1* transcript (Fig. 3.5A). A global feeding *coq-1* RNAi assay with this "Miller *coq-1* RNAi" clone produces GABA neuron degeneration levels comparable to that of previous experiments with the Ahringer RNAi clone (Fig. 3.5B), and thus demonstrates that the "Miller *coq-1* RNAi" region is sufficient to induce a potent *coq-1* RNAi phenotype. For cell-specific RNAi, the *pGABA::coq-1 RNAi* transgenes were expressed in the *eri-1(mg366); punc-25::GFP(juIs76)* background that was also used for induction of GABA degeneration by global *coq-1* RNAi knockdown (Fig. 2.2). *pGABA::coq-1 RNAi* alone (no global RNAi treatment, data not shown) and control (empty-vector) RNAi conditions did not result in GABA neuron death (Fig. 3.5C-D). Furthermore, *pGABA::coq-1 RNAi* does not enhance the degeneration induced by global *coq-1* RNAi (Fig. 3.5C-D).

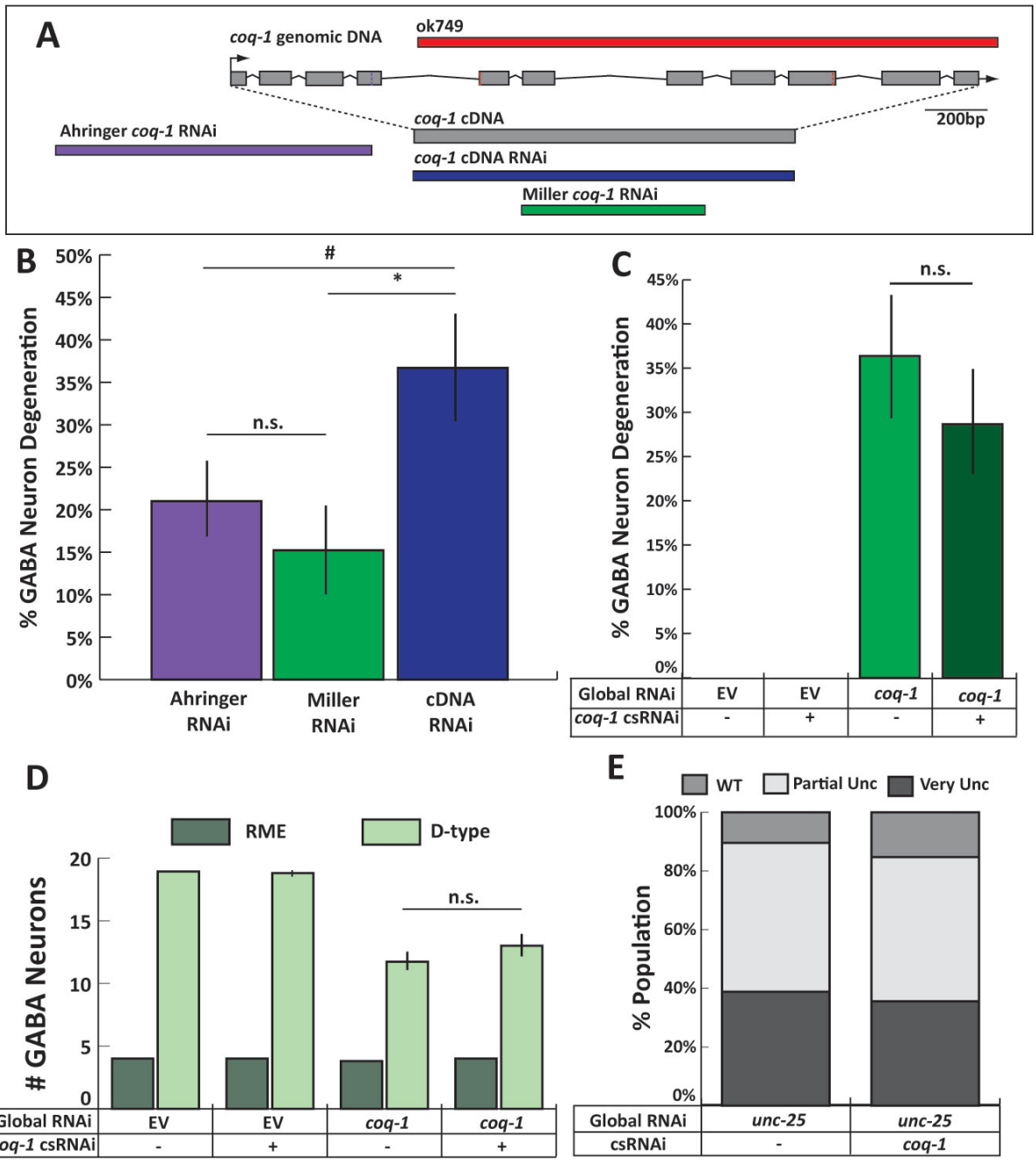
A
coq-1 genomic DNA
ok749
200bp
Ahringer coq-1 RNAi
coq-1 cDNA
coq-1 cDNA RNAi
Miller coq-1 RNAi
B
% GABA Neuron Degeneration
50%
45%
40%
35%
30%
25%
20%
15%
10%
5%
0%
#
*
n.s.
Ahringer RNAi
Miller RNAi
cDNA RNAi
C
% GABA Neuron Degeneration
45%
40%
35%
30%
25%
20%
15%
10%
5%
0%
n.s.
Global RNAi
coq-1 csRNAi
EV
EV
coq-1
coq-1
-
+
-
+
D
GABA Neurons
20
15
10
5
0
RME
D-type
n.s.
Global RNAi
coq-1 csRNAi
EV
EV
coq-1
coq-1
-
+
-
+
E
WT
Partial Unc
Very Unc
% Population
100%
80%
60%
40%
20%
0%
Global RNAi
csRNAi
unc-25
unc-25
-
coq-1

Figure 3.5: GABA neuron-specific knockdown of *coq-1* does not produce a GABA neurodegeneration defect. A. Schematic of *coq-1* genomic DNA, *coq-1* coding sequence (gray boxes), and *ok749* deletion (1860bp). Regions of *coq-1* targeted by RNAi clones are indicated: Ahringer (genomic), *coq-1* cDNA (cDNA), Miller *coq-1* (cDNA). **B.** "Miller *coq-1* RNAi" GABA neurodegeneration levels are not significantly (n.s.) different than with "Ahringer *coq-1* RNAi" treatment. The "cDNA *coq-1* RNAi" clone targets the entire coding sequence of *coq-1* and shows significantly higher levels of GABA neuron degeneration, # $p<0.02$, * $p<0.005$, $n>20$. **C.** Cell-specific RNAi (i.e., csRNAi) of *coq-1* exclusively in GABA neurons does not induce degeneration of GABA neuron processes. Under global *coq-1* RNAi treatment, the csRNAi transgene does not significantly (n.s.) enhance GABA degeneration versus animals without GABA neuron-specific knockdown. **D.** Quantification of the number of GABA neurons (RME, D-type) remaining after feeding control (EV) or *coq-1* RNAi. Cell-specific RNAi of *coq-1* does not reduce GABA neuron number or enhance the loss of GABA neuron cell bodies by global *coq-1* knockdown. **E.** Global RNAi of *unc-25* induces equally penetrant "shinker" (Unc) phenotypes in both the wild-type (WT) and *coq-1* csRNAi strains.

The *coq-1*-csRNAi transgenic array did not impair GABA neuron RNAi sensitivity as indicated by identical "shrinker" phenotypes in a global *unc-25* RNAi knockdown assay (Fig. 3.5E). These results suggest that robust *coq-1* production in GABA neurons is not required for their viability provided CoQ production is maintained in other tissues. Thus, the viability of GABA neurons under these conditions (i.e., GABA neuron-specific *coq-1* RNAi) likely results from the provision of CoQ by other cells. This model is supported by findings reported below, that the overall viability of CoQ-deficient animals can be rescued by CoQ expression in specific tissues. Alternatively, GABA neuron degeneration arising from a global CoQ deficit could be triggered by a "death signal" from another CoQ-deficient tissue. This question can be resolved by determining if CoQ synthesis in other cell types (e.g., body muscle, Fig. 3.6) can restore GABA neuron viability under conditions that otherwise result in GABA neuron degeneration (e.g, *coq-2* mutant).

Exogenous COQ-1::GFP localizes to mitochondria and rescues *coq-1(ok749)* defects

CoQ biosynthesis is predicted to occur in mitochondria because terminal CoQ biosynthetic enzymes (e.g., Coq2) localize to the inner mitochondrial matrix (Gin & Clarke 2005; A. Johnson et al. 2005; Tran & Clarke 2007). To determine the subcellular localization of COQ-1 in *C. elegans*, I generated a C-terminal GFP fusion (Fig. 3.6A) and co-expressed it in body-wall muscle with an outer mitochondrial membrane marker (TOM20::mRFP) (Ichishita et al. 2008). Co-localization of COQ-1::GFP and TOM20::mRFP confirms that COQ-1 also localizes to the mitochondria in *C. elegans* (Fig 3.6B).

Most *coq-1(ok749)* animals arrest at the L3 larval stage and are infertile. However, ubiquitous expression of COQ-1::GFP with the *sur-5* promoter restored *coq-1* mutant development and resulted in fertile adults that generated viable offspring (Fig 3.6C). The incomplete rescue of *coq- 1(ok749)* brood size by *psur-5::COQ-1::GFP* is likely due to mosaic inheritance of the rescuing

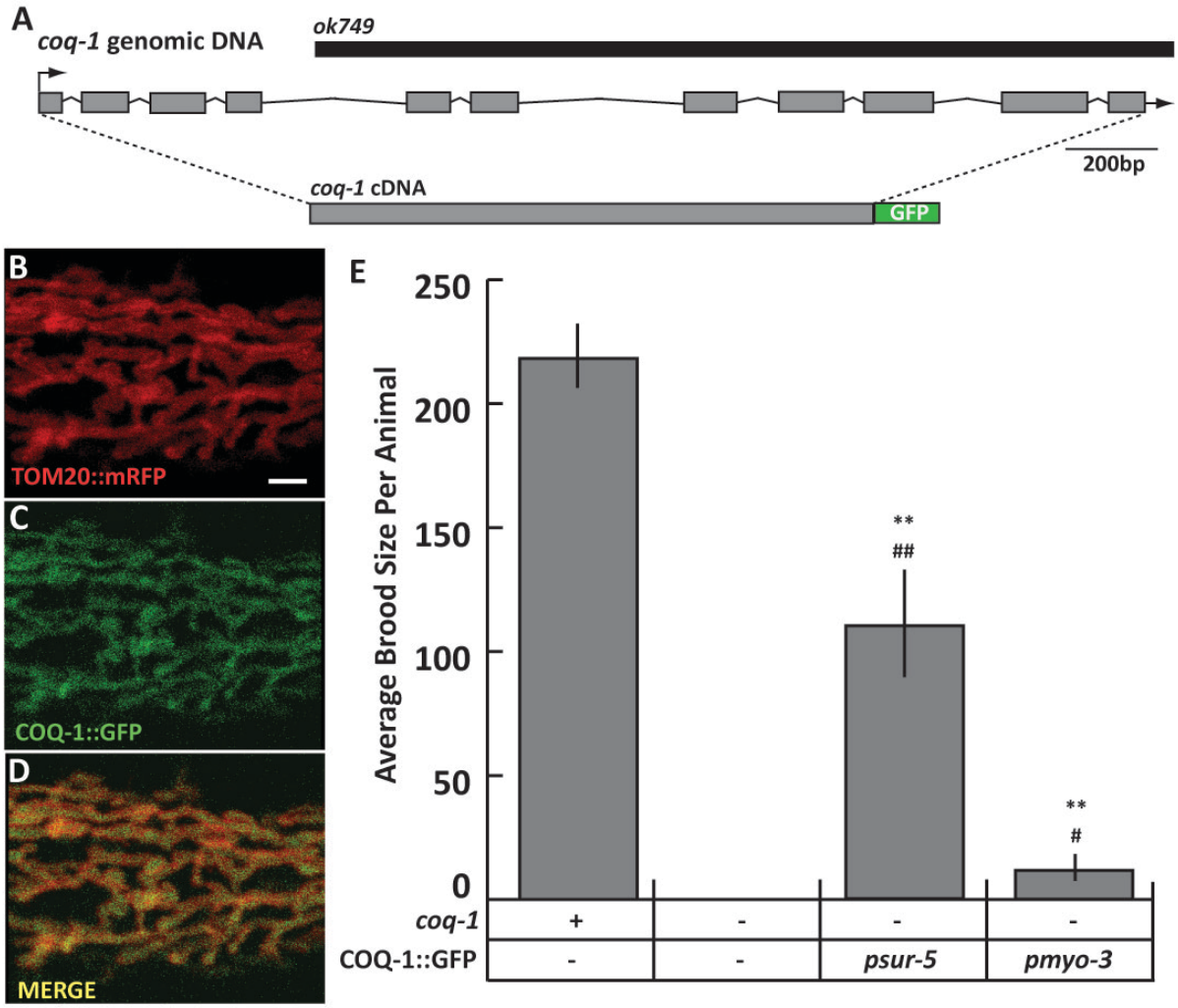

Figure 3.6: COQ-1::GFP localizes to mitochondria and rescues *coq-1* defects with either ubiquitous or muscle-specific expression. A. *coq-1* cDNA is C-terminally tagged with GFP. The region of the *ok749* deletion is indicated (black rectangle) **B.** TOM20::mRFP labels the outer mitochondrial membrane in body-wall muscle. Scale bar = 2µM. **C.** COQ-1::GFP also localizes to mitochondrial, as depicted in the merged image (**D**). **E.** Restoration of fertility in the *coq-1(ok749)* [i.e., *coq-1*(-)]mutant with ubiquitous (*psur-5*) or body-wall muscle-specific (*pmyo-3*) expression of COQ-1::GFP demonstrates restoration of function with the exogenous fusion protein. All strains contain the *juIs223 (pttr-39::mCherry)* transgenic background. **p<0.0001 vs *coq-1*(+), ##p<0.0001 vs *coq-1*(-), #p<0.0001 vs *coq-1(-); psur-5::COQ-1::GFP*, n=20. Note: *coq-1(-)* animals never produce progeny (brood size = 0), and p<0.03 for *coq-1(-); pmyo-3::COQ-1::GFP* vs *coq-1*(-).

transgenic array. This result shows that the COQ-1::GFP fusion protein is functional and thus that the C-terminal GFP tag does not disrupt COQ-1 enzymatic activity.

COQ-1::GFP expression in specific tissues restores fertility to *coq-1* mutant animals

Since GABA neuron-specific knockdown of *coq-1* did not recapitulate the neurodegeneration phenotype observed with global CoQ depletion (Fig. 3.5) and because intercellular CoQ transport has been detected in other organisms (Padilla-López et al. 2009; Fernández-Ayala et al. 2005), I hypothesized that CoQ from other cell types can compensate for a lack of CoQ synthesis in GABA neurons. This model predicts that CoQ production in a subset of cells could be sufficient to restore viability to *coq-1* mutants.

Because dietary CoQ_9 overcame the L3 lethality of *coq-1* mutants (Fig. 3.3), I reasoned that this phenotype (i.e., developmental arrest) would be a useful readout for CoQ intercellular transport. Based on previous experiments demonstrating functional rescue of *coq-1* mutants by ubiquitous COQ-1::GFP (Fig. 3.6), I constructed transgenic lines for expression of COQ-1::GFP in several different *C. elegans* tissues. Transgenic expression of COQ-1::GFP in pharyngeal muscle, intestine, nervous system, or GABA motor neurons did not overcome the larval arrest of *coq-1(ok749)* mutants (Table 3.7). Expression of the COQ-1 fusion protein was confirmed by presence of a GFP signal in these cell types (data not shown). In contrast, body muscle-specific expression of COQ-1::GFP overcame the developmental and sterility defects of *coq-1* animals (Fig. 3.6, Table 3.2). In these animals, the GFP signal (from COQ-1::GFP) was exclusively detected in body muscle (data not shown) and therefore suggests Coenzyme Q production is restricted to this tissue. Since body muscle function is not directly required for fertility, this result strongly supports the hypothesis that CoQ synthesized from muscle is transported to other CoQ-deficient tissues (e.g., germline, somatic gonad, etc) that are required for viability and fertility. The lack of rescue by COQ-1::GFP expression

Table 3.7: COQ-1 expression in body-wall muscle restores fertility to *coq-1* mutants.
COQ-1::GFP was expressed in specific tissues in the *coq-1(ok749)* mutant. Fertility is selectively rescued by either ubiquitous or body muscle-specific expression of COQ-1::GFP.

COQ-1::GFP Expression	Promoter	Genotype	Developmental Stage	Fertile
None	None	*coq-1*	L3	No
Ubiquitous	*sur-5*	*coq-1; wdEx926*	Adult	Yes (Fig. 3.6)
Pharynx	*ceh-22*	*coq-1; wdEx939*	L3	No
Intestine	*elt-2*	*coq-1; wdEx941*	L3	No
All neurons	*F25B3.3*	*coq-1; wdEx940*	L3	No
Body wall muscle	*myo-3*	*coq-1; wdEx934*	Adult	Yes (Fig. 3.6)
GABA neurons	*unc-25*	*coq-1; wdEx933*	L3	No

in the pharynx, intestine or nervous system could mean that CoQ production from specific tissues (e.g., muscle) is necessary for normal development. Alternatively, differential rescue could be due to higher levels of CoQ synthesis in muscle. This question could be resolved by quantifying CoQ production in these transgenic animals (Gomez et al. 2012).

Localization and function of human CoQ biosynthetic proteins are conserved in *C. elegans*

Proteins required for Coenzyme Q biosynthesis (Fig. 1.6) are highly conserved across phyla based on sequence homology and function; yeast Coq1, Coq2, Coq3 and Coq7 mutants are complemented by human homologues (Saiki et al. 2005; Forsgren et al. 2004; Jonassen & Clarke 2000; Vajo et al. 1999). However, human CoQ biosynthetic proteins have not been tested for function in multicellular organisms. To address this question, I obtained wild-type human PDSS1, PDSS2 (COQ-1 homologues) and COQ2 (Mollet et al. 2007). The Rotig lab also kindly provided mutant versions of these genes that were originally isolated from patients with Primary Coenzyme Q Deficiency. Here, I describe results demonstrating that the human COQ2 enzyme can drive CoQ biosynthesis in *C. elegans*.

COQ-1 shares phylogenetic similarity to PDSS1

Human PDSS1 and PDSS2 (Prenyl Diphosphate Synthase, Subunit 1 & 2) are homologues of *C. elegans* COQ-1. Long-chain *trans*-prenyl diphosphate synthases function as either homomers (i.e., *S.cerevisiae, A. thaliana*) or heteromers (i.e., *S. pombe, M. musculus, H. sapiens*) (Saiki et al. 2005), and the presence of only one polyprenyl diphosphate synthase in *C. elegans* suggests that it functions as a homomer. Phylogenetic analysis and protein sequence alignment reveals that COQ-1 most strongly resembles PDSS1 (Fig. 3.7), because PDSS2 lacks the aspartate-rich motifs in two of the seven conserved domains (II and IV) of *trans*-prenyl diphosphate synthases (Saiki et al. 2005).

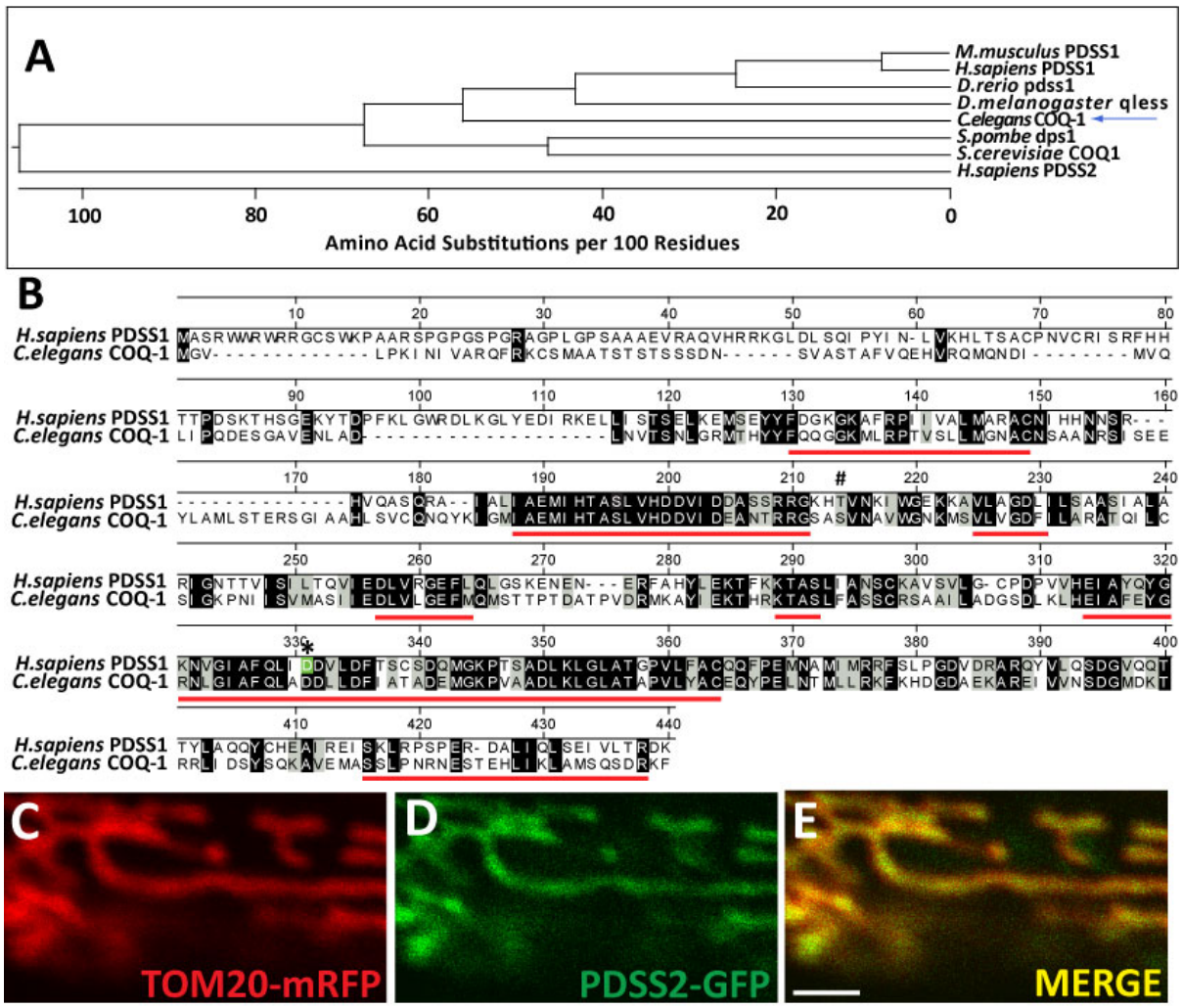

Figure 3.7: *C. elegans* COQ-1 is homologous to mitochondrially-localized human PDSS1 and PDSS2. **A.** Phylogenetic analysis of polyprenyl transferases implicated in Coeznyme Q production reveals that *C. elegans* COQ-1 (blue arrow) is more similar to human PDSS1 than PDSS2. **B.** Protein sequence alignment of Human PDSS1 and *C. elegans* COQ-1 shows 47% identity (black boxes) and 64% similarity (gray boxes). The seven conserved domains of polyprenyl transferases are denoated with the red underline (Jun et al. 2004). A missense mutation (S215N) in the *Drosophila qless* locus is marked (#) (Grant et al. 2010). A conserved aspartate (D) residue (*, green) is mutated (D308E) in a Coenzyme Q deficiency patient (Mollet et al. 2007). **C-E.** *C. elegans* body muscle mitochondria are labeled with the mitochondrial marker TOM20::mRFP (C) and with PDSS2::GFP (D). A merged image (E) confirms localization of PDSS2::GFP to mitochondria. Scale bar = 2 µM.

Exogenous PDSS2::GFP localizes to mitochondria

Trans-prenyl diphosphate synthases are reported to localize to mitochondrial (Gin & Clarke 2005) and also to ER, Golgi, and peroxisome membranes in some species (Jun et al. 2004; Turunen et al. 2004). Subcellular localization of the human proteins (PDSS1 and PDSS2) has not been investigated. PDSS2 labeled with a C-terminal GFP tag (PDSS2::GFP) was co-expressed with an outer mitochondrial membrane marker (TOM20::mRFP) in *C. elegans* body wall muscle. This experiment revealed that PDSS2::GFP localizes to mitochondria (Fig. 3.7C-E). Ubiquitously expressed PDSS1::mCherry also displays a punctate pattern consistent with mitochondrial localization (data not shown). This conclusion is also supported by the mitochondrial localization of PDSS2 since these proteins are predicted to form heteromeric complex (Saiki et al. 2005).

The mitochondrial localization of PDSS1 and PDSS2 in *C. elegans* suggests that these enzymes are properly trafficked to the site of CoQ biosynthesis (Fig. 3.7) (Tran & Clarke 2007). Future experiments could investigate whether these human homologues of COQ-1 also complement the *C. elegans coq-1* mutation. As mentioned previously, human PDSS1 and PDSS2 form a heterotetrameric enzyme that assembles the isoprenoid tail of Coenzyme Q (Saiki et al. 2005). Both PDSS1 and PDSS2 are required to rescue defects in *E. coli* and *S. pombe* (Saiki et al. 2005), and expression of wild-type PDSS1 alone was not sufficient to rescue growth defects to *S. cerevisiae coq1* mutants (Mollet et al. 2007). Based on these observations, I hypothesize that expression of both PDSS1 and PDSS2 will be required in *C. elegans* to rescue *coq-1* defects.

Fertility of C. elegans coq-2(ok1066) is rescued with expression of human COQ2

COQ2 corresponds to the *para*hydroxybenzoate polyprenyl transferase that generates the first membrane-bound molecule in the CoQ biosynthetic pathway (attaches the benzoquinone ring to the isoprene tail) (Fig. 1.6). Additionally, COQ2 is predicted to be an integral membrane protein in

the CoQ pathway. Tran and Clarke proposed that COQ2 is also a key structural component that anchors the CoQ biosynthetic complex to the inner mitochondrial membrane (Tran & Clarke 2007). These results suggest that COQ2 is not only required for a specific step in CoQ synthesis but that it is also needed for proper positioning of soluble protein components of the CoQ biosynthetic pathway.

The *C. elegans* homologue of COQ2 is predicted to produce five *coq-2* isoforms (COQ-2A-E, Fig. 3.1). The *coq-2* developmental and GABA neurodegeneration phenotypes were generated by a deletion allele (*ok1066*) that is predicted to disrupt expression of all five *coq-2* isoforms (Fig. 3.1). It is currently unclear if a specific *coq-2* splice-variant is responsible for tissue-specific phenotypes (i.e., fertility or GABA neuron protection), but this question would be interesting to investigate in future studies.

To date, six COQ2 mutations have been identified in patients with Primary CoQ Deficiency (Quinzii et al. 2006; Mollet et al. 2007; Diomedi-Camassei et al. 2007; Jakobs et al. 2013). Protein sequence alignment indicates that *C. elegans* COQ-2A is the closest homologue of the human COQ2 protein (Fig. 3.8A). All five of the residues that are altered in human CoQ missense mutations are conserved in *C. elegans* (Fig. 3.8A) (Quinzii et al. 2006; Mollet et al. 2007; Diomedi-Camassei et al. 2007; Jakobs et al. 2013). A sixth mutation (N401fsX415) deletes nucleotide 1198 to produce a frame shift that alters the last 21 amino acids of human COQ2. This region changes the global charge of the C-terminus and also disrupts part of a transmembrane domain of COQ2 (Mollet et al. 2007). Therefore, the N401fsX415 mutation could interfere with COQ2 localization to the inner mitochondrial membrane and thus also disrupt co-localization of other CoQ biosynthetic proteins to this region. Mollet *et al.* demonstrated that wild-type COQ2 rescued growth defects of *S. cerevisae coq2* and showed that COQ2 N401fsX415 was insufficient to complement the yeast mutation (Mollet et al. 2007).

A

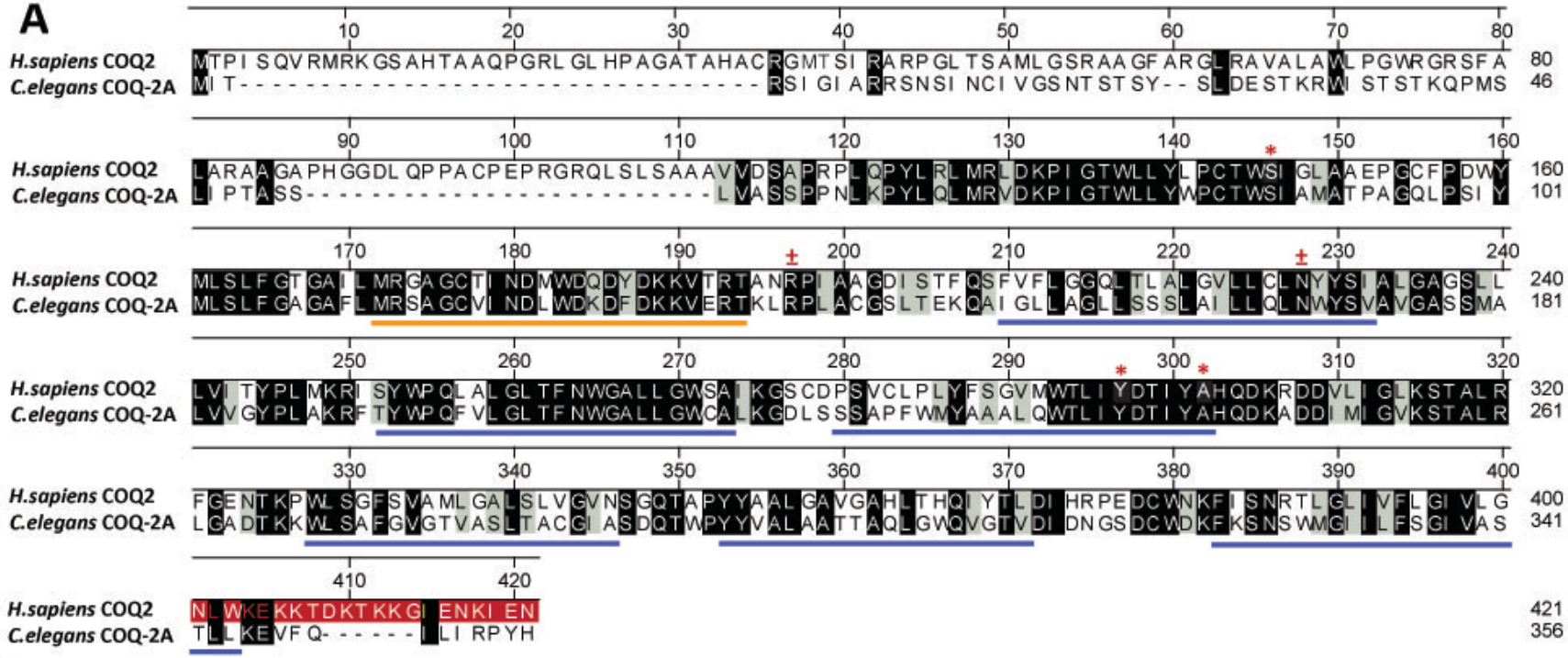

B

Genotype	Brood Size	Produces Embryos?
coq-2(ok1066)	0	no
coq-2(ok1066); psur-5::human COQ-2 wt	38.25 ± 7.2	yes, viable
coq-2(ok1066); psur-5::human COQ-2 mutant	0	yes, dead

Figure 3.8: Human COQ2 rescues infertility of *coq-2(ok1066)*. A. Alignment of *H. sapiens* COQ2 and *C. elegans* COQ-2A demonstrates strong conservation at the protein level (identity = black boxes, similarity = gray boxes). Homozygous (*) and heterozygous (±) mutations isolated from Primary Coenzyme Q Deficiency patients are indicated in red text (Quinzii et al. 2006; Diomedi-Camassei et al. 2007; Jakobs et al. 2013). The red box denotes the region of COQ2 altered by the c1198 delT, N401fsX415 mutation (Mollet et al. 2007). Predicted protein domains include a substrate (i.e., isoprenoid tail)-binding site (orange underline) and six transmembrane regions (blue underline) (Forsgren et al. 2004). **B.** Ubiquitous expression of wild-type (wt) Human COQ2 rescues the infertility defects of *coq-2(ok1066)* whereas the mutant COQ2 (N401fsX415, red box in Panel A) does not fully rescue (i.e., embryos produced but they are inviable).

Functional conservation of COQ2 in a more complex organism has not been previously tested. To address this question, human COQ2 was expressed in *C. elegans coq-2(ok1066)* mutant with a ubiquitous promoter (*sur-5*). Normally, *coq-2(ok1066)* animals develop to adulthood but do not produce viable embryos (Table 3.6). However, ubiquitous expression of human COQ2 restores fertility to *coq-2(ok1066)* animals (Fig. 3.8B). This result provides the first direct evidence that a protein from the human Coenzyme Q biosynthetic pathway can complement CoQ biosynthesis defects in a different multicellular organism.

The N401fsX415 COQ2 mutation was isolated from a patient with fatal infantile multiorgan disease (Mollet et al. 2007). In contrast to wild-type COQ2, ubiquitous expression of the mutant version of COQ2 (N401fsX415) in *coq-2(ok1066)* mutants resulted in limited rescue; embryos were produced but did not hatch (Fig. 3.8B). The incomplete rescue of the *coq-2* defect is consistent with the pathogenic effects of the COQ2 N401fsX415 mutation in humans and parallels the failure to complement a *coq2* mutation in yeast (Mollet et al. 2007).

DISCUSSION AND FUTURE DIRECTIONS

Summary

Coenzyme Q is synthesized in the mitochondria by a set of highly conserved enzymes (Coq1-Coq9, Fig. 1.6) (Turunen et al. 2004). Despite its mitochondrial production, CoQ is present in other cell membranes where it performs a variety of functions (discussed in **Chapter 1**). The presence of CoQ in non-mitochondrial locations indicates that there are cellular mechanisms for its distribution. Additionally, the clinical improvement of Coenzyme Q deficiency patients with CoQ_{10} supplementation suggests that exogenous CoQ can be both imported into a cell and also transported to distinct membrane locations to rescue metabolic defects. Therefore, in addition to

mechanisms that distribute CoQ throughout the cellular membranes, there are also processes that incorporate exogenous Coenzyme Q into the cell.

In this chapter, I performed cell-specific knockdown and transgenic rescue experiments that suggest CoQ transport mechanisms are conserved in *C. elegans*. The existence of robust mechanisms of intercellular CoQ transport likely explains my observation that selective knockdown of CoQ in GABA neurons does not result in degeneration whereas global CoQ deficiency consistently results in GABA neuron death. (Fig. 3.5). To test this model, I generated transgenic lines that expressed wild-type COQ-1 (i.e., restored CoQ production) in specific tissues. This experiment revealed that COQ-1 production in body muscle rescued *coq-1* mutants whereas expression of COQ-1 in other cell types (pharynx, intestine, nervous system, GABA neurons) failed to restore viability to *coq-1* animals (Fig. 3.6). This finding supports the hypothesis that Coenzyme Q can be transferred between cells in cases of CoQ deficiency but may also indicate that intercellular transport from some tissues (e.g., body muscle) is more efficient than from other cell types (e.g., intestine). Alternatively, overall CoQ production in muscle may be significantly greater than in cell types that do not restore viability to *coq-1* mutants. It should be possible resolve this question by comparing overall CoQ levels in rescuing (e.g., body muscle) versus non-rescuing (e.g., intestine) COQ-1 expressing transgenic lines.

Additionally, *coq-2* mutants were complemented with human COQ2, thus demonstrating the conservation of CoQ biosynthetic enzymes in *C. elegans*. A pathogenic COQ2 mutation originally isolated from a patient with Primary Coenzyme Q deficiency was unable to fully rescue fertility of the *coq-2* mutant, paralleling similar attempts to complement a mutant yeast *coq2* allele (Mollet et al. 2007). These studies broadly address how cells adapt to Coenzyme Q deficiency and provide the first evidence that wild-type and pathogenic features of human CoQ biosynthetic enzymes are conserved in a multicellular model organism.

A narrow range of CoQ levels permits both animal viability and GABA neuron death

I propose a Coenzyme Q threshold model to explain the range in phenotypes observed with various CoQ deficiency backgrounds (Table 3.6, Fig. 3.9). This model assumes that a minimum level of Coenzyme Q is necessary for development to adulthood and but is not sufficient to protect GABA neurons from degeneration. CoQ levels outside of this range result in either animal inviability (i.e., CoQ concentration is too low) or lack of GABA neurodegeneration (i.e., CoQ concentration is too high). This threshold model could explain why the different means of disrupting Coenzyme Q synthesis produced a range of developmental phenotypes and varying levels (and onset) of GABA neuron degeneration.

The fact that *coq-1* animals grown on dietary CoQ_9 overcome L3 arrest and reach adulthood (Fig. 3.3) also aligns with a CoQ threshold model of development and neurodegeneration. In this instance, dietary CoQ_9 allows *coq-1* animals to reach adult stages but is not sufficient to prevent GABA neurodegeneration. However, these *coq-1* animals also show severe defects in other tissues and thus degeneration is not limited to GABA neurons under these conditions.

coq-1 RNAi resulted in conditions that produce robust GABA neurodegeneration while also maintaining the viability of other neuron subtypes (e.g., adjacent cholinergic neurons in the ventral nerve cord) (Fig. 2.2). Mutants in CoQ biosynthetic enzymes also result in GABA neuron death (Fig. 2.2, Fig. 3.2). These CoQ pathway mutants, however, are typically subviable due to either larval arrest or sterility (Table 3.6). These results underscore the idea that the selective death of GABA neurons may occur at a specific CoQ threshold such that higher levels of CoQ do not induce GABA neurodegeneration whereas lower levels of CoQ result in ubiquitous tissue degeneration. Future studies could directly test this threshold model by quantifying CoQ_9 levels in the CoQ deficiency strains described in this chapter.

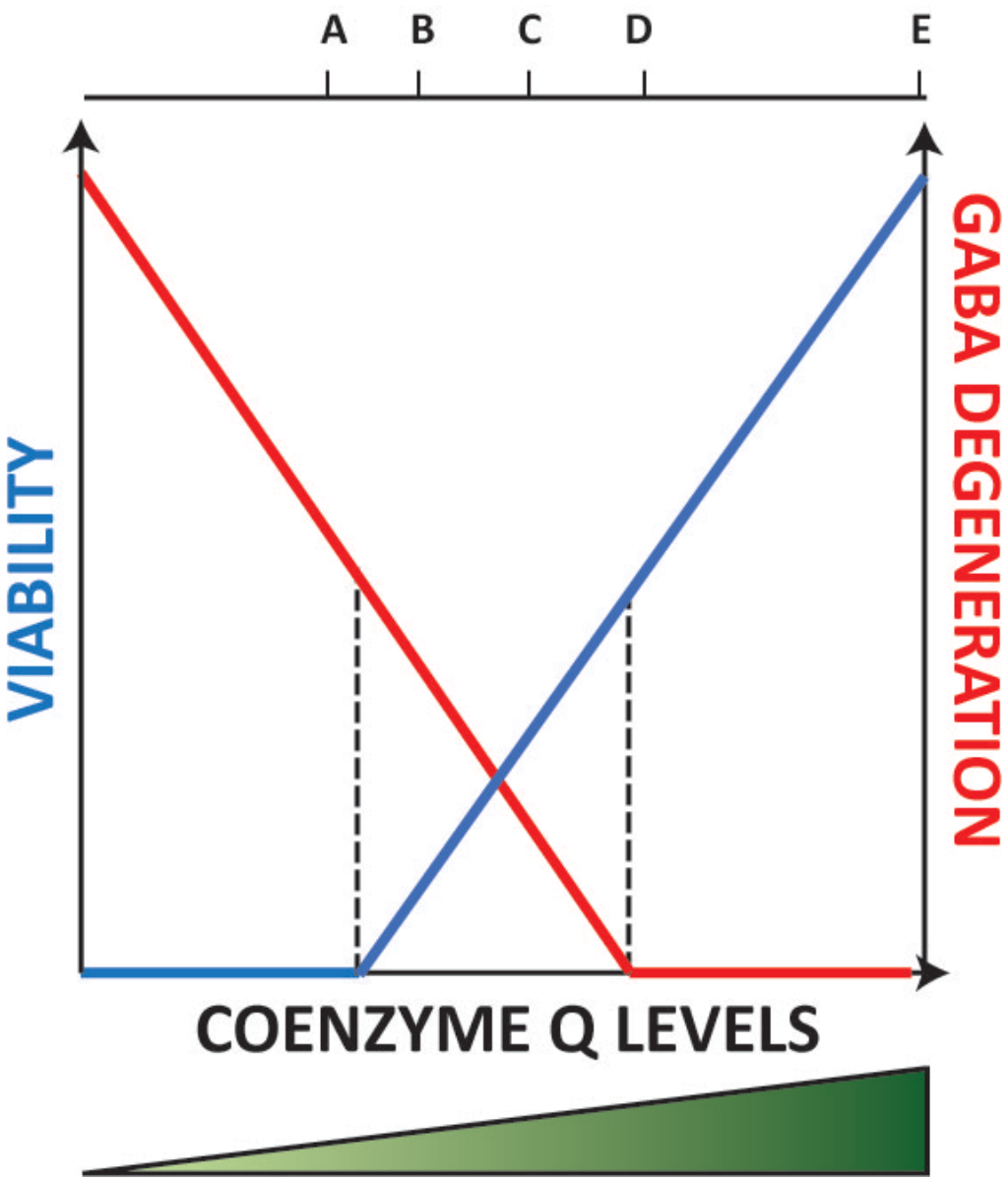

Figure 3.9: Coenzyme Q level threshold for viability and GABA neurodegeneration. A narrow range of Coenzyme Q concentration in *C. elegans* is required to observe GABA neuron degeneration in adult animals. **A.** Coenzyme Q biosynthetic pathway mutants with severe defects and thus strong reduction in CoQ levels are inviable and their GABA neurodegeneration cannot be assessed. **B.** Robust GABA neurodegeneration occurs in animals with enough CoQ to maintain animal viability but other tissues are also severely affected by low CoQ levels (i.e., *coq-1* mutants fed dietary CoQ_9). **C.** Selective GABA neuron death occurs in animals that develop normally but signs of CoQ deficiency manifest as adults (i.e., *coq-1* RNAi or *coq-2* mutants). **D.** Alternatively, weak depletion of CoQ levels permits animal viability but GABA neurons do not degenerate, likely due to intercellular CoQ transport mechanisms that supplement GABA neurons with CoQ (Fig. 3.10D). **E.** Wild-type animals are viable and do not show GABA neuron death.

C. elegans as a model system to study intercellular CoQ transport

GABA neuron-specific COQ-1 production is not necessary for their survival

Results from this chapter point to robust mechanisms of intercellular transport in *C. elegans*. This idea was initially suggested by the surprising finding that experiments designed to deplete CoQ specifically in GABA neurons (i.e., cell-specific RNAi) did not produce the GABA neurodegeneration phenotype that arises from global knockdown of CoQ levels (Fig. 3.4). One potential explanation for this result is that *coq-1*-deficient GABA neurons receive CoQ from other cells and thus are protected from degeneration (Fig. 3.10B). If this model holds true, then CoQ production from both GABA neurons as well as other from nearby tissues should be sufficient to prevent neuron degeneration (Fig. 3.10C-D). Future studies could test this hypothesis by testing for GABA neurodegeneration in the various transgenic strains that express COQ-1 in specific cell types (Table 3.7) (see **Future Directions**).

Muscle-specific CoQ production overcomes developmental defects of coq-1 mutants

Further evidence to support a model of Coenzyme Q transfer between cells comes from experiments in which COQ-1 is selectively expressed in specific tissues. Only muscle-specific expression of COQ-1 rescues the fertility of *coq-1* mutants (Fig. 3.6), whereas the restoration of COQ-1 (and CoQ synthesis) to the pharynx, intestine or nervous system did result in viable offspring (Table 3.7). Normally, CoQ concentration approaches saturation in cellular membranes (Turunen et al. 2004), and rescue experiments of CoQ pathway mutants in *S. pombe* revealed that $1/30^{th}$ of wild-type levels of CoQ was sufficient to rescue growth defects (Saiki et al. 2005). These observations suggest that individual cells normally produce more than enough CoQ to meet basic intracellular needs (Saiki et al. 2005). Therefore, it is seems likely that CoQ synthesized in muscle is sufficiently high to afford rescue of other CoQ-deficient tissues.

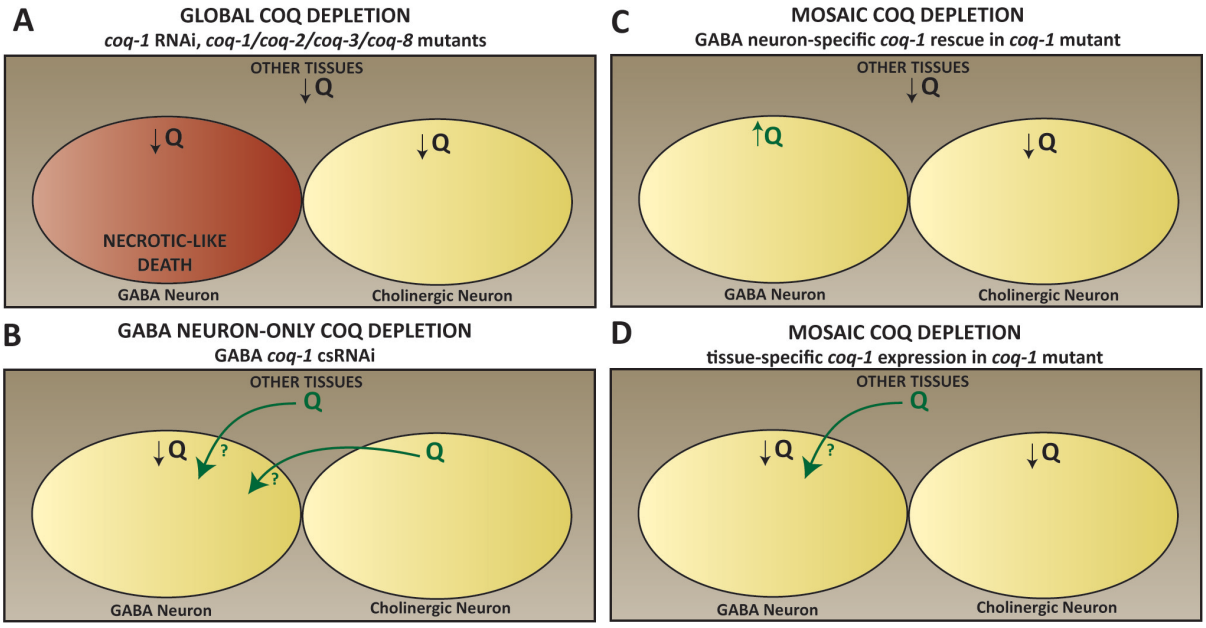

Figure 3.10. Model for intercellular Coenzyme Q transport as a mechanism to protect GABA neurons from degeneration. A. Under conditions of global Coenzyme Q depletion (i.e., *coq-1* RNAi, CoQ biosynthetic mutants), GABA neurons undergo selective degeneration. **B.** GABA neuron-specific knockdown of CoQ production (Fig. 3.5) (*coq-1* csRNAi) does not induce degeneration because of CoQ transport from other CoQ-rich tissues. **C.** GABA neuron-specific restoration of CoQ production rescues the GABA neurodegeneration phenotype induced by global CoQ deficiency. **D.** CoQ transport from specific tissues rescues GABA neurodegeneration under conditions of global CoQ deficiency.

Two alternative models could explain how CoQ is transported between cells: (1) CoQ distribution occurs by passive transport (i.e., diffusion) or (2) CoQ movement is controlled by a specific pathway. Recent studies of this question favor an active mechanism of CoQ distribution that requires the endomembrane system (Fernández-Ayala et al. 2005; Padilla-López et al. 2009). For example, in *S. cerevisiae,* exogenous CoQ_6 rescues growth defects in the *coq7* mutant strain; however, external CoQ is not taken up in *coq7* mutants in which endocytosis is impaired (Padilla-López et al. 2009). Membrane trafficking mutants that disrupt endocytosis at various steps (i.e., *erg2*/internalization, *tlg2*/endosome formation, *pep12*/vacuole maturation) are unable to incorporate exogenous CoQ. Similarly, both endogenous transport from the mitochondria and external import of CoQ into cultured human cells require the endomembrane system (Fernández-Ayala et al. 2005).

In addition to mechanisms that bring CoQ into the cell, it also seems likely that specific carrier proteins could facilitate CoQ transport to distinct membrane locations. Selective lipid-binding proteins have been identified for other membrane antioxidants that assist transport of essential lipids. For example, α-Tocopherol transfer protein (αTTP) is expressed in the liver and selectively binds α-tocopherol to facilitate its transport between membranes (Arita et al. 1995). Coq10p is the only protein identified thus far that is predicted to bind and transport Coenzyme Q (Barros et al. 2005; Busso et al. 2010). Coq10p shuttles CoQ from its site of synthesis (inner mitochondrial membrane, matrix side) to the electron transport chain suggesting that it functions in the inner mitochondrial membrane. The discovery of Coq10p indicates that CoQ movement within a cell is not simply a passive process but instead requires specific molecular chaperones to ensure its proper membrane localizations. A better understanding of CoQ transport could have immense therapeutic benefit and thus warrants further investigation.

Human COQ2, a CoQ biosynthetic protein, is functionally conserved in *C. elegans*

Experiments described in this chapter, showed that ubiquitous expression of human COQ2 restored movement and fertility to a *coq-2* mutant in *C. elegans* (Fig. 3.8). Conversely, expression of mutant human COQ2 failed to rescue *coq-2* defects. Together, these results provide the first evidence of functional conservation of both wild-type and pathogenic alleles of a CoQ biosynthetic gene between humans and another multicellular organism.

Future Directions

Coenzyme Q_{10} supplementation is used to ameliorate symptoms in patients with CoQ deficiency (Rötig et al. 2000; Montini et al. 2008). The positive impact of this treatment indicates that cells use active mechanisms of CoQ uptake in states of deficiency. However, not all patients with CoQ deficiency benefit from treatment with exogenous CoQ_{10} and myopathic forms are often more responsive than neurologic ataxia phenotypes (Montero et al. 2007). This inefficiency and tissue selectivity has been attributed to lack of CoQ bioavailability (large molecular weight and insolubility in water) and thus warrants investigations to enhance the therapeutic benefit of CoQ supplementation. Previous attempts to increase CoQ uptake tested Coenzyme Q derivatives with increased solubility in water. However, these hydrophilic forms of CoQ were largely ineffective probably because the lipid solubility of Coenzyme Q is important to its membrane-localized functions (Esposti et al. 1996). These results warrant additional research on the mechanism of CoQ uptake and intercellular distribution as a strategy for developing effective therapies for treating CoQ deficiency.

Vesicular transport mechanisms of the endomembrane system have been identified as necessary for CoQ import and intracellular distribution in yeast and in human cells (Padilla-López et al. 2009; Fernández-Ayala et al. 2005). Future studies in *C. elegans* could test this model by

determining if mutants in specific endocytic components (e.g., *rme-8*) prevent rescue in one of the CoQ transport systems described in this chapter (i.e., muscle-specific COQ-1 rescue in *coq-1* mutants). For example, if the endomembrane system is required to transport CoQ synthesized in the muscle to other tissues (e.g., somatic gonad) to rescue fertility defects of *coq-1* mutants, genetic mutations in endocytic genes should inhibit this transport and thus result in animal sterility. Additionally, the muscle-specific COQ-1-rescued strain could be especially well suited for unbiased, forward-genetic approaches to identify novel regulators of CoQ uptake in a multicellular organism (discussed in **Chapter 6**).

Muscle-specific COQ-1 expression rescued developmental arrest and infertility of *coq-1* mutants (Fig. 3.6), whereas CoQ production from other tissues (pharynx, intestine, nervous system) did not ameliorate these defects (Table 3.7). This finding raises the question of whether the location of CoQ production is important (e.g., body muscle) or whether a minimum threshold of CoQ overcomes these deficits. Future studies could distinguish between these two models by quantifying CoQ_9 levels in tissue-specific COQ-1 transgenic *coq-1* animals. Body-wall muscle is a large tissue and perhaps CoQ production from muscle produces such robust levels that it can compensate for global CoQ deficiency. However, the intestine is also a large organ but does not rescue *coq-1* mutants with intestine-specific COQ-1 production. Therefore, comparison of CoQ_9 in *coq-1* mutants with muscle- and intestine-specific CoQ production could address whether levels or location of CoQ is important for viability. If both tissues produce comparable CoQ levels, this would suggest that the location of CoQ synthesis is important. If muscle-specific COQ-1 expression has significantly higher CoQ levels, this would implicate that a threshold of CoQ production, regardless of the source, must be met. In this scenario, combinations of tissue-specific rescue (i.e., intestine and nervous system) could be used to elevate overall CoQ levels and further test this hypothesis.

A key question surrounding the GABA neuron degeneration arising from CoQ depletion is whether activation of this pathway is due to an inability of GABA neurons to synthesize CoQ or if CoQ deficiency in other cell types causes GABA neurons to die. In this chapter, cell-specific RNAi experiments revealed that GABA neurons-specific expression of *coq-1* is not required for their survival (Fig. 3.5). This result implicates a non-cell autonomous role for Coenzyme Q (Fig. 3.10B). Future studies could test whether *coq-1* is sufficient to prevent GABA neuron death in animals globally deficient in CoQ production (Fig. 3.10C). Additionally, the tissue-specific COQ-1 strains described in this chapter could also be used to test the model that GABA neuron viability is maintained by uptake of CoQ from other cells (Fig. 3.10D).

CHAPTER IV

CED-3/CASPASE ANTAGONIZES A CED-4/APAF-1-DEPENDENT DEATH PATHWAY IN COENZYME Q-DEFICIENT GABA NEURONS

INTRODUCTION

Members of the core apoptotic machinery (CED-4 and CED-3) (Fig. 1.3) are required for somatic and germline cell deaths in *C. elegans* (Dong et al. 2009; Gartner et al. 2008). Apoptotic induction occurs when CED-9/Bcl2 releases CED-4/Apaf-1 for oligomerization and formation of the "apoptosome." In this state, CED-4 interacts with CED-3 via a shared Caspase Activation Recruitment Domain (CARD) to trigger CED-3 caspase activity. In addition to this well-documented functional relationship with the canonical apoptotic pathway, CED-3 and CED-4 can also function independently to regulate cell death. For example, PVL-5 (unknown molecular identity) blocks a cell death pathway in the *C. elegans* epidermis that requires *ced-3* but not *ced-4* (Joshi & Eisenmann 2004). Conversely, genetic ablation of *icd-1*/βNAC activates apoptosis in neurons through a pathway dependent on *ced-4* but not requiring *ced-3* (Bloss et al. 2003). These examples suggest that CED-3 and CED-4 can either function together as in the canonical apoptotic pathway or alternatively as independent players in atypical cell death mechanisms activated in specific tissues or cellular contexts.

CED-3 belongs to a conserved family of caspases (cysteine-dependent aspartyl proteases) that are known for their essential death-promoting roles in apoptosis. In recent years, however, many non-apoptotic duties for caspases have been identified in the nervous system, including caspase-dependent neuronal plasticity (Huesmann & Clayton 2006), ischemic preconditioning (McLaughlin et al. 2003), dendritic pruning (Williams et al. 2006), and neuronal regeneration (Pinan-

Lucarre et al. 2011). Localized and highly regulated activation of caspases in these cellular contexts is predicted to account for their non-death-inducing roles, as uncontrolled caspase activation leads to apoptotic death (Dong et al. 2009; Williams et al. 2006; Gartner et al. 2008; Joshi & Eisenmann 2004; Chelur & Chalfie 2007).

In **Chapter 2**, I presented evidence that CED-4/Apaf-1 activity is required for degeneration of CoQ-deficient GABA neurons, whereas *ced-3* mutants showed partial suppression of GABA neuron death (Fig. 2.6). Here, additional experiments were performed to better understand the relationship between CED-3 and CED-4 during CoQ depletion-induced GABA neuron death. Our data now suggest that CED-3 antagonizes a cell degeneration pathway in CoQ-deficient GABA neurons. The proteolytic activity of CED-3 is neuroprotective in GABA neurons, which suggests that caspase activity in this context actually blocks cell death. This result is surprising because it suggests that CED-3 and CED-4 have opposite roles in this cell death pathway. Furthermore, epistasis analysis suggests that *ced-4* either functions downstream or in parallel to *ced-3*. This finding was also unexpected given the well-studied relationship between these two proteins during programmed cell death (i.e., CED-3 is activated downstream of CED-4). Thus, these findings support a new mechanism in which CED-3 could either inhibit activation of CED-4 or potentially function independently to oppose a CED-4-driven neurodegeneration pathway (Fig. 4.7). Due to the high conservation of apoptotic regulators from nematode to vertebrates, we propose that similar stress-induced caspase-dependent neuronal protection mechanisms could also be activated in mammals.

MATERIALS AND METHODS

Nematode Strains and Genetics

Nematodes were cultured using previously described methods (Brenner 1974). Mutant alleles, primers used to verify the mutations and source of the original strains used for this study are listed in Table 4.1. Strains generated for data analysis are listed in Table 4.2.

Molecular Biology and Transgenic Strains

Cloning primers are listed in Table 4.3, and Table 4.4 lists the plasmids that were created for this study. Transgenic arrays were generated by microinjection of DNA at concentrations listed in Table 4.5. See **Materials and Methods** sections of **Chapter 2** for a description of the *unc-25* promoter and **Chapter 3** for details of the *ttr-39* promoter construction.

Wild-type (WT) and caspase-dead (C358S) ced-3

ced-3 cDNA was amplified (Phusion High-Fidelity DNA Polymerase, New England Biolabs) from pG2M24 (WT) and pG2M25 (C358S) and inserted into pMLH117 with 5'AscI/3'SacII (added to primer sequences) to create pMLH162 and pMLH163, respectively. pG2M24 and pG2M25 were kindly provided by Shai Shaham (Shaham 1998).

Reconstituted ced-3

GABA neuron-specific promoters (*ttr-39* and *unc-25*) were sub-cloned into TU#806 [*CZ-ced-3 (p17)*] and TU#807 [*ced-3(p15)-NZ*] (Chelur & Chalfie 2007) (from Addgene) with 5'HindIII/3'BamHI to make pMLH209 and pMLH207, respectively.

Table 4.1. Mutant alleles used in this study and their source of origin (Caenorhabditis Genetics Center = CGC).

Mutant	Source	Genotyping Primers	Reference
coq-1 (ok749) I	CGC	AAAAATGTTACGGCCGACTG	(Gavilan et al. 2005)
		CGTGTCCCTCAAAATGACCT	
		AGTCAGTGCTCGTCGGAGAT	
ced-4 (n1162) III	CGC	TCATCCACGACTTTGAACCA	(Yuan & Horvitz 1992)
		GCAAGCGTCACGAAATATCA	
ced-4 (n1894) III	CGC	ATTGGAAAGTCGAGGATTAGTC	(Yuan & Horvitz 1992)
		TTAACAGCATGCAAAATTTTTGAGG	
ced-4 (n3040) III	Robert Horvitz	GCTATTGTATATTCTCCAGCTA	(F. Chen et al. 2000)
		GAGCTTGTGATGCAATTACTG	
ced-4 (ot248) III	CGC	GCTATTGTATATTCTCCAGCTA	(Sarin et al. 2007)
		GAGCTTGTGATGCAATTACTG	
ced-9 (n1950gf) III	CGC	CGGACAACTCGCTGACGAAT	(Hengartner & Horvitz 1994)
		TTCCTTCCAGTTGTTGCGGA	
coq-2 (ok1066) III	CGC	ATGCACATGGAGCATAGCAATG	(Gavilan et al. 2005)
		GCGTGGTTTCACACAGATACAA	
eri-1 (mg366) IV	CGC	CATGCAATTTCAATGCCTTTTA	(Kennedy et al. 2004)
		TGCATCATCCAATCCACTATGT	
ced-3 (n717) IV	CGC	AGACTTTGCCAAACACGAATCA	(Yuan et al. 1993)
		TCAGCAGCTCAACAACATCC	
ced-3 (n718) IV	CGC	ATGATGCGTCAAGATAGAAG	(Shaham et al. 1999)
		GGCAGAGCGTCCTTTTGCAAGC	
ced-3 (n1949) IV	CGC	ATGATGCGTCAAGATAGAAG	(Yuan et al. 1993)
		GGCAGAGCGTCCTTTTGCAAGC	
ced-3 (n2433) IV	CGC	AAATTTCCCAGCCTTGTTCC	(Yuan et al. 1993)
		TCAGCAGCTCAACAACATCC	
ced-3 (n2888) IV	CGC	ATGATGCGTCAAGATAGAAG	(Shaham et al. 1999)
		TTCGTTGTCACAATTCGAGCATA	
ced-3 (ok2734) IV	CGC	AAATTTCCCAGCCTTGTTCC	N/A
		TCAGCAGCTCAACAACATCC	
		CTGATTGGTCGCAGTTTTCA	
egl-1 (n1084 n3082) V	CGC	CCGATTAGTCGTATTCTAACTTC	(Conradt & Horvitz 1998)
		TCATGGTACAAATTGGAGAAAAGT	
eri-1(mg366) IV	CGC	CATGCAATTTCAATGCCTTTTA	(Kennedy et al. 2004)
		TGCATCATCCAATCCACTATGT	
Transgene	**Source**	**Array**	**Reference**
juIs76 II	CGC	*punc-25::GFP, lin-15(+)*	(Jin et al. 1999)
hT2 (I;III)	CGC	*bli-4(e937) let(q782) qIs48*	(McKim et al. 1993)
nIs48	Robert Horvitz	*punc-30::ced-4, rol-6(d)*	(Shaham & Horvitz 1996b)
trIs10 I	CGC	*pmyo-3::MB::YFP, pmyo-2::YFP, pceh-23::HcRed, punc-25::DsRed, unc-129nsp::CFP*	(Dixon 2006)

Table 4.2. Table of strains used in this study.

Strain	Genotype
NC1405	*juIs76 [punc-25::GFP, lin-15(+)] II; eri-1 (mg366) IV*
NC1407	*juIs76 [punc-25::GFP, lin-15(+)] II; ced-4 (n1162) III; eri-1 (mg366) IV*
NC1959	*juIs76 [punc-25::GFP, lin-15(+)] II; coq-2(ok1066)/hT2 (I; III)*
NC2322	*juIs76 [punc-25::GFP, lin-15(+)] II; ced-3(ok2734) eri-1(mg366) IV*
NC2536	*juIs76 [punc-25::GFP, lin-15(+)] II; ced-4 (n1162) III; eri-1 (mg366) IV; wdEx847 [pttr-39::ced-4, punc-25::mCherry, pceh-22::GFP]*
NC2568	*juIs76 [punc-25::GFP, lin-15(+)] II; ced-3(ok2734) eri-1(mg366) IV; wdEx865 [pttr-39::ced-3 cDNA, punc-25::mCherry, pceh-22::GFP]*
NC2590	*juIs76 [punc-25::GFP, lin-15(+)] II; ced-3(ok2734) eri-1(mg366) IV; wdEx875 [pttr-39::ced-3 C358S cDNA, punc-25::mCherry, pceh-22::GFP]*
NC2617	*trIs10 [pmyo-3::MB::YFP, pmyo-2::YFP, pceh-23::HcRed, punc-25::DsRed, unc-129nsp::CFP] I; eri-1 (mg366) IV*
NC2627	*trIs10 [pmyo-3::MB::YFP, pmyo-2::YFP, pceh-23::HcRed, punc-25::DsRed, unc-129nsp::CFP] I; ced-3 (ok2734) eri-1 (mg366) IV*
NC2660	*juIs76 [punc-25::GFP, lin-15(+)] II; ced-3(n1949) eri-1(mg366) IV*
NC2664	*juIs76 [punc-25::GFP, lin-15(+)] II; ced-3(ok2734) eri-1(mg366) IV; wdEx904 [punc-25::ced-3-SM-nz, pttr-39::cz-ced-3-LG, punc-25::mCherry, pceh-22::GFP]*
NC2687	*juIs76 [punc-25::GFP, lin-15(+)] II; ced-3(n718) eri-1(mg366) IV*
NC2743	*coq-1(ok749)/hT2 (I; III); juIs76 [punc-25::GFP, lin-15(+)] II*
NC2749	*juIs76 [punc-25::GFP, lin-15(+)] II; coq-2(ok1066)/hT2 (I; III); ced-3(ok2734) IV*
NC2778	*juIs76 [punc-25::GFP, lin-15(+)] II; ced-4 (n1894) III; eri-1 (mg366) IV*
NC2779	*juIs76 [punc-25::GFP, lin-15(+)] II; ced-4 (n3040) III; eri-1 (mg366) IV*
NC2790	*juIs76 [punc-25::GFP, lin-15(+)] II; ced-4 (not248) III; eri-1 (mg366) IV; otIs114 [plim-6::GFP, rol-6(d)]*
NC2798	*coq-1(ok749)/hT2 (I; III); juIs76 [punc-25::GFP, lin-15(+)] II; ced-3(ok2734) IV*
NC2802	*juIs76 [punc-25::GFP, lin-15(+)] II; coq-2(ok1066)/hT2 (I; III); ced-3(n717) IV*
NC2803	*coq-1(ok749)/hT2 (I; III); juIs76 [punc-25::GFP, lin-15(+)] II; ced-4(n1162)/hT2 (I; III); ced-3(ok2734) IV*
NC2804	*coq-1(ok749)/hT2 (I; III); juIs76 [punc-25::GFP, lin-15(+)] II; ced-4(n1162)/hT2 (I; III)*
NC2817	*juIs76 [punc-25::GFP, lin-15(+)] II; coq-2(ok1066)/hT2 (I; III); ced-3(n2433) IV*
NC2818	*coq-1(ok749)/hT2 (I; III); juIs76 [punc-25::GFP, lin-15(+)] II; egl-1(n1084 n3082) V*
NC2825	*coq-1(ok749)/hT2 (I; III); juIs76 [punc-25::GFP, lin-15(+)] II; ced-9(n1950)/hT2 (I; III)*
NC2828	*juIs76 [punc-25::GFP, lin-15(+)] II; coq-2(ok1066)/hT2 (I; III); ced-3(n2888) IV*

Table 4.3. Molecular cloning primers used in this work. Restriction sites added to the primers are underlined.

Gene	Primer Name	Primer Sequence
ced-3 WT cDNA	ced-3_5p_AscI	GGGGCGCGCCATGATGCGTCAAGATAGAAG
	ced-3_3p_SacII	CCCCGCGGTTAGACGGCAGAGTTTCGTGCTTCC
ced-3 C358S cDNA	ced-3_5p_AscI	GGGGCGCGCCATGATGCGTCAAGATAGAAG
	ced-3_3p_SacII	CCCCGCGGTTAGACGGCAGAGTTTCGTGCTTCC
ced-4 cDNA	ced-4_5p_AscI	GGGGCGCGCCATGCTCTGCGAAATCGAATG
	ced-4_3p_SacII	CCCCGCGGTTAACAGCATGCAAAATTTTTG
pttr-39	pC04G2.1_5p_SphI	GGGGGGGCATGCATTATTATTTCTATCGGCTAC
	pC04G2.1_3p_AscI	GGGGGGGGCGCGCCATGATTTTTTGTTTTAACAA
punc-25	punc-25_5p_HindIII_SphI	GGGGGGAAGCTTGCATGCAAAAAACACCCAC
	punc-25_3p_AscI	GGGGGGGGCGCGCCATTTTTGGCGGTGAACTGAGC

Table 4.4. Plasmids generated and/or used in this study.

Vector	DNA	Additional Information
pG2M24	pET3a::ced-3 WT cDNA::FLAG	a gift from Shai Shaham
pG2M25	pET3a::ced-3 C358S cDNA::FLAG	a gift from Shai Shaham
pG2M39	*pmec-18::ced-3(p15)-nz [TU#806]*	purchased from Addgene
pG2M40	*pmec-18::cz-ced-3(p17) [TU#807]*	purchased from Addgene
pMLH001	*pttr-39* forward in pENTR D-TOPO	
pMLH004	*punc-25* forward in pENTR D-TOPO	
pMLH162	*pttr-39::ced-3 WT cDNA::unc-10 3'UTR*	
pMLH163	*pttr-39::ced-3 C358S cDNA::unc-10 3'UTR*	
pMLH174	*pttr-39::ced-4 cDNA::unc-10 3'UTR*	
pMLH188	*punc-25::ced-3::GFP::unc-54 3'UTR*	
pMLH189	*punc-25::ced-4::GFP::unc-54 3'UTR*	
pMLH190	*punc-25::csp-1B::GFP::unc-54 3'UTR*	
pMLH207	*punc-25::ced-3 (p15)-NZ::unc-54 3'UTR*	
pMLH209	*pttr-39::CZ-ced-3 (p17)::unc-54 3'UTR*	
Coinjection Markers		
pCW2.1	*pceh-22::GFP*	a gift from Oliver Hobert
pMLH132	*punc-25::mcherry::unc-54 3'UTR*	
pG2M30	*pBluescript II*	filler DNA for array

Table 4.5. Plasmid concentrations that were microinjected to generate the transgenic arrays used in this study. Refer to Table 4.4 for plasmid descriptions.

Transgenic Array	Genotype Injected	Plasmid Name	Concentration
wdEx865 [pttr-39::ced-3, punc-25::mCherry, pceh-22::GFP]	*juIs76 [punc-25::GFP, lin-15(+)] II; ced-3(ok2734) eri-1(mg366) IV*	pMLH162	25 ng/µL
		pMLH132	25 ng/µL
		pCW2.1	20 ng/µL
wdEx847 [pttr-39::ced-4, punc-25::mCherry, pceh-22::GFP]	*juIs76 [punc-25::GFP, lin-15(+)] II; ced-4 (n1162) III; eri-1 (mg366) IV*	pMLH174	25 ng/µL
		pMLH132	30 ng/µL
		pCW2.1	20 ng/µL
wdEx875 [pttr-39::ced-3(C358S), punc-25::mCherry, pceh-22::GFP]	*juIs76 [punc-25::GFP, lin-15(+)] II; ced-3(ok2734) eri-1(mg366) IV*	pMLH163	25 ng/µL
		pMLH132	25 ng/µL
		pCW2.1	20 ng/µL
wdEx904 [punc-25::ced-3(p15)-nz, pttr-39::cz-ced-3(p17), punc-25::mCherry, pceh-22::GFP]	*juIs76 [punc-25::GFP, lin-15(+)] II; ced-3(ok2734) eri-1(mg366) IV*	pMLH207	10 ng/µL
		pMLH209	10 ng/µL
		pMLH132	25 ng/µL
		pCW2.1	20 ng/µL
		pG2M30	35 ng/µL

ced-4

ced-4 cDNA was amplified (Phusion High-Fidelity DNA Polymerase, New England Biolabs) from DNA isolated from *nIs48* (*punc-30::ced-4 cDNA*) transgenic animals (Shaham & Horvitz 1996b) (a gift from H. Robert Horvitz) and inserted into pMLH162 with 5'AscI/3'SacII (added to the primers) to make pMLH174.

Synchronizing *coq-2* adults for neurodegeneration analysis

Strains were cultured at 20°C. Synchronized *coq-2/hT2* animals were maintained on NGM OP50 plates, and *coq-2* homozygotes were picked at the L3/L4 stage to new plates to avoid overgrowing and starvation. On Day 7 (unless otherwise indicated), homozygous *coq-2(ok1066)* animals were mounted on a 2% agarose pad and GABA neuron degeneration was examined on a Zeiss Axioplan compound microscope using a 100x objective. Percent (%) degeneration was scored as described in **Chapter 2 – Materials and Methods**. The experimenter was blinded to avoid bias.

Assay for "undead" RME neurons

Adult animals were mounted on a 2% agarose pad and examined on a Zeiss Axioplan compound microscope using a 100x objective. Total number of RME neurons (visualized by *punc-25::*GFP) were counted and animals with more than four RMEs were scored as "extra RME."

***coq-1* RNAi-induced GABA neurodegeneration assay**

Feeding RNAi assays (Kamath et al. 2003) were performed as described in **Chapter 2 – Materials and Methods** (Earls et al. 2010).

GABA neuron versus cholinergic neuron degeneration assay

A *coq-1* RNAi assay was used to quantify the number of GABAergic and cholinergic neurons in WT and *ced-3(ok2734)* mutants marked with the *trIs10* multi-color reporter (Dixon 2006). At Day 5 of the *coq-1* RNAi experiment, the total number of D-type GABAergic (VD3-VD11) and DA/DB cholinergic neurons (DB3-DA9) were counted. Wild-type animals have 13 GABAergic (Fig. 1.7) and 13 cholinergic neurons in this interval. Animals grown on empty vector (EV) control bacteria (i.e., backbone vector lacking an RNAi insert) did not show evidence of GABA neuron degeneration (data not shown).

Dietary Coenzyme Q_9 feeding plates

CoQ_9 bacterial plates were made as described in **Chapter 3 – Materials and Methods**.

Apoptotic versus necrotic GABA neurons

Differential interference contrast (DIC) microscopy on a Zeiss Axioplan compound microscope (using a 100x objective) was used to assess the distribution of apoptotic versus necrotic GABA neurons. Neurons with a raised, button-like appearance were scored as apoptotic and swollen cells were scored as necrotic.

Microscopy

Images in Figures 4.2 and 4.4 were obtained with a Leica TCS-SP5 confocal microscope using the Leica Application Suite Advanced Fluorescence (LAS-AF) software with a 40x objective. A Zeiss Axioplan compound microscope was used to capture the images in Figure 4.3 and 4.6.

Caspase cleavage site prediction

The CED-4 protein sequence (accession number NP_001021202.1) was analyzed using CASVM: Server for SVM Prediction of Caspase Substrates Cleavage Sites (Wee et al. 2006) to identify a single predicted caspase cleavage site at 89-DYID-92.

Experimental contributions

Meg Mitchell built the NC2778, NC2779, NC2790 and NC2819 strains and quantified the percent extra RME for all *ced-4* alleles in Figure 4.2.

RESULTS

Loss of CED-3 enhances GABA neurodegeneration induced by CoQ depletion

Our initial assessment of the role of CED-3 during GABA neurodegeneration relied on *coq-1* RNAi and detected partial suppression of degeneration by a *ced-3(n717)* mutant (Fig. 2.6). This result indicated that CED-3 functioned in parallel to an unknown factor to promote GABA neuron death. To confirm this finding I performed a parallel experiment with the *ced-3* deletion allele, *ok2734*, in a *coq-2(ok1066)* background. This experiment was designed to address two possible caveats with the interpretation of the results obtained with *ced-3(n717)*. First, the *ced-3(ok2734)* allele corresponds to a large deletion that spans the caspase active site and therefore likely represents the null phenotype (Fig. 4.1A). In contrast, the *ced-3(n717)* point mutation perturbs the fidelity of exon 7 splicing and can result in both wild-type and frame-shifted versions of *ced-3* mRNA (Shaham et al. 1999). Thus, *ced-3(n717)* could retain low levels of wild-type or neomorphic *ced-3* activity. My recent discovery of the sensitivity of *coq-1* RNAi effect to different genetic backgrounds (see **Appendix A**) also emphasizes the importance of validating the role of *ced-3* by using a genetic mutant to disable CoQ biosynthesis. Thus, I used the *coq-2(ok1066)* mutation to reduce CoQ levels in this experiment. In contrast to earlier experiments with *ced-3(n717)*, the *ced-3(ok2734)* allele reproducibly enhanced GABA neuron degeneration in the *coq-2(ok1066)* background. This new finding suggested the opposite role for CED-3 as a negative regulator of CoQ-deficient GABA neuron degeneration.

To address this disparity I also constructed double mutants of *coq-2(ok1066)* with *n717* and two additional strong apoptotic loss-of-function *ced-3* alleles: *n2888* (early stop codon) and *n2433* (missense mutation in the caspase active site) (Shaham et al. 1999) (Fig. 4.1A). In this experiment, GABA neurodegeneration was significantly enhanced by all four *ced-3* loss-of-function backgrounds, thereby supporting the hypothesis that CED-3 adopts a protective role in GABA neurons of CoQ-

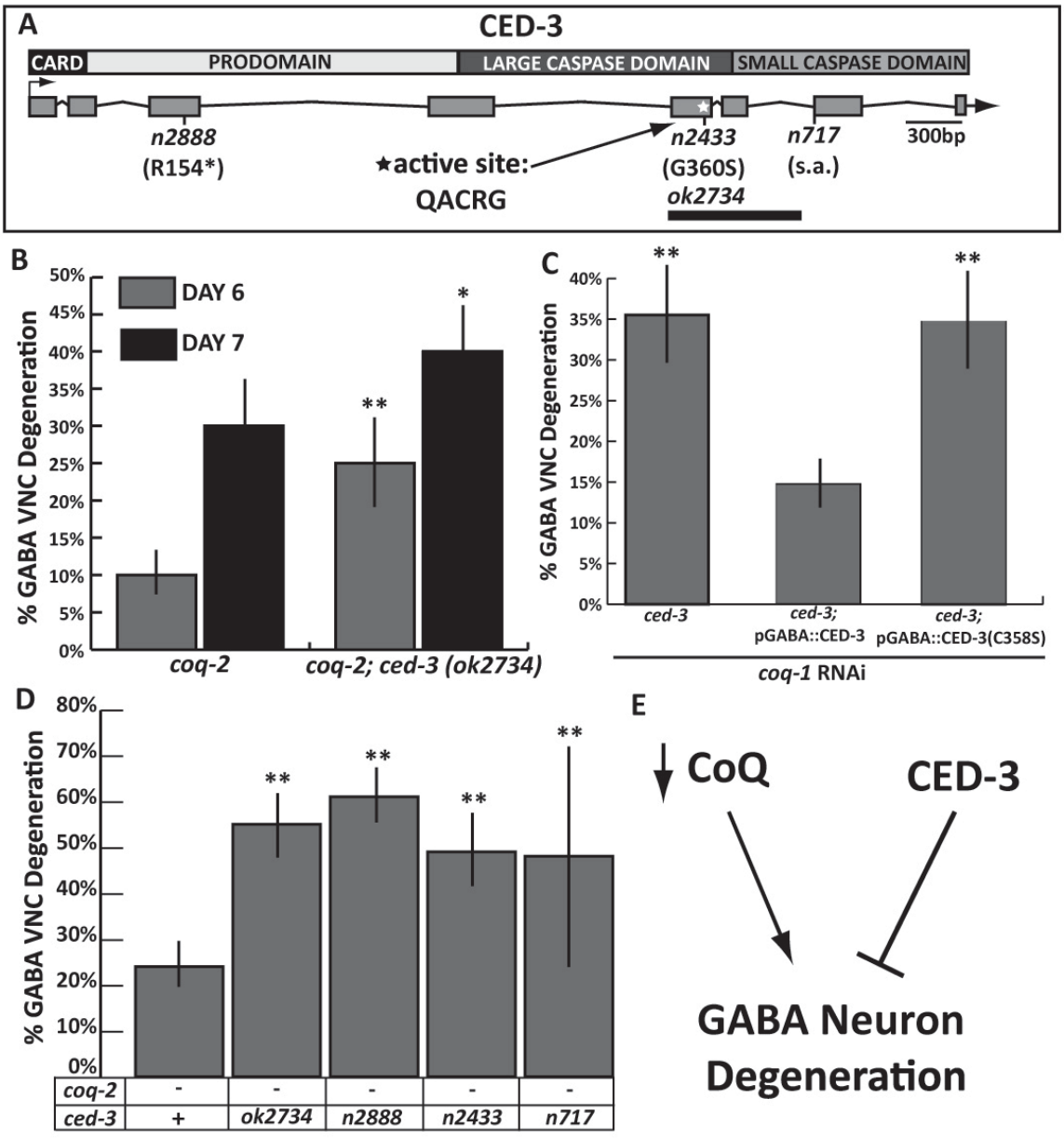
A
CED-3
CARD
PRODOMAIN
LARGE CASPASE DOMAIN
SMALL CASPASE DOMAIN
n2888
(R154*)
★active site:
QACRG
n2433
(G360S)
ok2734
n717
(s.a.)
300bp
B
% GABA VNC Degeneration
DAY 6
DAY 7
coq-2
coq-2; ced-3 (ok2734)
C
% GABA VNC Degeneration
ced-3
ced-3;
pGABA::CED-3
ced-3;
pGABA::CED-3(C358S)
coq-1 RNAi
D
% GABA VNC Degeneration
coq-2
ced-3
ok2734
n2888
n2433
n717
E
CoQ
CED-3
GABA Neuron
Degeneration

Figure 4.1: CED-3 caspase activity protects GABA neurons from degeneration induced by depletion of Coenzyme Q. A. *ced-3* mutants used in this study with protein domains: CARD = Caspase Activation Recruitment Domain. s.a. = splice acceptor mutant, * = premature stop codon, CED-3 active site = QACRG (star). *n2433* (G360S) mutates G of the active site and the caspase-dead construct (C358S) changes the active site C to S. **B.** GABA neuron degeneration is significantly enhanced in *coq-2(ok1066); ced-3(ok2734)* mutants versus *coq-2* single mutants. ** p<0.003 vs *coq-2*/Day 6, * p<0.02 vs *coq-2*/Day 7. **C.** GABA neuron-specific expression of CED-3 reduces GABA neurodegeneration induced by *coq-1* RNAi in *ced-3(ok2734)* mutants. Caspase-dead (C358S) *ced-3* expression does not suppress degeneration of GABA neurons. All strains share the *ced-3(ok2734) eri-1(mg366); unc-25::GFP(juIs76)* genetic background. n>25, ** p<0.002. **D.** Multiple loss-of-function *ced-3* alleles show enhanced GABA neuron degeneration. ** p<0.007, n>20. **E.** Model: Coenzyme Q deficiency triggers a GABA neuron degeneration pathway that is opposed by CED-3.

deficient animals (Fig. 4.1E). Although GABA neurodegeneration was enhanced, we note a highly variable phenotype in *ced-3(n717); coq-2* double mutants. This range of neurodegeneration may reflect the dominant-negative nature of the *n717* gene product that we speculate accounts for the discrepancy between the *coq-1* RNAi assay and these new findings.

Caspase activity of CED-3 is cell autonomously required to protect GABA neurons

CED-3 is a caspase that functions cell autonomously to promote programmed cell death during development (Ellis & Horvitz 1986; Yuan & Horvitz 1990; Shaham & Horvitz 1996b). Our data indicate that this otherwise canonical pro-apoptotic gene adopts a novel, neuroprotective role in CoQ-deficient animals. To address whether the death-inhibiting role of CED-3 is cell autonomous, I asked if GABA neuron-specific expression of wild-type CED-3 could rescue the *ced-3* mutant phenotype of enhanced neurodegeneration by *coq-1* RNAi. GABA neuron-specific restoration of *ced-3* significantly reduced degeneration compared to control *ced-3(ok2734)* animals (Fig. 4.1C). Expression of CED-3 with an active site mutation (C358S, Fig. 4.1A) did not reduce GABA neuron degeneration and thus suggests that CED-3 caspase activity is required for its neuroprotective role (Fig. 4.1C). This results parallels our finding that the *ced-3(n2433)* mutant (which also specifically disrupts the active site) shows enhanced neurodegeneration in *coq-1* RNAi-treated animals (Fig. 4.1B). These studies demonstrate that CED-3 proteolytic activity is required in GABA neurons to inhibit neurodegeneration induced by CoQ deficiency.

Forced CED-3 activation kills GABA neurons through apoptosis

The unexpected finding that CED-3 inhibits a cell death pathway in GABA neurons raised the question of whether CED-3 is capable of executing an apoptotic program in this cell type. We and others have shown that overexpression of wild-type *ced-3* does not force an apoptotic death in

GABA neurons (Fig. 4.1C) (Shaham & Horvitz 1996b). This result is interesting because ectopic *ced-3* expression is sufficient to induce apoptosis in mechanosensory neurons (Shaham & Horvitz 1996b). To investigate whether robust levels of CED-3 activation are neuroprotective, we used a reconstituted caspase system to force CED-3 activation in GABA neurons (Chelur & Chalfie 2007). In this system, large and small caspase catalytic subunits are attached to antiparallel leucine-zipper domains and expressed independently using cell-specific promoters. Presence of both leucine-zipper domains in a cell facilitates caspase activation (Fig. 4.2A). In this experiment, expression of constitutively active CED-3 in GABA neurons induced an apoptotic response with GABA neurons adopting a compact, button-like morphology (Fig. 4.2D-F). Movement was also impaired, with *pGABA::rec-ced-3* transgenic animals showing a "shrinker" movement defect (data not shown), a hallmark of impaired GABA neuron function (McIntire, Jorgensen & Horvitz 1993a).

The forced apoptotic death by CED-3 reconstitution indicates a high level of CED-3 caspase activity is sufficient to kill GABA neurons. This striking apoptotic response was not altered under CoQ-deficient conditions (Fig. 4.2G). This finding argues that CoQ deficiency activates CED-3 by a mechanism that is likely independent of the pathway that triggers an apoptotic role for CED-3 and that despite the ability of GABA neurons to die through CED-3-dependent apoptosis, Coenzyme Q deficiency triggers an alternative function for this caspase.

Apoptosis is impaired in GABA neuron precursor cells in *ced-3* and *ced-4* mutants

Our discovery that CED-3 adopts alternative roles in apoptotic versus neurodegenerative pathways prompted us to ask if these CED-3 functions are unique to GABA neurons. To address this question, we considered the fate of cells that are generated as RME GABA neurons in the head region. Normally, the lineal sisters of RME L/R and the "aunt" of RMEV GABA neurons undergo apoptosis (Fig. 4.3A). In addition to robust D-type GABA motor neuron death, we also observe RME

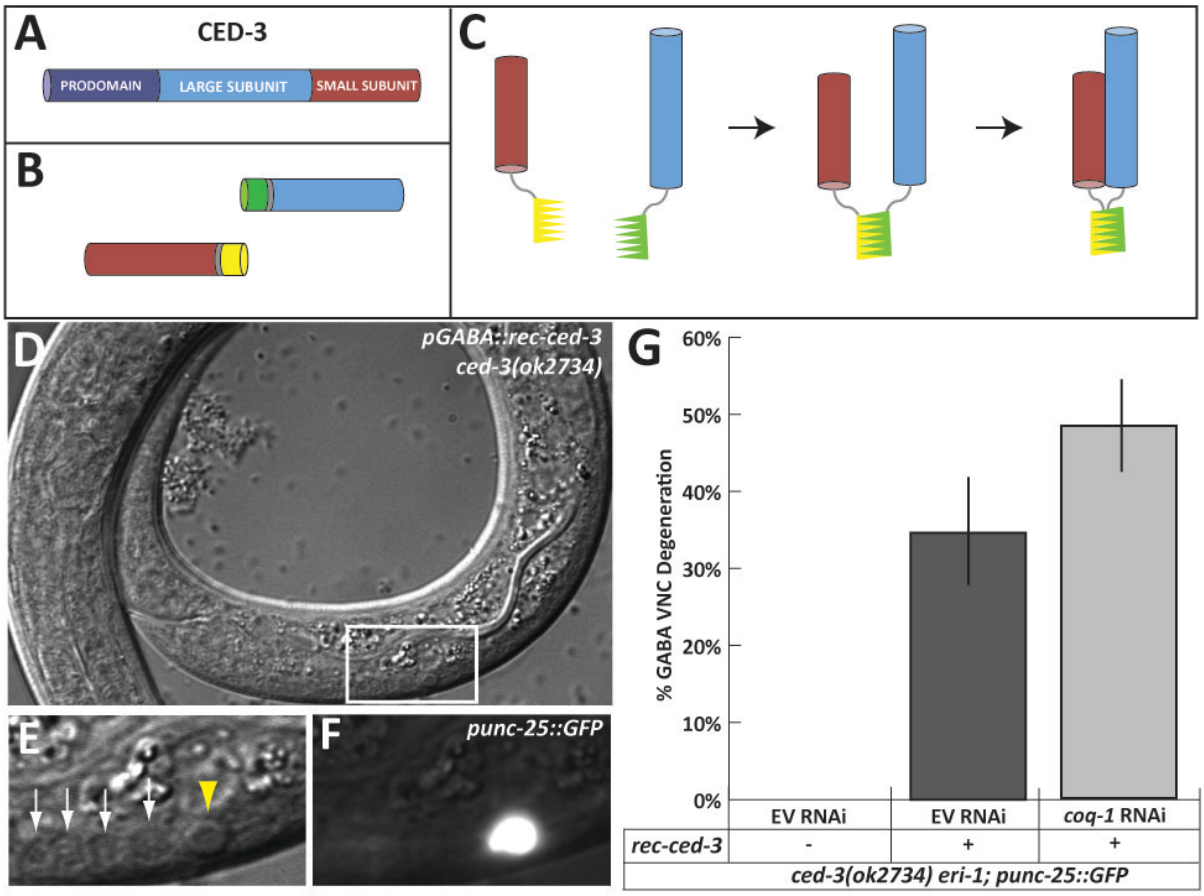

Figure 4.2: Forced CED-3 activation kills GABA neurons through apoptosis. A. CED-3 procaspase (zymogen) subunits. **B.** Reconstituted-CED-3 (rec-CED-3) has two components: large (blue) and small (red) caspase subunit domains are attached to leucine zipper domains (green and yellow) by a linker (gray). **C.** rec-CED-3 is formed by interaction between the antiparallel leucine zipper domains that activates CED-3. Panels A-C are modified from Chelur *et al.* (Chelur & Chalfie 2007). **D.** DIC image of a button-like neuron in an L2 *ced-3(ok2734)* animal that expresses rec-CED-3 in GABA neurons. **E.** Magnified inset shows an apoptotic neuron (yellow arrowhead) and four healthy neighboring neurons (white arrows). **F.** The apoptotic neuron expresses *punc-25::GFP* and is therefore GABAergic. **G.** Forced CED-3 activation (*pGABA::rec-ced-3)* kills GABA neurons under control (EV) RNAi conditions and enhances degeneration with *coq-1* RNAi. *p<0.08 versus EV RNAi + *rec-ced-3*, n>20.

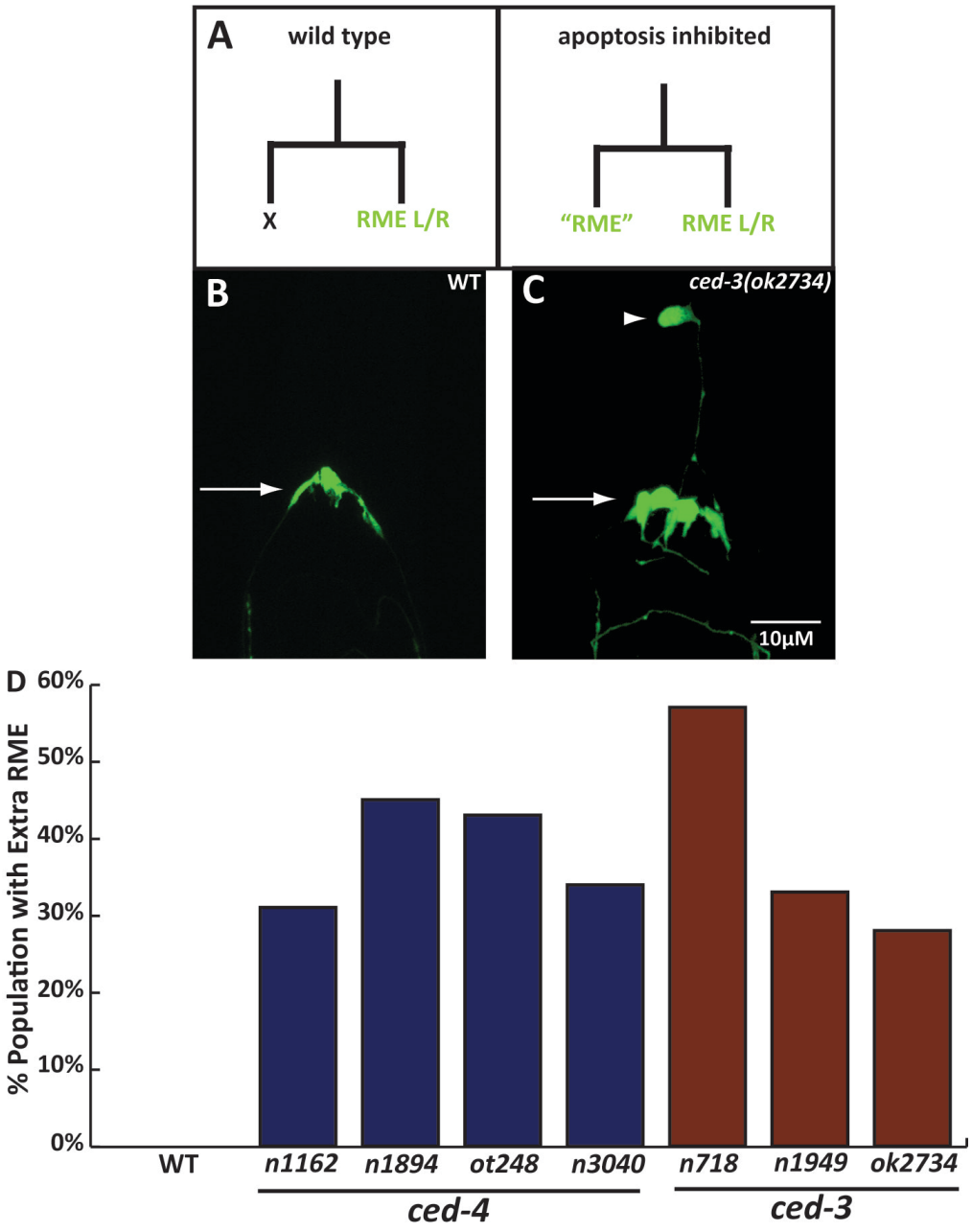

Figure 4.3: *ced-3* alleles block apoptosis in GABA neuron precursor cells. A. Inhibition of core apoptotic machinery (i.e., *ced-3* and *ced-4*) prevents programmed cell death of RME cells in the GABAergic lineage (image adapted from (Frank et al. 2005)). **B.** Wild-type animals have four *punc-25::GFP*(+) RME neurons (white arrow). **C.** *ced-3* mutants have additional RME-like neurons that often migrate anteriorly (white arrowhead). Anterior up, ventral right. **D.** Extra/undead RME neurons are not found in wild-type animals but are prevalent in *ced-4* and *ced-3* mutants.

GABA neurodegeneration under CoQ-deficient conditions (Fig. 2.4, Fig. 5.3). I determined that *ced-4* mutants resulted in ectopic RME-like GABA neurons (Fig. 4.3B) to confirm an earlier report that the "undead" relatives of RME neurons can adopt a GABA neuron-like fate (Frank et al. 2005) (Fig. 4.3C). This result also verified that *ced-4* mutations that perturb neurodegeneration in CoQ-deficient GABA neurons are also sufficient to block apoptosis in these cells. As shown in Fig. 4.3, *ced-3* mutations that enhanced degeneration of CoQ-deficient GABA neurons also prevent the death of the lineal sisters of RME neurons. These results are consistent with a model in which the core apoptotic components, CED-3 and CED-4, can adopt alternative roles in GABA neurons that are activated for degeneration by deficient CoQ production.

Cholinergic neuron sensitivity to CoQ depletion is not enhanced by loss of CED-3

In previous studies, we showed that CoQ deficiency preferentially affects the GABA neurons, with other neuronal subtypes and body wall muscle showing less sensitivity to CoQ depletion (Fig. 2.2, Fig. 2.4, Fig. 2.5) (Earls et al. 2010). Given our recent discovery that loss of CED-3 activity enhances GABA neuron degeneration with CoQ depletion, it was interesting to consider the possibility that CED-3 activity might also protect other classes of CoQ-deficient neurons from death. To address this question, I examined ventral cord cholinergic neurons (DA/DB) for degeneration in *coq-1* RNAi-treated *ced-3(ok2734)* mutants. However, this experiment did not result in detectable loss of cholinergic neurons (Fig. 4.4). Thus, these data suggest that CED-3 activity protects GABA neurons from the stress caused by CoQ deficiency but is not required for this neuroprotective role in other neuron types (i.e.,cholinergic neurons) that do not degenerate with CoQ-deficient animals.

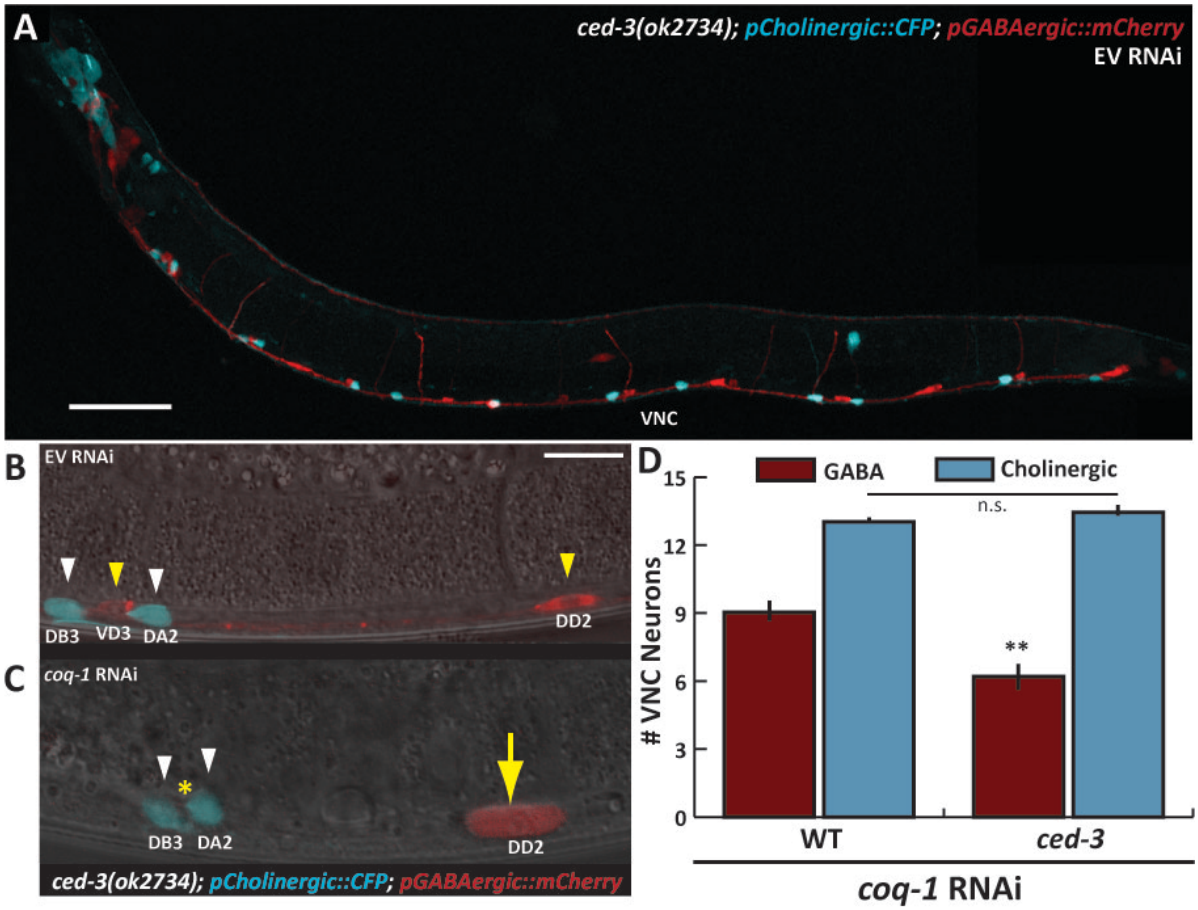

Figure 4.4: Cholinergic neurons are not more sensitive to Coenzyme Q depletion in *ced-3* mutants. **A.** Adult empty vector (EV, control) RNAi-treated *ced-3* animal retains the full complement of GABAergic or Cholinergic neurons in the ventral nerve cord (VNC). Scale bar = 50 µM. **B.** Cholinergic neurons (white arrowhead) and GABAergic neurons (yellow arrowhead) in EV RNAi-treated *ced-3* mutants. **C.** VNC GABA neurons either missing (VD3, asterisk) or appear swollen (DD2, yellow arrow) in *coq-1* RNAi-treated *ced-3* mutants but cholinergic motor neurons (DB3, DA2, white arrowheads) show normal morphology. Scale bar = 10 µM. **D.** *coq-1* RNAi-treated *ced-3* mutants show a significant reduction in the number of VNC GABAergic neurons compared to wild-type (WT), whereas the wild-type number of VNC cholinergic neurons is retained. EV control RNAi-treated WT and *ced-3* mutant adults do not have missing cells from VD3-VD11 (13 D-type GABA neurons) and DB3-DA9 (13 DA/DB neurons) (data not shown) ** $p<0.001$ vs WT GABA, $n>20$, n.s. = not significant.

***ced-4*/Apaf-1 functions cell autonomously and is epistatic *ced-3*/caspase**

The Apaf-1 homologue *ced-4* functions cell-autonomously in the canonical apoptotic pathway (Shaham & Horvitz 1996a). We previously identified *ced-4* as an essential component of the CoQ depletion-induced GABA cell death pathway (Fig. 2.6) (Earls et al. 2010). With *coq-1* RNAi treatment, transgenic expression of CED-4 in GABA motor neurons restored degeneration to *ced-4(n1162)* mutants (Fig. 4.5B). Thus, *ced-4* functions cell-autonomously to kill GABA neurons in response to CoQ depletion.

To address the genetic relationship between *ced-4* (promotes death) and *ced-3* (antagonizes death), I performed an epistasis experiment by examining the degeneration phenotype of a *ced-4; ced-3* double mutant in a *coq-1(ok749)* background. For this experiment, *coq-1(ok749)* mutants were grown on an *E. coli* background (KO229) that produces CoQ_9 and supports growth to the adult stage for scoring signs of GABA neurodegeneration (see **Chapter 3**). Consistent with our earlier results obtained using *coq-2* mutants (Fig. 4.1B) or by *coq-1* RNAi (Fig 4.1C), *coq-1(ok749)* adults show enhanced degeneration in a *ced-3(ok2734)* background compared to *coq-1* single mutants (Fig. 4.5C). This experimental paradigm is also validated by the finding that *ced-4* is required for GABA degeneration in *coq-1* mutants as previously observed in other CoQ-deficient conditions (*coq-1* RNAi and *coq-3* mutants, Fig. 2.6 (Earls et al. 2010)). GABA neuron degeneration is significantly reduced in the *coq-1; ced-4; ced-3* triple mutant (Fig. 4.5C) which indicates that *ced-4* is epistatic to *ced-3* in the GABA neuron death pathway of CoQ-deficient animals. This genetic result is consistent with a mechanism in which CED-4 functions either downstream or in parallel to CED-3 (Fig. 4.7).

GABA neurons adopt apoptotic or necrotic features in *coq-1* mutants fed KO229 *E. coli*

As described above, we used *E. coli* strain KO229 to provide sufficient dietary CoQ_9 to sustain *coq-1(ok749)* mutant animals to the adult stage for scoring GABA neuron death. Although

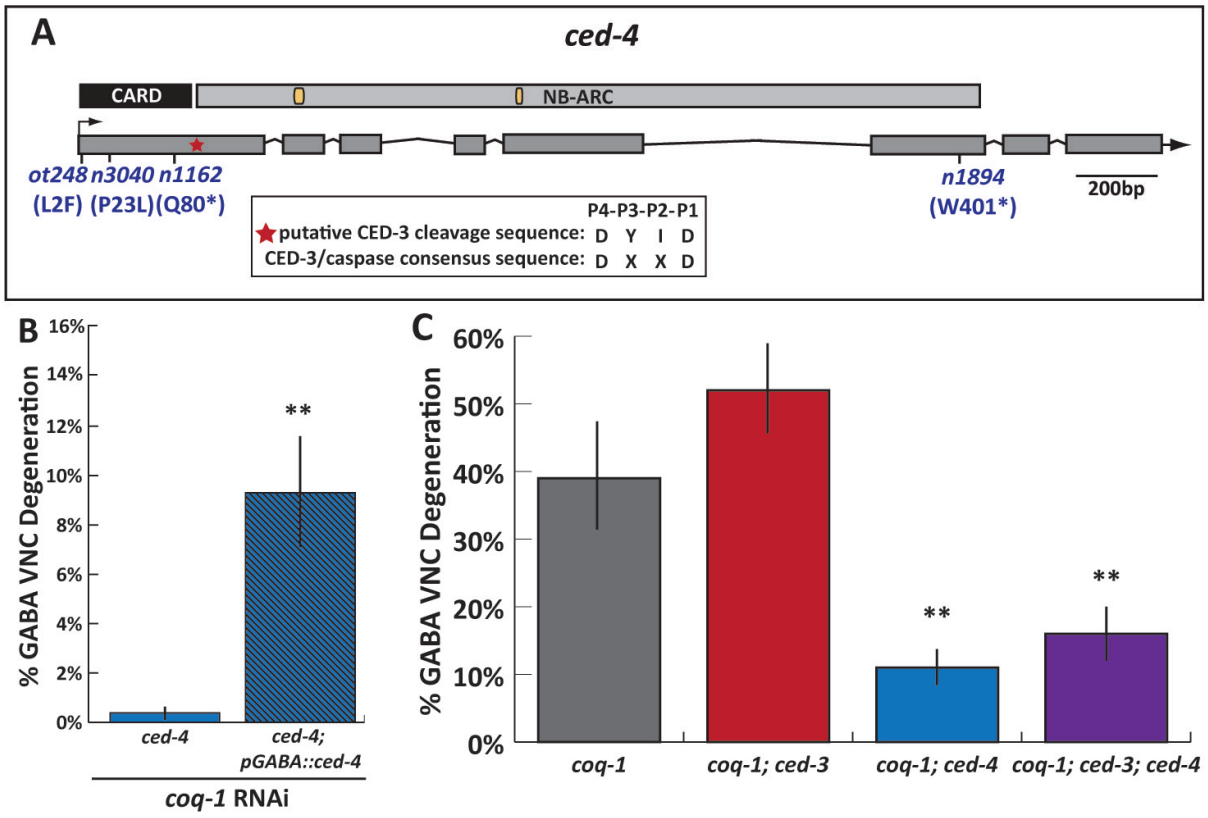

Figure 4.5: *ced-4* is epistatic to *ced-3* and functions cell autonomously to kill GABA neurons.
A. *ced-4* gene model with the location of CARD and NB-ARC domains. Yellow boxes are predicted P-loop/ATP-binding sequences (Zou et al. 1997). Red star = putative CED-3 cleavage sequence (89-DYID-92) (Wee et al. 2006). Mutant alleles used in this study are indicated; premature stop codon (*). **B.** GABA neuron-specific expression of *ced-4* restores degeneration with *coq-1* RNAi. Both strains share the *ced-4(n1162) eri-1(mg366); unc-25::GFP(juIs76)* background. ** p<0.0001, n>50. **C.** Neurodegeneration in the *coq-1(ok749); ced-4(n1162); ced-3(ok2734)* triple mutant resembles that of the *coq-1(ok749); ced-4(n1162)*, indicating that *ced-4* is epistatic to *ced-3* in this pathway. **p<0.0001 vs *coq-1*, n>40. The neurodegeneration enhancement in *coq-1; ced-3* is not statistically significant from *coq-1* in this instance (p<0.06), however the results of multiple independent experiments have confirmed significantly enhanced cell death (data not shown).

our treatment resulted in the expected complement of necrotic (i.e., swollen) GABA neurons, growth of *coq-1* mutants on KO229 bacteria also produced a significant fraction (~20%) of dying GABA neurons with the compact nuclei that are hallmarks of apoptotic cells (Fig. 4.6). This combination of GABA neurons with either necrotic or apoptotic features was uniquely observed in CoQ biosynthetic mutants on KO229 *E. coli; coq-1* RNAi and growth of *coq-2, coq-3* and *coq-8* on OP50 (normal *E. coli* diet) exclusively resulted in GABA neurons with swollen (i.e., necrotic) cell bodies (Fig. 2.2, Fig. 3.2). The reason for this difference is unclear but the appearance of apoptotic cells in *coq-1* mutants indicates that CoQ-deficiency can trigger either of these cell death mechanisms. In this experimental paradigm, both types of cell death (necrotic and apoptotic) require *ced-4* (Fig. 4.5C). In contrast, *ced-3* antagonizes GABA neuron death by either of these mechanisms. Thus, the apoptotic pathway that is induced in *coq-1* mutants must differ from the canonical apoptotic mechanism for which *ced-3* function is essential (Ellis & Horvitz 1986).

DISCUSSION AND FUTURE DIRECTIONS

The work presented in this chapter describes a novel, neuroprotective role for the canonical apoptotic caspase CED-3 in CoQ-deficient GABA neurons (Fig. 4.1). We demonstrate that CED-3 caspase activity is necessary for this function. Furthermore, our results show that CED-3 antagonizes a cell-killing pathway that is promoted by CED-4/Apaf-1 (Fig. 4.5). Our genetic results showing that *ced-4* is epistatic to *ced-3* indicate that CED-4 functions either downstream or in parallel to CED-3. This result is particularly striking because CED-4/Apaf-1 functions upstream of CED-3/caspase in the canonical apoptotic pathway (Shaham & Horvitz 1996b; Shaham & Horvitz 1996a). Furthermore, we noted that the occurrence of GABA neurons with apoptotic features in *coq-1* mutant animals was not blocked by genetic ablation of *ced-3* and is thus also suggestive of a novel apoptotic mechanism.

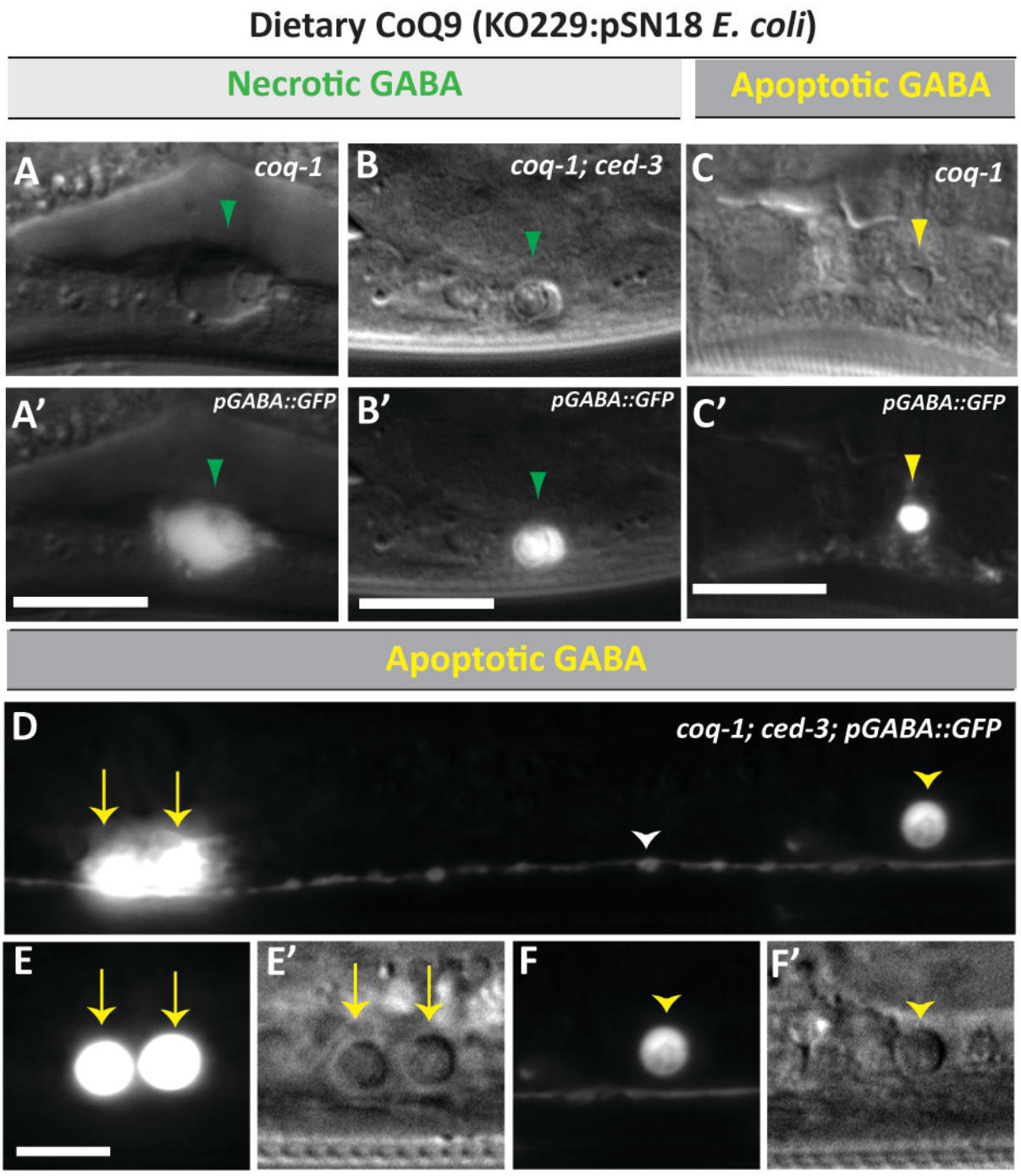
Dietary CoQ9 (KO229:pSN18 E. coli)
Necrotic GABA
Apoptotic GABA
A
coq-1
B
coq-1; ced-3
C
coq-1
A'
pGABA::GFP
B'
pGABA::GFP
C'
pGABA::GFP
Apoptotic GABA
D
coq-1; ced-3; pGABA::GFP
E
E'
F
F'

Figure 4.6: Coenzyme Q deficiency-induced GABA neuron death occurs independently of CED-3. **A-A'.** A GABA neuron in a *coq-1(ok749)* animal (green arrowhead) is swollen (i.e., necrotic). **B-B'.** Necrotic features are also displayed in a GABA neuron (green arrowhead) in a *coq-1; ced-3* double mutant. **C-C'.** A button-like apoptotic GABA neuron (yellow arrowhead) is also observed in a *coq-1* mutant. **D.** Three apoptotic GABA neurons are shown in *coq-1; ced-3* double mutants along the ventral nerve cord (white arrowhead). **E-E'.** Two neighboring GABA neurons from Panel D (yellow arrows) show pronounced apoptotic morphology. **F-F'**. A third GABA neuron shows rounded, button-like morphological features in *coq-1; ced-3* double mutants (yellow arrowhead). All images were collected from animals fed KO229:pSN18 (CoQ_9-producing) *E. coli*. *pGABA::GFP = punc-25::GFP.* Scale bars = 10μM.

Nonetheless, GABA neurons can undergo *ced-3*-dependent apoptotic death in other contexts, for example, with over-expression of activated CED-3 or during neuronal development (Fig. 4.2, Fig. 4.3). These results are indicative of diverse mechanisms of cell death in GABA neurons and suggest that CED-3 can adopt different roles in these distinct pathways.

Restricted CED-3 activation protects GABA neurons from CoQ depletion-induced death

Our findings indicate that CED-3 may either promote or inhibit cell killing pathways in *C. elegans* GABAergic neurons and that these opposite roles likely depend on mechanisms that regulate CED-3 activity. We showed that expression of an activated form of CED-3 induced robust apoptosis of GABA neurons. In contrast, transgenic expression of CED-3 in its inactive zymogen form did not result in GABA neuron death but was sufficient to antagonize degeneration induced by CoQ deficiency. Regulation of caspase activity is also a likely determining factor in other neuronal contexts in which caspase-dependent pathways either trigger apoptosis or lead to alternative outcomes such as regeneration (Pinan-Lucarre et al. 2011) or dendritic pruning (Williams et al. 2006).

CED-3 and CED-4 adopt opposing roles in CoQ-depleted GABA neurons

In the canonical apoptotic pathway, CED-4 activates CED-3 to trigger cell death (Fig. 1.3). Our results indicate that these two proteins (CED-3 and CED-4) can also function through an alternative mechanism in adult GABA motor neurons under CoQ-deficient conditions. In this setting, CED-3 antagonizes a CED-4-dependent death pathway. In addition, our genetic epistasis results indicate that CED-4 functions either downstream or in parallel to CED-3. Here, I discuss potential mechanisms to explain the novel roles of CED-3 and CED-4 in this neurodegeneration pathway.

GABA neuron degeneration and regeneration pathways share common components

Recent studies have revealed that CED-3 promotes regeneration of axotomized GABAergic and mechanosensory motor neurons in *C. elegans* (Pinan-Lucarre et al. 2011). In this experimental paradigm, CED-3 function is cell autonomous and necessary for efficient regrowth of injured neuronal processes. Additionally, CED-3 acts upstream of the conserved regeneration kinase DLK-1 (p38-like MAPK pathway). We speculate that axotomy and CoQ deficiency may activate a common set of stress signals to counteract the cellular injury. It is reasonable to imagine for example, that CoQ deficiency triggers a neurodegeneration pathway that is countered by a regeneration mechanism that depends on CED-3. Thus, in this model, a loss-of-function *ced-3* mutation could indirectly enhance the degeneration phenotype by preventing a regeneration response to mediate the injurious pathway (Fig. 4.7A). Interestingly, a recent review of proteomics literature identified many common pathways (involving axonal transport, molecular chaperones, cytoskeletal components) that are modified in response to both regeneration and degeneration (F. Sun & Cavalli 2010). This finding is consistent with the idea that cellular injury (CoQ depletion or axotomy) could induce similar responses to repair damaged subcellular compartments (e.g., neurites).

The possibility of shared mechanisms for the axotomy-induced regeneration pathway and the CoQ-deficient response that we have discovered in GABA neurons is also underscored by the parallel findings that the upstream apoptotic regulators EGL-1 and CED-9 are not required for either mechanism (Pinan-Lucarre et al. 2011) (Fig. 2.7). In addition, both pathways require the calcium-binding chaperone protein calreticulin (CRT-1) (Fig. 2.6) and are thus likely regulated by intracellular calcium. The roles of CED-4 in these pathways may differ, however. Whereas CED-4 promotes degeneration with CoQ deficiency, CED-4 function is required for efficient regeneration of GABA neurons injured by axotomy. Perhaps CoQ deficiency triggers a degeneration response that is not

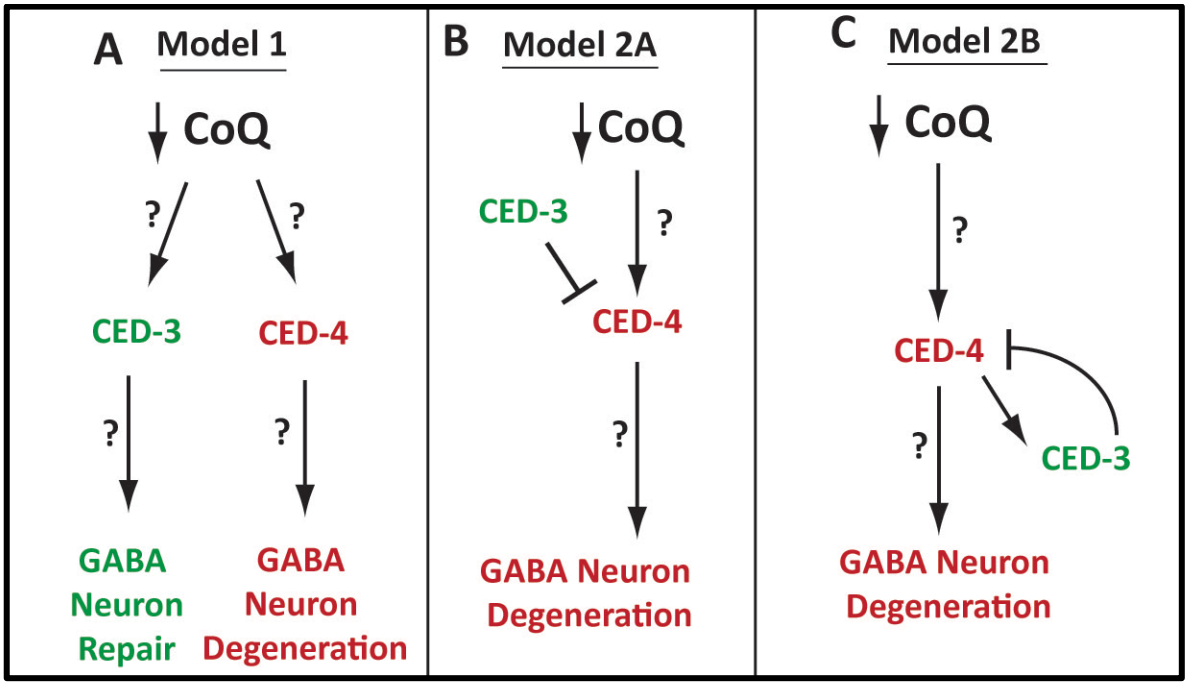

Figure 4.7: Proposed models to explain epistatic interactions between *ced-3* and *ced-4*. A. Model 1: Reduced CoQ levels triggers parallel pathways in GABA neurons. A CED-3-dependent mechanism is activated to repair the damage caused by CoQ deficiency and a CED-4-dependent pathway promotes GABA neuron cell death. In the absence of both *ced-4* and *ced-3* function, the CoQ-deficiency pathway is blocked and thus accounts for GABA neuron survival in the *coq-1; ced-3; ced-4* triple mutant. **B.** Model 2A: CoQ deficiency activates CED-4 in a GABA neuron degeneration pathway that is antagonized by CED-3. A *ced-3* mutation enhances degeneration but this effect is blocked by mutations that disable *ced-4.* **C.** Model 2B: CED-4 is activated in response to CoQ depletion and subsequently activates both CED-3 and other unknown death-promoting factors. Activated CED-3/caspase provides feedback inhibition of CED-4, perhaps through proteolytic cleavage/inactivation.

activated by axotomy. In this scenario, CED-4 could function in both of these competing pathways (degeneration and regeneration) such that CoQ-deficient GABA neurons show net degeneration.

To test whether CED-3 functions to promote regeneration in parallel to CED-4 (Fig. 4.7A), members of the core GABA neuron regeneration pathway (e.g., *dlk-1*) could be knocked out in CoQ mutants to determine if their absence phenocopies the enhanced degeneration seen in *ced-3* mutants. Overexpression of regeneration proteins such as DLK-1/MAPKKK in GABA neurons accelerates axonal regeneration (Hammarlund et al. 2009) and it would be interesting to determine whether overexpression of this MAP kinase signaling cascade was neuroprotective following CoQ depletion.

The idea that CED-3 and CED-4 could function in parallel pathways as noted above is consistent with our genetic epistasis results (i.e., *ced-4* is epistatic to *ced-3*). This genetic interaction could also be explained by an alternative mechanism in which CED-4 functions downstream of CED-3 (Fig. 4.7B). However, the order of action of these gene products is reversed in the canonical apoptotic pathway (where CED-4 functions upstream of CED-3). In this instance (under CoQ-deficient conditions), CED-4 is downstream of CED-3. Recent evidence from other organisms points to a potential mechanism whereby CED-3 could function to inactivate CED-4.

Mechanisms of caspase-dependent proteolysis of Apaf-1 are conserved

Apaf-1 is proteolytically cleaved and inactivated by caspase-3 following apoptotic stimulation in human cell culture and *in vitro* (Bratton et al. 2001; Lauber 2001). Similarly, *Drosophila* homologue of CED-4 (Dark) is also cleaved by caspases (Akdemir 2006). Apaf-1 is inactivated by cleavage at a site near the N-terminus that removes the CARD domain (Bratton et al. 2001; Lauber 2001). In considering this mechanism, I have identified a putative CED-3 cleavage site (89-DYID-92) between the N-terminal CARD domain and the C-terminal NB-ARC domain of CED-4

(Fig. 4.5A). This DYID site matches the CED-3 consensus cleavage site of DXXD and is the only such site in the CED-4 protein sequence. The existence of this candidate CED-3 cleavage site is consistent with a model in which CED-3 antagonizes CED-4-dependent neurodegeneration by proteolytic inactivation of CED-4 function (Fig. 4.7B).

One curious feature of a model in which CED-3 functions upstream of CED-4 is that it does not explain how CED-3 becomes activated. The developmental apoptotic pathway relies on CED-4 to activate CED-3 (Shaham & Horvitz 1996b; Shaham & Horvitz 1996a). A more complex model of how CED-4 functions downstream of CED-3 could involve CED-4 (promotes death) activating CED-3 (prevents death) through a canonical mechanism (similar to CED-3 activation during programmed cell death) (Fig. 4.7C). Unlike apoptosis, however, activated CED-3 does not promote an apoptotic response but could instead inactivate CED-4. Under this paradigm, CED-3 activation elicits a negative feedback perhaps by directly cleaving and inactivating CED-4. This model would explain how loss of CED-3 enhances degeneration due to the absence of CED-4 inhibition, and without CED-4 there is no degeneration which aligns with our *ced-4* and *ced-4; ced-3* double mutant analysis. Currently, we have a basic understanding of the interplay between CED-3 and CED-4, where CED-4 is either in parallel or downstream of CED-3. Future experiments should be designed to distinguish between these models and to provide a clearer understanding of how these canonical apoptotic regulators function antagonistically in adult GABA neurons.

To investigate the possibility that CED-3 cleaves CED-4, biochemical experiments could be used to determine if CED-3 cleaves CED-4 at the proposed DYID site. Furthermore, mutagenesis strategies could also be used to disrupt the putative DYID sequence of CED-4; aspartate-to-alanine mutations in caspase-recognition sites abrogate caspase-dependent cleavage (Ditzel et al. 2003). If CED-3 cleaves at this site to inhibit CED-4 *in vivo*, then expression of this mutant form of CED-4 (DYIA) could potentially enhance degeneration with CoQ deficiency due to elimination of the

damping effect of CED-3-dependent cleavage of CED-4. In fact, transgenic expression of CED-4(DYIA) in the GABA neurons is predicted to phenocopy the enhanced neurodegenerative effects of CED-3 since CED-4 is not cleaved by CED-3. These experiments will begin to distinguish between our proposed models (Fig. 4.7) and provide insight into the antagonistic relationship between CED-3 and CED-4 during CoQ deficiency-induced death.

A novel mechanism for CED-4 activation and execution of necrotic-like death

Based on our analysis, CED-4 promotes GABA neuron death without requiring its canonical downstream caspase CED-3. Another CED-4-dependent/CED-3-independent apoptotic mechanism has been reported (Bloss et al. 2003), but currently no downstream components of this pathway have been identified. In addition to the novelty of CED-4 regulating a necrotic-like death pathway, our results also introduce the intriguing question of how CED-4 could promote cell death in the absence of a downstream "killing" role for CED-3. An additional caspase CSP-1 has recently been assigned to a death-promoting role in *C. elegans* (Denning et al. 2013). In this pathway, however, CSP-1 is maternally provided to kill a subset of embryonic cells in a pathway that does not require CED-4 for activation. Perhaps CoQ depletion induces CSP-1 expression in GABA neurons where it is activated by CED-4. Future experiments to investigate whether this additional caspase is required for GABA neurodegeneration in *coq-1* mutants using a *csp-1* loss-of-function background will determine whether CED-4 potentially activates another caspase or whether novel death proteins are employed. Denning *et al.* (2013) also identify examples of apoptosis that are independent of caspase function which suggests that cell death can be executed by alternative downstream effectors (Denning et al. 2013).

Our work in **Chapter 2** used *coq-1* RNAi to demonstrate that *ced-4* is activated by a novel mechanism. In these experiments, mutations in the canonical upstream regulators of *ced-4* (*ced-9*

and *egl-1*) did not perturb degeneration of CoQ-deficient GABA neurons (Fig. 2.7). However, given my recent discovery that RNAi efficacy varies with genotype (see **Appendix A**), more experiments should be replicated in a genetic model of CoQ deficiency (e.g., *coq-1* mutant). Since all CoQ depletion-induced GABA neuron deaths (apoptotic or necrotic) are promoted by CED-4 and inhibited by CED-3 it seems likely that our experiments with a *coq-1* mutant will confirm earlier results obtained with *coq-1* RNAi. In that event, future experiments could pursue the important question of how CED-4 is activated in this neurodegeneration pathway.

CED-9-independent activation of CED-4 has been observed with neuronal regeneration (Pinan-Lucarre et al. 2011) and hypoxic conditioning (Dasgupta et al. 2007); however neither of these studies identified upstream regulators of CED-4. Recently, a member of the Adenine Nucleotide Translocator (ANT) family of mitochondrial proteins (*wan-1)* was reported to physically interact with CED-4 and promote apoptosis in *C. elegans* (Q. Shen et al. 2009). ANT is a conserved mitochondrial protein that exchanges cytosolic ADP with mitochondrial ATP. As discussed in **Chapter 1**, ANT is also a key component of the mitochondrial permeability transition pore (PTP) complex that releases death-inducing factors from the mitochondria to promote cell death in mammals (Galluzzi et al. 2010). It is therefore reasonable to speculate that ANT is also required for CED-4 activation in CoQ-deficient GABA neurons. Knockout of ANT family members (*wan-1, wan-2, wan-3, wan-4*) in CoQ mutant backgrounds would provide a genetic way to test this hypothesis (further discussed in **Chapter 6**).

Apoptotic and necrotic death of CoQ-deficient GABA neurons occurs independently of CED-3

Our studies in **Chapter 3** are suggestive of a model in which GABA neuron degeneration requires a minimum threshold of CoQ function that is sufficient to maintain overall animal viability but which is not adequate to prevent GABA neuron death (Fig. 3.9). We have also observed that CoQ

deficiency can result in GABA neurons adopting the characteristic features of either apoptotic or necrotic cells (Fig. 4.6). Although the exact mechanisms that distinguish between these alternative outcomes are not known, this observation that both do occur suggest that stress signals resulting from CoQ deficiency can activate either necrotic or apoptotic killing pathways.

It was recently discovered that expression of HBx (Hepatitis B virus protein X) triggers apoptotic and necrotic death in *C. elegans* and that CED-9/Bcl-2 is an essential regulator of both death pathways (Geng et al. 2012). Interestingly, the mechanism by which CED-9 promotes apoptosis (canonical release of CED-4 and CED-3 activation) is distinct from its activation of necrosis, which occurs through mitochondrial permeability transition (MPT)-dependent calcium increase. Our data indicate that CoQ deficiency can also stimulate two morphologically distinct modes of cell death in GABA neurons that are both promoted by CED-4/Apaf-1 and antagonized by CED-3/caspase. Thus, our findings place CED-4 at a key nexus where it responds to cellular injury to promote alternative cell death mechanisms.

CHAPTER V

GENETIC AND ULTRASTRUCTURAL ANALYSIS OF A NECROTIC DEATH PATHWAY ACTIVATED IN COENZYME Q-DEFICIENT MOTOR NEURONS

INTRODUCTION

Coenzyme Q is an essential component of the mitochondrial electron transport chain (ETC) (Fig. 1.2) and ETC dysfunction is linked to cellular stresses such as increased reactive oxygen species (ROS) and depletion of cellular ATP levels (Petrozzi et al. 2007). Both of these insults are known to trigger apoptotic (Kasahara et al. 1997) and necrotic cell death pathways (Zong & Thompson 2006). As discussed in **Chapter 1**, neurodegenerative disease is correlated with impaired electron transport chain function (Fig. 1.1); additionally, we have shown that global ATP levels are reduced in CoQ-deficient animals (Fig. 2.10). However, Coenzyme Q may also exercise roles that are independent of ETC function (discussed in **Chapter 1**) and thus could support GABA neuron viability through mechanisms that do not involve the electron transport chain.

My work is focused on understanding the mechanism whereby CoQ depletion triggers GABA neuron degeneration. My findings indicate that GABA neuron death in this experimental paradigm depends on the canonical apoptotic genes that appear to act through novel mechanisms (see **Chapter 4**). Coenzyme Q deficiency models in *Drosophila* and zebrafish detect elevated caspase activity in animals with reduced Coenzyme Q production (Heeringa et al. 2011; Grant et al. 2010). Other studies have presented evidence that Coenzyme Q prevents apoptosis by inhibiting mitochondrial permeability pore opening (Papucci et al. 2003). Although my results have also detected roles for apoptotic genes in our *C. elegans* model of CoQ deficiency, the affected GABA neurons show the swollen morphology of necrotic cell death (Fig. 2.2, Fig. 3.2).

It is currently unclear whether CED-4/Apaf-1 regulates a strictly necrotic death or if dying neurons share features of both apoptosis and necrosis. Ultrastructural analysis is often used to distinguish between these two cell death pathways (Table 5.5) (Zong & Thompson 2006; Kerr et al. 1972) and transmission electron microscopy (TEM) has also identified cells that share features of both pathways (Formigli et al. 2000). I therefore examined ultrastructural features of dying motor neurons to better understand how apoptotic proteins regulate necrotic-like death.

Like apoptosis, necrosis also activates distinct proteases that are responsible for cellular demise. The most well-studied necrosis paradigm in *C. elegans* results from overactivation of neuronal ion channels where an influx of cations causes cell swelling and ultimately necrotic death (Syntichaki et al. 2002). Necrosis depends on multiple proteases including two calpains TRA-3 & CLP-1 that act in parallel and also upstream of two aspartyl proteases ASP-3 and ASP-4 (Fig. 1.4). Canonical apoptotic regulators (CED-3, CED-4, etc) (Fig. 1.3) are not required for this necrotic-like death, indicating that this pathway is molecularly distinct from programmed cell death. Based on our observation that GABA neurons swell under CoQ-deficient conditions, I hypothesized that components of the necrotic pathway (Fig. 1.4) were also likely components of this cell killing machinery. Here, I report that additional proteases adopt both predicted and novel roles in the GABA neurodegeneration pathway.

Work in this chapter seeks to better understand how Coenzyme Q deficiency kills GABA neurons by addressing key questions: How is cell death triggered? What proteases are required to kill CoQ-deficient neurons? What type of death occurs in GABA neurons? What might prevent other cells from degenerating? My studies reveal that initiation of the GABA neurodegeneration pathway by CoQ depletion is not solely a result of ETC dysfunction. This work also identifies necrotic proteases that regulate GABA neuron death. Finally, ultrastructural analysis of CoQ-deficient motor neurons reveals physical traits that are characteristic of necrosis.

MATERIALS AND METHODS

Nematode Strains and Genetics

Nematodes were maintained as previously described (Brenner 1974). Mutant alleles and genotyping primers are listed in Table 5.1. Strains used in this study are in Table 5.2.

Molecular biology

cDNA and *unc-25* RNAi generation were previously described in **Chapter 3.**

Verifying RNAi clones

RNAi clones (all derived from the pL4440 vector) were sequenced using M13F21. The *asp-3/H22K11.1* RNAi clone in the Ahringer library is listed under X-3H21; however the sequence of its bacterial clone aligns with a neighboring gene *H22K11.2*. The *nuo-2* RNAi clone from I-3M05 is also mislabeled, as it corresponds to a neighboring gene T0E9.6. The following Ahringer library RNAi clones are correctly annotated were verified by sequencing: *D2030.4, cyc-1, F26E4.6, atp-3, mev-1, gas-1, tra-3*.

RNAi

Feeding RNAi plates were made as described in **Chapter 2 – Materials and Methods**.

Movement assay

Adult animals on Day 6 of the RNAi experiment were tapped once or twice on the head and backward movement was scored as follows: “WT” (wild-type) = moves 2+ body bends backward, “Unc” = only moves 1 body bend backward, “Very Unc” = cannot move backward but does not shrink, “Shrinker” = shrinks when touched on the head. n>50 unless there were not enough adults

Table 5.1. Mutant alleles and transgenes used in this chapter.

Allele	Source	Genotyping Primers	Reference
asp-4(ok2693)	CGC	GCAACCAGTGAACCAGGAAT	(Geng et al. 2012)
		ATCTGTTGCTTAGTGGCGCT	
clp-1(tm858)	NBRP	AAAAAAGGAAACGAGACATGGCG	(Bano et al. 2009)
		ATGCATATAGAGAAGCTCGCCG	
eri-1(mg366) IV	CGC	CATGCAATTTCAATGCCTTTTA	(Kennedy et al. 2004)
		TGCATCATCCAATCCACTATGT	
gas-1(fc21) X	CGC	TTTTTCTGGATGTTCGAGGG	(Kayser et al. 1999)
		TCTTGTTGAGGCACTGATGC	
mev-1(kn1) III	CGC	CACTCGCCAAGGATAAAAGG	(Ishii et al. 1998)
		ATGGCGAGAGCAAGAATAGC	
tra-3(ok2207) IV	CGC	TGCTTATGCAGTTAGTGCCG	N/A
		TGTCGAAAATGTATTGCGGA	
		ATCCGACTTCAAAATCCGTG	
Transgene	**Source**	**Array**	**Reference**
hT2 (I;III)	CGC	*bli-4(e937) let(q782) qIs48*	(McKim et al. 1993)
juIs76 II	CGC	*punc-25::GFP, lin-15(+)*	(Jin et al. 1999)
trIs10 I	CGC	*pmyo-3::MB::YFP, pmyo-2::YFP, pceh-23::HcRed, punc-25::DsRed, unc-129nsp::CFP*	(Dixon 2006)
wpIs36 I	Marc Hammarlund	*punc-47::mCherry*	Unpublished
wpSi1 II	Marc Hammarlund	*punc-47::rde-1:SL2:sid-1, C. briggsae unc-119(+)*	Unpublished
wpIs39 X	Marc Hammarlund	*punc-47::mCherry*	Unpublished

Table 5.2. Strains generated for use in this study.

Strain	Genotype
NC1140	*juIs76 [punc-25::GFP, lin-15(+)] II;*
NC1405	*juIs76 [punc-25::GFP, lin-15(+)] II; eri-1 (mg366) IV*
NC1798	*juIs76 [punc-25::GFP, lin-15(+)] II; tra-3 (ok2207) eri-1(mg366)IV*
NC1799	*juIs76 [punc-25::GFP, lin-15(+)] II; clp-1(tm858) III; eri-1(mg366)IV*
NC1834	*juIs76 [punc-25::GFP, lin-15(+)] II; clp-1(tm858) III; tra-3 (ok2207) eri-1(mg366)IV*
NC2811	*juIs76 [punc-25::GFP, lin-15(+)] II; coq-2(ok1066)/hT2 (I; III); tra-3 (ok2207) IV*
NC1959	*juIs76 [punc-25::GFP, lin-15(+)] II; coq-2(ok1066)/hT2 (I; III)*
XE1375	*lin-15(n744) X ; eri-1(mg366) IV ; rde-1(ne219) V ; wpSi1[Punc-47::rde-1:SL2:sid-1, Cbunc-119(+)] II ; wpIs36[Punc-47::mCherry] I*

on the plate (*). For all movement and degeneration assays, the experimenter was blinded to genotype to avoid bias.

GABA neurodegeneration assays

ETC RNAi

At least 15 adults were examined for breaks in VNC GABAergic processes. Apoptotic GABA neurons were photographed at 63x on a Zeiss Axioplan compound microscope.

RME Degeneration Assay

RME degeneration was scored on a Zeiss Axioplan compound microscope by counting the number of *punc-25::GFP*-positive neurons in the head of the synchronized animals at Day 7 (i.e., 7 days after hatching). Wild-type (WT) animals have four RME neurons (Fig. 1.7).

D-Type Neuron Degeneration Assay

Degeneration of the D-Type GABA neurons was quantified by counting the number of *punc-25::GFP*-positive neurons along the ventral nerve cord (VNC) of synchronized animals at Day 7. WT animals have 19 D-Type GABA neurons (Fig. 1.7).

Microscopy

A Zeiss Axioplan compound microscope with a 100x objective was used to capture the images in Figure 5.1. The representative images collected for Figure 5.2 and Figure 5.3 were obtained on a Leica TCS-SP5 confocal microscope with a 40x objective using the Leica Application Suite Advanced Fluorescence (LAS-AF) software.

Transmission Electron Microscopy (TEM)

The RNAi experiment was initiated at Vanderbilt University and samples were sent to Albert Einstein College of Medicine (AECOM) for TEM preparation (fixation, sectioning and staining). *juIs76 [punc-25::GFP, lin-15(+)]; eri-1 (mg366)* animals were treated with EV (control) or *coq-1* RNAi and collected for fixation on Day 5 of the RNAi experiment. Because of the variability of RNAi among a population (Fraser et al. 2000; Simmer et al. 2003), I used a stereomicroscope to select adult animals with clear indications of multiple necrotic GABA neurons (i.e., enlarged GFP-positive cells). Selected animals were fixed by high-pressure freezing (HPF) in a BalTec HM 010 High-Pressure Freezer. Freeze substitution was performed using a BalTec Freeze Substitution device. The sample blocks were sectioned using a RMC Powertome at 50 nm and stained with uranyl acetate and lead citrate. Images were collected on a Philips CM-10 transmission electron microscope (TEM) with a Morada digital camera system.

Experimental contributions

Meg Mitchell built the pMBM009 vector and the NC2811 strain. She also collected the data for Figure 5.3C-D. David Hall (Albert Einstein College of Medicine, AECOM) prepared the TEM samples (fixation, sectioning, and staining) and provided training and use of his transmission electron microscope at AECOM.

RESULTS

Global electron transport chain knockdown results in developmental arrest but not GABA neuron degeneration

GABA neurons in hypomorphic mutants of ETC Complex I and Complex II do not degenerate

To test the hypothesis that ETC dysfunction underlies the neurodegeneration pathway initiated by Coenzyme Q depletion, I examined GABA neurons in hypomorphic mutants of protein subunits of ETC Complexes I and II, *gas-1(fc21)* and *mev-1(kn1)*, respectively. These mutants show significantly decreased ETC activity (reduced by 80-90% versus wild-type) (Kayser et al. 2001; Ishii et al. 1998), increased oxidative stress (Hartman et al. 2001) and *ced-3*/*ced-4*-dependent supernumerary apoptosis (Senoo-Matsuda 2003). However, neither hypomorphic mutant displayed noticeable signs of GABA neuron degeneration at any developmental age (data not shown). Interpretation of this negative result is difficult since these alleles do not completely eliminate gene function. Unfortunately, animals with more severe ETC mutations (i.e., *atp-2*/Complex V, *nuo-1*/Complex I*, isp-1*/Complex III (Tsang & Lemire 2003; Ndegwa & Lemire 2004; Ventura & Rea 2007)) do not reach adulthood and therefore cannot be examined for GABA neurodegeneration.

Global RNAi of ETC genes induces developmental arrest

Because it was not possible to test null alleles ETC genes for GABA neuron degeneration defects, I instead used RNAi to knock down ETC components to determine if this impairment phenocopies the GABA neurodegeneration observed with Coenzyme Q deficiency. For this experiment, I used the same RNAi-sensitized genetic background (*juIs76; eri-1)* that shows robust GABA neurodegeneration with *coq-1* RNAi (Fig. 2.2). Global RNAi knockdown of ETC genes (*gas-1, nuo-1, cyc-1, cco-1, F26E4.6, atp-3*) delayed or arrested the first generation progeny (Table 5.3) and therefore prevented analysis of adult neurons.

We next decreased overall sensitivity to ETC knockdown by examining animals without the neuronal RNAi-enhancing mutation *eri-1(mg366)* (Kennedy et al. 2004); however, many of the ETC RNAi populations (*gas-1, D2030.4, cyc-1, atp-3)* still arrested during larval development with global RNAi treatment (Table 5.4). Knockdown of two ETC genes (*mev-1* and *F26E4.6*) in this genetic background allowed the first generation progeny to reach adulthood but we did not observe GABA degeneration in these adults (data not shown). Thus, these findings indicate that the severity of global RNAi knockdown of ETC genes hinder our effort to assess potential degeneration of adult GABA neurons.

GABA neuron-specific knockdown of ETC genes does not induce their degeneration

Given the developmental delay caused by global knockdown of ETC genes, I decided to use a GABA neuron-specific RNAi strain (XE1375) generously provided by Marc Hammarlund (Yale University). Mutations in *lin-15b* (Wang et al. 2005) and *eri-1*/RNase (Kennedy et al. 2004) enhance sensitivity to RNAi, and the *rde-1/*Argonaut (Tabara et al. 1999) is required to process dsRNA for gene interference. The *wpSi1* [*punc-47::rde-1::SL2::sid-1*] transgene drives GABA neuron-specific expression of wild-type RDE-1/Argonaut as well as SID-1, a dsRNA gated channel protein (Shih & Hunter 2011) that enhances RNAi in cells where it is overexpressed and decreases RNAi of non-transgenic cells (Calixto et al. 2010). Together, this combination of RNAi-enhancing mutations and transgenic rescue of key components of the RNAi pathway in GABA neurons allows the function of otherwise lethal genes to be assessed exclusively in these neurons. I inspected GABA neurons of ETC knockdown animals in the GABA neuron-specific RNAi background. With the exception of a rare button-like (i.e., apoptotic) GABA neuron in a single *gas-1* RNAi-treated animal (Fig. 5.1B-C), I did not detect signs of GABA neuron death (data not shown). To verify RNAi efficacy in GABA neurons of this genetic background, I used RNAi to knock down *unc-25*/Glutamic Acid Decarboxylase and quantified

Table 5.3: Knockdown of electron transport chain (ETC) components results in developmental arrest. Global RNAi of *eri-1(mg366); juIs96* was used to knock down genes encoding ETC components. Loss of these essential genes resulted in lethality or developmental arrest for the F1 generation.

Gene Targeted by RNAi	ETC Complex	Quantity of F1 Generation	Development of F1 Generation
EV	n/a	many	Adults
gas-1	I	very few	L1 - L2
nuo-1	I	very few, many dead eggs	L1
cyc-1	III	very few	L1-L2
cco-1	IV	very few	L1-L2
F26E4.6	IV	very few	L1-L2
atp-3	V	none	n/a

Table 5.4: ETC RNAi treatment of animals without *eri-1(mg366)* progress to later developmental stages but do not display GABA neuron degeneration. Removal of the RNAi-sensitizing *eri-1(mg366)* mutation allows ETC knockdown populations to develop to later stages. F1 adults of *mev-1* or *F26E4.6* do not have GABA neuron degeneration while *coq-1* knockdown animals show dying GABA neurons.

Gene Targeted by RNAi	ETC Complex	F1 Generation		
		Quantity	Stage	GABA neuron Degeneration
EV	n/a	many	adults	0%
gas-1	I	many	L3/L4	0%
D2030.4	I	few	L3	0%
mev-1	II	many	small adults	0%
cyc-1	III	very few	L2	0%
F26E4.6	IV	many	adults	0%
atp-3	V	very few	L2/L3	0%
coq-1	(CoQ)	many	adults	13%

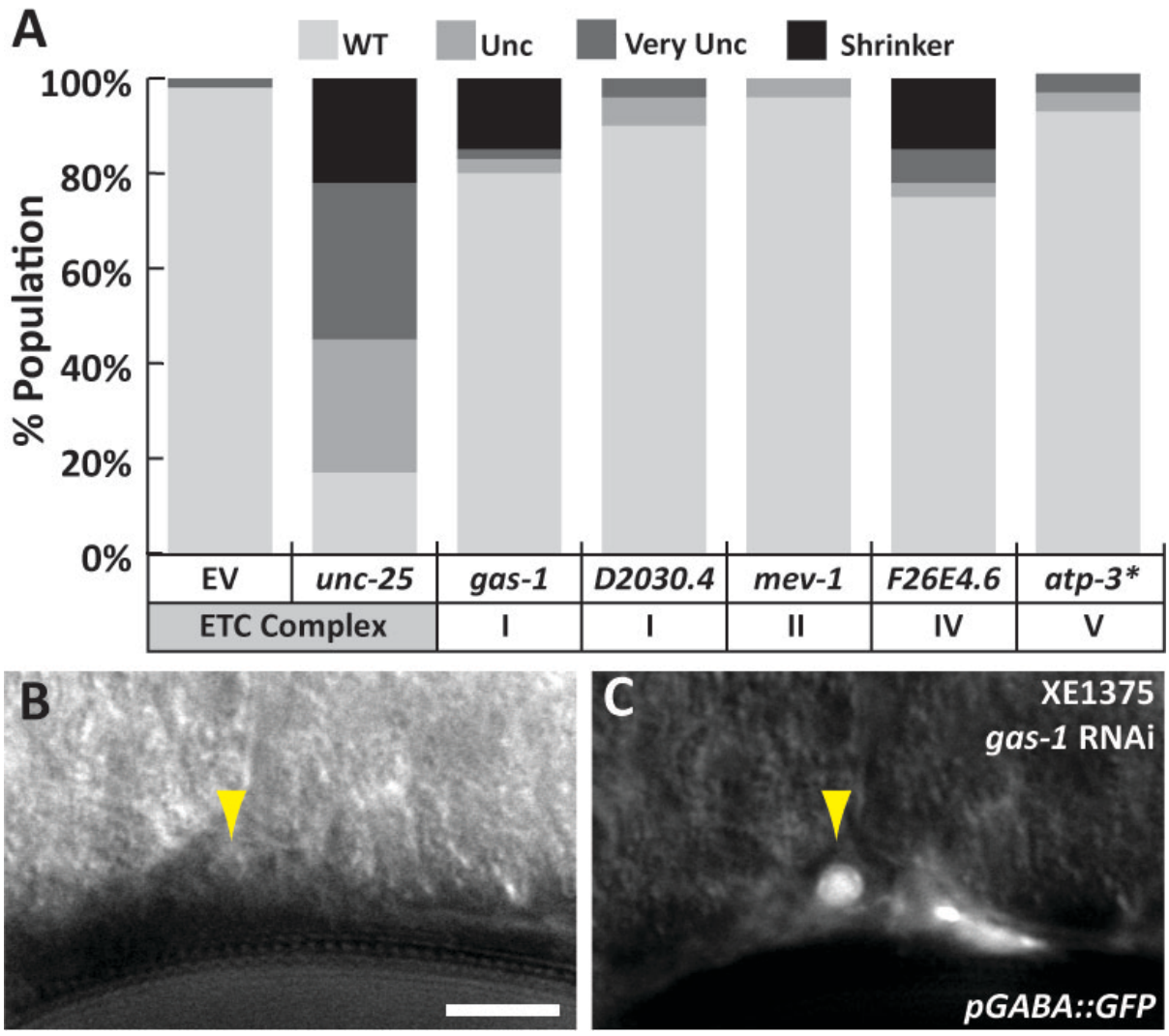

Figure 5.1: GABA neuron-specific knockdown of electron transport chain (ETC) genes does not phenocopy the robust degeneration defect of Coenzyme Q-depleted animals. A. Movement (WT, Unc, Very Unc, Shrinker) was scored in XE1375 animals treated with RNAi that targeted components of the ETC as well as controls (empty vector and *unc-25*/GAD). Scale bar = 5μM, n > 50 except *atp-3* which did not have enough F1 progeny to score (*), in which case n = 20. **B.** DIC image of a single apoptotic GABA neuron (yellow arrowhead) in an adult XE1375 animal with *gas-1* RNAi. This image is not representative of overall GABA neuron morphology and notes the rare presence of apoptotic features. **C.** GABAergic identity is confirmed by expression of *punc-25::GFP* in the dying neuron.

movement defects caused by reduction of this GABA biosynthetic enzyme. The XE1375 strain showed a robust Unc phenotype with *unc-25* knockdown, showing the characteristic "shrinker" defect observed in nematodes without functional GABA neurons (McIntire, Jorgensen, Kaplan, et al. 1993b) (Fig. 5.1A). This result confirmed that GABA neurons are sensitized to feeding RNAi in the XE1375 sensitized background. The GABA neuron specific "shrinker" phenotype was also visible in ~20% of the populations targeted for RNAi of *gas-1*/Complex I and *F26E4.6*/Complex IV. The "shrinker" phenotype induced by the RNAi treatment suggests that the function of these ETC genes was reduced specifically in GABA neurons and yet we did not induce GABA neurodegeneration. These data suggest that ETC impairment alone does not explain the cell death observed in GABA neurons of CoQ-deficient animals.

Specific calpain and cathepsin proteases are differentially required in the GABA neurodegeneration pathway

Despite the involvement of key apoptotic genes to in the CoQ depletion-induced neurodegeneration pathway (see **Chapter 4**), the swollen morphology of dying GABA neurons is characteristic of necrotic death (Fig. 2.2, Fig. 3.2). Studies in *C. elegans* have identified mutants in which specific hyperactive cation channels induce necrotic death in the affected neurons (Syntichaki et al. 2002). Mutations that disable either of two classes of proteases, calpains (CLP-1 and TRA-3) and cathepsins (ASP-3 and ASP-4) (Fig. 1.4), block the necrosis pathway in this experimental paradigm (Syntichaki et al. 2002). To determine if these necrotic proteases are also required for CoQ depletion-induced GABA neurodegeneration, I examined genetic mutants of *clp-1, tra-3* and *asp-4* in a *coq-1* RNAi assay. At the time of analysis, it was not possible to test the cathepsin/aspartyl protease *asp-3* due to the lack of a genetic mutant. Recently, two *asp-3* mutant alleles were generated (*tm4450* and *tm4559*) that could be used in future experiments to investigate the role of

this cathepsin. In comparison to wild-type animals treated with *coq-1* RNAi, there was significant reduction in GABA neuron degeneration in *asp-4(ok2693)* mutants (Fig. 5.2A). This result is consistent with the death-promoting role of ASP-4 in other *C. elegans* necrotic pathways (Syntichaki et al. 2002; Geng et al. 2012). However, these experiments also revealed that GABA neurodegeneration did not depend on CLP-1 and was significantly enhanced by loss of TRA-3 function (Fig. 5.2A-B). These results indicate that the GABA neurodegeneration pathway shares the aspartyl protease ASP-4 with other necrotic mechanisms but also shows important differences: CLP-1 is not required and TRA-3/calpain appears to function in a neuroprotective role.

RME GABA neurons are severely affected by CoQ depletion in *tra-3* mutants

To confirm enhanced GABA neuron degeneration of *tra-3(ok2207)* mutants with CoQ depletion, GABA neuron death was also examined in the *coq-2(ok1066)* mutants. For this assay, I examined two distinct populations of GABA neurons: the four RME neurons in the head and the 19 D-Type GABA neurons in the ventral nerve cord (VNC) (Fig. 1.7). Significant enhancement of both RME (Fig. 5.3A-C) and D-type GABA neuron (Fig. 5.3D) degeneration was observed in *coq-2; tra-3* double mutants compared to *coq-2* single mutants. These data strongly support a model in which Coenzyme Q deficiency activates a GABA neuron degeneration pathway that is antagonized by TRA-3/calpain (Fig. 5.3E).

Transmission electron microscopy reveals ultrastructural features of Coenzyme Q-deficient motor neurons

Genetic data from my studies indicate that both apoptotic (see **Chapter 2** and **Chapter 4**) and necrotic (Fig. 5.2, Fig. 5.3) regulators are involved in the GABA neurodegeneration pathway induced by CoQ depletion. Additionally, light microscopy reveals that dying GABA neurons adopt a

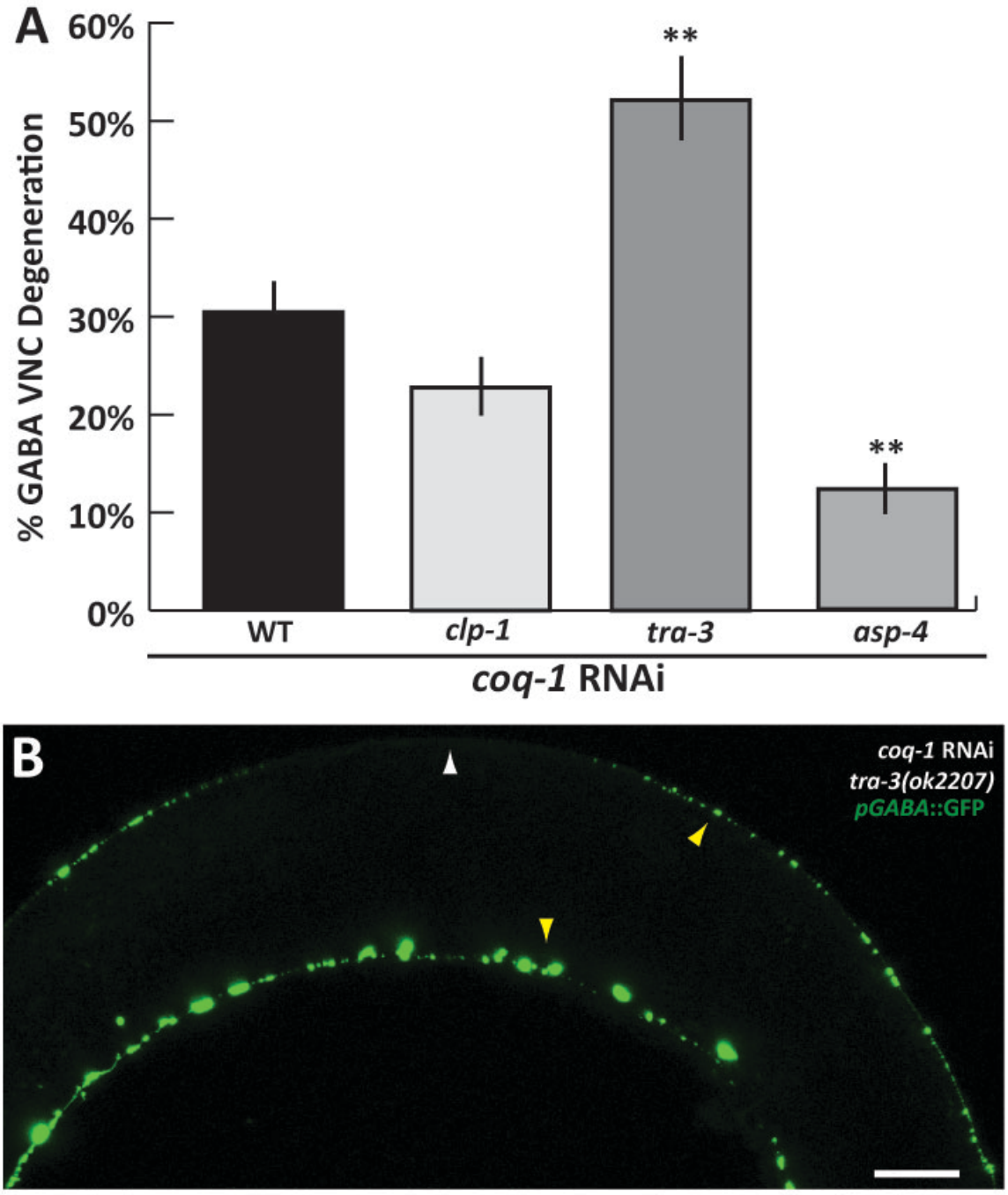

Figure 5.2: Specific proteases from the necrotic death pathway are differentially required for GABA neurodegeneration induced by Coenzyme Q depletion. A. *coq-1* RNAi induces GABA neuron degeneration that is enhanced by the *tra-3(ok2207)* mutation and suppressed in *asp-4(ok1653)* mutants. n >60 except for *clp-1; tra-3* (n=20), ** p<0.0001 vs wild-type (WT). Degeneration levels in *clp-1; tra-3* does not differ statistically from WT (data not shown). **B.** Confocal image showing severe GABA neuron degeneration (i.e., neuronal process blebbing – yellow arrowhead and break in neuronal process – white arrowhead) in *tra-3* mutants with *coq-1* knockdown. *pGABA::GFP = punc-25::GFP,* scale bar = 25µM.

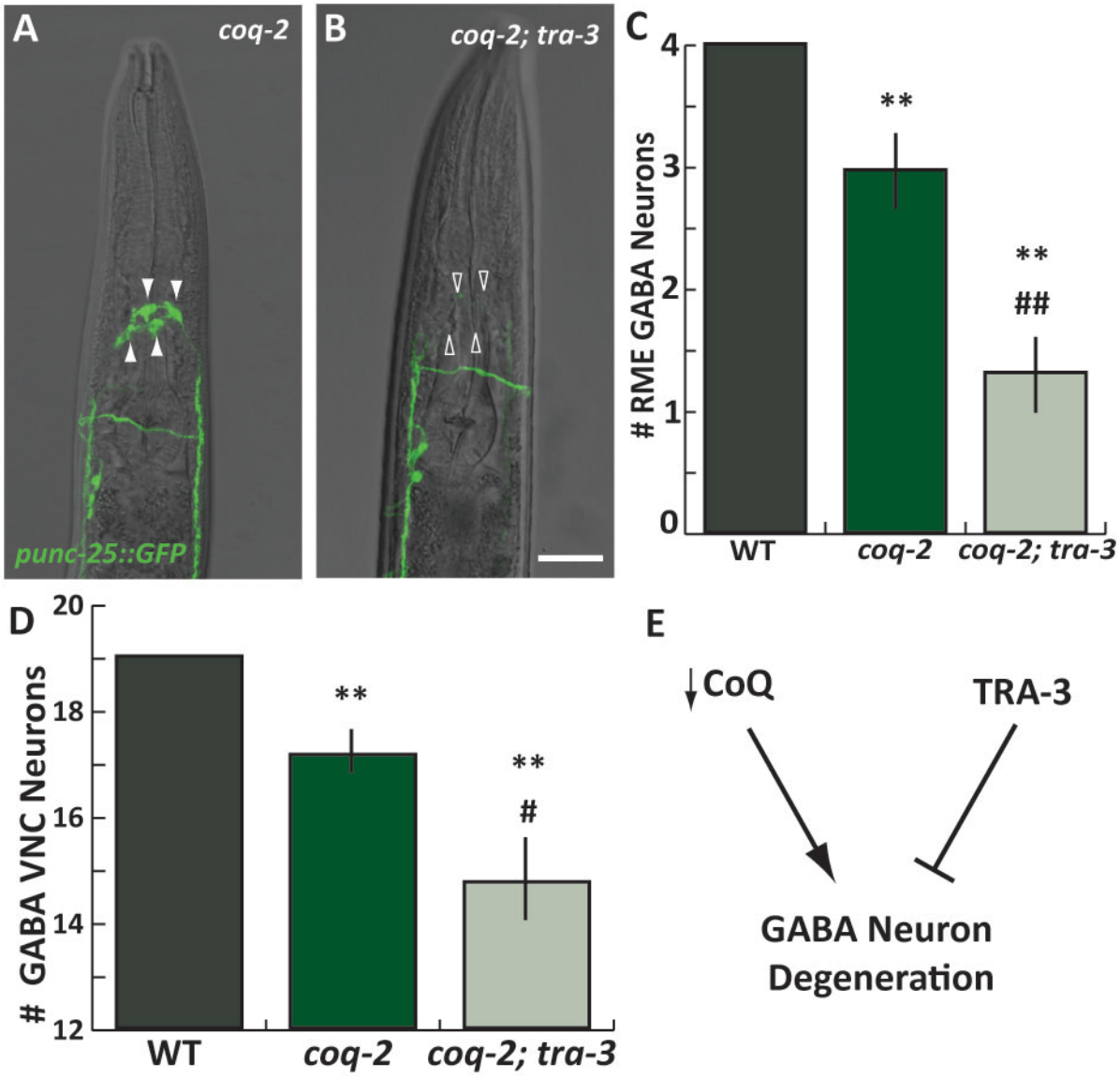

Figure 5.3: GABA neuron degeneration is enhanced in *coq-2; tra-3* double mutants. A. All four RME neurons are visible in a Z-axis projection of *punc-25::GFP* and DIC confocal images in a *coq-2(ok1066)* adult. **B.** RME neurons are missing (empty arrowheads) from the head region of this representative *coq-2(ok1066); tra-3(ok2207)* animal. Scale bar = 25µM. **C.** An average of ~1 GABAergic RME degenerates in *-2* adult animals scored at Day 6. RME degeneration at Day 6 is significantly enhanced in the *coq-2*; *tra-3* background (~2.5 missing RMEs). n>25, ** p<0.0002 vs WT, ## p<0.0001 vs *coq-2*. **D.** *coq-2*; *tra-3* double mutants also have significantly fewer VNC D-Type GABA neurons versus *coq-2*. n>25, ** p<0.0001 vs WT, # p<0.06 vs *coq-2*. **E.** Loss of Coenzyme Q activates a pathway that requires TRA-3 to block GABA neuron degeneration.

swollen, necrotic-like morphology (Fig. 2.2, Fig. 3.2). Taken together, these results suggest that either apoptotic genes regulate a necrotic death pathway or that a hybrid death mechanism, with shared features of both apoptosis and necrosis, is activated in the GABA neurons of CoQ-depleted animals. Since apoptotic and necrotic features are distinguishable at the ultrastructural level (Table 5.5), I used transmission electron microscopy (TEM) to address this question.

Table 5.5. Ultrastructural features that distinguish apoptotic versus necrotic cell death. Characteristics of apoptotic and necrotic death revealed through ultrastructural analysis (Zong & Thompson 2006; Kerr et al. 1972; Hall et al. 1997).

Apoptosis	Necrosis
Chromatin condensation	Extensive cytoplasmic vacuolation
DNA fragmentation	Mitochondrial swelling
Overall cell shrinking	Dilation of the endoplasmic reticulum
Plasma membrane blebbing	Plasma membrane rupture
Formation of apoptotic bodies	Membranous whorls

Longitudinal sectioning allows ultrastructural features of neighboring motor neurons to be visualized using transmission electron microscopy

We previously demonstrated that CoQ deficiency results in the degeneration of GABA neurons but not nearby cholinergic neurons in the ventral nerve cord (Fig. 2.2, Fig. 2.4). The striking difference in cellular responses to CoQ depletion between these neighboring neuron classes motivated us to examine motor neurons side-by-side using transmission electron microscopy (TEM). This goal was achieved by generating longitudinal sections of the ventral nerve cord (VNC). Analysis of control animals confirmed the utility of this sectioning strategy, which produced an ultrastructural representation of adjacent motor neurons cell bodies in the ventral nerve cord (Fig. 5.4).

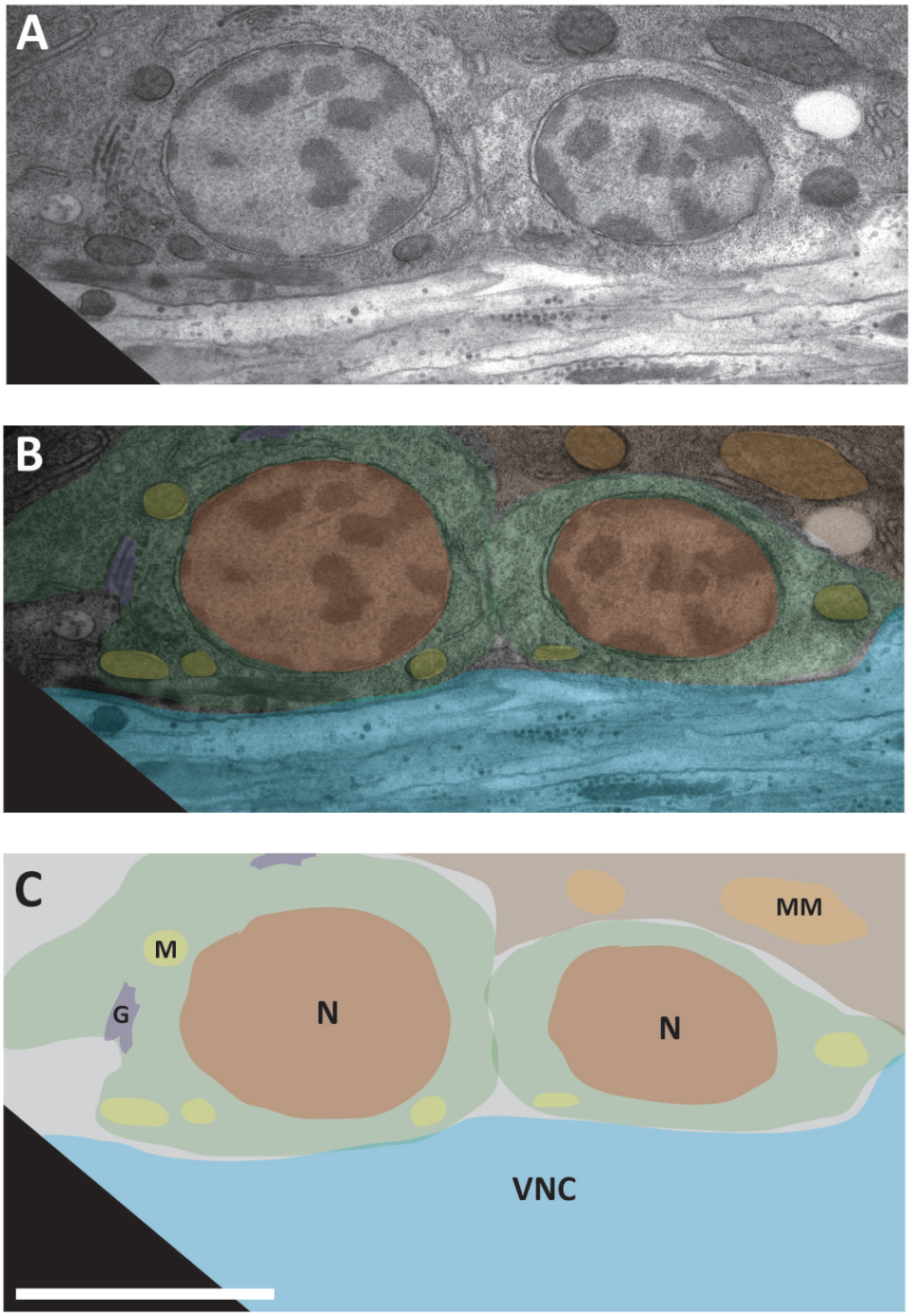

Figure 5.4: Transmission electron micrograph shows ultrastructural features of wild-type ventral nerve cord (VNC) motor neurons. A. Two neighboring motor neuron cell bodies in control (EV) RNAi-treated samples**. B.** Pseudocolored micrograph of motor neurons (green). **C.** Pseudocolor schematic highlights features of wild-type motor neuron cell bodies on the dorsal side of the VNC (blue). Nucleus (N), neuronal mitochondria (M), Golgi (G), ventral nerve cord (VNC), muscle mitochondria (MM). Scale bar = 2µM.

Transmission electron micrographs of these motor neurons clearly delineated prominent subcellular structures such as mitochondria, Golgi and the cell nucleus. These images of normal motor neurons provide a wild-type control for comparison to potential intracellular changes in CoQ-depleted neurons.

Ultrastructural analysis of coq-1 knockdown animals reveals necrotic characteristics of dying motor neurons

Next, I examined transmission electron micrographs of motor neurons in adult animals treated with *coq-1* RNAi. A dying motor neuron near the vulva (Fig. 5.5), displayed several characteristics suggestive of necrotic cell death. These features include: (1) extensive intracellular proteolysis (i.e., lack of cytoplasmic electron density), (2) a large cytoplasmic vacuole, (3) rupture of the plasma membrane, (4) a membranous whorl, and (5) mitochondrial swelling (see Fig. 5.5 legend). Each of these features has been previously identified in necrotic *C. elegans* neurons (Hall et al. 1997). Mitochondrial distortion and electron-dense membranous whorls are also observed in cytotoxic death induced by dominant mutations in *lin-24* (homology to bacterial toxins) and *lin-33* (unknown gene function) (Galvin et al. 2008), but other features of cytotoxic death (i.e., nuclear envelope dilation, electron-dense nuclear punctae) were not observed in CoQ-deficient motor neurons. The neuron depicted in Figure 5.5A is likely to be GABAergic motor neuron VD7 based on its position next to the vulva and frequent swollen VD7 neurons in the light microscope (Fig. 3.2). Similar features were observed in TEM images from a second *coq-1* knockdown animal that showed an elongated swollen neuron (Fig. 5.5E) with a striking resemblance to the appearance of CoQ-depleted GABA neurons in the light microscope (Fig. 2.2C). Based on our light microscopy studies in which GABA neurons are the predominant, if not exclusive, type of VNC motor neuron to swell with *coq-1* knockdown, we infer that the cells depicted in Figure 5.5 are also GABAergic neurons.

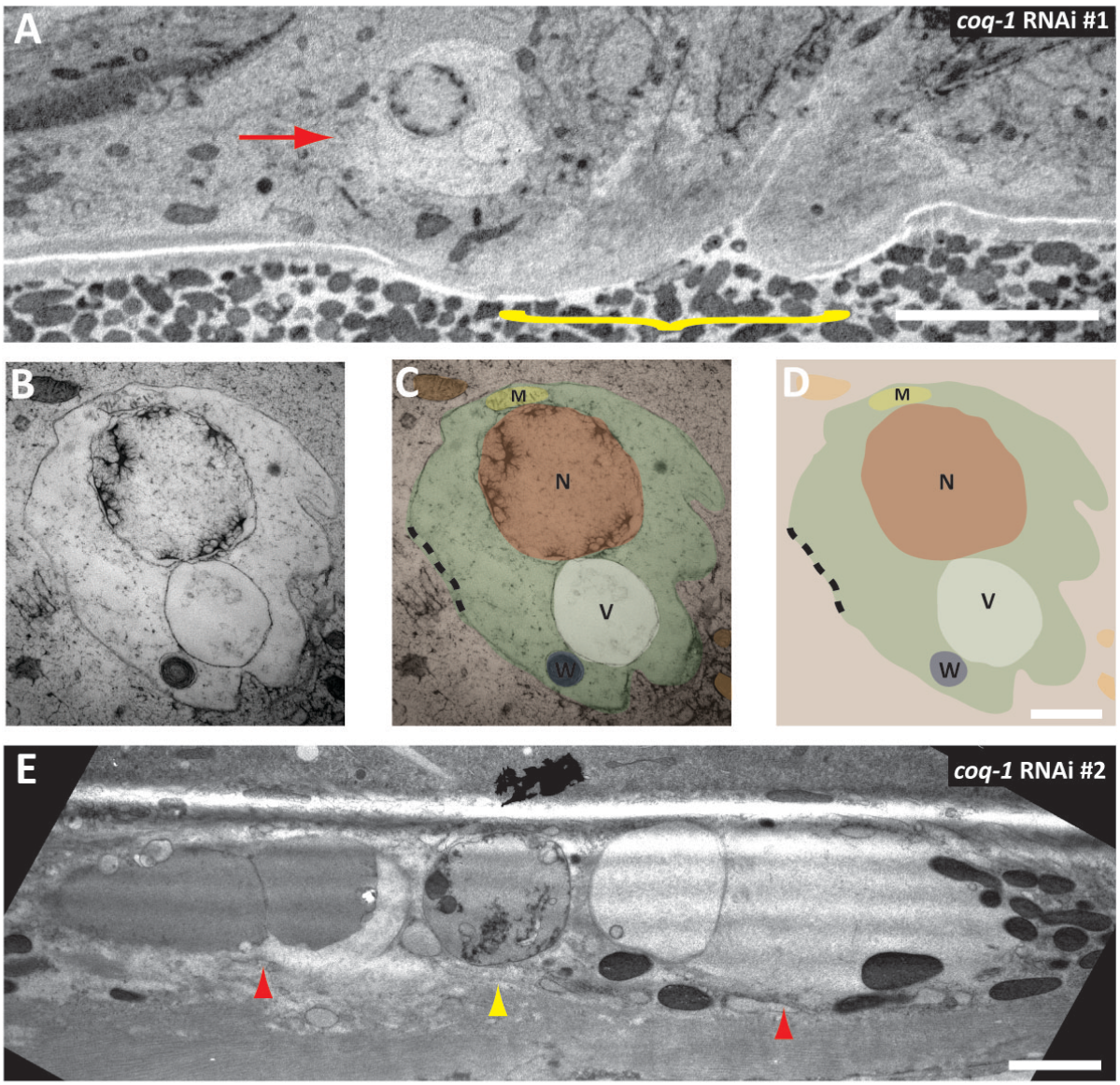

Figure 5.5: Ultrastructural analysis of *coq-1* knockdown animals reveals necrotic features of dying motor neurons. A. A dying motor neuron (red arrow) near the vulva (yellow bracket) of *coq-1* RNAi treated animal #1. Anterior left, ventral down. Scale bar = 5µM. **B.** TEM image of the neuron in Panel A. **C.** Pseudocolor overlay distinguishes various features of the cell: M = ruptured neuronal mitochondrion, N = nucleus, V = intracellular vacuole, W = electron-dense membranous whorl, dotted line = plasma membrane rupture. **D.** Pseudocolor. Scale bar = 1µM. **E.** Large vacuoles (red arrowheads) flank the nucleus (yellow arrowhead) of a dying cell in *coq-1* RNAi-treated animal #2. Scale bar = 2µM.

Autophagic characteristics are observed in coq-1 depleted neurons

Interestingly, I also identified VNC neurons with features consistent with autophagy. Autophagy is a self-digestion mechanism that is associated both with cell survival and cell death pathways (Kourtis & Tavernarakis 2009). During autophagy, double-membrane vesicles engulf cytoplasmic material, and these vesicles (i.e., autophagosomes) fuse with lysosomal machinery, where its contents are degraded. In a CoQ-deficient animal, we noted a neuron containing several membrane-enclosed structures (Fig. 5.6) (Sigmond et al. 2008). It is currently unclear whether this neuron is GABAergic or cholinergic, and additional experiments are required to definitively test for a role for autophagy in GABA neurodegeneration. Perhaps GABA neuron necrosis is preceded by activation of autophagic mechanisms. Alternatively, other cell types in the VNC may activate autophagy instead of necrosis in response to CoQ depletion, perhaps as a cell-survival mechanism. We note that the autophagic cell depicted in Figure 5.6A-B is adjacent to a vacuolated region that likely corresponds to the position of a necrotic GABA neuron that already died at the time of analysis. This finding is interesting because it could point to an important role for autophagy in the survival of cholinergic neurons in the VNC of CoQ-depleted animals. In addition to neurons with features of either necrotic or autophagic cells, these electron micrographs also revealed VNC neurons with the normal morphology of viable cells (Fig. 5.6 A, C). Thus, this TEM analysis is important because it confirms our findings in the light microscope of both necrotic and normal appearing VNC motor neurons in CoQ-deficient animals.

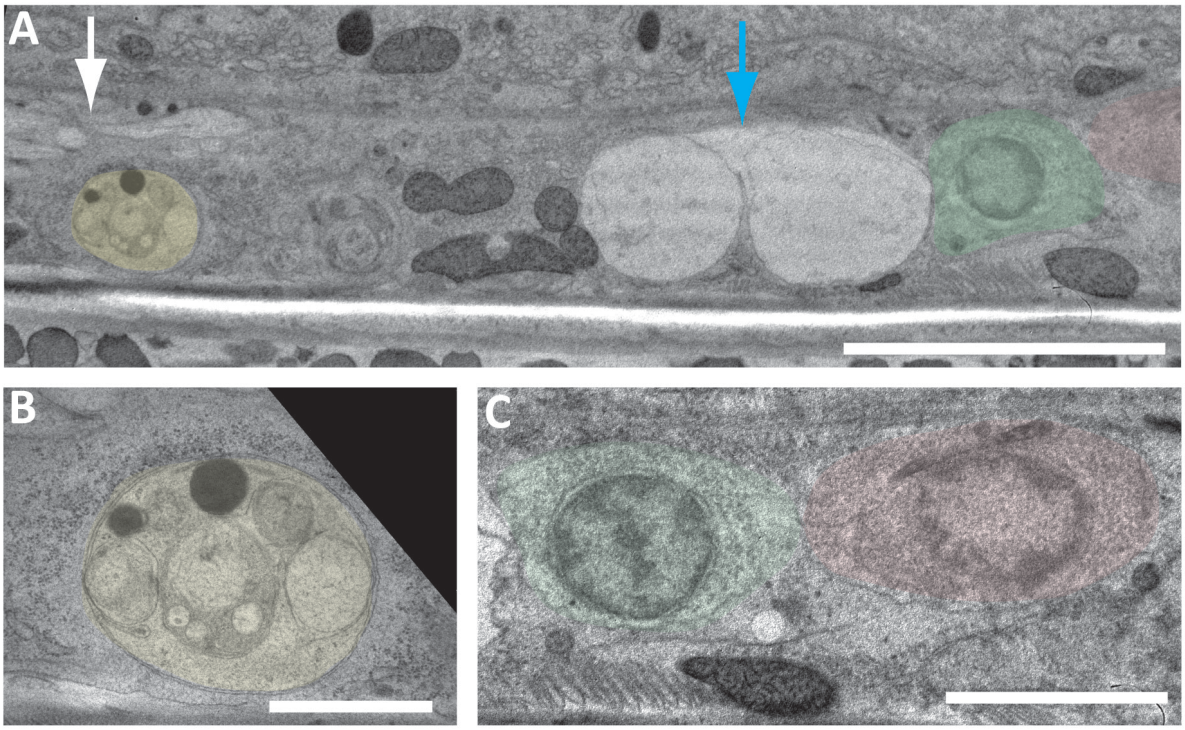

Figure 5.6: Diverse cellular responses to *coq-1* depletion are revealed by transmission electron micrographs. A. Neurons along the ventral nerve cord (white arrow) display a range of features: autophagic cell (yellow pseudocolor), large vacuolated area (blue arrow) and a normal neuron (green pseudocolor). Scale bar = 5µM. **B.** Magnified image of the autophagic cell from Panel A shows membrane-bound structures in the cytoplasm. Scale bar = 1µM. **C.** Motor neurons with wild-type features from Panel A. Note: the red pseudocolored cell was not fully visible in Panel A. Scale bar = 2µM.

DISCUSSION AND FUTURE DIRECTIONS

Summary

Impairing ETC function in adult animals is technically challenging due to the essential nature of the proteins that make up the multisubunit complexes. However, by using a genetic background that selectively sensitizes GABA neurons to RNAi, I was able to reveal that knockdown of ETC genes does not elicit a GABA neurodegeneration phenotype. This result suggests that GABA neurons degenerate due to the disruption of a CoQ function that is independent of its role in the ETC. I also identified specific necrotic proteases that regulate GABA neuron death. These experiments revealed that the CoQ depletion-induced death pathway is controlled by proteases with death-promoting (ASP-4/cathepsin) or death-preventing (TRA-3/calpain) functions. Examination of dying motor neurons in the electron microscope revealed ultrastructural hallmarks of necrosis as well as signs of autophagy in CoQ-deficient animals. Taken together, these findings enhance our understanding of how GABA neurons degenerate and implicate an ETC-independent function of Coenzyme Q for neuronal viability.

Electron transport chain knockdown does not phenocopy GABA neurodegeneration observed with Coenzyme Q depletion

As discussed in **Chapter 1**, although Coenzyme Q functions as critical component of the mitochondrial electron transport chain, it also is required for additional cellular activities such as membrane oxidative stress defense (Turunen et al. 2004) and energy coupling at plasma and lysosomal membranes (Crane 2001; Gille & Nohl 2000). GABA neuron-specific ablation of ETC components did not phenocopy the cell death phenotype that accompanies global Coenzyme Q depletion. This negative result argues against a model in which GABA neuron degeneration arises from disruption of the ETC. Our initial hypothesis was based on findings that correlate ETC

dysfunction with ATP depletion and elevated ROS that then initiate both apoptotic and necrotic death pathways. However, these results now favor ETC-independent roles of Coenzyme Q such as its antioxidant properties (Turunen et al. 2004) and regulation of the mitochondrial permeability transition pore (PTP) (Fontaine et al. 1998; Papucci et al. 2003; Devun et al. 2010; Sahach et al. 2007) as potentially involved in GABA neuron necrosis. Our results are also consistent with the finding that global reduction of Coenzyme Q content by as much as 60-70% does not decrease ETC activity in *C. elegans* (Asencio et al. 2003). While we have not directly measured the level of Coenzyme Q deficiency achieved with our RNAi or genetic approaches, it is possible that CoQ depletion is not sufficient to impair ETC function. In any case, our results suggest that CoQ levels that are sufficient to support overall animal viability are not adequate to prevent GABA neuron degeneration (Fig. 3.10).

In addition to its electron transfer function during oxidative phosphorylation, Coenzyme Q is also a potent antioxidant in lipid membranes. I hypothesize that depletion of Coenzyme Q results in increased oxidative stress, which in turn could trigger GABA neurodegeneration. Future studies to address question could utilize genetic knockouts of enzymes with antioxidant function such as superoxide dismutases (*sod-1, sod-2*) or catalases (*ctl-1, ctl-2, ctl-3*). If increased ROS is responsible for the death of GABA neurons in CoQ-depleted animals, then GABA neuron degeneration should be enhanced in these genetic backgrounds. Conversely, if elevated oxidative stress of CoQ-depleted animals causes GABA neuron, then overexpression of antioxidant enzymes (e.g., *sod-1, ctl-1*) could counteract this effect and suppress neurodegeneration.

Necrotic proteases adopt opposing roles in the CoQ deficiency-induced GABA cell death pathway

TRA-3/calpain antagonizes GABA neurodegeneration

TRA-3 is an atypical calpain that has been shown to be necessary for the necrotic-like death of neurons induced by hyper-activation of DEG/ENac cation channels (Syntichaki et al. 2002). My results offer the unexpected finding of the opposite role for TRA-3 of protecting neurons from a necrotic pathway induced by CoQ depletion (Fig. 5.2, Fig. 5.3). This finding indicates that Coenzyme Q deficiency-induces a necrotic pathway that differs from the necrotic mechanism induced by DEG/ENac channel hyperactivity. Additionally, TRA-3-dependent necrotic death occurs in touch receptor neurons (Syntichaki et al. 2002), and it is possible that different types of neurons activate distinct necrotic responses.

Data from another study are consistent with our finding that TRA-3 antagonizes a neurodegeneration pathway. Knockdown of *tra-3* sensitizes animals to necrosis stimulated by treatment with a pharmacological ETC Complex IV inhibitor sodium azide (Luke et al. 2007). This independent observation coupled with our discovery that TRA-3 protects GABA neurons from CoQ depletion-induced death suggests that this calpain functions downstream of mitochondrial stress to prevent cell death. A similar phenomenon has been reported for human Calpain 10 for which knockdown induces apoptosis (Smith & Schnellmann 2012). In addition, Calpain 10 proteolytically cleaves components of the ETC after calcium overload and that this role could prevent a buildup of damaged substrates that may contribute to both mitochondrial and cellular injury that induces cell death. A similar mechanism may also explain why loss of TRA-3 enhances CoQ depletion-induced GABA neuron degeneration.

In addition to calpain 10 protecting against apoptosis (Smith & Schnellmann 2012), calpain-dependent cleavage of apoptotic regulators has been reported. For example, calcium-induced activation of calpain enzymes leads to cleavage of Bax (Bcl-2 family member) and Apaf-1 (CED-4

homologue) (Wood et al. 1998; Reimertz et al. 2001). Therefore, perhaps TRA-3 inhibits GABA neurodegeneration by degrading pro-death machinery (i.e., CED-4/Apaf-1). Epistasis analysis of *tra-3* and the death-promoting genes we have identified (i.e., *ced-4, drp-1, crt-1, asp-4*) will begin to shed light onto the relationship between this protective protease and the neurodegeneration pathway.

Interestingly, TRA-3 expression is reportedly excluded from GABA neurons (Joyce et al. 2012); therefore, analysis of potential non cell-autonomous roles for TRA-3 could also be insightful for delineating the mechanism by which this protease protects against GABA neuron death. Our studies also do not indicate whether the protease activity of TRA-3 is required for its protective function and mutagenesis of its active site (C83S, (Moldoveanu et al. 2002; Sokol & Kuwabara 2000)) could be used to address this question.

ASP-4/cathepsin promotes GABA neurodegeneration

Results in this chapter show that aspartyl protease ASP-4 is required for GABA neuron degeneration with CoQ depletion. Due to inconsistencies of RNAi efficacy between genetic backgrounds (see **Appendix A**), this result should next be confirmed in a CoQ synthetic pathway mutant background. Once its death-promoting role is validated in an RNAi-independent assay, future studies to understand how this protease promotes degeneration could focus on addressing whether ASP-4 promotes GABA neuron death cell autonomously. During hyperactive ion-channel-induced necrotic death, ASP-4 is downstream of TRA-3, and both proteases promote cell death (Syntichaki et al. 2002); however, we discovered that TRA-3 antagonizes a death pathway that is promoted by ASP-4. Genetic epistasis analysis of the *tra-3; asp-4* double mutant could determine whether these proteases act in the same or parallel pathways in response to CoQ depletion.

Ultrastructural studies reveal canonical necrotic features in dying motor neurons and implicate autophagy as a mechanism of neuroprotection

Our transmission electron microscopy analysis strongly suggests that CoQ-deficient GABA neurons die through a necrotic pathway. The ultrastructural resolution afforded by this technique allowed us to compare intracellular features of motor neurons to distinguish between various modes of cell death. Based on their location (adjacent to the ventral nerve cord) and our reproducible observation in the light microscope that GABA neurons are preferentially affected by CoQ depletion, we have tentatively identified these cells as GABAergic neurons. I performed preliminary analysis on four *coq-1* knockdown TEM samples and identified the regions in each that contain the ventral nerve cord. Further examination of these TEM samples could be pursued to confirm the findings of this pilot study.

Because we chose to section longitudinally, we were able to observe neurons with normal ultrastructural features adjacent to others with clear signs of distress (Fig. 5.6A). Most notably, we detected signs of autophagy (e.g., multiple membrane-bound structures contained inside the cell) (Fig. 5.6B). Autophagy refers to a cellular self-degradation pathway that has been tied to both cell survival and cell death (Kourtis & Tavernarakis 2009). Until acquiring these high-resolution images, only necrosis was observed in CoQ-deficient animals (Fig. 2.2, Fig. 3.2), with rare instances of apoptosis (Fig. 3.3, Fig. 4.6). Interestingly, primary Coenzyme Q deficiency models in other systems have reported signs of autophagy (Rodriguez-Hernandez et al. 2009; Peng et al. 2004; Peng et al. 2008), suggesting that an adaptive response to Coenzyme Q depletion is conserved across phylogeny.

A long-standing point of intrigue regarding CoQ deficiency in *C. elegans* is why GABA neurons die and neighboring cholinergic neurons are spared. In *C. elegans*, autophagy is required for protection against hypoxic injury (Samokhvalov et al. 2008). We speculate that the autophagic cell

identified in our TEM study (Fig. 5.6) is a non-GABAergic neuron that has activated autophagy as a cell-survival mechanism to overcome deprivation of CoQ. Alternatively, autophagy has also been recognized as an independent cell death pathway (i.e., Type II death), and it is also upregulated upon induction of necrosis in *C. elegans* neurons (Samara et al. 2008; Samokhvalov et al. 2008). It is therefore possible that the autophagic cell is a GABA neuron during a stage of necrotic degeneration without soma swelling. Future studies can distinguish between these models by knocking down autophagy regulators (i.e., *unc-51/*Atg1, *bec-1/*Atg6, *lgg-1/*Atg8) and examining both GABAergic and cholinergic neurons in animals with CoQ depletion. If autophagy were a neuroprotective mechanism in cholinergic neurons, loss of autophagic regulators would then induce cholinergic neurodegeneration with CoQ deficiency. Alternatively, if autophagy were essential for GABA neuron necrotic death, its inhibition would suppress degeneration. The outcome of this analysis could provide insight into why GABA neurons preferentially degenerate versus cholinergic neurons.

CHAPTER VI

GENERAL DISCUSSION AND FUTURE DIRECTIONS

The work in this dissertation explores the mechanism of GABA neuron degeneration in a *C. elegans* model of Coenzyme Q deficiency. This model shares key features with neurodegenerative diseases, including selective neuronal vulnerability, age-related onset, and mitochondrial dysfunction. Thus, my studies of this phenomenon in *C. elegans* have the potential to reveal key determinants of neuropathogenic disease in humans. The molecular pathway activated in CoQ-deficient GABA neurons is regulated by a novel combination of elements including canonical components of both apoptotic (**Chapter 2** and **Chapter 4**) and necrotic (**Chapter 2** and **Chapter 5**) mechanisms. My work has also uncovered evidence of robust mechanisms for intercellular trafficking of CoQ that is sufficient to protect otherwise CoQ-deficient GABA neurons from degeneration (**Chapter 3**). These studies emphasize the power of using a simple, genetic organism to investigate complex cellular responses to mitochondrial dysfunction. The strong conservation of core biological processes between nematodes and mammals suggests that these findings in *C. elegans* could contribute to our understanding of how mitochondrial impairment leads to neurodegenerative disease. Here, I discuss key findings and future directions to further investigate the effects of Coenzyme Q deficiency in *C. elegans*.

Specific proteases antagonize CoQ deficiency-induced GABA neurodegeneration

CED-3/caspase

Our studies in **Chapter 4** introduced a novel role for CED-3/caspase in CoQ-deficient GABA neurons; in this context CED-3 antagonizes a CED-4-dependent killing pathway. Whereas the mechanism of this neuroprotective role of CED-3 is unclear, another recently discovered function for

CED-3 could explain how an executioner caspase antagonizes GABA neuron degeneration. In this finding, laser axotomy of GABA neurons triggers a regeneration pathway that depends on CED-3 function. This mechanism is also calcium dependent and requires the ER calcium binding protein, CRT-1/calreticulin (Pinan-Lucarre et al. 2011). Notably, we previously demonstrated that CoQ depletion-induced GABA neuron death also requires CRT-1/calreticulin-dependent calcium signaling (**Chapter 2**). As described in **Chapter 4**, we favor a hypothesis in which CoQ deficiency and axotomy induce similar stress responses. This model predicts that these signals activate a common pathway to neutralize the cellular damage in GABA motor neurons. In this paradigm, CoQ deficiency triggers a CED-4-dependent degeneration pathway that is antagonized by a CED-3-requiring regeneration mechanism (Fig. 4.7A). Studies in *C. elegans* have identified conserved signaling pathways (i.e., DLK-1, MAP kinase-dependent) that are required for efficient neuron regeneration (Bejjani & Hammarlund 2011). Thus, future experiments to test this model could examine regeneration-deficient mutants (i.e., *dlk-1*) under CoQ-depletion conditions. If DLK-1-dependent regeneration pathways are activated in response to CoQ deficiency, then animals lacking *dlk-1* function are predicted to display the enhanced neurodegeneration phenotype of *ced-3* mutants.

The robust degeneration of GABA neurons that occurs with CoQ deficiency suggests that the CED-4-dependent cell-killing pathway ultimately overpowers the neuroprotective effects of CED-3 function. This observation raises the question of whether a stronger regenerative response to CoQ deficiency could also offer more neuroprotection. For instance, neuronal regeneration in axotomized GABA neurons is accelerated by overexpression of DLK-1 (Hammarlund et al. 2009). Therefore, if it is discovered that *dlk-1* mutants phenocopy *ced-3* loss-of-function (as suggested above), it would be interesting to determine if overexpression of DLK-1 in CoQ-deficient GABA neurons is sufficient to inhibit neuron death. This result would suggest that the balance between cell protection and cell death could be manipulated to sustain neuron viability.

Neuroprotective roles for active caspases have also been detected in cellular responses to ischemia (McLaughlin et al. 2003). The term "preconditioning" refers to a process in which sub-toxic challenges confer tolerance to subsequent insults. For example, exposure to acute stressors (i.e., disrupted ROS or ATP levels) induces up-regulation of pro-survival genes that in turn protect against future injury. Sublethal ischemic conditions activate caspase-3, such that the affected cells are relatively protected against subsequent ischemic insults. In this paradigm, the application of caspase inhibitors abrogated the neuroprotective response, and therefore supports the hypothesis that caspase-3 is required for neuronal preconditioning. For animals that are exposed to CoQ-deficient conditions throughout life, damage to GABA neurons could accumulate over time to eventually activate cell death at the adult stage. Perhaps young CoQ-deficient animals activate CED-3 acutely in a response similar to caspase-3 activation during ischemic preconditioning (McLaughlin et al. 2003). CED-3 activity could provide cytoprotective effects that prevent activation of a neurodegeneration pathway. However, as animals age, two potential mechanisms could explain how this neuroprotection is overridden. First, as mentioned above, the cumulative intracellular damage inflicted by CoQ-deficiency could reach a level of severity in adulthood that can no longer be inhibited by neuroprotective mechanisms. Alternatively, development from L3 to adulthood is a very energetically demanding process (due to a large expansion in mitochondria DNA (mtDNA) (Tsang & Lemire 2002)). As the animal transitions from larval to adult stages, the reduced levels of ATP that results from CoQ depletion coupled with this robust energy requirement could trigger neurodegeneration, despite early CED-3 neuroprotection.

Although the exact mechanism of caspase-3-dependent ischemic neuroprotection is not well-understood, caspase-3 activation is required for induction of neuroprotective heat-shock proteins (HSPs) which function as molecular chaperones under conditions of stress (McLaughlin et al. 2003). HSPs and hypoxia inducible factor (HIF) are up-regulated as a result of preconditioning

stresses (Albers et al. 2010). HIF is a conserved transcription factor that mediates the induction of hundreds of genes in response to hypoxia. In *C. elegans, hif-1* is also required for survival of hypoxic conditions (C. Shen & Powell-Coffman 2003), induced by mitochondrial ETC inhibitors (i.e., rotenone/Complex I, antimycin/Complex III). Although our studies showed that ETC dysfunction is not sufficient to account for degeneration of CoQ-deficient GABA neurons (**Chapter 5**), it is reasonable to hypothesize that CoQ deficiency likely reduces ETC function and therefore simulates hypoxic conditions. The role of hypoxic response genes in this pathway has not been investigated, but the association of caspases with the preconditioning effect (McLaughlin et al. 2003) suggests that CED-3 could functions through a similar mechanism in response to CoQ depletion. In this model, the neuroprotective mechanism fails in *ced-3* mutants, which thus show more robust GABA neuron death. This model predicts that *hif-1* mutants could phenocopy the enhanced GABA neuron degeneration defect of *ced-3* loss-of-function mutants. The precise mechanism of CED-3-mediated neuroprotection is unclear but future studies of neuronal regeneration or cellular preconditioning could be informative.

Investigating the role of autophagy under CoQ-deficient conditions

If additional studies confirm that HIF-1 is required for GABA neuroprotection, then a role for hypoxic response pathways in CoQ-deficient animals could be further investigated. For instance, autophagy protects against hypoxia in *C. elegans,* and we identified ultrastructural features consistent with autophagy in the ventral nerve cord (VNC) of CoQ-deficient animals (**Chapter 5)** Perhaps, in this instance, a GABA neuron has activated autophagy as a cell-survival mechanism in response to CoQ-deficient conditions. As described in **Chapter 5**, future studies could use mutants of known autophagy genes to investigate the role of autophagy in the CoQ-deficient neurons. Because autophagy can contribute to both cell survival and cell death pathways (Kourtis & Tavernarakis

2009), alternative mechanisms could account for the autophagic neuron observed in our TEM studies. The following models (Fig. 6.1) and potential outcomes are considered for this analysis: (1) Autophagy is activated in GABA neurons to protect against degeneration. Over time, however, these neurons succumb to necrosis. In this model, mutations in autophagy genes would enhance GABA neuron death. (2) GABA neurons activate a necrotic pathway that requires autophagy (as discussed in **Chapter 5**); therefore, inhibiting autophagy in this case should block GABA neurodegeneration. (3) Cholinergic neurons survive CoQ deficiency by activating autophagy as a cell-survival mechanism. Therefore, inhibiting autophagy could result in degeneration of cholinergic neurons. The third outcome would be particularly interesting, as it would suggest a rationale for why cholinergic neurons fail to degenerate with CoQ deficiency.

TRA-3/calpain

My work identified another protease TRA-3/calpain as a negative regulator of the CoQ depletion-induced GABA neuron death pathway (**Chapter 5**). TRA-3 has been shown to promote death in other models of necrosis (Syntichaki et al. 2002). However, in the context of CoQ-deficient GABA neurons, my evidence suggests that TRA-3 exerts the opposite role, antagonizing cell death. *tra-3* mutants show enhanced neurodegeneration (**Chapter 5**) resembling that of *ced-3* loss-of-function animals (**Chapter 4**). The identification of two different proteases, CED-3 and TRA-3, that antagonize GABA neuron death strengthens the hypothesis that both cell-killing and cell-survival mechanisms are activated in CoQ-deficient GABA neurons.

Calpain-dependent antagonism of death pathways has also been observed in mammals. For example, mitochondrial calpain 10 protects against apoptotic cell death (Covington et al. 2008). Calpain-dependent degradation of pro-apoptotic proteins (i.e., Bax and Apaf-1) has also been reported (Wood et al. 1998; Reimertz et al. 2001). These examples are consistent with a model in

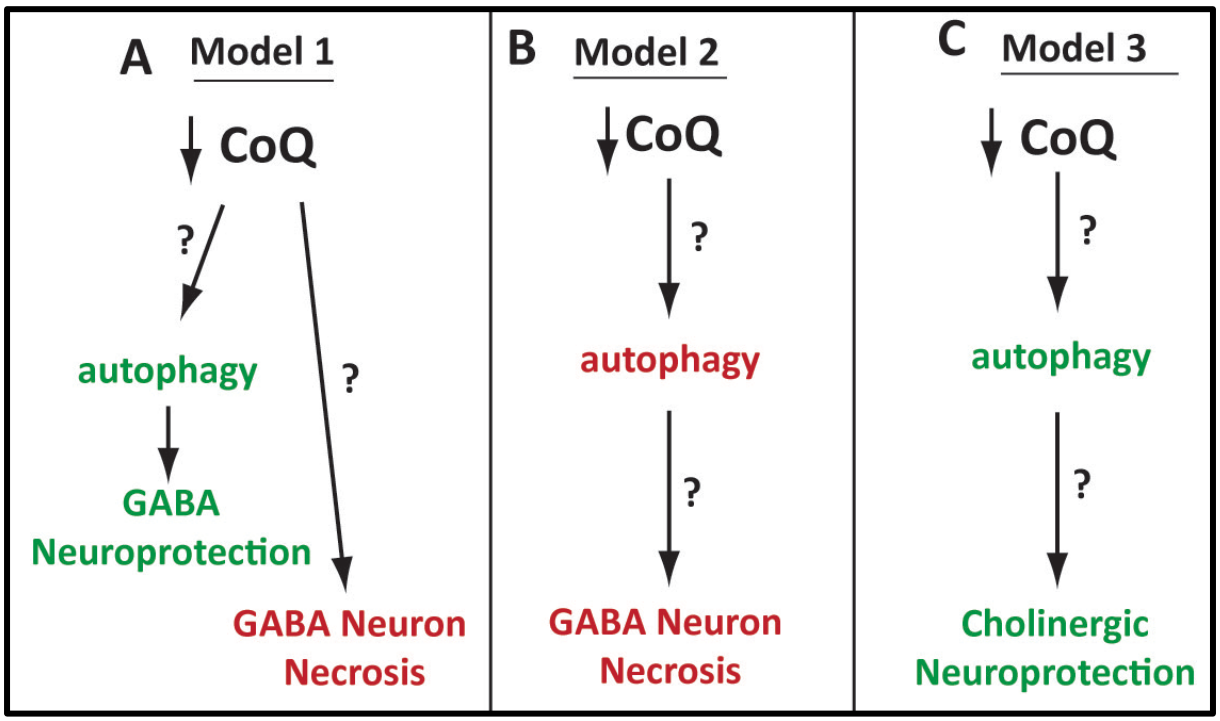

Figure 6.1: Models of how autophagy could prevent or promote neurodegeneration.
A. Model 1: Autophagy is activated in response to CoQ deficiency to protect GABA neurons from death. However, over time, injuries accumulate and necrosis is activated to kill GABA neurons. **B.** Model 2: CoQ deficiency triggers a necrotic pathway that requires autophagy. **C.** Model 3: Activation of the autophagy pathway protects cholinergic neurons from degeneration with CoQ deficiency.

which TRA-3 inhibits the GABA neuron death pathway through proteolysis of the killing machinery. Future studies could test this model by genetic epistasis experiments (see below) or biochemical assays to determine if TRA-3 cleaves proteins that promote GABA neuron degeneration (i.e., CED-4).

To better understand how CED-3 and TRA-3 antagonize neurodegeneration, epistatic relationships between these proteases and positive regulators of the pathway (e.g., *ced-4, asp-4, crt-1, drp-1*) could be investigated. Our studies of *ced-3* and *ced-4* uncovered a novel epistatic interaction that places *ced-4* either downstream or in parallel to *ced-3* (**Chapter 4**). This finding led to testable models that could be explored in future studies (see **Chapter 4**). The idea that TRA-3 inhibits degeneration through direct cleavage of death-promoting proteins could be tested with these epistasis experiments. For example, if TRA-3 functions similarly to mammalian calpain to cleave CED-4, then this TRA-3-dependent activity would effectively reduce the executioner function of CED-4 in the mechanism of GABA neuron death. It follows then that this inhibition of CED-4 would be relieved in a *tra-3* mutant and thus result in enhanced neurodegeneration. In this model, the *tra-3; ced-4* double mutant is predicted to phenocopy *ced-4* single mutants (i.e., *ced-4* is epistatic and degeneration is suppressed). Similar genetic epistasis experiments should be highly useful for future studies that seek to place these genes in the pathway that controls GABA neuron death.

CED-4/Apaf-1 promotes necrosis in CoQ-deficient GABA neurons

In this work, morphological features of dying GABA neurons were examined using light microscopy (**Chapter 2** and **Chapter 3**) and transmission electron microscopy (**Chapter 5**). Based on the appearance of canonical necrotic features of GABA motor neurons (e.g., swollen cell soma, extensive proteolysis, and mitochondrial rupture), we concluded that CoQ-deficient GABA neurons activate a necrotic death pathway. Evidence of necrosis is further supported by the requirement of necrotic genes (*asp-4*/cathepsin and *crt-1*/calreticulin) for GABA neurodegeneration. (**Chapter 5**).

Intriguingly, we also showed that a core member of the canonical apoptotic pathway, CED-4, functions as a key regulator of GABA neuron necrotic death (**Chapter 2**). In addition, we discovered that CED-4 does not promote neurodegeneration through its canonical apoptotic caspase CED-3 (**Chapter 4**). Although the most well-documented function of CED-4 is to promote programmed cell death (Shaham & Horvitz 1996a), alternative roles for CED-4 have been identified in other biological processes. For example, CED-4 and Apaf-1 share a conserved function of mediating DNA-damage-induced cell-cycle arrest (Zermati et al. 2007; Mouhamad et al. 2007). Additionally, hypoxic preconditioning and cell-size-regulation are also controlled by CED-4 (Dasgupta et al. 2007; L. Chen et al. 2008). Notably, all of these non-apoptotic functions of CED-4 occur independently of its downstream caspase CED-3 (Zermati et al. 2007; Dasgupta et al. 2007; L. Chen et al. 2008). Some of these non-apoptotic roles for CED-4 are also induced by cellular stresses (i.e., DNA-damage and hypoxia). Therefore, the activation of a CED-4-dependent function in CoQ-deficient neurons that does not require other members of the canonical apoptotic pathway may involve mechanisms that also occur under other conditions of cell stress. Together, these findings suggest that CED-4 functions as a critical stress-sensing protein that can be activated by a range of different environmental conditions.

Potential mechanisms of CED-4 activation

A worm adenine nucleotide translocase (WAN-1/ANT) was recently identified as a core component of the *C. elegans* programmed cell death machinery (Q. Shen et al. 2009). Adenine nucleotide translocases regulate the mitochondrial permeability transition pore (PTP) complex (Galluzzi et al. 2010). As discussed in **Chapter 1**, mitochondrial PTP opening (i.e., mitochondrial permeability transition or MPT) can be induced by ROS or calcium, and prolonged pore opening can lead to cell death (Vaseva et al. 2012; Geng et al. 2012). Overexpression of ANT (Bauer et al. 1999)

or WAN-1 (Q. Shen et al. 2009) induces apoptosis, whereas ANT inhibition blocks cell death (Marzo et al. 1998; Q. Shen et al. 2009). Because ANT is a critical regulator of PTP opening, mechanisms that control ANT activity are likely to limit inappropriate cell death.

Interestingly, Coenzyme Q may inhibit apoptosis by physically interacting with the PTP, although a specific CoQ-binding protein in this complex has yet to be identified (Papucci et al. 2003; Devun et al. 2010; Sahach et al. 2007). Loss of Coenzyme Q could stimulate pore opening either directly (i.e., by removal of inhibition of PTP opening) or indirectly (i.e., by increasing ROS production, which induces PTP opening). In considering this evidence, I hypothesize that the mitochondrial PTP opens through a WAN-1/ANT-dependent manner in CoQ-deficient GABA neurons to promote CED-4-dependent necrosis.

Future studies could test this model by examining CoQ depletion-induced GABA neurodegeneration in ANT-deficient genetic backgrounds. If ANT promotes GABA neuron death, then genetic ablation of ANT function is predicted to block neurodegeneration (similar to loss of *ced-4*). This requirement for ANT during GABA degeneration would raise the question of whether MTP is involved (as in HBx-induced necrosis (Geng et al. 2012), described below) or if ANT directly activates CED-4 without PTP opening (as in apoptosis (Q. Shen et al. 2009), described above). In addition to ANT, the PTP complex also contains VDAC (voltage-dependent anion channel) and cyclophilin D (discussed in **Chapter 1**) (Galluzzi et al. 2010). A recent study in *C. elegans* described a necrotic pathway initiated by ectopic expression of Hepatitis B virus protein X (HBx) that functions through the MPT (Geng et al. 2012). Inhibition of MPT was achieved using *cyn-1/*Cyclophilin D mutants that prevented necrotic cell death. Similar genetic experiments (i.e., *cyn-1/*Cyclophilin D mutants) could be performed in CoQ-deficient animals to determine if MPT is required for GABA neurodegeneration. If inactivation of the PTP (independent of ANT/WAN-1) does not suppress

degeneration, this result would suggest that WAN-1 functions independently of PTP to promote CED-4-dependent necrosis.

Shen *et al.* report that overexpression of WAN-1 induces ectopic apoptotic death (Q. Shen et al. 2009). In the case of CoQ-deficient GABA neurons, however, we are considering the possibility that WAN-1 would promote necrosis. Cellular ATP concentration can determine whether a cell undergoes apoptosis or necrosis (Yakovlev & Faden 2004) (Fig. 1.5), with high levels of ATP required for apoptosis and low ATP levels resulting in necrosis. We have shown that CoQ deficiency reduces ATP levels (Fig. 2.10). Therefore, the decreased ATP production and likely increased ROS that accompany CoQ deficiency could shift WAN-1/ANT-dependent cell death from apoptosis (Q. Shen et al. 2009) (wild-type CoQ levels) to necrosis (reduced CoQ levels). Therefore, if ANT were identified as a component of the GABA neurodegeneration pathway, it would be interesting to investigate whether ectopic WAN-1 expression in CoQ-deficient backgrounds enhances the necrotic phenotype.

Intercellular Coenzyme Q transport in *C. elegans*

Initially, I considered the hypothesis that GABA neuron degeneration results from decreased synthesis of Coenzyme Q in the affected GABA neurons. However, selective knockdown of *coq-1* in GABA neurons did not trigger neurodegeneration (**Chapter 3**). Because global reduction of CoQ results in GABA neuron degeneration, I reasoned that the necrotic phenotype must result from low CoQ levels but that GABA neurons fail to degenerate with cell specific *coq-1* knockdown because other cells compensate for the lack of *de novo* CoQ synthesis in GABA neurons (Fig. 3.9). In this paradigm, CoQ provided from Q-replete cells is capable of rescuing Q-deficient tissues. This hypothesis is reinforced by our discovery that restoration of CoQ production in muscle is sufficient to overcome growth and fertility defects of *coq-1* mutants (**Chapter 3**).

Studies of uptake of exogenous CoQ and intracellular trafficking have implicated the endomembrane system but the molecular mechanisms that govern these key processes are largely unknown (Padilla-López et al. 2009; Fernández-Ayala et al. 2005). As described in **Chapter 3**, this deficit could be addressed by forward genetic screens in *C. elegans*. For example, in *coq-1* mutant animals that are viable with muscle-only COQ-1 expression (see **Chapter 3**), genetic mutations that inhibit CoQ transport would result in lethality. Alternatively, mutations that enhance CoQ intercellular transport should result in improved viability (i.e., increased brood size, Fig. 3.5). Mutations in known endocytic components could validate the screen and potentially new regulators (i.e., CoQ-binding chaperones) may also be discovered. The impact of these studies could have important therapeutic implications, as the effectiveness of CoQ supplementation is currently limited by its inefficient uptake from exogenous sources.

Model of CoQ deficiency-induced GABA neurodegeneration

My studies have identified a range of proteins that adopt either canonical or unexpected roles in the neurodegenerative response to CoQ deficiency. Here, I describe a model (Fig. 6.2) that incorporates my current knowledge of this pathway. Based on hypotheses introduced in this **Discussion**, I speculate on the interactions between these components that ultimately lead to GABA neuron death. Confirmation of this model will depend on future studies to delineate the exact sequence of events that trigger degeneration of CoQ-deficient GABA neurons.

Events that lead to GABA neuron death under CoQ deficient-conditions

Global CoQ deficiency ultimately results in a broad array of defects in many tissues but GABA neurons are preferentially sensitive to a degenerative response (**Chapter 2**). Despite the prominent role of CoQ in the electron transport chain (ETC), our studies suggest that ETC-

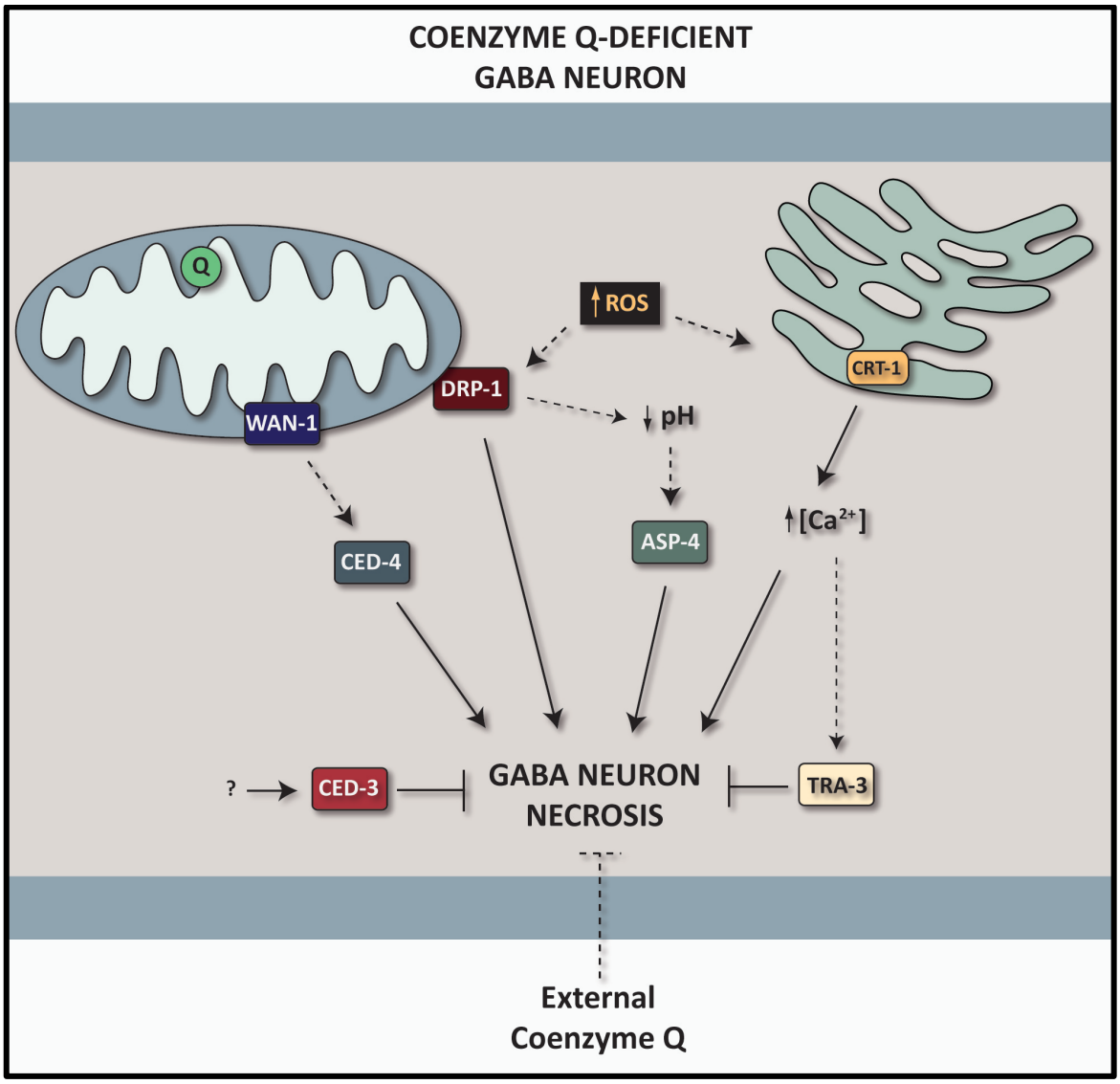

Figure 6.2: Model of CoQ deficiency-induced GABA neurodegeneration. Reduced Coenzyme Q levels in GABA neurons increases ROS production, which in turn triggers a necrotic pathway. CED-4/Apaf-1, DRP-1/Dynamin-Related Protein, ASP-4/aspartyl protease, and CRT-1-dependent calcium release promote GABA neurodegeneration. Conversely, GABA neuron death is antagonized by proteases (CED-3/caspase and TRA-3/calpain). GABA neurons that cannot synthesize CoQ can import CoQ from external sources and to prevent activation of the necrotic pathway. Solid lines = experimentally supported, dashed lines = hypothesized.

independent CoQ functions (e.g., antioxidant defense) antagonize this death pathway (**Chapter 5**). I hypothesize that the loss of Coenzyme Q reduces its robust antioxidant function and thus results in increased ROS production. This oxidative stress (i.e., damage to proteins, lipids, nucleotides) accumulates throughout the lifetime of the animal and manifests as a degenerative response during adulthood (**Chapter 2**). In this model, increased oxidative stress results in elevated cytosolic calcium through CRT-1-dependent release from the endoplasmic reticulum (ER) (**Chapter 2**). High calcium concentrations coupled with elevated ROS could trigger ANT/WAN-1-dependent mitochondrial permeability transition (MPT). Additionally, Coenzyme Q deficiency may disrupt the CoQ-dependent inhibition of MPT and thus sensitize the permeability transition pore for opening by elevated ROS or calcium. ANT/WAN-1 could then release CED-4 (**Chapter 2** and **Chapter 4**), allowing it to promote necrosis through unidentified downstream effectors. In parallel to elevating cytoplasmic calcium, ROS also promotes DRP-1-dependent mitochondrial fragmentation (**Chapter 2**). Mitochondrial fragmentation and PTP opening would then release unknown death-promoting factors from the mitochondria into the cytosol. Additionally, mitochondrial fragmentation acidifies the cell (D. Johnson & Nehrke 2010) and activates cathepsin proteases (i.e., ASP-4, **Chapter 5**) that require low pH for optimal enzymatic activity (Syntichaki et al. 2002). These cellular stresses and proteolytic events culminate in necrotic cell death of GABA motor neurons.

Mechanisms that antagonize GABA neurodegeneration

The cascade of events described above is based on our current understanding of the molecular components that promote GABA neurodegeneration. Our studies have also revealed mechanisms that antagonize GABA neuron death (Fig. 6.2). For example, with tissue-specific CoQ depletion, GABA neurons that are blocked for *de novo* CoQ synthesis may incorporate CoQ from other cells, thus preventing the cell death response (**Chapter 3**). When the death-promoting

mechanism is triggered by global CoQ reduction, specific proteases (CED-3/**Chapter 4** and TRA-3/**Chapter 5**) function to antagonize this pathway. I hypothesize that increased intracellular calcium levels (described above) activates the calcium-dependent protease TRA-3. TRA-3/calpain could antagonize neuron death by degrading pro-death proteins, thus dampening their neurodegenerative effects. Additionally, the neuronal stresses caused by CoQ depletion activate CED-3 (through an unknown mechanism), which could perhaps cleave substrates required for neuronal regeneration (**Chapter 4**). Ultimately, however, the degenerative pathway overrides these proteolytic neuroprotective events and the neuron dies.

CONCLUSIONS

My studies have begun to elucidate the complex molecular response to injury induced by CoQ deficiency. This chapter emphasized important aspects of CoQ deficiency that could be pursued in future studies: (1) The neuronal protection offered by proteolysis; (2) The activation mechanism of CED-4 to promote necrotic cell death; (3) Intercellular Coenzyme Q transport and uptake. The outcome of these future studies could have translational implications for neurodegenerative disease by enhancing our understanding of neuronal protection mechanisms, mitochondria cell death activation, and potential therapeutic avenues for enhanced CoQ treatment.

REFERENCES

Akdemir, F., 2006. Autophagy occurs upstream or parallel to the apoptosome during histolytic cell death. *Development*, 133(8), pp.1457–1465.

Albers, E.L., Bichell, D.P. & McLaughlin, B., 2010. New approaches to neuroprotection in infant heart surgery. *Pediatr Res*, 68(1), pp.1–9.

Altun-Gultekin, Z. et al., 2001. A regulatory cascade of three homeobox genes, ceh-10, ttx-3 and ceh-23, controls cell fate specification of a defined interneuron class in C. elegans. *Development*, 128(11), pp.1951–1969.

Andrew J Duncan, M.B.-G.B.M.H.C.I.P.H.L.C.L.M.H.C.M.Q.M.I.S.J.H.A.S.P.T.C.S.R., 2009. A Nonsense Mutation in COQ9 Causes Autosomal-Recessive Neonatal-Onset Primary Coenzyme Q10 Deficiency: A Potentially Treatable Form of Mitochondrial Disease. *American Journal of Human Genetics*, 84(5), p.558.

Arita, M. et al., 1995. Human alpha-tocopherol transfer protein: cDNA cloning, expression and chromosomal localization. *Biochem J*, 306 (Pt 2), pp.437–443.

Arroyo, A. et al., 2006. Coenzyme Q is irreplaceable by demethoxy-coenzyme Q in plasma membrane of Caenorhabditis elegans. *FEBS Lett*, 580(7), pp.1740–1746.

Asencio, C. et al., 2009. Coenzyme Q supports distinct developmental processes in Caenorhabditis elegans. *Mech Ageing Dev*, 130(3), pp.145–153.

Asencio, C. et al., 2006. Differential expression pattern of coq-8 gene during development in Caenorhabditis elegans. *Gene Expr Patterns*, 6(4), pp.433–439.

Asencio, C. et al., 2003. Silencing of ubiquinone biosynthesis genes extends life span in Caenorhabditis elegans. *The FASEB Journal*, 17(9), pp.1135–1137.

Atamna, H. & Frey, W.H., 2007. Mechanisms of mitochondrial dysfunction and energy deficiency in Alzheimer's disease. *Mitochondrion*, 7(5), pp.297–310.

Bano, D. et al., 2009. Alteration of the nuclear pore complex in Ca2+-mediated cell death. *Cell death and differentiation*, 17(1), pp.119–133.

Barros, M.H. et al., 2005. The Saccharomyces cerevisiae COQ10 gene encodes a START domain protein required for function of coenzyme Q in respiration. *J Biol Chem*, 280(52), pp.42627–42635.

Barsoum, M.J. et al., 2006. Nitric oxide-induced mitochondrial fission is regulated by dynamin-related GTPases in neurons. *EMBO J*, 25(16), pp.3900–3911.

Bauer, M.K. et al., 1999. Adenine nucleotide translocase-1, a component of the permeability transition pore, can dominantly induce apoptosis. *Journal of Cell Biology*, 147(7), pp.1493–1502.

Beal, M.F., 2005. Mitochondria take center stage in aging and neurodegeneration. *Ann Neurol.*, 58(4), pp.495–505.

Bejjani, El, R. & Hammarlund, M., 2011. Neural Regeneration in Caenorhabditis elegans. *Annu Rev Genet*, 46(1), p.120913144909001.

Bergmann, A. & Steller, H., 2010. Apoptosis, stem cells, and tissue regeneration. *Science signaling*, 3(145), p.re8.

Bertram, L., 2005. The genetic epidemiology of neurodegenerative disease. *J. Clin. Invest.*, 115(6), pp.1449–1457.

Betarbet, R. et al., 2000. Chronic systemic pesticide exposure reproduces features of Parkinson's disease. *Nat Neurosci*, 3(12), pp.1301–1306.

Bird, T.D. et al., 1983. Alzheimer's disease: choline acetyltransferase activity in brain tissue from clinical and pathological subgroups. *Ann Neurol.*, 14(3), pp.284–293.

Bloss, T., Witze, E. & Rothman, J., 2003. Suppression of CED-3-independent apoptosis by mitochondrial betaNAC in Caenorhabditis elegans. *Nature*, 424(6952), pp.1066–1071.

Bonfoco, E. et al., 1995. Apoptosis and necrosis: two distinct events induced, respectively, by mild and intense insults with N-methyl-D-aspartate or nitric oxide/superoxide in cortical cell cultures. *Proc Natl Acad Sci U S A*, 92(16), pp.7162–7166.

Bossy-Wetzel, E. et al., 2003. Mitochondrial fission in apoptosis, neurodegeneration and aging. *Current Opinion in Cell Biology*, 15(6), pp.706–716.

Bossy-Wetzel, E., Petrilli, A. & Knott, A.B., 2008. Mutant huntingtin and mitochondrial dysfunction. *Trends in Neurosciences*, pp.1–8.

Bras, M. et al., 2007. Drp1 mediates caspase-independent type III cell death in normal and leukemic cells. *Molecular and Cellular Biology*, 27(20), pp.7073–7088.

Bratton, S.B. et al., 2001. Caspase-3 cleaves Apaf-1 into an approximately 30 kDa fragment that associates with an inappropriately oligomerized and biologically inactive approximately 1.4 MDa apoptosome complex. *Cell Death Differ*, 8(4), pp.425–433.

Breckenridge, D.G. et al., 2008. Caenorhabditis elegans drp-1 and fis-2 Regulate Distinct Cell-Death Execution Pathways Downstream of ced-3 and Independent of ced-9. *Molecular Cell*, 31(4), pp.586–597.

Breckenridge, D.G. et al., 2003. Caspase cleavage product of BAP31 induces mitochondrial fission through endoplasmic reticulum calcium signals, enhancing cytochrome c release to the cytosol. *The Journal of Cell Biology*, 160(7), pp.1115–1127.

Bredesen, D.E., Rao, R.V. & Mehlen, P., 2006. Cell death in the nervous system. *Nature*, 443(7113), pp.796–802.

Brennan, M.A. & Cookson, B.T., 2000. Salmonella induces macrophage death by caspase-1-dependent necrosis. *Mol Microbiol*, 38(1), pp.31–40.

Brenner, S., 1974. The genetics of Caenorhabditis elegans. *Genetics*, 77(1), pp.71–94.

Brookes, P.S. et al., 2004. Calcium, ATP, and ROS: a mitochondrial love-hate triangle. *Am J Physiol, Cell Physiol*, 287(4), pp.C817–33.

Brouillet, E. et al., 1999. Replicating Huntington's disease phenotype in experimental animals. *Progress in Neurobiology*, pp.1–42. Available at: http://ac.els-cdn.com/S0301008299000052/1-s2.0-S0301008299000052-main.pdf?_tid=d8fc854e-85bf-11e2-a0c6-00000aab0f26&acdnat=1362507160_a6c9d156656250ee11b1cbbf65f59535.

Busso, C. et al., 2010. Saccharomyces cerevisiae coq10 null mutants are responsive to antimycin A. *FEBS Journal*, 277(21), pp.4530–4538.

Calixto, A. et al., 2010. Enhanced neuronal RNAi in C. elegans using SID-1. *Nature Methods*.

Campagnola, P.J. et al., 2002. Three-dimensional high-resolution second-harmonic generation imaging of endogenous structural proteins in biological tissues. *Biophys J*, 82(1 Pt 1), pp.493–508.

Canevari, L., Clark, J.B. & Bates, T.E., 1999. beta-Amyloid fragment 25-35 selectively decreases complex IV activity in isolated mitochondria. *FEBS Lett*, 457(1), pp.131–134.

Catarina M Quinzii, S.D.M.H., 2007. Human Coenzyme Q10 Deficiency. *Neurochemical Research*, 32(4-5), pp.723–727.

Chelur, D.S. & Chalfie, M., 2007. Targeted cell killing by reconstituted caspases. *Proceedings of the National Academy of Sciences of the United States of America*, 104(7), pp.2283–2288.

Chen, F. et al., 2000. Translocation of C. elegans CED-4 to Nuclear Membranes During Programmed Cell Death. *Science signaling*, 287(5457), pp.1485–1489.

Chen, L. et al., 2008. ced-4 and Proto-Oncogene tfg-1 Antagonistically Regulate Cell Size and Apoptosis in C. elegans. *Current Biology*, 18(14), pp.1025–1033.

Chung, C.Y. et al., 2005. Cell type-specific gene expression of midbrain dopaminergic neurons reveals molecules involved in their vulnerability and protection. *Human Molecular Genetics*, 14(13), pp.1709–1725.

Chung, S. et al., 2000. A common set of engulfment genes mediates removal of both apoptotic and necrotic cell corpses in C. elegans. *Nat Cell Biol*, 2(12), pp.931–937.

Conradt, B. & Horvitz, H.R., 1998. The C. elegans protein EGL-1 is required for programmed cell death and interacts with the Bcl-2-like protein CED-9. *Cell*, 93(4), pp.519–529.

Covington, M.D., Arrington, D.D. & Schnellmann, R.G., 2008. Calpain 10 is required for cell viability and is decreased in the aging kidney. *AJP: Renal Physiology*, 296(3), pp.F478–F486.

Crane, F.L., 2001. Biochemical Functions of Coenzyme Q10. *Journal of the American College of Nutrition*, pp.1–8.

Crane, F.L. et al., 1957. *Isolation of a quinone from beef heart mitochondria*,

Dacey, D.M. et al., 2005. Melanopsin-expressing ganglion cells in primate retina signal colour and irradiance and project to the LGN. *Nature*, 433(7027), pp.754–760.

Darios, F., 2003. Parkin prevents mitochondrial swelling and cytochrome c release in mitochondria-dependent cell death. *Human Molecular Genetics*, 12(5), pp.517–526.

Dasgupta, N. et al., 2007. Hypoxic Preconditioning Requires the Apoptosis Protein CED-4 in C. elegans. *Current Biology*, 17(22), pp.1954–1959.

Demaurex, N. & Distelhorst, C., 2003. Cell biology. Apoptosis--the calcium connection. *Science*, 300(5616), pp.65–67.

Denning, D.P., Hatch, V. & Horvitz, H.R., 2013. Both the Caspase CSP-1 and a Caspase-Independent Pathway Promote Programmed Cell Death in Parallel to the Canonical Pathway for Apoptosis in Caenorhabditis elegans. *PLoS Genet*, 9(3), p.e1003341.

Devun, F. et al., 2010. Ubiquinone Analogs: A Mitochondrial Permeability Transition Pore-Dependent Pathway to Selective Cell Death A. Lewin, ed. *PLoS ONE*, 5(7), p.e11792.

DiMauro, S., Quinzii, C.M. & Hirano, M., 2007. Mutations in coenzyme Q10 biosynthetic genes. *J. Clin. Invest.*, 117(3), pp.587–589.

Diomedi-Camassei, F. et al., 2007. COQ2 Nephropathy: A Newly Described Inherited Mitochondriopathy with Primary Renal Involvement. *Journal of the American Society of Nephrology*, 18(10), pp.2773–2780.

Ditzel, M. et al., 2003. Degradation of DIAP1 by the N-end rule pathway is essential for regulating apoptosis. *Nat Cell Biol*, 5(5), pp.467–473.

Dixon, S.J., 2006. FGF negatively regulates muscle membrane extension in Caenorhabditis elegans. *Development*, 133(7), pp.1263–1275.

Do, T.Q. et al., 2001. A defect in coenzyme Q biosynthesis is responsible for the respiratory deficiency in Saccharomyces cerevisiae abc1 mutants. *J Biol Chem*, 276(21), pp.18161–18168.

Dong, Z. et al., 2009. Programmed Cell Death in C. elegans. pp.355–373.

Driscoll, M. & Gerstbrein, B., 2003. Dying for a cause: invertebrate genetics takes on human neurodegeneration. *Nature Reviews Genetics*, 4(3), pp.181–194.

Du, C. et al., 2000. Smac, a mitochondrial protein that promotes cytochrome c-dependent caspase activation by eliminating IAP inhibition. *Cell*, 102(1), pp.33–42.

Dueñas, A.M., Goold, R. & Giunti, P., 2006. Molecular pathogenesis of spinocerebellar ataxias. *Brain*,

129(Pt 6), pp.1357–1370.

Earls, L.R. et al., 2010. Coenzyme Q protects Caenorhabditis elegans GABA neurons from calcium-dependent degeneration. *Proceedings of the National Academy of Sciences of the United States of America*, 107(32), pp.14460–14465.

Ellis, H.M. & Horvitz, H.R., 1986. Genetic control of programmed cell death in the nematode C. elegans. *Cell*, 44(6), pp.817–829.

Emmanuele, V. et al., 2012. Heterogeneity of coenzyme Q10 deficiency: patient study and literature review. *Arch Neurol*, 69(8), pp.978–983.

Ernster, L. & Dallner, G., 1995. Biochemical, physiological and medical aspects of ubiquinone function. *Biochim Biophys Acta*, 1271(1), pp.195–204.

Esposti, M.D. et al., 1996. The interaction of Q analogs, particularly hydroxydecyl benzoquinone (idebenone), with the respiratory complexes of heart mitochondria. *Archives of Biochemistry and Biophysics*, 330(2), pp.395–400.

Faber, P.W. et al., 1999. Polyglutamine-mediated dysfunction and apoptotic death of a Caenorhabditis elegans sensory neuron. *Proceedings of the National Academy of Sciences of the United States of America*, 96(1), pp.179–184.

Farooqui, T. & Farooqui, A.A., 2009. Aging: An important factor for the pathogenesis of neurodegenerative diseases. *Mechanisms of Ageing and Development*, 130(4), pp.203–215.

Fernández-Ayala, D.J.M. et al., 2005. Coenzyme Q distribution in HL-60 human cells depends on the endomembrane system. *Biochimica et Biophysica Acta (BBA) - Biomembranes*, 1713(2), pp.129–137.

Ferrante, R.J. et al., 2002. Therapeutic effects of coenzyme Q10 and remacemide in transgenic mouse models of Huntington's disease. *Journal of Neuroscience*, 22(5), pp.1592–1599.

Fontaine, E., Ichas, F. & Bernardi, P., 1998. A ubiquinone-binding site regulates the mitochondrial permeability transition pore. *J Biol Chem*, 273(40), pp.25734–25740.

Formigli, L. et al., 2000. Aponecrosis: morphological and biochemical exploration of a syncretic process of cell death sharing apoptosis and necrosis. *J Cell Physiol*, 182(1), pp.41–49.

Forsgren, M. et al., 2004. Isolation and functional expression of human COQ2, a gene encoding a polyprenyl transferase involved in the synthesis of CoQ. *Biochem J*, 382(Pt 2), pp.519–526.

Frank, C.A. et al., 2005. C. elegans HAM-1 positions the cleavage plane and regulates apoptosis in asymmetric neuroblast divisions. *Developmental Biology*, 284(2), pp.301–310.

Fraser, A.G. et al., 2000. Functional genomic analysis of C. elegans chromosome I by systematic RNA interference. *Nature*, 408(6810), pp.325–330.

Fukushige, T., Hawkins, M.G. & McGhee, J.D., 1998. The GATA-factor elt-2 is essential for formation

of the Caenorhabditis elegans intestine. *Developmental Biology*, 198(2), pp.286–302.

Galluzzi, L. et al., 2007. Cell death modalities: classification and pathophysiological implications. *Cell death and differentiation*, 14(7), pp.1237–1243.

Galluzzi, L. et al., 2010. Mitochondrial gateways to cancer. *Molecular aspects of medicine*, 31(1), pp.1–20.

Galpern, W.R. & Cudkowicz, M.E., 2007. Coenzyme Q treatment of neurodegenerative diseases of aging. *Mitochondrion*, 7, pp.S146–S153.

Galvin, B.D., Kim, S. & Horvitz, H.R., 2008. Caenorhabditis elegans genes required for the engulfment of apoptotic corpses function in the cytotoxic cell deaths induced by mutations in lin-24 and lin-33. *Genetics*, 179(1), pp.403–417.

Garcia-Corzo, L. et al., 2012. Dysfunctional Coq9 protein causes predominant encephalomyopathy associated with CoQ deficiency. *Human Molecular Genetics*.

Gartner, A., Boag, P.R. & Blackwell, T.K., 2008. Germline survival and apoptosis*. pp.1–20.

Gavilan, A. et al., 2005. C. elegans knockouts in ubiquinone biosynthesis genes result in different phenotypes during larval development. *Biofactors*, 25(1-4), pp.21–29.

Gempel, K. et al., 2007. The myopathic form of coenzyme Q10 deficiency is caused by mutations in the electron-transferring-flavoprotein dehydrogenase (ETFDH) gene. *Brain*, 130(Pt 8), pp.2037–2044.

Geng, X. et al., 2012. Hepatitis B virus X protein targets the Bcl-2 protein CED-9 to induce intracellular Ca2+ increase and cell death in Caenorhabditis elegans. *Proceedings of the National Academy of Sciences of the United States of America*, 109(45), pp.18465–18470.

Gille, L. & Nohl, H., 2000. The existence of a lysosomal redox chain and the role of ubiquinone. *Archives of Biochemistry and Biophysics*, 375(2), pp.347–354.

Gilleard, J.S., Barry, J.D. & Johnstone, I.L., 1997. cis regulatory requirements for hypodermal cell-specific expression of the Caenorhabditis elegans cuticle collagen gene dpy-7. *Molecular and Cellular Biology*, 17(4), pp.2301–2311.

Gin, P. & Clarke, C.F., 2005. Genetic evidence for a multi-subunit complex in coenzyme Q biosynthesis in yeast and the role of the Coq1 hexaprenyl diphosphate synthase. *J Biol Chem*, 280(4), pp.2676–2681.

Gomez, F. et al., 2009. Characterizing Two coq-3 Mutants in Caenorhabditis elegans. *17th International C. elegans Meeting*, pp.1–1.

Gomez, F. et al., 2012. Restoring de novo coenzyme Q biosynthesis in Caenorhabditis elegans coq-3 mutants yields profound rescue compared to exogenous coenzyme Q supplementation. *Gene*, pp.1–11.

Grad, L.I., Sayles, L.C. & Lemire, B.D., 2007. Isolation and functional analysis of mitochondria from the nematode Caenorhabditis elegans. *Methods in molecular biology (Clifton, NJ)*, 372, pp.51–66.

Grant, J., Saldanha, J.W. & Gould, A.P., 2010. A Drosophila model for primary coenzyme Q deficiency and dietary rescue in the developing nervous system. *Disease Models and Mechanisms*, 3(11-12), pp.799–806.

Gu, T., Orita, S. & Han, M., 1998. Caenorhabditis elegans SUR-5, a novel but conserved protein, negatively regulates LET-60 Ras activity during vulval induction. *Molecular and Cellular Biology*, 18(8), pp.4556–4564.

Hall, D.H. et al., 1997. Neuropathology of degenerative cell death in Caenorhabditis elegans. *J Neurosci*, 17(3), pp.1033–1045.

Hallam, S. et al., 2000. The C. elegans NeuroD homolog cnd-1 functions in multiple aspects of motor neuron fate specification. *Development*, 127(19), pp.4239–4252.

Hammarlund, M. et al., 2009. Axon regeneration requires a conserved MAP kinase pathway. *Science*, 323(5915), pp.802–806.

Hargreaves, I.P., Lane, A. & Sleiman, P.M.A., 2008. The coenzyme Q10 status of the brain regions of Parkinson's disease patients. *Neurosci Lett*, 447(1), pp.17–19.

Hartman, P.S. et al., 2001. Mitochondrial mutations differentially affect aging, mutability and anesthetic sensitivity in Caenorhabditis elegans. *Mech Ageing Dev*, 122(11), pp.1187–1201.

Hedlund, E. et al., 2010. Global gene expression profiling of somatic motor neuron populations with different vulnerability identify molecules and pathways of degeneration and protection. *Brain*, 133(8), pp.2313–2330.

Heeringa, S.F. et al., 2011. COQ6 mutations in human patients produce nephrotic syndrome with sensorineural deafness. *J. Clin. Invest.*, 121(5), pp.2013–2024.

Hengartner, M.O. & Horvitz, H.R., 1994. Activation of C. elegans cell death protein CED-9 by an amino-acid substitution in a domain conserved in Bcl-2. *Nature*, 369(6478), pp.318–320.

Hihi, A.K., Gao, Y. & Hekimi, S., 2002. Ubiquinone is necessary for Caenorhabditis elegans development at mitochondrial and non-mitochondrial sites. *J Biol Chem*, 277(3), pp.2202–2206.

Hihi, A.K., Kebir, H. & Hekimi, S., 2003. Sensitivity of Caenorhabditis elegans clk-1 mutants to ubiquinone side-chain length reveals multiple ubiquinone-dependent processes. *J Biol Chem*, 278(42), pp.41013–41018.

Hodgkin, J. & Barnes, T.M., 1991. More is Not Better: Brood Size and Population Growth in a Self-Fertilizing Nematode. *Proceedings of the Royal Society B: Biological Sciences*, 246(1315), pp.19–24.

Horvath, R. et al., 2006. Coenzyme Q10 deficiency and isolated myopathy. *Neurology*, 66(2), pp.253–

255.

Huesmann, G.R. & Clayton, D.F., 2006. Dynamic role of postsynaptic caspase-3 and BIRC4 in zebra finch song-response habituation. *Neuron*, 52(6), pp.1061–1072.

Ichishita, R. et al., 2008. SUPP.2 - An RNAi screen for mitochondrial proteins required to maintain the morphology of the organelle in Caenorhabditis elegans. *Journal of Biochemistry*, 143(4), pp.449–454.

Ishii, N. et al., 1998. A mutation in succinate dehydrogenase cytochrome b causes oxidative stress and ageing in nematodes. *Nature*, 394(6694), pp.694–697.

Jakobs, B.S. et al., 2013. A novel mutation in COQ2 leading to fatal infantile multisystem disease. *Journal of the Neurological Sciences*.

Jellinger, K.A., 2000. Cell death mechanisms in Parkinson's disease. *Journal of neural transmission (Vienna, Austria : 1996)*, 107(1), pp.1–29.

Jin, Y. et al., 1999. The Caenorhabditis elegans gene unc-25 encodes glutamic acid decarboxylase and is required for synaptic transmission but not synaptic development. *J Neurosci*, 19(2), pp.539–548.

Johnson, A. et al., 2005. COQ9, a New Gene Required for the Biosynthesis of Coenzyme Q in Saccharomyces cerevisiae. *Journal of Biological Chemistry*, 280(36), pp.31397–31404.

Johnson, D. & Nehrke, K., 2010. Mitochondrial fragmentation leads to intracellular acidification in caenorhabditis elegans and mammalian cells. *Mol Biol Cell*, 21(13), pp.2191–2201.

Jonassen, T. & Clarke, C.F., 2000. Isolation and functional expression of human COQ3, a gene encoding a methyltransferase required for ubiquinone biosynthesis. *J Biol Chem*, 275(17), pp.12381–12387.

Jonassen, T., Larsen, P.L. & Clarke, C.F., 2001. A dietary source of coenzyme Q is essential for growth of long-lived Caenorhabditis elegans clk-1 mutants. *Proc Natl Acad Sci U S A*, 98(2), pp.421–426.

Joshi, P. & Eisenmann, D.M., 2004. The Caenorhabditis elegans pvl-5 gene protects hypodermal cells from ced-3-dependent, ced-4-independent cell death. *Genetics*, 167(2), pp.673–685.

Joyce, P.I. et al., 2012. The Atypical Calpains: Evolutionary Analyses and Roles in Caenorhabditis elegans Cellular Degeneration A. D. Chisholm, ed. *PLoS Genet*, 8(3), p.e1002602.

Jun, L. et al., 2004. Identification and subcellular localization of two solanesyl diphosphate synthases from Arabidopsis thaliana. *Plant & cell physiology*, 45(12), pp.1882–1888.

K, O. et al., 1997. The ispB gene encoding octaprenyl diphosphate synthase is essential for Growth of Escherichia coli. *JOURNAL OF BACTERIOLOGY*, pp.1–3.

Kalén, A. et al., 2002. Ubiquinone biosynthesis by the microsomal fraction from rat liver. *Biochim Biophys Acta*, 926(1), pp.70–78. Available at: http://ac.els-cdn.com/0304416587901838/1-s2.0-

0304416587901838-main.pdf?_tid=1853c3fae4ffb2928455eb173e181533&acdnat=1337615538_d0f65ef0554ac8ade5ec7f24e84647dc.

Kalén, A., Appelkvist, E.L. & Dallner, G., 1989. Age-related changes in the lipid compositions of rat and human tissues. *Lipids*, 24(7), pp.579–584.

Kamath, R.S. et al., 2003. Systematic functional analysis of the Caenorhabditis elegans genome using RNAi. *Nature*, 421(6920), pp.231–237.

Kasahara, Y. et al., 1997. Involvement of reactive oxygen intermediates in spontaneous and CD95 (Fas/APO-1)-mediated apoptosis of neutrophils. *Blood*, 89(5), pp.1748–1753.

Kawamura, Y. et al., 1981. Morphometric comparison of the vulnerability of peripheral motor and sensory neurons in amyotrophic lateral sclerosis. *Journal of neuropathology and experimental neurology*, 40(6), pp.667–675.

Kayser, E.-B., Morgan, P.G. & Sedensky, M.M., 1999. GAS-1: A Mitochondrial Protein Controls Sensitivity to Volatile Anesthetics in the Nematode Caenorhabditis elegans. *Anesthesiology*, pp.545–554.

Kayser, E.B. et al., 2001. Mitochondrial expression and function of GAS-1 in Caenorhabditis elegans. *J Biol Chem*, 276(23), pp.20551–20558.

Kennedy, S., Wang, D. & Ruvkun, G., 2004. A conserved siRNA-degrading RNase negatively regulates RNA interference in C. elegans. *Nature*, 427(6975), pp.645–649.

Kerr, J.F., Wyllie, A.H. & Currie, A.R., 1972. Apoptosis: a basic biological phenomenon with wide-ranging implications in tissue kinetics. *British journal of cancer*, 26(4), pp.239–257.

Knott, A.B. & Bossy-Wetzel, E., 2008. Impairing the mitochondrial fission and fusion balance: a new mechanism of neurodegeneration. *Annals of the New York Academy of Sciences*, 1147, pp.283–292.

Knott, A.B. et al., 2008. Mitochondrial fragmentation in neurodegeneration. *Nature Reviews Neuroscience*, 9(7), pp.505–518. Available at: http://www.ncbi.nlm.nih.gov/entrez/query.fcgi?db=pubmed&cmd=Retrieve&dopt=AbstractPlus&list_uids=18568013.

Kourtis, N. & Tavernarakis, N., 2009. Autophagy and cell death in model organisms. *Cell death and differentiation*, 16(1), pp.21–30.

Kraemer, B.C. et al., 2006. Molecular pathways that influence human tau-induced pathology in Caenorhabditis elegans. *Human Molecular Genetics*, 15(9), pp.1483–1496.

Kroemer, G., Galluzzi, L. & Brenner, C., 2007. Mitochondrial Membrane Permeabilization in Cell Death. *Physiological Reviews*, 87(1), pp.99–163.

Kwong, J.Q., Beal, M.F. & Manfredi, G., 2006. The role of mitochondria in inherited

neurodegenerative diseases. *Journal of Neurochemistry*, 97(6), pp.1659–1675.

Lagido, C. et al., 2008. SUPPLEMENTAL Bridging the phenotypic gap: real-time assessment of mitochondrial function and metabolism of the nematode Caenorhabditis elegans. *BMC Physiol*, 8, p.7.

Lagier-Tourenne, C. et al., 2008. ADCK3, an ancestral kinase, is mutated in a form of recessive ataxia associated with coenzyme Q10 deficiency. *Am J Hum Genet*, 82(3), pp.661–672.

Lalani, S.R. et al., 2005. Isolated mitochondrial myopathy associated with muscle coenzyme Q10 deficiency. *Arch Neurol*, 62(2), pp.317–320.

Langston, J.W. et al., 1983. Chronic Parkinsonism in humans due to a product of meperidine-analog synthesis. *Science*, 219(4587), pp.979–980.

Larsen, P.L. & Clarke, C.F., 2002. Extension of life-span in Caenorhabditis elegans by a diet lacking coenzyme Q. *Science*, 295(5552), pp.120–123.

Lauber, K., 2001. The Adapter Protein Apoptotic Protease-activating Factor-1 (Apaf-1) Is Proteolytically Processed during Apoptosis. *Journal of Biological Chemistry*, 276(32), pp.29772–29781.

Lee, R.Y. et al., 1999. EAT-4, a homolog of a mammalian sodium-dependent inorganic phosphate cotransporter, is necessary for glutamatergic neurotransmission in caenorhabditis elegans. *J Neurosci*, 19(1), pp.159–167.

Lemire, B.D. et al., 2009. C. elegans longevity pathways converge to decrease mitochondrial membrane potential. *Mech Ageing Dev*, 130(7), pp.461–465.

Lettre, G. & Hengartner, M.O., 2006. Developmental apoptosis in C. elegans: a complex CEDnario. *Nat Rev Mol Cell Biol*, 7(2), pp.97–108.

Levavasseur, F. et al., 2001. Ubiquinone is necessary for mouse embryonic development but is not essential for mitochondrial respiration. *J Biol Chem*, 276(49), pp.46160–46164.

Lin, M.T. & Beal, M.F., 2006. Mitochondrial dysfunction and oxidative stress in neurodegenerative diseases. *Nature*, 443(7113), pp.787–795.

Liu, J. et al., 2011. Drosophila sbo regulates lifespan through its function in the synthesis of coenzyme Q in vivo. *Journal of Genetics and Genomics*, 38(6), pp.225–234.

Liu, X. et al., 1996. Induction of apoptotic program in cell-free extracts: requirement for dATP and cytochrome c. *Cell*, 86(1), pp.147–157.

López, L.C. et al., 2006. Leigh syndrome with nephropathy and CoQ10 deficiency due to decaprenyl diphosphate synthase subunit 2 (PDSS2) mutations. *Am J Hum Genet*, 79(6), pp.1125–1129.

Luke, C. et al., 2007. An intracellular serpin regulates necrosis by inhibiting the induction and sequelae of lysosomal injury. *Cell*, 130(6), pp.1108–1119.

Maduro, M. & Pilgrim, D., 1995. Identification and cloning of unc-119, a gene expressed in the Caenorhabditis elegans nervous system. *Genetics*, 141(3), pp.977–988.

Mancuso, M. et al., 2009. Coenzyme Q10 and Neurological Diseases. *Pharmaceuticals*, 2(3), pp.134–149.

Martin, J.B. & Gusella, J.F., 1986. Huntington's disease. Pathogenesis and management. *The New England Journal of Medicine*, 315(20), pp.1267–1276.

Marzo, I. et al., 1998. Bax and adenine nucleotide translocator cooperate in the mitochondrial control of apoptosis. *Science*, 281(5385), pp.2027–2031.

Matthews, R.T. et al., 1998. Coenzyme Q10 administration increases brain mitochondrial concentrations and exerts neuroprotective effects. *Proc Natl Acad Sci U S A*, 95(15), pp.8892–8897.

Mattson, M.P., 2000. APOPTOSIS IN NEURODEGENERATIVE DISORDERS. pp.1–10.

Mattson, M.P., 2007. Calcium and neurodegeneration. *Aging Cell*, 6(3), pp.337–350.

Mattson, M.P. & Magnus, T., 2006. Ageing and neuronal vulnerability. *Nature reviews Neuroscience*, 7(4), pp.278–294.

Matyja, E. et al., 2005. The mode of spinal motor neurons degeneration in a model of slow glutamate excitotoxicity in vitro. *Folia neuropathologica / Association of Polish Neuropathologists and Medical Research Centre, Polish Academy of Sciences*, 43(1), pp.7–13.

McCarter, J. et al., 1997. Soma-germ cell interactions in Caenorhabditis elegans: multiple events of hermaphrodite germline development require the somatic sheath and spermathecal lineages. *Developmental Biology*, 181(2), pp.121–143.

McIntire, S.L., Jorgensen, E.M. & Horvitz, H.R., 1993a. Genes required for GABA function in Caenorhabditis elegans. *Nature*, 364(6435), pp.334–337.

McIntire, S.L., Jorgensen, E.M., Kaplan, J.M., et al., 1993b. The GABAergic nervous system of Caenorhabditis elegans. *Nature*, 364(6435), pp.337–341.

McKim, K.S., Peters, K. & Rose, A.M., 1993. Two types of sites required for meiotic chromosome pairing in Caenorhabditis elegans. *Genetics*, 134(3), pp.749–768.

McLaughlin, B. et al., 2003. Caspase 3 activation is essential for neuroprotection in preconditioning. *Proc Natl Acad Sci U S A*, 100(2), pp.715–720.

Menzies, F.M. et al., 2002. Mitochondrial dysfunction in a cell culture model of familial amyotrophic lateral sclerosis. *Brain*, 125(Pt 7), pp.1522–1533.

Metzstein, M.M., Stanfield, G.M. & Horvitz, H.R., 1998. Genetics of programmed cell death in C. elegans: past, present and future. *Trends Genet*, 14(10), pp.410–416.

Michalak, M. et al., 1999. Calreticulin: one protein, one gene, many functions. *Biochem J*, 344 Pt 2, pp.281–292.

Miller, K.G. et al., 1996. A genetic selection for Caenorhabditis elegans synaptic transmission mutants. *PNAS*, 93(22), pp.12593–12598.

Moldoveanu, T. et al., 2002. A Ca(2+) switch aligns the active site of calpain. *Cell*, 108(5), pp.649–660.

Mollet, J. et al., 2008. CABC1 gene mutations cause ubiquinone deficiency with cerebellar ataxia and seizures. *Am J Hum Genet*, 82(3), pp.623–630.

Mollet, J. et al., 2007. Prenyldiphosphate synthase, subunit 1 (PDSS1) and OH-benzoate polyprenyltransferase (COQ2) mutations in ubiquinone deficiency and oxidative phosphorylation disorders. *J. Clin. Invest.*, 117(3), pp.765–772.

Montero, R. et al., 2007. Clinical, biochemical and molecular aspects of cerebellar ataxia and Coenzyme Q10 deficiency. *Cerebellum*, 6(2), pp.118–122.

Montini, G., Malaventura, C. & Salviati, L., 2008. Early Coenzyme Q10 Supplementation in Primary Coenzyme Q10 Deficiency. pp.1–2.

Mouhamad, S. et al., 2007. Apaf-1 Deficiency Causes Chromosomal Instability. *Cell Cycle*, 6(24), pp.3103–3107.

Nakai, D. et al., 2001. Mouse Homologue of coq7/clk-1, Longevity Gene in Caenorhabditis elegans, Is Essential for Coenzyme Q Synthesis, Maintenance of Mitochondrial Integrity, and Neurogenesis. *Biochemical and Biophysical Research Communications*, 289(2), pp.463–471.

Nass, R. et al., 2002. Neurotoxin-induced degeneration of dopamine neurons in Caenorhabditis elegans. *Proceedings of the National Academy of Sciences of the United States of America*, 99(5), pp.3264–3269.

Navas, P. et al., 2002. Ceramide-dependent caspase 3 activation is prevented by coenzyme Q from plasma membrane in serum-deprived cells. *Free Radic Res*, 36(4), pp.369–374.

Ndegwa, S. & Lemire, B.D., 2004. Caenorhabditis elegans development requires mitochondrial function in the nervous system. *Biochemical and Biophysical Research Communications*, 319(4), pp.1307–1313.

Nohl, H. & Gille, L., 2001. The existence and significance of redox-cycling ubiquinone in lysosomes. *Protoplasma*, 217(1-3), pp.9–14.

Obeso, J.A. et al., 2008. Functional organization of the basal ganglia: Therapeutic implications for Parkinson's disease. *Movement Disorders*, 23(S3), pp.S548–S559.

Okada, K. et al., 1998. Molecular cloning and mutational analysis of the ddsA gene encoding decaprenyl diphosphate synthase from Gluconobacter suboxydans. *European journal of biochemistry / FEBS*, 255(1), pp.52–59.

Okada, K. et al., 1996. Polyprenyl diphosphate synthase essentially defines the length of the side chain of ubiquinone. *Biochim Biophys Acta*, 1302(3), pp.217–223.

Okkema, P.G. et al., 1995. Sequence Requirementsfor Myosin Gene Expression and Regulation in Caenorhabditis elegans

. *Genetics*, 135, pp.385–404.

Okkema, P.G. et al., 1997. The Caenorhabditis elegans NK-2 homeobox gene ceh-22 activates pharyngeal muscle gene expression in combination with pha-1 and is required for normal pharyngeal development. *Development*, 124(20), pp.3965–3973.

Orr, A.L. et al., 2008. N-terminal mutant huntingtin associates with mitochondria and impairs mitochondrial trafficking. *J Neurosci*, 28(11), pp.2783–2792.

Padilla-López, S. et al., 2009. Genetic evidence for the requirement of the endocytic pathway in the uptake of coenzyme Q6 in Saccharomyces cerevisiae. *BBA - Biomembranes*, 1788(6), pp.1238–1248.

Papucci, L. et al., 2003. Coenzyme q10 prevents apoptosis by inhibiting mitochondrial depolarization independently of its free radical scavenging property. *J Biol Chem*, 278(30), pp.28220–28228.

Parrish, J. et al., 2001. Mitochondrial endonuclease G is important for apoptosis in C. elegans. *Nature*, 412(6842), pp.90–94.

Peng, M. et al., 2004. Mutant prenyltransferase-like mitochondrial protein (PLMP) and mitochondrial abnormalities in kd/kd mice. *Kidney international*, 66(1), pp.20–28.

Peng, M. et al., 2008. Primary Coenzyme Q Deficiency in Pdss2 Mutant Mice Causes Isolated Renal Disease D. Beier, ed. *PLoS Genet*, 4(4), p.e1000061.

Petersen, S.C. et al., 2011. A Transcriptional Program Promotes Remodeling of GABAergic Synapses in Caenorhabditis elegans. *Journal of Neuroscience*, 31(43), pp.15362–15375.

Petrozzi, L. et al., 2007. Mitochondria and neurodegeneration. *Biosci Rep*, 27(1-3), pp.87–104.

Pich, S. et al., 2005. The Charcot-Marie-Tooth type 2A gene product, Mfn2, up-regulates fuel oxidation through expression of OXPHOS system. *Human Molecular Genetics*, 14(11), pp.1405–1415.

Pinan-Lucarre, B. et al., 2011. The core apoptotic executioner proteins CED-3 and CED-4 promote initiation of neuronal regeneration in *Caenorhabditis elegans*. *PLoS Biol*, 10(5), p.e1001331. Available at: http://dx.plos.org/10.1371/journal.pbio.1001331.t001.

Portera-Cailliau, C. et al., 1995. Evidence for apoptotic cell death in Huntington disease and excitotoxic animal models. *J Neurosci*, 15(5 Pt 2), pp.3775–3787.

Praitis, V. et al., 2001. Creation of low-copy integrated transgenic lines in Caenorhabditis elegans. *Genetics*, 157(3), pp.1217–1226.

Putcha, G.V. & Johnson, E.M., 2004. Men are but worms: neuronal cell death in C elegans and vertebrates. *Cell death and differentiation*, 11(1), pp.38–48.

Quinzii, C.M. et al., 2006. A mutation in para-hydroxybenzoate-polyprenyl transferase (COQ2) causes primary coenzyme Q10 deficiency. *Am J Hum Genet*, 78(2), pp.345–349.

Quinzii, C.M. et al., 2005. Coenzyme Q deficiency and cerebellar ataxia associated with an aprataxin mutation. *Neurology*, 64(3), pp.539–541.

Reimertz, C. et al., 2001. Ca(2+)-induced inhibition of apoptosis in human SH-SY5Y neuroblastoma cells: degradation of apoptotic protease activating factor-1 (APAF-1). *Journal of Neurochemistry*, 78(6), pp.1256–1266.

Rodriguez-Hernandez, A. et al., 2009. Coenzyme Q deficiency triggers mitochondria degradation by mitophagy. *Autophagy*, 5(1), pp.19–32.

Rodríguez-Aguilera, J.C. et al., 2005. The role of ubiquinone in Caenorhabditis elegans longevity. *Ageing Res Rev*, 4(1), pp.41–53.

Roy, M.K. et al., 2006. Apoptosis, necrosis and cell proliferation-inhibition by cyclosporine A in U937 cells (a human monocytic cell line). *Pharmacol Res*, 53(3), pp.293–302.

Rötig, A. et al., 2000. Quinone-responsive multiple respiratory-chain dysfunction due to widespread coenzyme Q10 deficiency. *Lancet*, 356(9227), pp.391–395.

Sahach, V.F. et al., 2007. [Inhibition of mitochondrial permeability transition pore is one of the mechanisms of cardioprotective effect of coenzyme Q10]. *Fiziolohichnyĭ zhurnal (Kiev, Ukraine : 1994)*, 53(4), pp.35–42.

Saiki, R. et al., 2005. Characterization of solanesyl and decaprenyl diphosphate synthases in mice and humans. *FEBS Journal*, 272(21), pp.5606–5622.

Saiki, R., Lunceford, A.L., Bixler, T., et al., 2008a. Altered bacterial metabolism, not coenzyme Q content, is responsible for the lifespan extension in Caenorhabditis elegans fed an Escherichia coli diet lacking coenzyme Q. *Aging Cell*, 7(3), pp.291–304.

Saiki, R., Lunceford, A.L., Shi, Y., et al., 2008b. Coenzyme Q10 supplementation rescues renal disease in Pdss2kd/kd mice with mutations in prenyl diphosphate synthase subunit 2. *AJP: Renal Physiology*, 295(5), pp.F1535–F1544.

Samara, C., Syntichaki, P. & Tavernarakis, N., 2008. Autophagy is required for necrotic cell death in Caenorhabditis elegans. *Cell death and differentiation*, 15(1), pp.105–112.

Samokhvalov, V., Scott, B.A. & Crowder, C.M., 2008. Autophagy protects from hypoxic injury in C. elegans. *Autophagy*, 4(8).

Sarin, S. et al., 2007. Genetic screens for Caenorhabditis elegans mutants defective in left/right asymmetric neuronal fate specification. *Genetics*, 176(4), pp.2109–2130.

Schuske, K., Beg, A. & Jorgensen, E.M., 2004. The GABA nervous system in C. elegans. *Trends Neurosci*, 27(7), pp.407–414.

Senoo-Matsuda, N., 2003. A Complex II Defect Affects Mitochondrial Structure, Leading to ced-3- and ced-4-dependent Apoptosis and Aging. *Journal of Biological Chemistry*, 278(24), pp.22031–22036.

Shaham, S., 1998. Identification of multiple Caenorhabditis elegans caspases and their potential roles in proteolytic cascades. *J Biol Chem*, 273(52), pp.35109–35117.

Shaham, S. & Horvitz, H.R., 1996a. An alternatively spliced C. elegans ced-4 RNA encodes a novel cell death inhibitor. *Cell*, 86(2), pp.201–208.

Shaham, S. & Horvitz, H.R., 1996b. Developing Caenorhabditis elegans neurons may contain both cell-death protective and killer activities. *Genes & Development*, 10(5), pp.578–591.

Shaham, S. et al., 1999. Mutational analysis of the Caenorhabditis elegans cell-death gene ced-3. *Genetics*, 153(4), pp.1655–1671.

Shani, G. et al., 2001. Autophosphorylation restrains the apoptotic activity of DRP-1 kinase by controlling dimerization and calmodulin binding. *EMBO J*, 20(5), pp.1099–1113.

Shen, C. & Powell-Coffman, J.A., 2003. Genetic analysis of hypoxia signaling and response in C elegans. *Annals of the New York Academy of Sciences*, 995, pp.191–199. Available at: http://onlinelibrary.wiley.com/store/10.1111/j.1749-6632.2003.tb03222.x/asset/j.1749-6632.2003.tb03222.x.pdf?v=1&t=heub0yav&s=aab7f6779adc5679b43931037422318a92025122.

Shen, Q. et al., 2009. Adenine nucleotide translocator cooperates with core cell death machinery to promote apoptosis in Caenorhabditis elegans. *Molecular and Cellular Biology*, 29(14), pp.3881–3893.

Shih, J.D. & Hunter, C.P., 2011. SID-1 is a dsRNA-selective dsRNA-gated channel. *RNA*, 17(6), pp.1057–1065.

Sigmond, T. et al., 2008. Chapter Twenty-Eight Qualitative and Quantitative Characterization of Autophagy in Caenorhabditis elegans by Electron Microscopy. In *Methods in Enzymology*. Methods in Enzymology. Elsevier, pp. 467–491.

Simmer, F. et al., 2003. Genome-wide RNAi of C. elegans using the hypersensitive rrf-3 strain reveals novel gene functions. *PLoS Biol*, 1(1), p.E12.

Smith, M.A. & Schnellmann, R.G., 2012. Calpains, mitochondria, and apoptosis. *Cardiovascular Research*, 96(1), pp.32–37.

Sohmiya, M. et al., 2005. An increase of oxidized coenzyme Q-10 occurs in the plasma of sporadic ALS patients. *J Neurol Sci*, 228(1), pp.49–53.

Sokol, S.B. & Kuwabara, P.E., 2000. Proteolysis in Caenorhabditis elegans sex determination:

cleavage of TRA-2A by TRA-3. *Genes & Development*, 14(8), pp.901–906.

Sun, F. & Cavalli, V., 2010. Neuroproteomics Approaches to Decipher Neuronal Regeneration and Degeneration. *Molecular & Cellular Proteomics*, 9(5), pp.963–975.

Sun, I.L. et al., 1992. Requirement for coenzyme Q in plasma membrane electron transport. *Proc Natl Acad Sci U S A*, 89(23), pp.11126–11130.

Syntichaki, P. et al., 2002. Specific aspartyl and calpain proteases are required for neurodegeneration in C. elegans. *Nature*, 419(6910), pp.939–944.

Sze, J.Y. et al., 2000. Food and metabolic signalling defects in a Caenorhabditis elegans serotonin-synthesis mutant. *Nature*, 403(6769), pp.560–564.

Tabara, H. et al., 1999. The rde-1 gene, RNA interference, and transposon silencing in C. elegans. *Cell*, 99(2), pp.123–132. Available at: http://ac.els-cdn.com/S009286740081644X/1-s2.0-S009286740081644X-main.pdf?_tid=4e8916cc-6bdc-11e2-a5ae-00000aab0f02&acdnat=1359660653_bbf5721c530b517de91c2e38ee107edb.

Taira, T. et al., 2004. DJ-1 has a role in antioxidative stress to prevent cell death. *EMBO Rep*, 5(2), pp.213–218.

Takayuki Kanazawa, M.D.Z.A.H.A.P.W.E.D.N.-S.K.F.B.K.M.C.A.M.A.M.V.D.B., 2008. The C. elegans Opa1 Homologue EAT-3 Is Essential for Resistance to Free Radicals. *PLoS Genetics*, 4(2), p.e1000022.

Tao, W., Walke, D.W. & Morgan, J.I., 1999. Oligomerized Ced-4 kills budding yeast through a caspase-independent mechanism. *Biochemical and Biophysical Research Communications*, 260(3), pp.799–805.

Tavernarakis, N. et al., 2000. Heritable and inducible genetic interference by double-stranded RNA encoded by transgenes. *Nat Genet*, 24(2), pp.180–183.

Thellmann, M., Hatzold, J. & Conradt, B., 2003. The Snail-like CES-1 protein of C. elegans can block the expression of the BH3-only cell-death activator gene egl-1 by antagonizing the function of bHLH proteins. *Development*, 130(17), pp.4057–4071.

Timmons, L., Court, D. & Fire, A.Z., 2001. Ingestion of bacterially expressed dsRNAs can produce specific and potent genetic interference in Caenorhabditis elegans. *Gene*, 263(1-2), pp.103–112.

Tran, U. & Clarke, C.F., 2007. Endogenous synthesis of coenzyme Q in eukaryotes. *Mitochondrion*, 7 Suppl, pp.S62–71.

Tsang, W.Y. & Lemire, B.D., 2003. Mitochondrial ATP synthase controls larval development cell nonautonomously in Caenorhabditis elegans. *Developmental Dynamics*, 226(4), pp.719–726.

Tsang, W.Y. & Lemire, B.D., 2002. Mitochondrial Genome Content Is Regulated during Nematode Development. *Biochemical and Biophysical Research Communications*, 291(1), pp.8–16.

Tsang, W.Y. et al., 2001. Mitochondrial respiratory chain deficiency in Caenorhabditis elegans results in developmental arrest and increased life span. *J Biol Chem*, 276(34), pp.32240–32246.

Turunen, M., Olsson, J. & Dallner, G., 2004. Metabolism and function of coenzyme Q. *Biochimica et Biophysica Acta (BBA) - Biomembranes*, 1660(1-2), pp.171–199. Available at: http://www.ncbi.nlm.nih.gov/entrez/query.fcgi?db=pubmed&cmd=Retrieve&dopt=AbstractPlus&list_uids=14757233.

Vajo, Z. et al., 1999. Conservation of the Caenorhabditis elegans timing gene clk-1 from yeast to human: a gene required for ubiquinone biosynthesis with potential implications for aging. *Mammalian genome : official journal of the International Mammalian Genome Society*, 10(10), pp.1000–1004.

Valente, E.M. et al., 2004. PINK1 mutations are associated with sporadic early-onset parkinsonism. *Ann Neurol.*, 56(3), pp.336–341.

Vaseva, A.V. et al., 2012. p53 Opens the Mitochondrial Permeability Transition Pore to Trigger Necrosis. *Cell*, 149(7), pp.1536–1548.

Ventura, N. & Rea, S.L., 2007. Caenorhabditis elegans mitochondrial mutants as an investigative tool to study human neurodegenerative diseases associated with mitochondrial dysfunction. *Biotechnol J*, 2(5), pp.584–595.

Wallace, K.B. & Starkov, A.A., 2000. Mitochondrial targets of drug toxicity. *Annu Rev Pharmacol Toxicol*, 40, pp.353–388.

Wang, 2010. Selective neuronal vulnerability to oxidative stress in the brain. *Frontiers in Aging Neuroscience*.

Wang, D. et al., 2005. Somatic misexpression of germline P granules and enhanced RNA interference in retinoblastoma pathway mutants. *Nature*, 436(7050), pp.593–597.

Wang, H. et al., 2008. Effects of overexpression of Huntingtin proteins on mitochondrial integrity. *Human Molecular Genetics*, 18(4), pp.737–752.

Wang, X. et al., 2007. C. elegans mitochondrial factor WAH-1 promotes phosphatidylserine externalization in apoptotic cells through phospholipid scramblase SCRM-1. *Nat Cell Biol*, 9(5), pp.541–549.

Wang, X. et al., 2003. Necrotic cell death in response to oxidant stress involves the activation of the apoptogenic caspase-8/bid pathway. *J Biol Chem*, 278(31), pp.29184–29191.

Wee, L.J., Tan, T. & Ranganathan, S., 2006. SVM-based prediction of caspase substrate cleavage sites. *BMC Bioinformatics*, 7(Suppl 5), p.S14.

White, J.G. et al., 1986. The structure of the nervous system of the nematode Caenorhabditis elegans. *Philos Trans R Soc Lond, B, Biol Sci*, 314(1165), pp.1–340.

Williams, D.W. et al., 2006. Local caspase activity directs engulfment of dendrites during pruning.

Nat Neurosci, 9(10), pp.1234–1236.

Wochna, A. et al., 2007. A possible role of oxidative stress in the switch mechanism of the cell death mode from apoptosis to necrosis--studies on rho0 cells. *Mitochondrion*, 7(1-2), pp.119–124.

Wood, D.E. et al., 1998. Bax cleavage is mediated by calpain during drug-induced apoptosis. *Oncogene*, 17(9), pp.1069–1078.

Xie, L.X. et al., 2011. Expression of the human atypical kinase ADCK3 rescues coenzyme Q biosynthesis and phosphorylation of Coq polypeptides in yeast coq8 mutants. *Biochimica et Biophysica Acta (BBA) - Molecular and Cell Biology of Lipids*, 1811(5), pp.348–360.

Xu, K., Tavernarakis, N. & Driscoll, M., 2001. Necrotic cell death in C. elegans requires the function of calreticulin and regulators of Ca(2+) release from the endoplasmic reticulum. *Neuron*, 31(6), pp.957–971.

Yakovlev, A.G. & Faden, A.I., 2004. Mechanisms of neural cell death: implications for development of neuroprotective treatment strategies. *NeuroRx : the journal of the American Society for Experimental NeuroTherapeutics*, 1(1), pp.5–16.

Yamashima, T., 2000. Implication of cysteine proteases calpain, cathepsin and caspase in ischemic neuronal death of primates. *Progress in Neurobiology*, 62(3), pp.273–295.

Yan, N. et al., 2004. Structural, biochemical, and functional analyses of CED-9 recognition by the proapoptotic proteins EGL-1 and CED-4. *Mol Cell*, 15(6), pp.999–1006.

Yang, X., Chang, H.Y. & Baltimore, D., 1998. Essential role of CED-4 oligomerization in CED-3 activation and apoptosis. *Science*, 281(5381), pp.1355–1357.

Yang, Y.-Y. et al., 2009. The effect of different ubiquinones on lifespan in Caenorhabditis elegans. *Mechanisms of Ageing and Development*, 130(6), pp.370–376. Available at: http://www.ncbi.nlm.nih.gov/entrez/query.fcgi?db=pubmed&cmd=Retrieve&dopt=AbstractPlus&list_uids=19428456.

Yi, C.H. & Yuan, J., 2009. The Jekyll and Hyde Functions of Caspases. *Dev Cell*, 16(1), pp.21–34.

Youle, R.J. & Karbowski, M., 2005. Mitochondrial fission in apoptosis. *Nat Rev Mol Cell Biol*, 6(8), pp.657–663.

Young, K.W. et al., 2010. Different pathways lead to mitochondrial fragmentation during apoptotic and excitotoxic cell death in primary neurons. *Journal of biochemical and molecular toxicology*.

Yuan, J. & Horvitz, H.R., 1992. The Caenorhabditis elegans cell death gene ced-4 encodes a novel protein

and is expressed during the period of extensive programmed cell death. *Development*, 116, pp.309–320.

Yuan, J. et al., 1993. The C. elegans cell death gene ced-3 encodes a protein similar to mammalian

interleukin-1 beta-converting enzyme. *Cell*, 75(4), pp.641–652.

Yuan, J.Y. & Horvitz, H.R., 1990. The Caenorhabditis elegans genes ced-3 and ced-4 act cell autonomously to cause programmed cell death. *Developmental Biology*, 138(1), pp.33–41.

Zeevalk, G.D. et al., 2005. Mitochondrial inhibition and oxidative stress: reciprocating players in neurodegeneration. *Antioxidants & Redox Signaling*, 7(9-10), pp.1117–1139.

Zermati, Y. et al., 2007. Nonapoptotic Role for Apaf-1 in the DNA Damage Checkpoint. *Molecular Cell*, 28(4), pp.624–637.

Zhang, D. et al., 2009. RIP3, an Energy Metabolism Regulator that Switches TNF-Induced Cell Death from Apoptosis to Necrosis. *Science*.

Zoghbi, H.Y., 1995. Spinocerebellar ataxia type 1. *Clinical neuroscience (New York, N.Y.)*, 3(1), pp.5–11.

Zong, W. & Thompson, C., 2006. Necrotic death as a cell fate. *Genes Dev*, 20(1), pp.1–15.

Zou, H. et al., 1997. Apaf-1, a human protein homologous to C. elegans CED-4, participates in cytochrome c-dependent activation of caspase-3. *Cell*, 90(3), pp.405–413.

APPENDIX A

LIMITATIONS OF USING RNA INTERFERENCE AS A BIOASSAY TO IDENTIFY COMPONENTS OF A MOLECULAR PATHWAY

SUMMARY

Many of the initial experiments to investigate the mechanism Coenzyme Q deficiency-induced GABA neuron degeneration were performed using *coq-1* RNAi. Unlike CoQ biosynthetic pathway mutants that either developmentally arrest before degeneration is observed or have a weak neurodegenerative phenotype, knockdown of *coq-1* provided a large number of adult animals with robust GABA neuron cell death. However, use of RNAi as the means of perturbing CoQ levels in order to study GABA neurodegeneration presented many experimental challenges that are highlighted in this appendix.

MATERIALS AND METHODS

Nematode strains and genetics

Nematodes used for this study were maintained as previously described (Brenner 1974). The CGC was the source of all of the mutants [*eri-1(mg366), ced-3(n718), ced-3(n1040), ced-3(n1949), ced-3(n2888), ced-3(ok2734), csp-1(ok2570)]* and integrated transgenes [*juIs76, trIs10*] used in this work. Experiments in this appendix used strains listed in Table A.1.

Molecular Biology

See **Materials and Methods** sections of **Chapter 2** for a description of the *unc-25* promoter used and **Chapter 5** for construction of the *unc-25 RNAi* clone. Plasmids used in this appendix are listed in Table A.2.

TOM20::mRFP and TOM20::GFP (Outer Mitochondrial Membrane Localization)

See **Chapter 3 – Materials and Methods** for a description of *TOM20::mRFP*. pMLH161 was made by replacing mRFP from pMLH035 with GFP from pMLH084 with 5'KpnI/3'ApaI.

acr-2 Promoter (Cholinergic neurons)

The 3.2kb *acr-2* promoter was amplified (GoTaq, Promega) from pG2M63 with primers that added 5'SphI/3'AscI and inserted into a pCR8/GW/TOPO vector by TOPO TA Cloning (Invitrogen) to make pMLH074. pMLH127 was created by inserting the *acr-2* promoter from pMLH074 into pMLH035 with 5'SphI/3'AscI. *acr-2* primers: 5'GGGGCATGCCGAGGTCGACATTCTTGGAATT, 5'GGGGGCGCGCCCTGGTTCGTGAAGACAACTAAA.

Microscopy

Images for Figure A.1 were obtained on a Leica TCS-SP5 confocal microscope with a 63x objective using the Leica Application Suite Advanced Fluorescence (LAS-AF) software. GABA neuron degeneration was scored on a Zeiss Axioplan microscope with a 100x objective.

Additional Methods

Additional experimental methods are described in the **Materials and Methods** sections of **Chapter 2** (RNAi) and **Chapter 5** (*unc-25* RNAi movement assay).

Table A.1: *C. elegans* strains used in this appendix.

Strain	Genotype
NC1405	*juIs76 [punc-25::GFP, lin-15(+)] II; eri-1 (mg366) IV*
NC2236	*wdEx707 [punc-25::TOM20mRFP+elt-2::GFP+pha-1(+)]; pha-1(e2123); lon-2(e678)X*
NC2479	*wdEx783 [punc-25::TOM20::GFP, pacr-2::TOM20::mRFP, pceh-22::GFP]*
NC2617	*trIs10 [pmyo-3::MB::YFP, pmyo-2::YFP, pceh-23::HcRed, punc-25::DsRed, unc-129nsp::CFP] I; eri-1 (mg366) IV*
NC2627	*trIs10 [pmyo-3::MB::YFP, pmyo-2::YFP, pceh-23::HcRed, punc-25::DsRed, unc-129nsp::CFP] I; ced-3 (ok2734) eri-1 (mg366) IV*
NC2628	*trIs10 [pmyo-3::MB::YFP, pmyo-2::YFP, pceh-23::HcRed, punc-25::DsRed, unc-129nsp::CFP] I; csp-1 (ok2570) II; ced-3 (ok2734) eri-1 (mg366) IV*
NC2626	*trIs10 [pmyo-3::MB::YFP, pmyo-2::YFP, pceh-23::HcRed, punc-25::DsRed, unc-129nsp::CFP] I; csp-1 (ok2570) II; eri-1 (mg366) IV*
NC2660	*juIs76 [punc-25::GFP, lin-15(+)] II; ced-3(n1949) eri-1(mg366) IV*
NC2676	*juIs76 [punc-25::GFP, lin-15(+)] II; ced-3(n1040) eri-1(mg366) IV*
NC2675	*juIs76 [punc-25::GFP, lin-15(+)] II; ced-3(n2888) eri-1(mg366) IV*
NC2687	*juIs76 [punc-25::GFP, lin-15(+)] II; ced-3(n718) eri-1(mg366) IV*

Table A.2: Plasmids used in this work.

Vector	DNA	Additional Information
pMBM09	*unc-25 RNAi* in pL4440 (HT115 *E. coli*)	made by Meg Mitchell
pMLH001	*punc-25* (5'SphI/3'AscI) FWD in pENTR D-TOPO	
pMLH035	*punc-25::TOM20::mRFP::unc-10 3'UTR*	
pMLH074	*pacr-2 (5'SphI/3'AscI) in pCR8/GW/TOPO*	
pMLH084	*punc-25::GFP::unc-10 3'UTR*	
pMLH127	*pacr-2::TOM20::mRFP::unc-10 3'UTR*	
pMLH161	*punc-25::TOM20::GFP::unc-10 3'UTR*	
pG2M02	*pmyo-3::TOM20::mRFP*	a gift from Toshihiko Oka
pG2M17	*pelt-2::NLS::GFP*	a gift from Oliver Hobert
pG2M19	*pceh-22::GFP (pCW2.1)*	a gift from Oliver Hobert
pG2M30	*pBlueScript II*	
pG2M63	*pacr-2::YFP (pSC391*)	a gift from Yishi Jin
pG2M64	*pha-1(+) (pBX)*	

Table A.3: Plasmid concentrations used to make transgenic arrays used for this study.

Transgenic Array	Genotype Injected	Plasmid Name	Concentration
wdEx707 [punc-25::TOM20mRFP, elt-2::GFP, pha-1(+)]	*pha-1(e2123)* III*; lon-2(e678)* X	pMLH035	25 ng/µL
		pG2M17	25 ng/µL
		pG2M30	25 ng/µL
		pG2M64	25 ng/µL
wdEx783 [punc-25::TOM20::GFP, pacr-2::TOM20::mRFP, pceh-22::GFP]	N2	pMLH127	25 ng/µL
		pMLH161	25 ng/µL
		pG2M19	15 ng/µL

RESULTS

Mislabeled clones in the Ahringer RNAi library

The Ahringer RNAi library is a useful source of bacterial clones that target more than 85% of the *C. elegans* genome (Kamath & Ahringer 2003; Kamath et al. 2003; Fraser et al. 2000). However, as indicated in **Chapter 5**, some of the RNAi clones selected for analysis were incorrectly annotated in the Ahringer RNAi library. Additionally, the *coq-1* RNAi bacterial strain was initially discovered in a location designated, and also containing, a bacterial clone targeted toward another gene (*arl-1*). An estimated clone error rate of 7% is acknowledged by the Ahringer lab and other groups have performed more detailed analysis on the Ahringer RNAi library reliability (Qu et al. 2011). Therefore, use of bacterial clones in this library should first be confirmed by sequencing before experimentation.

Transgene silencing by the RNAi pathway limits use of extrachromosomal transgenic arrays

RNAi-induced Transcriptional Gene Silencing (RNAi-TGS) is a phenomenon in which somatic transgenes are silenced by a mechanism induced by feeding RNAi. The effect is suggested to arise from promiscuous transcription of dsRNAs from sequences that are shared between the RNAi vector backbone and the transgenic array (Grishok 2005). Induction of this silencing pathway presents experimental challenges for assays that rely on RNAi-induced phenotypes.

We also observed muted transgenic array expression in genetic backgrounds containing *eri-1(mg366)*, an RNAi-sensitizing mutation (Kennedy et al. 2004) that is required to achieve robust GABA neurodegeneration with *coq-1* knockdown. This combination of potential transgene silencing by RNAi treatment and the need to use a genetic background that also reduces transgene expression complicated experiments that relied on the use of extrachromosomal arrays.

One example of an experiment that could not be performed due to RNAi-TGS was designed to address the potential role of the mitochondrial fission and fusion machinery in the GABA neurodegeneration pathway (see **Chapter 2**) (Earls et al. 2010). The idea for this experiment was to use a transgenically-expressed fluorescent marker to monitor changes in mitochondria (*i.e.,* size, distribution, number) as a result of *coq-1* knockdown. The mitochondrial membrane localization sequence (TOM20) was fused to mRFP (Ichishita et al. 2008) and expressed in GABA neurons; this reporter labeled mitochondria in both the cell soma and neuronal processes (Fig. A.1). However, the TOM20::RFP marker was too dim after RNAi-induced *coq-1* knockdown to investigate changes in mitochondrial morphology.

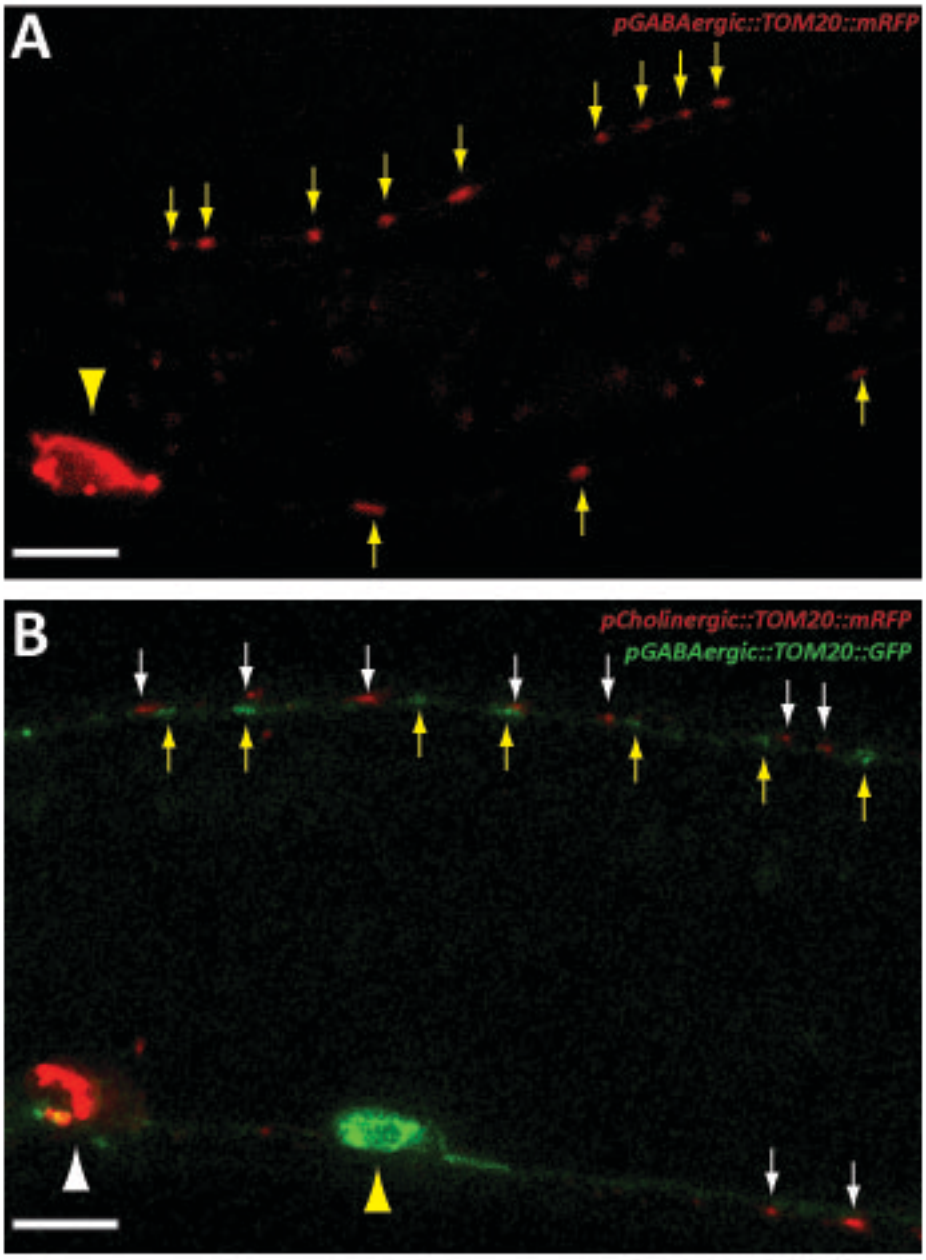

Figure A.1: Neuronal mitochondria are visualized by outer-mitochondrial membrane tagged (TOM20) fluorophores. A. TOM20::mRFP labels mitochondria in GABA neurons. The TOM20::mRFP mitochondrial signal accumulates in the cell soma (white arrowhead) and labels individual mitochondria in GABAergic processes (white arrows). **B.** Mitochondria from GABA (white arrows/arrowhead) and cholinergic (yellow arrows/arrowhead) neurons are labeled with TOM20::mRFP and TOM20::GFP, respectively. Anterior left, ventral down. Scale bar = 5µM.

Interpretation of GABA neurodegeneration levels induced by coq-1 knockdown is difficult due to varying sensitivities of genetic backgrounds to RNAi treatment

To investigate the mechanism of GABA neuron degeneration arising from CoQ depletion, I generated multiple strains with loss of function mutations in candidate death-related genes (*e.g., ced-4*). These strains also contained the RNAi-sensitizing mutation *eri-1(mg366*) and GABA neuron reporter *punc-25::GFP* (*juIs76*). *coq-1* RNAi knockdown was used to induce GABA neuron cell death and levels of degeneration in these mutants were compared to control (*eri-1; juIs76* alone).

With the goal of confirming that RNAi sensitivity was equivalent across these different genetic backgrounds, I performed a control RNAi experiment targeting *unc-25*/Glutamic Acid Decarboxylase (GAD), a gene selectively required in GABA neurons for GABA biosynthesis (McIntire et al. 1993). RNAi knockdown of *unc-25* results in a characteristic "shrinker" movement defect due to excessive muscle contraction (McIntire et al. 1993). I reasoned that strains with equal RNAi sensitivity would show comparable Unc-25 shrinker phenotypes. The results of this control experiment, however, detected variable levels of impaired movement in different genetic backgrounds (Fig. A.2). For example, two independently-generated "wild-type" (*eri-1; juIs76*) strains showed significantly different sensitivities to *unc-25* RNAi. Additionally, transgenic lines built with different *ced-3* alleles also displayed variable levels of penetrance for the *unc-25* RNAi movement defect. These results suggested that apparent differences in GABA neurodegeneration could be due to variable, strain-specific sensitivity to RNAi and rather an indication of an effect of tested genetic mutant on the degeneration pathway.

The unexpected range of sensitivities to *unc-25* RNAi prompted us to examine this effect in concert with GABA neuron degeneration induced by *coq-1* RNAi knockdown. For this experiment, I used a second transgenic GABAergic reporter (*trIs10*) in combination with the RNAi-sensitizing *eri-1* mutation, and treated WT, *ced-3 (ok2734), csp-1(ok2570),* and the *ced-3; csp-1* double mutant with

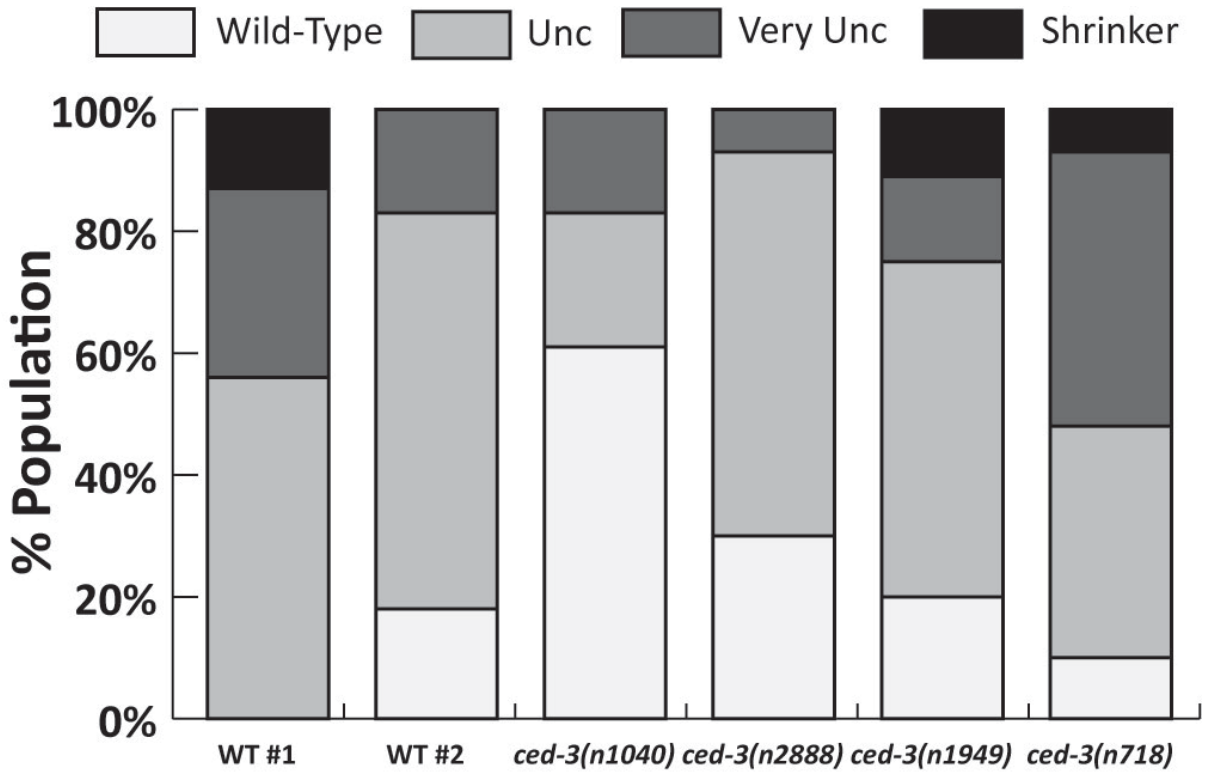

Figure A.2: Sensitivity to feeding RNAi is variable between controls strains and among animals with different *ced-3* mutant backgrounds. RNAi knockdown of *unc-25*/GAD presents a range of Uncoordinated (Unc) phenotypes in two groups of animals sharing the *eri-1(mg366); juIs76 [punc-25::GFP, lin-15(+)]* genetic background (WT #1 *vs* WT #2). Among the *ced-3* mutants, the n718 allele is significantly more sensitive than the others.

RNAi against both *coq-1* and *unc-25*. The extent of GABA neurodegeneration in these experiments indicated that *ced-3(ok2734)* enhanced degeneration, *csp-1(ok2570)* suppressed it, and animals mutant for both *ced-3* and *csp-1* showed significantly enhanced GABA neuron degeneration (Fig. A.3A). The wild-type control for this experiment did not display signs of GABA neuron death with *coq-1* knockdown. Unc-25 movement defects paralleled these results with *ced-3* and *ced-3; csp-1* mutants showing a strong Unc-25 phenotype whereas most of the *csp-1* mutant animals displayed wild-type movement (Fig. A.3B). I therefore concluded that differences in RNAi sensitivity are likely to account for the varying levels of GABA neuron degeneration among these mutant strain rather than specific effects of cell death pathway mutants (*e.g., ced-3* and *csp-1*) on the degeneration pathway. In addition to noting varying levels of RNAi sensitivity for different genetic backgrounds, these experiments were also plagued by highly variable levels of *coq-1* RNAi-induced GABA neuron degeneration in the wild type reference strain (Fig A.2). On the basis of these results, I concluded that the use of RNAi to knockdown *coq-1* could result in misleading conclusions. The mechanisms that accounts for variability in RNAi penetrance between different genetic strains and experimental replicates are unknown.

DISCUSSION AND FUTURE DIRECTIONS

The finding that GABA neurons preferentially degenerate under conditions of CoQ deficiency was initially recognized in *coq-1* RNAi knockdown animals (**Chapter 2**). Because *coq-1* mutants arrest before the onset of GABA neurodegeneration in the adult stage (**Chapter 3**), it is fortuitous that these first experiments were conducted with *coq-1* RNAi-treated animals, which survive to adulthood. It is now clear, however, that the RNAi effect is highly variable and sensitive to genetic backgrounds and thus must be interpreted with caution.

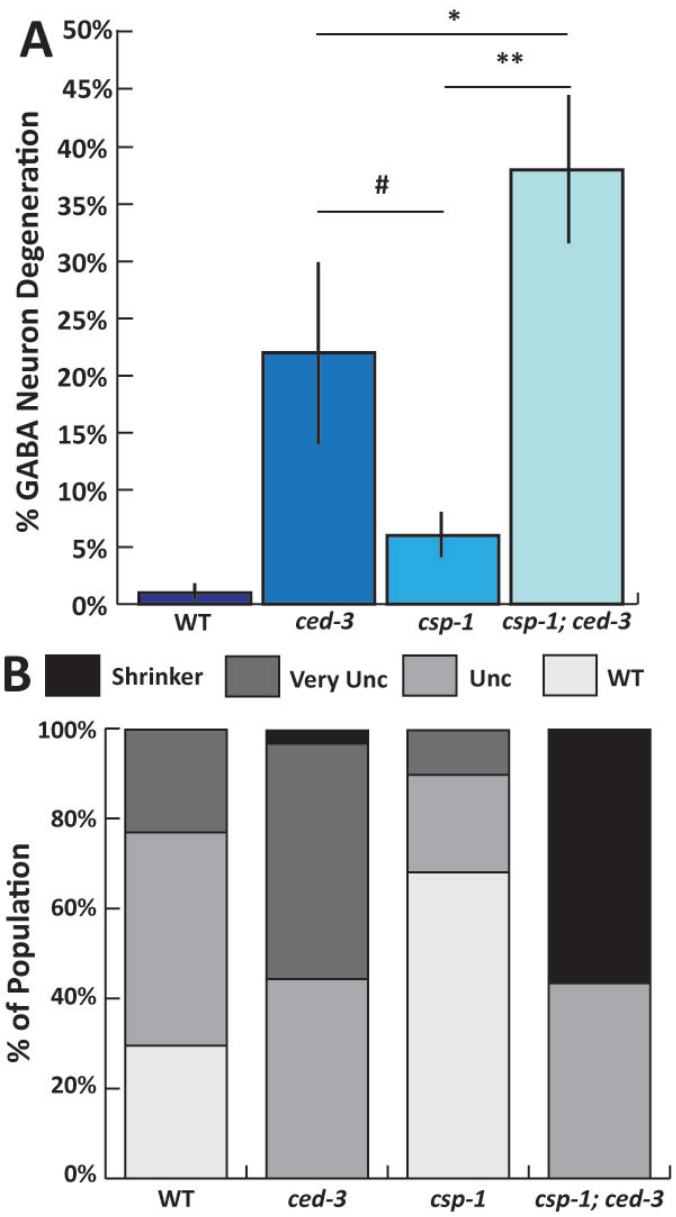

Figure A.3: Knockdown of *unc-25*/GAD reveals differential sensitivity to RNAi in GABA neurons among mutants used for CoQ neurodegeneration assays. A. Global *coq-1* RNAi produces a wide range of neurodegeneration levels between the four genotypes tested. The *csp-1; ced-3* double mutant has significantly enhanced GABA VNC degeneration compared to both wild-type (WT) and *csp-1* single mutants. # $p<0.04$ * $p<0.08$ ** $p<0.0001$. n>15. **B.** Movement defects induced by *unc-25* RNAi treatment mirrors the GABA neuron degeneration levels observed in **Panel A**. n>30. All strains share the *eri-1(mg366); trIs10 [pmyo-3::MB::YFP, pmyo-2::YFP, pceh-23::HcRed, punc-25::DsRed, unc-129nsp::CFP]* background.

We optimized experimental conditions using CoQ biosynthetic pathway mutants that now allow us to reproducibly observe GABA neurodegeneration (see **Chapter 3**). We have used this technique to validate components of the GABA cell death pathway that were originally identified using *coq-1* RNAi. This RNAi-independent system has confirmed that *ced-4* is necessary for GABA neuron death (see **Chapter 4**) and two proteases (*ced-3* and *tra-3*) antagonize this pathway (see **Chapters 4 and 5**). Our analysis of components of this pathway by both RNAi and genetic knockout of CoQ biosynthetic genes provides convincing evidence supporting their involvement in this degenerative process.

Future Directions

Despite technical hurdles with RNAi-induced Transcriptional Gene Silencing, efforts to examine GABAergic mitochondria in CoQ-depleted animals warrant further pursuit. Differences in mitochondrial number, size, and distribution (Labrousse et al. 1999) between wild-type and CoQ deficient animals are predicted based on our genetic and RNAi studies with the mitochondrial fission (*drp-1*) and fusion (*fzo-1*) genes (see **Chapter 2**, (Earls et al. 2010)). Additionally, two-color labeling of mitochondria in GABAergic and cholinergic neurons can be used to detect potential differential sensitivity of mitochondria to CoQ depletion in neighboring GABAergic versus cholinergic motor neurons. (Fig. A.1B). With our discovery of experimental conditions for detecting robust GABA neuron degeneration in CoQ pathway mutants (see **Chapter 3**), it should be possible to analyze mitochondria in these distinct neuronal populations independent of the transgene silencing effects associated with the RNAi pathway.

APPENDIX B

MODIFICATION OF AN *IN VIVO* CASPASE REPORTER TO DETECT CED-3 PROTEOLYTIC ACTIVITY IN *C. ELEGANS*

SUMMARY

We have shown that CED-3/caspase antagonizes a death pathway in GABA neurons caused by CoQ deficiency (see **Chapter 4**). Genetic and transgenic experiments indicate that the caspase activity of CED-3 is required for its neuroprotection. We wanted to characterize this non-canonical function of CED-3 and pursued a methodology that would allow us to detect caspase activation *in vivo*. For this, we modified a caspase biosensor (Apoliner) originally introduced in *Drosophila* (Bardet et al. 2008) for use in *C. elegans*. Our adapted caspase reporter (Apoworm) has enhanced expression and can detect apoptotic events in live animals. However, experimental outcomes described in this appendix bring the fidelity of this reporter into question. Apoworm therefore requires further optimization before it can be used as a reliable indicator of caspase activity. Despite current technical hurdles, this biosensor has immense potential to detect *in vivo* caspase-dependent events in *C. elegans*.

MATERIALS AND METHODS

Nematode Strains and Genetics

Nematodes were cultured as described previously (Brenner 1974). The following strains were obtained from the CGC: *opIs56 [pegl-1::2X::NLS::GFP]* (Hofmann et al. 2002)*, ced-1(e1735) I; ced-5(n1812) IV* (Reddien & Horvitz 2004)*, ced-3(ok2734) IV, sid-1(pk3321) V* (Calixto et al. 2010)*; uIs69 [pmyo-2::mCherry + punc-119::sid-1] V*. JR100 [*ced-1(e1735); wEx15(hs::p35 + pRF4)]* (Abraham et al. 2007) was a gift from Shai Shaham.

Molecular Biology

Table B.1 contains primers used for molecular cloning, and plasmids generated/used are listed in Table B.2. Plasmids were injected at concentrations listed in Table B.3.

Apoliner

The caspase reporter Apoliner was amplified (GoTaq, Promega) from pG2M03 with primers that added 5'AscI/3'KpnI and TA TOPO cloned into pCR2.1/TOPO to make pMLH024.

Apoliner(DEVD)

The caspase cleavage sequence was changed from DQVD to DEVD by introducing a G-to-A change at nucleotide 1390 into a primer that also contained the AgeI restriction site within Apoliner (between mCD8 and mRFP, Fig. B.1A). pG2M03 was used as template for the PCR reaction (GoTaq, Promega) and the amplicon (5'AgeI-[BIR1-NLS-GFP]-KpnI-3') was inserted into pCR8/GW/TOPO by TA TOPO cloning (Invitrogen) to make pMLH075. Due to a missense mutation in the mRFP domain of pMLH024 introduced by PCR, an intermediate vector (pMLH120) was made to create a multiple cloning site (MCS) containing restriction sites necessary for piecing together the full Apoliner(DEVD). This was done by amplifying an unrelated sequence (from pCJS03) with primers that added AscI-XhoI-SacII and AgeI-BamHI-KpnI to the pMLH116 vector using 5'AscI/3'KpnI to make pMLH120. pMLH137 was made by assembling pieces of Apoliner-DEVD from the following sources into pMLH007 (5'AscI/3'KpnI): pMLH024 (5'AscI/3'SacII), pG2M04 (5'SacII/3'AgeI) and pMLH074 (5'AgeI/3'KpnI).

Apoliner-CED-9

A region of *ced-9* cDNA containing two *in vitro* CED-3 cleavage sites (DAQD, ESID) (Xue & Horvitz 1997; Taylor et al. 2007) was selected to replace the BIR1 domain of Apoliner (Fig. B.1A). The size of the region (~450bp) is comparable to that of the BIR1 domain (Fig. B.5B). pMLH158 was used as template to amplify (GoTaq, Promega) this region of *ced-9* and insert it into pMLH142 (5'AgeI/3'BamHI) to make pMLH204.

Apoworm

The mCD8 domain of Apoliner-DEVD was replaced with the *pat-3* transmembrane domain (Mb) to make Apoworm. Lysate from *trIs10 [pmyo-3::Mb::YFP, pmyo-2::YFP, pceh-23::HcRed, punc-25::DsRed, unc-129nsp::CFP]* (Dixon 2006) animals was used as template to amplify (GoTaq, Promega) *pat-3* Mb (from pPD133.58 contained the *trIs10* array). The amplicon was cloned into pMLH103 (5'BamHI/3'AgeI) to make pMLH221. *pat-3* Mb was subsequently inserted into pMLH142 with 5'AscI/3'SacII to create pMLH237.

egl-1 Promoter

The 2.7kb *egl-1* promoter (Neukomm et al. 2011) was amplified (Phusion High-Fidelity Polymerase, New England Biolabs) from DNA lysate collected from *opIs56* [*pegl-1::2xNLS::GFP*] transgenic animals (Hofmann et al. 2002). pMLH157 was generated by inserting the *egl-1* promoter PCR product into pMLH137 with 5'SphI/3'AscI (added to the primers).

ced-9 RNAi

The Miller *ced-9* RNAi clone targets most of *ced-9* cDNA sequence (Figure B.5B). *ced-9* was amplified from N2 cDNA (GoTaq, Promega) with primers that flanked it with PmeI sites and inserted

into pCR8/GW/TOPO by a TOPO TA reaction (Invitrogen) to make pMLH152. pMLH158 was made by using a PmeI digest to add *ced-9* from pMLH152 to the pL4440 vector in pMLH128.

p35

The p35 gene was PCR amplified from JR100 [*ced-1(e1735); wEx15(hs::p35 + pRF4)*] (Abraham et al. 2007) (a gift from Shai Shaham) and cloned into pMLH84 with 5'AscI/3'SacII to generate pMLH247.

Apoworm-DXVA

Caspase cleavage is abrogated by mutating the aspartate in the P1 position (DXXD) of the caspase consensus sequence to alanine (DXXA) (Ditzel et al. 2003). The 5'AgeI-3'KpnI region of pG2M04 (DQVA) was amplified (Phusion High-Fidelity Polymerase, New England Biolabs) and inserted into pMLH240 to make pMLH241. The same primer that introduced the Q-to-E mutation to make Apoliner-DEVD was used to make pMLH243; pMLH241 was used as a template and the amplicon was inserted into pMLH237 (5'AgeI/3'KpnI).

Additional Molecular Biology

See **Materials and Methods** of the following chapters for previously described molecular biology: **Chapter 2** – *unc-25*/GABA promoter, **Chapter 3** – *ttr-39*/GABA promoter, *F25B3.3*/Pan-Neural promoter, **Chapter 4** – reconstituted CED-3.

Table B.1. Molecular cloning primers used to generate the plasmids (see **Table B.2**) used in this study.

Gene/Amplicon	Primer Name	Primer Sequence
Apoliner	Apo_5p_AscI	AAGGCGCGCCATGGCCTCACCGTTGACCCG
	Apo_3p_KpnI	AAGGTACCTTATTTGTATAGTTCATCCA
Apoliner-DEVD & Apoliner–DEVA	apo_DEVD_5p_AgeI	ACCGGTGCATCTGTTGTAGCTGATCTTCCGTCTTATGGACCTATCGCTTTTGATGAGGTG
	Apo_3p_KpnI	AAGGTACCTTATTTGTATAGTTCATCCA
Apoliner MCS	Apo_MCS_5p	AAGGCGCGCCCTCGAGCCGCGGAAAAAGCAGGAGGAATCTAC
	Apo_MCS_3p	AAGGTACCGGATCCACCGGTCCAGATAAAGCATTTTCTCT
Apoliner-CED-9	ced-9_5p_AgeI_Apo	GAACCGGTCTGGGGATAAAAGGCA
	ced-9_3p_BamHI_Apo	GGGGATCCTAGACCTATCAAACGTCC
ced-9 RNAi (Miller)	ced-9_RNAi_5p_PmeI	AAGTTTAAACTGACACGCTGCACGGCG
	ced-9_RNAi_3p_PmeI	AAGTTTAAACCATCCGCCCACACACGAC
egl-1 promoter	pegl-1_5p_SphI_MLH	AAGCATGCTCGATTCTTATGGTTAAAACGAGCCTTG
	pegl-1_3p_AscI_MLH	AAGGCGCGCCTTGGTAGAAGATCCGAA
p35	p35_5p_AscI	GGGGCGCGCCCTTTACCATAGCAAAATGTGTGTA
	p35_3p_SacII	CCCCGCGGGAATTCTACTCGTAAAGCCAGTTC
pat-3 membrane localization	Mb_5p_AscI	AAGGCGCGCCTCTAGAGGATCCC
	Mb_3p_SacII	AACCGCGGACCTCGGATCTATCATGAAG

Table B.2. A list of plasmids used and/or generated in this work.

Vector	DNA	Additional Information
pMLH007	*punc-25::mCherry::gateway::unc-54 3'UTR*	
pMLH024	*Apoliner in pCR2.1/TOPO*	
pMLH075	*DEVD-BIR1-nls-GFP (Apoliner piece) in pCR8*	
pMLH103	*pttr-39::mCherry::unc-54 3'UTR*	
pMLH116	*pF25B3.3(minus 106bp)::Apoliner-DEVD (mutations)*	
pMLH120	*pF25B3.3(minus 106bp)::Apoliner MCS*	
pMLH128	*coq-1 RNAi (flanked PmeI) in pL4440*	
pMLH137	*punc-25::Apoliner-DEVD::unc-54 3'UTR*	
pMLH142	*pF25B3.3::Apoliner-DEVD::unc-54 3'UTR*	
pMLH152	*ced-9 cDNA in pCR8/GW/TOPO*	
pMLH157	*pegl-1::Apoliner-DEVD::unc-54 3'UTR*	
pMLH158	*ced-9* RNAi (Miller) in HT115 *E. coli*	
pMLH204	*pF25B3.3::Apoliner-ced-9::unc-54 3'UTR*	
pMLH207	*punc-25::ced-3(p15)-nz*	
pMLH210	*punc-25::cz-ced-3(p17)*	
pMLH212	*psur-5::Apoliner-ced-9::unc-54 3'UTR*	
pMLH213	*punc-25::Apoliner-ced-9::unc-54 3'UTR*	
pMLH221	*pttr-39::Mb-mCherry*	
pMLH222	*punc-25::NLS::GFP*	
pMLH237	*pF25B3.3::Apoworm::unc-54 3'UTR*	
pMLH240	*pegl-1::Apoworm::unc-54 3'UTR*	
pMLH241	*pegl-1::Apoworm-DQVA::unc-54 3'UTR*	
pMLH243	*pF25B3.3::Apoworm-DEVA::unc-54 3'UTR*	
pMLH247	*punc-25::p35::unc-10 3'UTR*	
pCJS03	*pF49H12.4::intron2::unc-5*	made by Cody Smith
pG2M03	*pC2::Apoliner (DQVD)*	a gift from Pierre-Luc Bardet
pG2M04	*pC2::Apomut (DQVA)*	a gift from Pierre-Luc Bardet
pG2M17	*pelt-2::NLS::GFP*	a gift from Oliver Hobert
pG2M20	*pcoel:GFP*	a gift from Daniel Colon-Ramoz
pG2M30	*pBluescript II*	

Table B.3: Plasmid concentrations of transgenic arrays generated for this study.

Transgene	Genotype Injected	Plasmid Name	Concentration
wdEx907 [pF25B3.3::Apoworm, pcoel::GFP]	N2	pMLH237	80 ng/µL
		pG2M20	20 ng/µL
wdEx803 [pegl-1::Apoliner-DEVD, pelt-2::GFP]	N2	pMLH157	20 ng/µL
		pG2M17	25 ng/µL
		pG2M30	45 ng/µL
wdEx911 [pF25B3.3::Apoworm, punc-25::cz-ced-3(p17), punc-25::ced-3(p15)-nz]	N2	pMLH207	5.8 ng/µL
		pMLH210	5 ng/µL
		pMLH237	90 ng/µL

RESULTS

Apoliner is an *in vivo* caspase sensor that contains a mRFP-GFP fusion protein that normally localizes to the plasma membrane (Fig. B.1E) (Bardet, Kolahgar, Mynett, Miguel-Aliaga, Briscoe, Meier & Vincent 2008a). These fluorescent proteins are separated by a sequence that is specifically cleaved by *Drosophila* effector caspases and this proteolysis separates mRFP (remains membrane localized) from GFP (translocates to the nucleus after caspase cleavage). The differential localization of these fluorophores indicates that active caspases are present within the cell (Fig. B.1F). A biosensor to detect caspase activation *in vivo* has not been reported in *C. elegans*. We therefore modified this reporter to enhance expression and CED-3/caspase recognition in the nematode.

Optimizing reporter expression and caspase recognition

Modifying the caspase consensus sequence

The caspase recognition domain in Apoliner is derived from DIAP1 (*Drosophila* inhibitor of apoptosis protein 1) and contains the minimal effector caspase consensus site (DQVD) as well as a

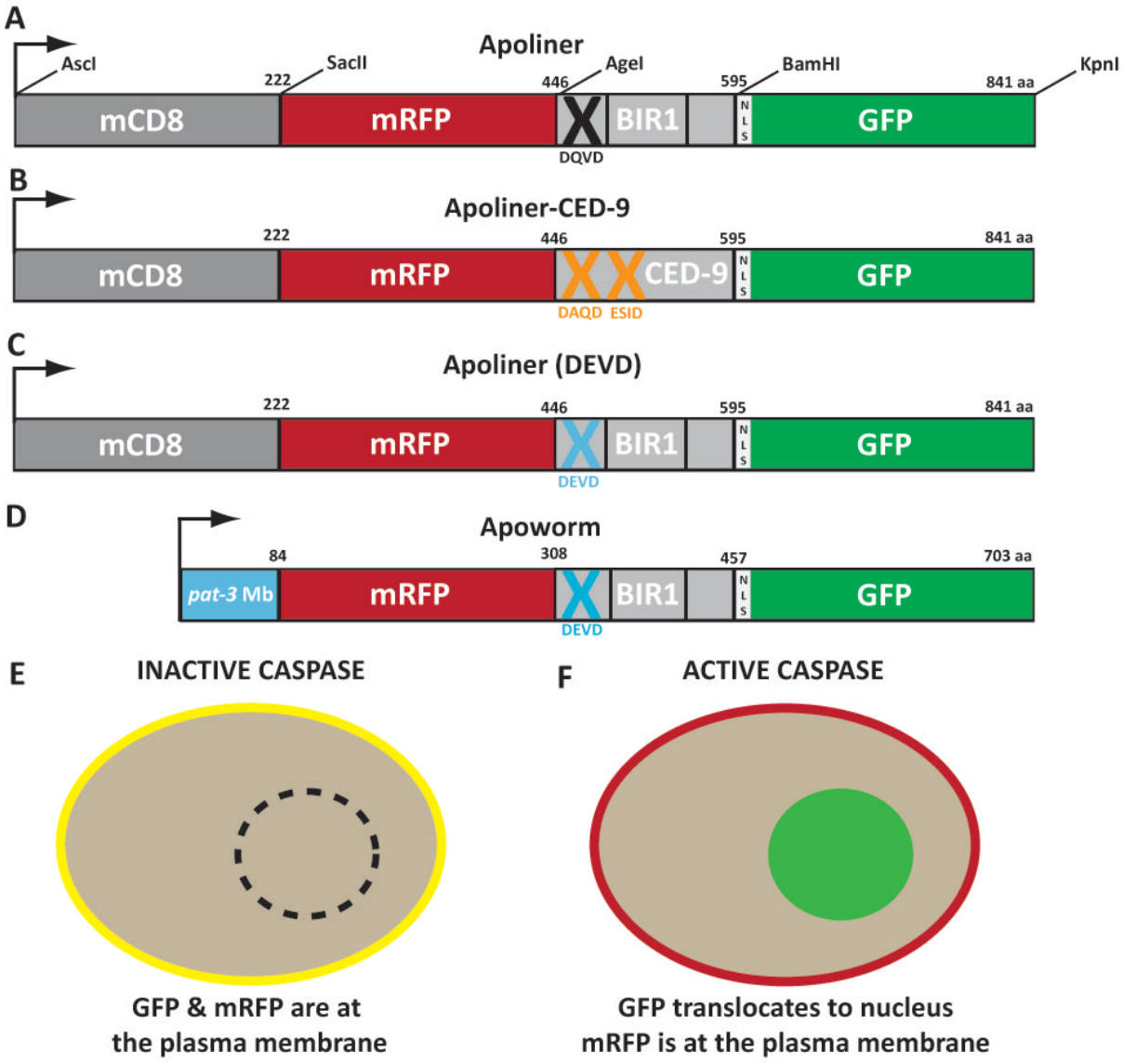

Figure B.1: Modifications to the *Drosophila* caspase biosensor (Apoliner) for enhanced expression and caspase recognition in *C. elegans* (Apoworm) A. Diagram of the *Drosophila* caspase reporter Apoliner. Restriction sites used for molecular cloning (see **Materials and Methods**) are indicated. **B.** Apoliner-CED-9: The *Drosophila* BIR1 domain is replaced by a sequence from *ced-9* with two CED-3 cleavage sites. **C.** Apoliner(DEVD): a single mutation in the caspase recognition sequence (DQVD to DEVD) is introduced to enhance CED-3 recognition. **D.** Apoworm: Mouse CD8 (mCD8) is replaced by the transmembrane domain of *C. elegans pat-3* for enhanced protein expression. Mb = membrane localization sequence. **E-F.** Schematic of fluorescent protein signals (GFP and mRFP) with inactive (**E**) and active (**F**) caspases in the cell.

BIR1 domain that enhances its recognition by caspases (Fig. B.1A) (Bardet, Kolahgar, Mynett, Miguel-Aliaga, Briscoe, Meier & Vincent 2008a). The preferred substrate sequence for *Drosophila* effector caspases (DQVD) is similar to that of CED-3 (DEVD) (Taylor et al. 2007); we mutated the P3 (Crawford & Wells 2011) glutamine (Q) in Apoliner to glutamic acid (E) to make Apoliner (DEVD) (Fig. B.1C).

For one version of the reporter, we replaced the BIR1 domain of Apoliner (DEVD) with a sequence from *ced-9*, an *in vitro* CED-3 substrate that contains two CED-3 cleavage sites (Fig. B.1B) (Xue & Horvitz 1997; Taylor et al. 2007). We were unable to detect Apoliner-CED-9 expression under the robust pan-neural/*F25B3.3* promoter (data not shown); we therefore reverted back to the version with the BIR1 domain, which has confirmed expression in *C. elegans* (Fig. B.2).

The egl-1 promoter-driven Apoliner (DEVD) is dimly expressed in cells undergoing PCD

To test whether Apoliner (DEVD) detects CED-3 activation during programmed cell death, we expressed it using the *egl-1* promoter, which is transcriptionally activated during programmed apoptosis (Fig. B.5A) (Conradt & Horvitz 1998). We were unable to detect *Apoliner(DEVD)* expression under the *egl-1* promoter in a wild-type background (data not shown), likely due to the swift execution and removal of dead cells (Sulston & Horvitz 1977; Robertson & Thomson 1982; Sulston et al. 1983; Ellis et al. 1991). Next, we expressed *pegl-1::Apoliner(DEVD)* in a strong corpse engulfment-deficient genetic background, *ced-1(e1735); ced-5(n1812)* (Reddien & Horvitz 2004). Because cell corpses persist in this background, we observed both GFP and mRFP fluroescence in dying cells (Fig. B.2). However, these events were both rare and difficult to detect due to dim fluorescent signal. Nevertheless, this analysis confirmed the *egl-1* promoter is capable of expressing Apoliner(DEVD) in cells that undergo programmed cell death.

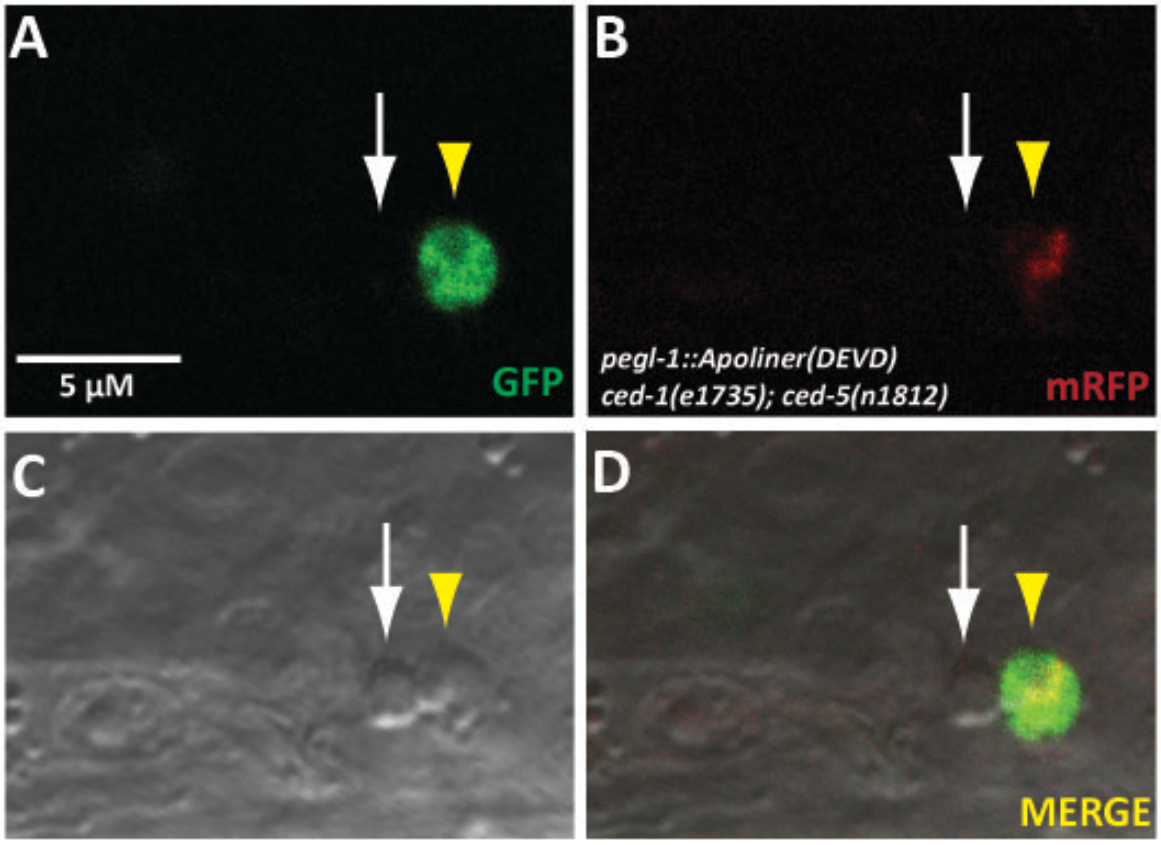

Figure B.2: The *egl-1* promoter-driven Apoliner(DEVD) is dimly expressed in cells undergoing programmed cell death. A. GFP signal in an apoptotic cell in the head of the animal under the control of the *egl-1* promoter (yellow arrowhead). **B.** Faint mRFP signal is also detected in the same cell. **C.** DIC shows two neighboring button-like, dying cells: one with Apoliner(DEVD) expressed (yellow arrowhead), one without (white arrow). **D.** Merged image. Anterior right, ventral down.

Modifying the membrane localization sequence

Preliminary data using multiple promoters (*egl-1*/programmed cell deaths*, unc-25*/GABA neurons*,* and *F25B3.3/*all neurons) to express Apoliner(DEVD) produced very weak fluorescence intensity compared to other fluorescent proteins (*i.e.* GFP alone) microinjected at similar concentrations (data not shown). Faint expression of vectors without introns has been documented (Hutter 2012), and the lack of introns in Apoliner(DEVD) may explain its diminished fluorescence.

To enhance the intensity of the fluorophore signal, we exchanged the mouse CD8 membrane localization sequence with a segment from the *pat-3* integrin that robustly localizes proteins to the plasma membrane in *C. elegans* (Gettner et al. 1995). This modification significantly enhanced of the fluorescent signal, and this version of the biosensor (Apoworm) was used for subsequent analyses.

Apoworm detects forced CED-3 activation in GABA neurons

Without robust expression using the *egl-1* promoter (Fig. B.2), we were unable to address whether Apoworm is cleaved in cells that normally undergo programmed cell death (PCD) during development. We also could not detect expression of the reporter in dying cells using either pan-neural/*F25B3.3* or ubiquitous/*sur-5* promoters (data not shown); we hypothesize this is because apoptotic cells do not activate these promoter regions before their death, which occurs shortly after their birth (Sulston et al. 1983).

We therefore took advantage of a reconstituted caspase system (described in **Chapter 4** (Chelur & Chalfie 2007)) to force CED-3 activation in a subset of cells also expressing Apoworm. Previous experiments demonstrated that expression of reconstituted CED-3 (rec-CED-3) in GABA neurons was sufficient to induce their apoptotic death (see **Chapter 4**). We used the *F25B3.3* promoter to express Apoworm throughout the nervous system and also reconstituted CED-3 in

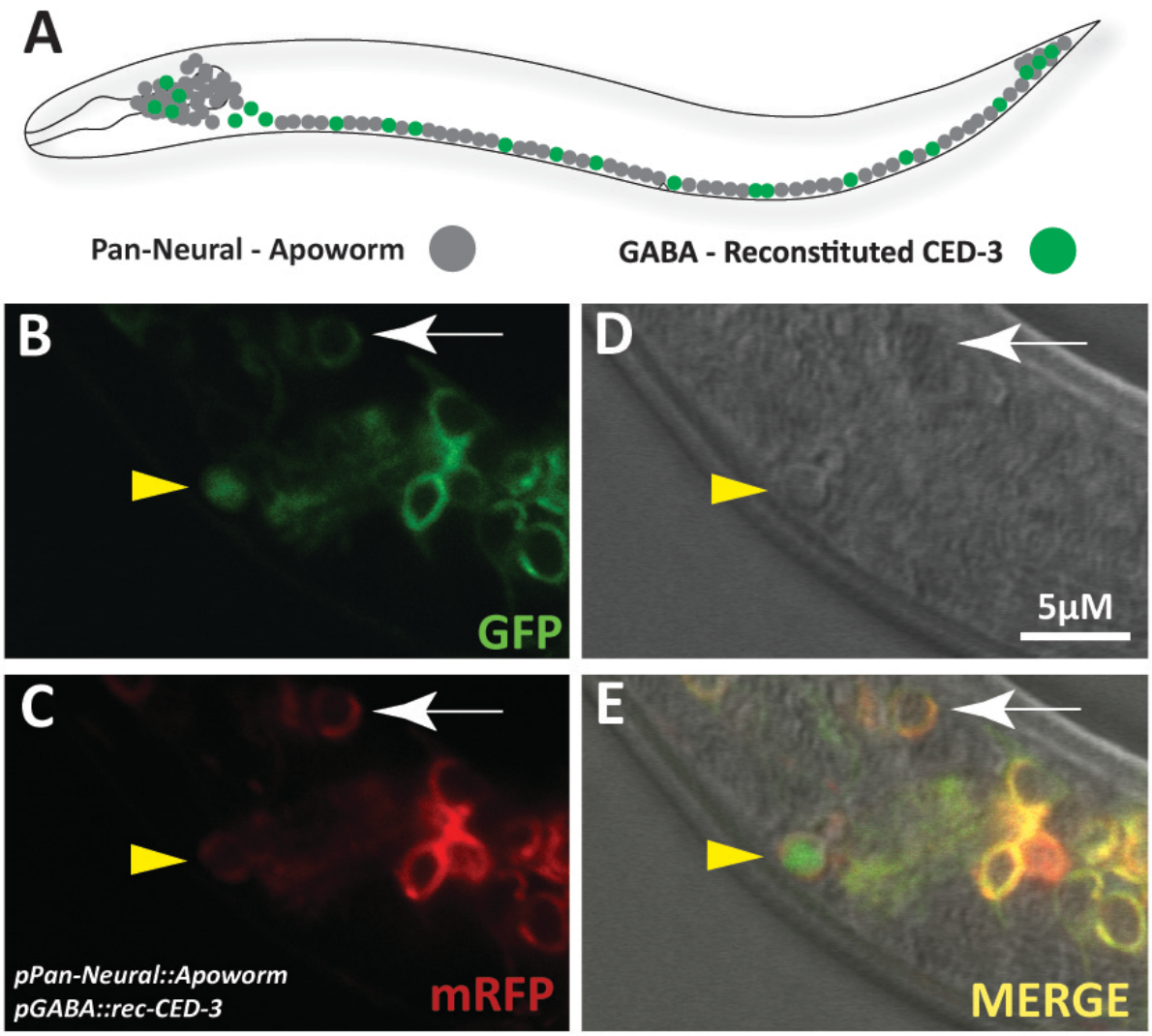

Figure B.3: Apoworm detects forced CED-3 activation in GABA neurons. A. Diagram illustrating the expression of Pan-Neural Apoworm (gray) and reconstituted CED-3 (rec-CED-3) in GABA neurons (green). **B.** Nuclear localization of GFP indicates Apoworm cleavage in an apoptotic GABA neuron (yellow arrowhead). **C.** In contrast, non-apoptotic neurons have both GFP and mRFP signals at the membrane (white arrow). **D.** DIC image shows button-like morphology of the apoptotic neuron. **E.** Merged (GFP/mRFP/DIC) image. Anterior left, ventral down.

GABA neurons (Fig. B.3A). Forced CED-3 activation allowed us to detect nuclear GFP (*i.e.* Apoworm cleavage) in button-like GABA neurons in the head of transgenic animals (Fig. B.3B-E). This finding indicates that Apoworm can be cleaved by activated CED-3/caspase.

Apoworm is cleaved independent of CED-3 in select neurons that do not die

After discovering that Apoworm can identify apoptotic events when CED-3 activation is transgenically induced (Fig. B.3), we wanted to know whether this reporter could also detect endogenous caspase activity. Because 105 of the 131 cells that undergo PCD are neurons (Putcha & Johnson 2004), we chose to focus on the nervous system. Using pan-neurally driven Apoworm, we examined neurons that express the caspase biosensor throughout development in hopes of catching an apoptotic event. Unfortunately, we did not see apoptotic neurons at any developmental stage in transgenic animals expressing this pan-neural caspase reporter (data not shown). Through this analysis, we noticed two neurons that had nuclear GFP and membrane-localized mRFP but did not display morphological features of apoptosis (Fig. B.4A-D). Both of these neurons are located in the head of the animal: one in the anterior bulb of the pharynx (cell identity unknown) and a second in the posterior bulb of the pharynx (believed to be either the M1 or I6 neuron). We noted a higher frequency of nuclear GFP for the neuron in the posterior bulb of the pharynx, and our quantification of this revealed that this neuron exhibits Apoworm cleavage throughout development (data not shown) and in almost half of the population (Fig. B.4E). Neither of these neurons died at any developmental stage (data not shown).

In addition to their role in cell death pathways, caspases participate in many other biological processes (see **Chapter 4**). We reasoned that the cleavage of Apoworm in these non-dying neurons was due to an uncharacterized, non-apoptotic role of CED-3. To test this hypothesis, we examined

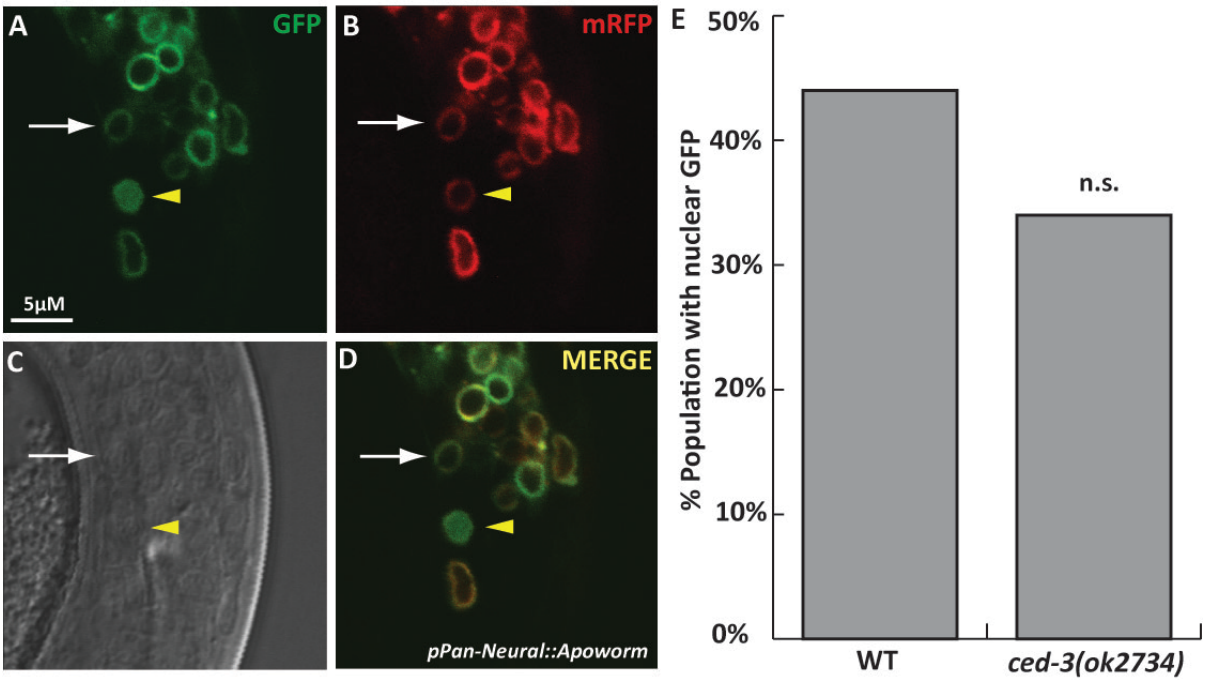

Figure B.4: Apoworm is cleaved in select neurons that do not die, independent of CED-3. A. Pan-neurally expressed Apoworm is uncleaved in head neurons (white arrow) except for one cell in the terminal bulb of the pharynx (yellow arrowhead). **B.** mRFP remains at the plasma membrane. **C.** DIC shows the neuron with cleaved Apoworm does not have apoptotic morphology. **D.** Merged image. Anterior up, ventral left. **E.** Percent of population with nuclear GFP signal (*i.e.* Apoworm cleavage) is not significantly (n.s.) reduced in *ced-3(ok2734)* versus wild-type (WT). n ≥ 25.

the frequency of Apoworm cleavage in the posterior pharyngeal bulb neuron in both wild-type (WT) and *ced-3(ok2734)*. Surprisingly, there was no significant difference in the frequency nuclear GFP between WT and *ced-3* mutants, which suggests that Apoworm cleavage in some cells occurs independent of CED-3.

Apoworm does not detect all apoptotic events

As previously described, pan-neurally driven Apoworm is not detected in cells that die during development. To address whether Apoworm could identify endogenous CED-3 activation, we used RNAi to knockdown *ced-9,* a negative regulator of apoptosis that functions upstream of *ced-3* (Fig. B.5A). Because global loss of *ced-9* is lethal (Hengartner & Horvitz 1994), we used a neuron-specific RNAi background [*sid-1; punc-119::sid-1*] (Calixto et al. 2010) to reduce *ced-9* function only in neurons. Knockdown of *ced-9* resulted in the rare apoptotic death of neurons that normally survive larval development (Fig. B.5C), but we were unable to see nuclear-localized GFP in these button-like cells. Furthermore, neighboring neurons that did not die had Apoworm cleavage (Fig. B.5C-E). Taken together, these results indicate that Apoworm is not cleaved in all apoptotic cells.

DISCUSSION AND FUTURE DIRECTIONS

In this appendix, we describe modifications to the *Drosophila* caspase sensor Apoliner (Bardet, Kolahgar, Mynett, Miguel-Aliaga, Briscoe, Meier & Vincent 2008a) to enhance expression and detection of CED-3 activation in *C. elegans*. By altering the membrane localization domain and including a substrate recognition sequence that is highly preferred by CED-3, we have generated a reporter that can detect CED-3 activation in cells undergoing apoptosis. With further optimization, this reporter may become a useful tool to uncover novel roles for CED-3 and other *C. elegans* proteases.

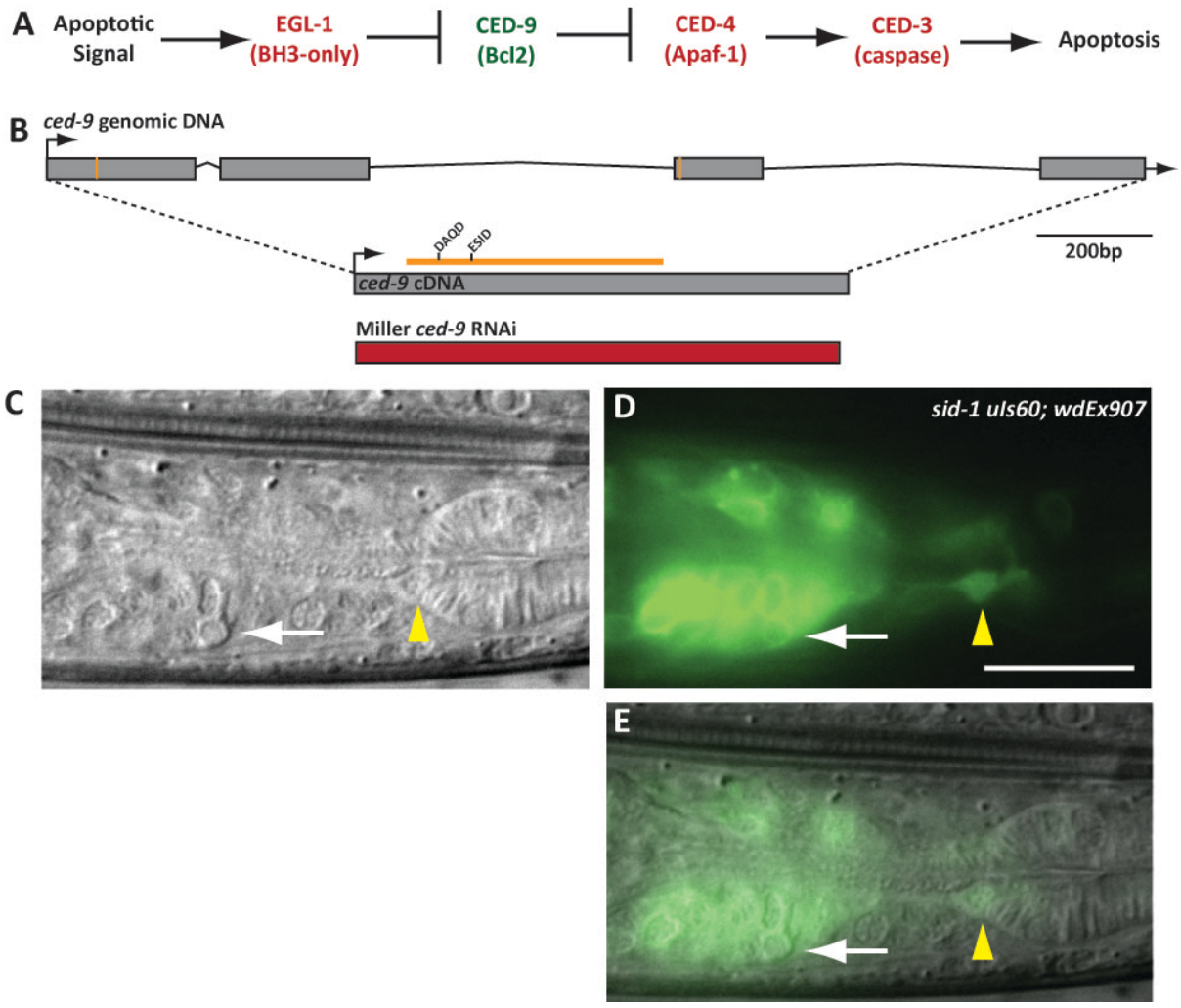

Figure B.5: Apoworm does not detect all CED-3-dependent apoptotic events induced by loss of CED-9 function. A. Diagram of the apoptotic pathway in *C. elegans*. **B.** *ced-9* genomic and cDNA are illustrated. The region of *ced-9* cDNA used to make Apoliner-CED-9 is orange – with the location of CED-3 cleavage sites (DAQD and ESID) annotated. The *ced-9* RNAi clone generated for this study covers most of the *ced-9* cDNA sequence. **C.** DIC image of a button-like apoptotic neuron (white arrow) caused by *ced-9* RNAi treatment of a *sid-1 (pk3321) uIs60 (pPan-Neural::sid-1); wdEx907 (pPan-Neural::Apoworm)* L1 animal. A neuron that does not have morphological characteristics of an apoptotic cell is also indicated (yellow arrowhead). **D.** The dying neuron (white arrow) has membrane-localized GFP (Apoworm not cleaved), while the non-apoptotic neuron (yellow arrowhead) has a pronounced nuclear GFP signal (Apoworm cleaved). Scale bar = 10 µm. **E.** Merged image. Anterior right, ventral down.

However, despite the progress made to optimize this sensor, there are specific issues that should be addressed for future use. First, we were unable to identify reporter cleavage in cells that normally undergo programmed cell death (PCD) during development. Attempts to express the sensor under the *egl-1* promoter (transcriptionally activated to begin apoptosis) were unsuccessful due to both dim reporter expression and rare apoptotic cells also expressing Apoliner(DEVD). The rapid execution and removal of apoptotic cells after *egl-1* induction (Maurer et al. 2007) may explain why we did not detect PCD events with this reporter.

Secondly, Apoworm is cleaved in a CED-3-independent manner in distinct neurons that do not undergo apoptosis (Figure B.4). This suggests that an additional protease is active and recognizes a region of the biosensor between the membrane-tagged mRFP and the NLS-GFP (Figure B.1D) in these neurons. It is unclear whether the DEVD sequence (*i.e.* CED-3 "specific") is recognized by this unidentified protease or another sequence within that region is cleaved. Finally, we detected an event where Apoworm failed to report CED-3 activity in a neuron with clear morphological signs of apoptosis (Figure B.5). Based on these preliminary analyses, we conclude that further optimization of Apoworm is required before it can be fully utilized as a reliable indicator of *in vivo* CED-3 activity.

Future Directions

Despite the aforementioned caveats of Apoworm, our work provides the foundation for further optimization that may lead to the creation of a reliable *in vivo* caspase reporter for *C. elegans*. Apoworm also has the potential to uncover novel, apoptotic-independent roles of CED-3. For example, CED-3 activity is required for neuron regeneration following axotomy (Pinan-Lucarre et al. 2011) and our work reveals a neuroprotective role for CED-3 that requires its caspase activity (see **Chapter 4**). Both of these non-apoptotic CED-3 roles are largely unstudied and require a detailed

mechanistic characterization. An *in vivo* CED-3 activity sensor could address many unanswered questions regarding caspase involvement in both regeneration and neuroprotection. However, it is worth noting that localized caspase activity is currently the favored model for CED-3-dependent neuronal regeneration (Pinan-Lucarre et al. 2011), and this reporter is designed to detect robust CED-3 activation (Figure B.1F). It will be difficult to detect minor or localized caspase activity with the sensor described here. Alternative approaches of detecting localized caspase activation currently include FRET-based systems (Figueroa et al. 2011) and these methods may be the desired technique to uncover subtle or localized caspase activity.

Additionally, CSP-1, another *C. elegans* caspase, was recently assigned an *in vivo* role, where it promotes programmed cell death through a mechanism independent of the core apoptotic machinery (Fig. 5A) (Denning et al. 2013). Work by Shai Shaham revealed that the preferential substrate sequence for CSP-1 (YVAD) is very distinct from that of CED-3 (DEVD) (Neukomm et al. 2011; Shaham 1998). By modifying the protease recognition sequence, this sensor could be used to assess properties of CSP-1-dependent apoptotic events. Furthermore, for proteases with unique substrate recognition sequences, this reporter could be extremely useful to investigate the timing and consequences of proteolytic activation in a variety of biological contexts.

We have also generated additional reagents that will be useful for future optimization of Apoworm. One such vector contains the pan-caspase inhibitor *p35* and could be used to verify the caspase-dependence of the biosensor. We have also mutated the caspase recognition sequence (an aspartate essential for caspase cleavage is mutated to alanine) and this reagent (Apoworm-DEVA) would provide a control to validate caspase substrate specificity.

Appendix C: List of plasmids (pMLH #1-303, pMBM #1-9)

Plasmid Name	Description	From
pMLH001	punc-25 FWD in pENTR 5' TOPO SphI/AscI	kanamycin
pMLH002	punc-25 REV in pENTR 5' TOPO SphI/AscI	kanamycin
pMLH003	yk1514f03 FWD in pCR8/GW TOPO	spectinomycin
pMLH004	pC04G2.1 FWD in pENTR 5' TOPO SphI/AscI	kanamycin
pMLH005	pC04G2.1 REV in pENTR 5' TOPO SphI/AscI	kanamycin
pMLH006	yk1514f03 REV in pCR8/GW TOPO	spectinomycin
pMLH007	punc-25:mcherry:gateway:unc-54 3'UTR	ampicillin
pMLH008	punc-25:gateway:YFP	ampicillin
pMLH009	punc-25:gateway:mcherry	ampicillin
pMLH010	punc-25:mcherry:yk1514f03:unc-54 3'UTR	ampicillin
pMLH011	punc-25 REV in pENTR 5' TOPO SacI/KpnI	kanamycin
pMLH012	punc-25:yk1514f03:mcherry (93A)	ampicillin
pMLH013	punc-25:yk1514f03 RC:mcherry (961)	ampicillin
pMLH014	coq-1 cDNA REV in pCR8/GW TOPO	spectinomycin
pMLH015	punc-25:rde-1 cDNA:mcherry:unc-10 3'UTR	ampicillin
pMLH016*	pwpro:unc-119:yk1514f03 IR:unc-54 3'UTR	ampicillin
pMLH017	pwpro:unc-119:yk1514f03	ampicillin
pMLH018	yk1749d10 in L4440 in HT115 cells	ampicillin
pMLH019	punc-25:mcherry:csp-3 genomic NO STOP	ampicillin
pMLH020	punc-25 in pCR2.1 TOPO AscI/PmeI	kanamycin
pMLH021	pcoq-1:gateway:mcherry	ampicillin
pMLH022	punc-25 in pCR2.1 TOPO SphI/SmaI	kanamycin
pMLH023	yk1479d10 FWD in pCR8/GW TOPO	spectinomycin
pMLH024	Apoliner in pCR2.1 TOPO AscI/KpnI	kanamycin
pMLH025	punc-25:csp-3 cDNA:mcherry	ampicillin
pMLH026	punc-25:luc+:GFP	ampicillin
pMLH027	punc-25:HyPer:unc-10 3'UTR	ampicillin
pMLH028	punc-25:gateway:SL2:mcherry	ampicillin
pMLH029	coq-1 cDNA Ahringer (5p) in pCR8/GW TOPO	spectinomycin
pMLH030	coq-1 cDNA 3prime end in pCR8/GW TOPO	spectinomycin
pMLH031	punc-4:HyPer:unc-10 3' UTR	ampicillin
pMLH032	coq-1 cDNA Ahringer (5p) in L4440	ampicillin
pMLH032	coq-1 cDNA Ahringer (5p) RNAi (in L4440)	ampicillin
pMLH033	punc-25::yk1479d10::SL2::mcherry::unc-10 3'UTR	ampicillin
pMLH034	pcoq-1:yk1479d10:SL2:mcherry:unc-10 3'UTR	ampicillin
pMLH035	punc-25:TOM20:mRFP:unc-10 3'UTR	ampicillin
pMLH036	punc-4:TOM20:mRFP	ampicillin
pMLH037	punc-25:rde-1:mcherry:unc-10 3'UTR + unc-119 mini gene	ampicillin
pMLH038	punc-25:HyPer:unc-10 3'UTR + unc-119 mini gene	ampicillin
pMLH039	punc-4:HyPer:unc-10 3'UTR + unc-119 mini gene	ampicillin
pMLH040	punc-25:TOM20:mRFP:unc-10 3'UTR + unc-119 mini gene	ampicillin
pMLH041	punc-25:mcherry:unc-54 3'UTR + unc-119 mini gene	ampicillin
pMLH042	pdes-2:mcherry:unc-54 3'UTR + unc-119 mini gene	ampicillin
pMLH043	punc-25:rde-1:mRFP:unc-10 3'UTR + unc-119 mini gene	ampicillin
pMLH044	punc-25:coq-1 (yk1479d10):SL2:mcherry + unc-119 mini gene	ampicillin
pMLH045	punc-25 in pCR8 ApaI/NcoI	spectinomycin
pMLH046	pttr-39::mcherry::unc-54 3'UTR + unc-119 mini gene	ampicillin
pMLH047	punc-25::yk1479d10::RC punc-25	ampicillin
pMLH048	punc-25::gateway::mRFP::unc-10 3'UTR	ampicillin
pMLH049	punc-25::gateway::GFP::unc-10 3'UTR	ampicillin
pMLH050	punc-25::gateway::SL2::GFP::unc-10 3'UTR	ampicillin
pMLH051	punc-25::gateway::SL2::mRFP::unc-10 3'UTR	ampcilin
pMLH052	punc-25::gateway::SL2::YFP::unc-54 3'UTR	ampicillin
pMLH053	punc-25::yk1479d10::SL2::mRFP::unc-10 3'UTR	ampicillin
pMLH054	punc-25::gateway::SL2::CFP::unc 54 3'UTR	ampicillin
pMLH055	pttr-39::egl-36(gf)::unc-54 3'UTR + unc-119 mini gene (same strand)	ampicillin

pMLH056	pttr-39::egl-36(gf)::unc-54 3'UTR + unc-119 mini gene (opp strand)	ampicillin
pMLH057	pttr-39::egl-36(lf)::unc-54 UTR + unc-119 mini gene (same strand)	ampicillin
pMLH058	pttr-39::egl-36(lf)::unc-54 3'UTR + unc-119 mini gene (opp strand)	ampicillin
pMLH059	yk1479d10 FWD (5' SacII- 3' AscI) in pCR8/GW TOPO	spectinomycin
pMLH059	yk1479d10 FWD in pCR8/GW TOPO (5'SacII-3'AscI)	spectinomycin
pMLH060	yk1479d10 REV in pCR8/GW TOPO (5'SacII-3'AscI)	spectinomycin
pMLH061	Gateway R1R2 cassette (5' AscI - 3' SacII) in pCR8/GW TOPO	spec + CAM
pMLH061	R1R2 Gateway in pCR8 GW/TOPO (5' AscI-3' SacII)	spectinomycin
pMLH062	punc-25::CFP + unc-119 minigene	ampicillin
pMLH063	pttr-39::coq-1 cDNA REV + unc-119 minigene	ampicillin
pMLH064	unc-30 cDNA minus TTAG FWD in pCR8/GW TOPO	spectinomycin
pMLH065	unc-30 cDNA minus TTAG REV in pCR8/GW TOPO	spectinomycin
pMLH066	yk1479d10 REV in pCR8/GW TOPO (5'AscI-3'SacII)	spectinomycin
pMLH067	yk1479d10 FWD in pCR8/GW TOPO (5'AscI-3'SacII)	spectinomycin
pMLH068	punc-25::gateway::SL2::mRFP + unc-119 minigene	ampicillin
pMLH069	mito::GFP PCR'd from bcEx620 FWD in pCR8/GW TOPO	spectinomycin
pMLH070	mito::GFP PCR'd from bcEx620 REV in pCR8/GW TOPO	spectinomycin
pMLH071	punc-25::unc-30 minus A in start::SL2::mRFP	ampicillin
pMLH072	punc-25::unc-30 minus TTAG in stop::SL2::mRFP + unc-119 minigene	ampicillin
pMLH073	pttr-39::coq-1 cDNA FOR::punc-25 RC + unc-119 minigene	ampicillin
pMLH074	pacr-2 5'SphI 3'AscI in pCR8 (REV)	spectinomycin
pMLH075	Apoliner DEVD piece in pCR8 FWD	spectinomycin
pMLH076	pttr-39::coq-1 cDNA FOR + unc-119 minigene	ampicillin
pMLH077	pttr-39::coq-1 FOR::punc-25 RC + unc-119 minigene	ampicillin
pMLH078	punc-25::mRFP + unc-119 minigene	ampicillin
pMLH079	pacr-2 5'SphI 3'AscI in pCR8 (FOR)	spectinomycin
pMLH080	psur-5 5'SphI 3'Asci in pCR8 (FOR)	spectinomycin
pMLH081	pF25B3.3 5'SphI 3'AscI in pCR8 (unknown direction)	spectinomycin
pMLH082	mitochondrial leader sequence (MLS)-GFP 5'AscI 3'SacII in pCR2.1	kanamycin/ampicillin
pMLH083	punc-25::gateway::SL2::mRFP 5'ApaI 3'ApaI in pCR8	chloramphenicol/spectinomycin
pMLH084	punc-25::GFP::unc-10 UTR	ampicillin
pMLH085	N/A	
pMLH086	punc-25::GFP::unc-10 UTR + unc-119 minigene	ampicillin
pMLH087	psur-5::mRFP + unc-119 minigene	ampicillin
pMLH088	pacr-2::TOM20::mRFP + unc-119 minigene	ampicillin
pMLH089	punc-25::mRFP in pENTR TOPO	kanamycin
pMLH090	psur-5::yk1479d10 + unc-119 minigene	ampicillin
pMLH091	pttr-39-yk1514f03-pu25reverse+unc119minigene and pdat-1mcherry	spectinomycin+ampicillin
pMLH092	pmyo-3::dsRed::unc-54 UTR FWD in pCR8	spectinomycin
pMLH093	pF25B3.3::GFP & punc-25::mcherry	ampicillin
pMLH094	pmyo-3::dsRed::unc-54 UTR REV in pCR8	spectinomycin
pMLH095	pttr-39::coq-1 cDNA REV + punc-25::mcherry	ampicillin
pMLH096	pttr-39::rde-1 cDNA + unc-119 minigene	ampicillin
pMLH097	drp-1 cDNA (unknown direction) in pCR8	spectinomycin
pMLH098	punc-25::drp-1 cDNA::unc-10 UTR	ampicillin
pMLH099	unc-30 cDNA AscI-KpnI in pCR8 (unknown direction)	spectinomycin
pMLH100	unc-30 cDNA AscI-KpnI in pCR8 (unknown direction)	spectinomycin
pMLH101	punc-25:unc-30::unc-54 3'UTR	ampicillin
pMLH102	pacr-2::unc-30::unc-54 3'UTR	ampicillin
pMLH103	pttr-39::mcherry::unc-54 3'UTR	ampicillin
pMLH104	coq-1 573bp RNAi from cDNA flanked PmeI in pCR8	spectinomycin
pMLH105	pttr-39::coq-1 RNAi FWD + unc-119(+)	ampicillin
pMLH106	pttr-39::(PmeI, no RNAi clone) + unc-119(+)	ampicillin
pMLH107	pttr-39::coq-1 RNAi FWD::punc-25::mCherry	ampicillin
pMLH108	pceh-22::mRFP	ampicillin
pMLH109	punc-4::TOM20::YFP::unc-54 3'UTR	ampicillin
pMLH110	punc-4::TOM20::GFP::unc-10 3'UTR	ampicillin
pMLH111	pttr-39::coq-1 RNAi FWD + unc-119(+)	ampicillin
pMLH112	pttr-39::coq-1 RNAi REV (flanked PmeI)	ampicillin
pMLH113	pF25B3.3(minus 106bp)::unc-30 cDNA	ampicillin

pMLH114	pacr-2::ApoDEVD missense mutations	ampicillin
pMLH115	pttr-39::coq-1 RNAi FWD (flanked PmeI)	ampicillin
pMLH116	pF25B3.3(minus 106bp)::ApoDEVD missense mutations	ampicillin
pMLH117	pttr-39::TOM20::GFP::unc-10 3'UTR	ampicillin
pMLH117	pttr-39::TOM20::GFP::unc-10 3'UTR	ampicillin
pMLH118	pttr-39::asp-4::GFP	ampicillin
pMLH119	punc-8 (FseI-AscI) FWD in pCR8	spectinomycin
pMLH120	pF25B3.3(minus 106bp)::Apoliner MCS	ampicillin
pMLH121	pF25B3.3(full)::unc-30 cDNA	ampicillin
pMLH122	pttr-39-coq-1 cDNA-mCherry	ampicillin
pMLH123	pF25B3.3 minus106bp::ApoMCS-AscI-SacII	ampicillin
pMLH124	punc-8::TOM20::GFP::unc-10 3'UTR	ampicillin
pMLH125	N/A	
pMLH126	N/A	
pMLH127	pacr-2::TOM20::mRFP::unc-10 3'UTR	ampicillin
pMLH128	coq-1 RNAi FWD in L4440 in XL1 Blues	ampicillin + tetracycline
pMLH129	coq-1 RNAi FWD in L4440 in HT115	ampicillin + tetracycline
pMLH130	punc-8::GFP::unc-10 3'UTR	ampicillin + tetracycline
pMLH131	C. briggsae (#5) coq-1 genomic REV in pCR8	spectinomycin
pMLH132	punc-25::mcherry::unc-54 3'UTR	ampicillin
pMLH133	phsp-16.2::GFP::unc-10 3' UTR	ampicillin
pMLH134	pF25B3.3 minus 106bp::Apoliner correct DEVD	ampicillin
pMLH135	N/A	
pMLH136	phsp-16.2::coq-1 RNAi FWD	ampicillin
pMLH137	punc-25::Apoliner-DEVD::unc-54 3'UTR	ampicillin
pMLH138	coq-1 & asp-3 RNAi clone in L440 in HT115	ampicillin + tetracycline
pMLH139	csp-1B cDNA no stop FWD AscI-KpnI in pCR8	spectinomycin
pMLH140	N/A	
pMLH141	pttr-39::csp-1B::GFP	ampicillin
pMLH142	pF25B3.3::Apoliner-DEVD::unc-54 3'UTR	ampicillin
pMLH143	punc-25::mcherry::unc-10 3'UTR + pmyo-2::mcherry	ampicillin
pMLH144	punc-25::GFP + pmyo-2::mcherry	ampicillin
pMLH145	psur-5::coq-1 RNAi REV + unc-119(+)	ampicillin
pMLH146	pacr-2::unc-30 cDNA + unc-119(+)	ampicillin
pMLH147	phsp-16.2::coq-1 FWD RNAi + pmyo-2::mcherry	ampicillin
pMLH148	pttr-39::csp-1B::GFP + unc-119(+)	ampicillin
pMLH149	pF25B3.3::Apoliner-DEVD + unc-119(+)	ampicillin
pMLH150	pacr-2::sod-1 genomic with mutation + unc-119(+)	ampicillin
pMLH151	C. briggsae (#2) coq-1 genomic FWD in pCR8	spectinomycin
pMLH152	ced-9 RNAi FWD (flanked PmeI) in pCR8	spectinomycin
pMLH153	ced-9 RNAi REV (flanked PmeI) in pCR8	spectinomycin
pMLH154	ced-9 RNAi REV in L4440 in XL1 Blues	ampicillin
pMLH155	wan-1 3'UTR (flanked PmeI) in pCR8	spectinomycin
pMLH156	pttr-39::tra-3 cDNA:: unc-10 3'UTR	ampicillin
pMLH157	pegl-1::Apoliner-DEVD	ampicillin
pMLH158	ced-9 RNAi in L4440 in HT115	ampicillin + tetracycline
pMLH159	wan-1 3'UTR in L4440 in HT115	ampicillin + tetracycline
pMLH160	pttr-39::asp-4 cDNA::unc-10 3'UTR	ampicillin
pMLH161	punc-25::TOM20::GFP	ampicillin
pMLH162	pttr-39::ced-3 cDNA::unc-10 3'UTR	ampicillin
pMLH163	pttr-39::ced-3 (C358S) cDNA::unc-10 3'UTR	ampicillin
pMLH164	pttr-39::ced-3 cDNA::unc-10 3'UTR (from my cDNA)	ampicillin
pMLH165	pttr-39::C. briggsae coq-1 cDNA::unc-10 3'UTR	ampicillin
pMLH166	pttr-39::C. briggsae coq-1 genomic DNA::unc-10 3'UTR	ampicillin
pMLH167	punc-25::C.briggsae coq-1 cDNA::unc-10 3'UTR	ampicillin
pMLH168	punc-25::C.briggsae coq-1 cDNA::unc-10 3'UTR	ampicillin
pMLH169	pttr-39::csp-1 cDNA::unc-10 3'UTR	ampicillin
pMLH170	punc-25::luc+::GFP::unc-10 3'UTR	ampicillin
pMLH171	psur-5::C.briggsae coq-1 cDNA::unc-10 3'UTR	ampicillin
pMLH172	pacr-2::GFP::unc-10 3'UTR	ampicillin

pMLH173	pF25B3.3::mcherry::unc-54 3'UTR	ampicillin
pMLH174	pttr-39::ced-4 cDNA::unc-10 3'UTR	ampicillin
pMLH175	pF25B3.3::GFP-H2B::unc-54 3'UTR	ampicillin
pMLH176	pacr-2::mcherry::unc-54 3'UTR	ampicillin
pMLH177	psur-5::C.briggsae coq-1 cDNA (STOP)-GFP::unc-54 3'UTR	ampicillin
pMLH178	csp-1 cDNA RNAi (FWD) in L4440 in XL1 Blues	ampicillin
pMLH179	ced-3 cDNA RNAi (FWD) in L4440 in XL1 Blues	ampicillin
pMLH180	pttr-39::csp-1 cDNA RNAi REV	ampicillin
pMLH181	psur-5::sod-2 gDNA::GFP::unc-54 3'UTR	ampicillin
pMLH182	pF25B3.3::C. briggsae coq-1 cDNA::unc-10 3'UTR	ampicillin
pMLH183	pttr-39::ced-3 RNAi FWD	ampicillin
pMLH184	punc-25::sod-2 gDNA::GFP::unc-54 3'UTR	ampicillin
pMLH185	pttr-39::csp-1 cDNA RNAi FWD	ampicillin
pMLH186	pttr-39::ced-3 cDNA RNAi REV	ampicillin
pMLH187	punc-25::drp-1 cDNA (STOP)::TAA-unc-54 3'UTR	ampicillin
pMLH188	punc-25::ced-3 cDNA::GFP::unc-54 3'UTR	ampicillin
pMLH189	punc-25::ced-4 cDNA::GFP::unc-54 3'UTR	ampicillin
pMLH190	punc-25::csp-1 cDNA::GFP::unc-54 3'UTR	ampicillin
pMLH191	punc-25::sod-2 gDNA (no stop)::TAA-unc-54 3'UTR	ampicillin
pMLH192	pttr-39::ctl-1 cDNA RNAi FWD	ampicillin
pMLH193	pttr-39-ctl-1_RNAi_FWD_flanked PmeI	ampicillin
pMLH194	pttr-39-ctl-1_RNAi_REV_flanked PmeI	ampicillin
pMLH195	N/A	
pMLH196	pttr-39_csp-1 genomic DNA-unc-10 UTR	ampicillin
pMLH197	punc-25-csp-1B-FLAG-unc-10UTR	ampicillin
pMLH198	pttr-39_csp-1B_C138S BUT ALSO K131R-	ampicillin
pMLH199	csp-1A cDNA FWD in pCR2.1-TOPO	ampicillin + kanamycin
pMLH200	pttr-39_csp-1A_cDNA w SNPs-unc-10	ampicillin
pMLH201	psur-5_csp-1_gDNA-unc-10 UTR	ampicillin
pMLH202	phsp-16-2_csp-1 gDNA-unc-10 UTR	ampicillin
pMLH203	pttr-39_csp-1A_cDNA w E136 -unc-10	ampicillin
pMLH204	pF25B3.3_Apoliner_ced-9-unc-54 3'UTR	ampicillin
pMLH205	pacr-2-rec-csp-1-large-unc-10-UTR	ampicillin
pMLH206	pttr-39-ced-3 (p15)-nz	ampicillin
pMLH207	punc-25-ced-3 (p15-SM)-nz	ampicillin
pMLH208	phsp-16.2-ced-3 (p15-SM)-nz	ampicillin
pMLH209	pttr-39-cz-ced-3 (p17)	ampicillin
pMLH210	punc-25-cz-ced-3 (p17-LG)	ampicillin
pMLH211	phsp-16.2-cz-ced-3 (p17-LG)	ampicillin
pMLH212	psur-5_Apoliner_ced-9-unc-54 3'UTR	ampicillin
pMLH213	punc-25_Apoliner_ced-9-unc-54 3'UTR	ampicillin
pMLH214	phsp_16.2_ced-3 cDNA-unc-10 UTR	ampicillin
pMLH215	pacr-2-csp-1(p10)-unc-10-UTR	ampicillin
pMLH216	pttr-39-csp-1 (p10)-nz	ampicillin
pMLH217	pttr-39-cz-csp-1 (p20)-unc-10 3'UTR	ampicillin
pMLH218	psur-5_Apoliner-DEVD_unc-54-UTR	ampicillin
pMLH219	psur-5_cz-csp-1(p20)-unc-10 UTR	ampicillin
pMLH220	phsp-16.2-csp-1 (p10)-nz	ampicillin
pMLH221	pttr-39-Mb-mCherry	ampicillin
pMLH223	psur-5_coq-1 RNAi FWD	ampicillin
pMLH224	psur-5-coq-1 RNAi REV flanked PmeI	ampicillin
pMLH226	psur-5_Mb-Apoliner-DEVD_unc-54-UTR	ampicillin
pMLH227	punc-25-Mb-Apoliner-DEVD	ampicillin
pMLH228	pcsp-1-GFP-unc-10UTR	ampicillin
pMLH229	pttr-39_ced-3-FLAG-unc-10 UTR	ampicillin
pMLH230	pttr-39_ced-3-C358S-FLAG-unc-10 UTR	ampicillin
pMLH231	pmec-4_Mb-Apoliner-DEVD_unc-54-UTR	ampicillin
pMLH232	pcsp-1 1.3kb FWD in pCR2.1-TOPO	ampicillin + kanamycin
pMLH233	pmyo-3-C-briggsae coq-1-unc-10 3'UTR	ampicillin
pMLH234	pmyo-3-csp-1 (p10)-nz unc-54 3'UTR	ampicillin

pMLH235	pmyo-3-GFP-unc-10 3'UTR	ampicillin
pMLH236	pttr-39_csp-1C_cDNA-unc-10 UTR	ampicillin
pMLH237	pF25B3.3-Mb-Apo-DEVD-unc-54 3'UTR	ampicillin
pMLH238	N/A	
pMLH239	N/A	
pMLH240	pegl-1_Mb-Apo_DEVD-unc-54 3'UTR	ampicillin
pMLH241	pegl-1_Mb-Apo_DQVA-unc-54 3'UTR	ampicillin
pMLH242	pegl-1_Mb-Apo_DEVA-unc-54 3'UTR	ampicillin
pMLH243	pF25B3.3-Mb-Apo-DEVA-unc-54 3'UTR	ampicillin
pMLH244	csp-1 FWD RNAi in L4440 (HT115)	ampicillin + tetracycline
pMLH245	ced-3 FWD RNAi in L4440 (HT115)	ampicillin + tetracycline
pMLH246	punc-25-WldS-unc-10 3'UTR	ampicillin
pMLH247	punc-25-p35-unc-10-3'UTR	ampicillin
pMLH248	pmec-4-csp-1 (p10)-nz	ampicillin
pMLH249	pttr-39_ced-3_NO-CARD_unc-10 UTR	ampicillin
pMLH250	pttr-39_csp-3_cDNA_unc-10 UTR	ampicillin
pMLH251	pdat-1_TOM20-GFP-unc-10 UTR	ampicillin
pMLH252	pdat-1_unc-30cDNA-unc-54 3'UTR	ampicillin
pMLH253	N/A	
pMLH254	punc-25_S-sp-ispB-incomplete_unc10UTR	ampicillin
pMLH255	psur-5-S sp-ispB-incomplete-unc-10 UTR	ampicillin
pMLH256	punc-25_coq-1-GFP-unc-54 3' UTR	ampicillin
pMLH257	psur-5-coq-1-GFP-unc-54 UTR	ampicillin
pMLH258	psur-5-coq-1-GFP-unc-54 UTR	ampicillin
pMLH259	N/A	
pMLH260	punc-25_coq-1-GFP-unc-54 3' UTR	ampicillin
pMLH261	punc-25 HindIII-SphI--XbaI-AscI-mCherry	ampicillin
pMLH262	punc-25 HindIII-SphI--XbaI-AscI-TOM20-GFP	ampicillin
pMLH263	pceh-22 HindIII-SphI--XbaI-AscI-TOM20-GFP	ampicillin
pMLH264	pmyo-3 HindIII-SphI--XbaI-AscI-TOM20-GFP	ampicillin
pMLH265	pF25B3.3-ced-3(p15)-nz-unc-54 3'UTR	ampicillin
pMLH266	pF25B3.3-cz-ced-3(p17)-unc-54 3'UTR	ampicillin
pMLH267	pmec-4-ced-3 (p15)-nz	ampicillin
pMLH268	pmec-4-cz-ced-3 (p17)	ampicillin
pMLH269	pceh-22 COQ-1-GFP	ampicillin
pMLH270	pmyo-3 COQ-1-GFP	ampicillin
pMLH271	pmyo-3-TOM20mRFP-unc-10 UTR	ampicillin
pMLH272	pmyo-3 COQ-1-mCherry	ampicillin
pMLH273	N/A	
pMLH274	N/A	
pMLH275	N/A	
pMLH277	psur-5_PDSS2_mut-S382L_human_cDNA-unc-10 UTR	ampicillin
pMLH278	psur-5::PDSS1-wt partial (missing 1st 500bp)	ampicillin
pMLH279	psur-5::PDSS1-mut partial (missing 1st 500bp)	ampicillin
pMLH280	psur-5-mCherry	ampicillin
pMLH281	psur-5::PDSS2-wt(no stop)	ampicillin
pMLH282	pmyo-3::PDSS2-wt(stop)	ampicillin
pMLH283	psur-5_PDSS2-wild-type-unc-10 UTR	ampicillin
pMLH284	pmyo-3-PDSS2 wild type-GFP	ampicillin
pMLH285	pttr-39::PDSS1 full pat-3 out-mcherry (intermediate vector)	ampicillin
pMLH286	psur-5::PDSS1 wild type::unc-10 3'UTR	ampicillin
pMLH287	psur-5::PDSS1(D308E)::unc-10 3'UTR	ampicillin
pMLH288	N/A	
pMLH289	N/A	
pMLH290	pdpy-7::COQ-1::GFP::unc-54 3'UTR	ampicillin
pMLH291	pelt-2::COQ-1::GFP::unc-54 3'UTR	ampicillin
pMLH294	psur-5::PDSS1-wt-stop-GFP::unc-54 3'UTR	ampicillin
pMLH295	pmyo-3::end-of-PDSS1::GFP	ampicillin
pMLH298	punc-25 (XbaI-KpnI)::COQ-1::GFP (intermediate vector)	ampicillin
pMLH299	psur-5::human COQ2 (missing stop)::unc-54 3'UTR	ampicillin

pMLH300	psur-5::PDSS1-mCherry::unc-54 3'UTR	ampicillin
pMLH301	psur-5::human COQ2 wild-type::unc-54 3'UTR	ampicillin
pMLH302	psur-5::human COQ2 N401fsX415::unc-54 3'UTR	ampicillin
pMLH303	psur-5::PDSS2::GFP	ampicillin
pMBM1	pttr-39::sod-1 genomic DNA + unc-119 minigene	ampicillin
pMBM3	punc-25::sod-1 genomic DNA::unc-10 3'UTR	ampicillin
pMBM4	punc-25::sod-2 genomic DNA::unc-10 3'UTR	ampicillin
pMBM5	punc-25::ctl-2 genomic DNA::unc-10 3'UTR	ampicillin
pMBM0	punc-25::ctl-1 cDNA::unc-10 3'UTR	ampicillin
pMBM7	punc-25::ctl-3 cDNA::unc-10 3'UTR	ampicillin
pMBM8	unc-25 cDNA RNAi in pCR2.1	ampicillin
pMBM9	unc-25 RNAi in pL4440 (in HT115 E. coli)	ampicillin + tetracycline

Appendix D: List of Gifts to Mal plasmids (pG2M#1-64)

Plasmid Name	Description	From	Institution	Reference
pG2M01	pcsp-3::csp-3::GFP	Ding Xue	UC Boulder	(Geng et al. 2008)
pG2M02	pmyo-3::TOM20::mRFP	Toshihikio Oka	Kyushu Universita, Japan	(Ichishita et al. 2008)
pG2M03	Apoliner	Jean-Paul Vincent / Pierre-Luc Bardet	MRC	(Bardet, Kolahgar, Mynett, Miguel-Aliaga, Briscoe, Meier & Vincent 2008b)
pG2M04	Apomut	Jean-Paul Vincent / Pierre-Luc Bardet	MRC	(Bardet, Kolahgar, Mynett, Miguel-Aliaga, Briscoe, Meier & Vincent 2008b)
pG2M05	odr-1::GFP	Geraldine Maro	Stanford	(Maro et al. 2009)
pG2M06	odr-1::RFP	Geraldine Maro	Stanford	(Maro et al. 2009)
pG2M07	odr-1::mcherry	Cori Bargmann	Rockafeller	(Lesch et al. 2009)
pG2M08	ced-3 RNAi clone	David Eisenman	University of Maryland	(Joshi & Eisenmann 2004)
pG2M09	ced-4 RNAi clone	David Eisenman	University of Maryland	(Joshi & Eisenmann 2004)
pG2M10	pTG96 (psur-5::NLS::GFP)	David Fay	University of Wyoming	(Kirienko et al. 2008)
pG2M11	pwpro::unc-119::ccdb	David Sattelle	Oxford	(Briese et al. 2006)
pG2M12	pwpro::myo-3::ccdb	David Sattelle	Oxford	(Briese et al. 2006)
pG2M13	L4440-Gateway	Addgene		
pG2M14	punc-8::mec-4(d)	Nektarios Tavernarakis	IMBB	(Syntichaki et al. 2002)
pG2M15	pasp-3::asp-3::GFP	Nektarios Tavernarakis	IMBB	(Syntichaki et al. 2002)
pG2M16	pasp-4::asp-4::GFP	Nektarios Tavernarakis	IMBB	(Syntichaki et al. 2002)
pG2M17	pelt-2::GFP	Oliver Hobert	Columbia	
pG2M18	pttx-3::GFP	Oliver Hobert	Columbia	
pG2M19	pceh-22::GFP	Oliver Hobert	Columbia	
pG2M20	coel::GFP	Daniel Colon-Ramoz (Cody)	Yale	
pG2M21	coel::RFP	Daniel Colon-Ramoz (Cody)	Yale	
pG2M22	pET3a-csp-1B-FLAG	Shai Shaham	Rockafeller	(Shaham 1998)
pG2M23	pET3a-csp-1B-C138S-FLAG	Shai Shaham	Rockafeller	(Shaham 1998)
pG2M24	pET3a-ced-3-FLAG	Shai Shaham	Rockafeller	(Shaham 1998)
pG2M25	pET3a-ced-3-C358S-FLAG	Shai Shaham	Rockafeller	(Shaham 1998)
pG2M26	GD1 (Q-less E.coli)	Cathy Clarke	UCLA	(Saiki et al. 2008)
pG2M27	K0229:pSN18 (CoQ-9 E. coli)	Cathy Clarke	UCLA	(Saiki et al. 2008)
pG2M28	him-14 RNAi	Randy Blakely (via Andrew Hardaway)	Vanderbilt	
pG2M29	pCFJ90 (pmyo-2::mcherry)	Addgene		
pG2M30	pBluescript II	unknown (old lab stocks)		
pG2M31	pRF4 (rol-6(d))	unknown (old lab stocks)		
pG2M32	pCM1.151 (mCherry::H2B)	Addgene		
pG2M33	pCM1.35 (GFP::H2B)	Addgene		
pG2M34	TU#730 (psto-	old Miller lab		

	6::cz::GFP)	stocks		
pG2M35	pPD95.69	old Miller lab stocks		
pG2M36	pJER1 (pmyo-3::dsRed)	old Miller lab stocks		
pG2M37	pmig-24::WldS (Wallerian Degeneration Slow)	Shai Shaham	Rockafeller	(Abraham et al. 2007)
pG2M38	coq-2 fosmid			
pG2M39	TU#806 (pmec-18::ced-3(p15)-nz)	Addgene		(Chelur & Chalfie 2007)
pG2M40	TU#807 (pmec-18::cz-ced-3(p17))			(Chelur & Chalfie 2007)
pG2M41	PDSS2			
pG2M42	unc-119 minigene (MM051)			
pG2M43	PDSS1 wt	Agnes Rotig		(Mollet et al. 2007)
pG2M44	PDSS1 D308E	Agnes Rotig		(Mollet et al. 2007)
pG2M45	PDSS2 wt	Agnes Rotig		(Mollet et al. 2007)
pG2M46	PDSS2 S382L	Agnes Rotig		(Mollet et al. 2007)
pG2M47	COQ2 wt	Agnes Rotig		(Mollet et al. 2007)
pG2M48	COQ2 N401fsX415	Agnes Rotig		(Mollet et al. 2007)
pG2M49	pJM360 (elt-2 promoter)	Jim McGhee		
pG2M50	pdpy-7::swip-10	Andrew Hardaway/Blakely Lab		
pG2M51	pHyPer-cyto			
pG2M52	pSLGCV			(Lagido et al. 2008)
pG2M53	pBC401 (drp-1 WT)	Barbara Conradt		(Jagasia et al. 2005)
pG2M54	pBC402 (drp-1 WT)			(Jagasia et al. 2005)
pG2M55	pBC403 (drp-1 DN)			(Jagasia et al. 2005)
pG2M56	pBC404 (drp-1 (DN)			(Jagasia et al. 2005)
pG2M57	yk1514f03			
pG2M58	yk1479d10			
pG2M59	pPD#S006 (pF25B3.3::GFP)			
pG2M60	pSC392 (punc-25::CFP)			
PG2M61	K0229:pKA3 (Q8)	Cathy Clarke	UCLA	(Saiki et al. 2008)
pG2M62	K0229:pLD23 (Q10)	Cathy Clarke	UCLA	(Saiki et al. 2008)
pG2M63	pSC391 (pacr-2::YFP)			
pG2M64	pBX (pha-1(+))			

APPENDICES REFERENCES

Abraham, M.C., Lu, Y. & Shaham, S., 2007. A morphologically conserved nonapoptotic program promotes linker cell death in Caenorhabditis elegans. *Dev Cell*, 12(1), pp.73–86.

Bardet, P., Kolahgar, G., Mynett, A., Miguel-Aliaga, I., Briscoe, J., Meier, P. & Vincent, J., 2008a. A fluorescent reporter of caspase activity for live imaging. *Proc Natl Acad Sci U S A*, 105(37), pp.13901–13905.

Bardet, P.-L., Kolahgar, G., Mynett, A., Miguel-Aliaga, I., Briscoe, J., Meier, P. & Vincent, J.-P., 2008b. A fluorescent reporter of caspase activity for live imaging. *Proceedings of the National Academy of Sciences of the United States of America*, 105(37), pp.13901–13905.

Brenner, S., 1974. The genetics of Caenorhabditis elegans. *Genetics*, 77(1), pp.71–94.

Briese, M. et al., 2006. pWormgatePro enables promoter-driven knockdown by hairpin RNA interference of muscle and neuronal gene products in Caenorhabditis elegans. *Invert Neurosci*, 6(1), pp.5–12.

Calixto, A. et al., 2010. Enhanced neuronal RNAi in C. elegans using SID-1. *Nature Methods*.

Chelur, D.S. & Chalfie, M., 2007. Targeted cell killing by reconstituted caspases. *Proceedings of the National Academy of Sciences of the United States of America*, 104(7), pp.2283–2288.

Conradt, B. & Horvitz, H.R., 1998. The C. elegans protein EGL-1 is required for programmed cell death and interacts with the Bcl-2-like protein CED-9. *Cell*, 93(4), pp.519–529.

Crawford, E.D. & Wells, J.A., 2011. Caspase Substrates and Cellular Remodeling. *Annual Review of Biochemistry*, 80(1), pp.1055–1087.

Denning, D.P., Hatch, V. & Horvitz, H.R., 2013. Both the Caspase CSP-1 and a Caspase-Independent Pathway Promote Programmed Cell Death in Parallel to the Canonical Pathway for Apoptosis in Caenorhabditis elegans. *PLoS Genet*, 9(3), p.e1003341.

Ditzel, M. et al., 2003. Degradation of DIAP1 by the N-end rule pathway is essential for regulating apoptosis. *Nat Cell Biol*, 5(5), pp.467–473.

Dixon, S.J., 2006. FGF negatively regulates muscle membrane extension in Caenorhabditis elegans. *Development*, 133(7), pp.1263–1275.

Earls, L.R. et al., 2010. Coenzyme Q protects Caenorhabditis elegans GABA neurons from calcium-dependent degeneration. *Proceedings of the National Academy of Sciences of the United States of America*, 107(32), pp.14460–14465.

Ellis, R.E., Jacobson, D.M. & Horvitz, H.R., 1991. Genes required for the engulfment of cell corpses during programmed cell death in Caenorhabditis elegans. *Genetics*, 129(1), pp.79–94.

Figueroa, R.A. et al., 2011. Anchored FRET sensors detect local caspase activation prior to neuronal degeneration. *Molecular Neurodegeneration*, 6(1), p.35.

Fraser, A.G. et al., 2000. Functional genomic analysis of C. elegans chromosome I by systematic RNA interference. *Nature*, 408(6810), pp.325–330.

Geng, X. et al., 2008. Inhibition of CED-3 zymogen activation and apoptosis in Caenorhabditis elegans by caspase homolog CSP-3. *Nat Struct Mol Biol*, 15(10), pp.1094–1101.

Gettner, S.N., Kenyon, C. & Reichardt, L.F., 1995. Characterization of beta pat-3 heterodimers, a family of essential integrin receptors in C. elegans. *Journal of Cell Biology*, 129(4), pp.1127–1141.

Grishok, A., 2005. Transcriptional silencing of a transgene by RNAi in the soma of C. elegans. *Genes & Development*, 19(6), pp.683–696.

Hengartner, M.O. & Horvitz, H.R., 1994. C. elegans Cell Survival Gene ced-9 Encodes a Functional Homolog of the Mammalian Proto-Onocogene bcl-2

. *Cell*, 76, pp.665–676.

Hofmann, E.R. et al., 2002. Caenorhabditis elegans HUS-1 is a DNA damage checkpoint protein required for genome stability and EGL-1-mediated apoptosis. *Current biology : CB*, 12(22), pp.1908–1918.

Hutter, H., 2012. Fluorescent Protein Methods: Strategies and Applications. In *Methods in Cell Biology*. Methods in Cell Biology. Elsevier, pp. 67–92.

Ichishita, R. et al., 2008. SUPP.2 - An RNAi screen for mitochondrial proteins required to maintain the morphology of the organelle in Caenorhabditis elegans. *Journal of Biochemistry*, 143(4), pp.449–454.

Jagasia, R. et al., 2005. DRP-1-mediated mitochondrial fragmentation during EGL-1-induced cell death in C. elegans. *Nature*, 433(7027), pp.754–760.

Joshi, P. & Eisenmann, D.M., 2004. The Caenorhabditis elegans pvl-5 gene protects hypodermal cells from ced-3-dependent, ced-4-independent cell death. *Genetics*, 167(2), pp.673–685.

Kamath, R. & Ahringer, J., 2003. Genome-wide RNAi screening in Caenorhabditis elegans. *Methods*, 30(4), pp.313–321.

Kamath, R.S. et al., 2003. Systematic functional analysis of the Caenorhabditis elegans genome using RNAi. *Nature*, 421(6920), pp.231–237.

Kennedy, S., Wang, D. & Ruvkun, G., 2004. A conserved siRNA-degrading RNase negatively regulates RNA interference in C. elegans. *Nature*, 427(6975), pp.645–649.

Kirienko, N.V., McEnerney, J.D.K. & Fay, D.S., 2008. Coordinated regulation of intestinal functions in C. elegans by LIN-35/Rb and SLR-2. *PLoS Genetics*, 4(4), p.e1000059.

Labrousse, A.M. et al., 1999. C. elegans dynamin-related protein DRP-1 controls severing of the mitochondrial outer membrane. *Mol Cell*, 4(5), pp.815–826.

Lagido, C. et al., 2008. SUPPLEMENTAL Bridging the phenotypic gap: real-time assessment of mitochondrial function and metabolism of the nematode Caenorhabditis elegans. *BMC Physiol*, 8, p.7.

Lesch, B.J. et al., 2009. Transcriptional regulation and stabilization of left-right neuronal identity in C. elegans. *Genes Dev*, 23(3), pp.345–358.

Maro, G.S., Klassen, M.P. & Shen, K., 2009. A beta-catenin-dependent Wnt pathway mediates anteroposterior axon guidance in C. elegans motor neurons. *PLoS ONE*, 4(3), p.e4690.

Maurer, C.W., Chiorazzi, M. & Shaham, S., 2007. Timing of the onset of a developmental cell death is controlled by transcriptional induction of the C. elegans ced-3 caspase-encoding gene. *Development*, 134(7), pp.1357–1368.

McIntire, S.L., Jorgensen, E.M. & Horvitz, H.R., 1993. Genes required for GABA function in Caenorhabditis elegans. *Nature*, 364(6435), pp.334–337.

Mollet, J. et al., 2007. Prenyldiphosphate synthase, subunit 1 (PDSS1) and OH-benzoate polyprenyltransferase (COQ2) mutations in ubiquinone deficiency and oxidative phosphorylation disorders. *J. Clin. Invest.*, 117(3), pp.765–772.

Neukomm, L.J. et al., 2011. Loss of the RhoGAP SRGP-1 promotes the clearance of dead and injured cells in Caenorhabditis elegans. *Nature*, 13(1), pp.79–86.

Pinan-Lucarre, B. et al., 2011. The core apoptotic executioner proteins CED-3 and CED-4 promote initiation of neuronal regeneration in *Caenorhabditis elegans*. *PLoS Biol*, 10(5), p.e1001331. Available at: http://dx.plos.org/10.1371/journal.pbio.1001331.t001.

Putcha, G.V. & Johnson, E.M., 2004. Men are but worms: neuronal cell death in C elegans and vertebrates. *Cell death and differentiation*, 11(1), pp.38–48.

Qu, W. et al., 2011. Reliability analysis of the Ahringer Caenorhabditis elegans RNAi feeding library: a guide for genome-wide screens. *BMC Genomics*, 12(1), p.170.

Reddien, P.W. & Horvitz, H.R., 2004. The engulfment process of programmed cell death in caenorhabditis elegans. *Annu Rev Cell Dev Biol*, 20(1), pp.193–221. Available at: http://www.ncbi.nlm.nih.gov/entrez/query.fcgi?db=pubmed&cmd=Retrieve&dopt=AbstractPlus&list_uids=15473839.

Robertson, A.M.G. & Thomson, J.N., 1982. Morphology of programmed cell death in the ventral nerve cord of Caenorhabditis elegans larvae. pp.1–12.

Saiki, R. et al., 2008. Altered bacterial metabolism, not coenzyme Q content, is responsible for the lifespan extension in Caenorhabditis elegans fed an Escherichia coli diet lacking coenzyme Q. *Aging Cell*, 7(3), pp.291–304.

Shaham, S., 1998. Identification of multiple Caenorhabditis elegans caspases and their potential roles in proteolytic cascades. *J Biol Chem*, 273(52), pp.35109–35117.

Sulston, J.E. & Horvitz, H.R., 1977. Post-embryonic cell lineages of the nematode, Caenorhabditis elegans. *Developmental Biology*, 56(1), pp.110–156.

Sulston, J.E. et al., 1983. The embryonic cell lineage of the nematode Caenorhabditis elegans. *Developmental Biology*, 100(1), pp.64–119.

Syntichaki, P. et al., 2002. Specific aspartyl and calpain proteases are required for neurodegeneration in C. elegans. *Nature*, 419(6910), pp.939–944.

Taylor, R.C. et al., 2007. Establishing a blueprint for CED-3-dependent killing through identification of multiple substrates for this protease. *J Biol Chem*, 282(20), pp.15011–15021.

Xue, D. & Horvitz, H.R., 1997. Caenorhabditis elegans CED-9 protein is a bifunctional cell-death inhibitor. pp.1–4.